ESL-TR-92-01

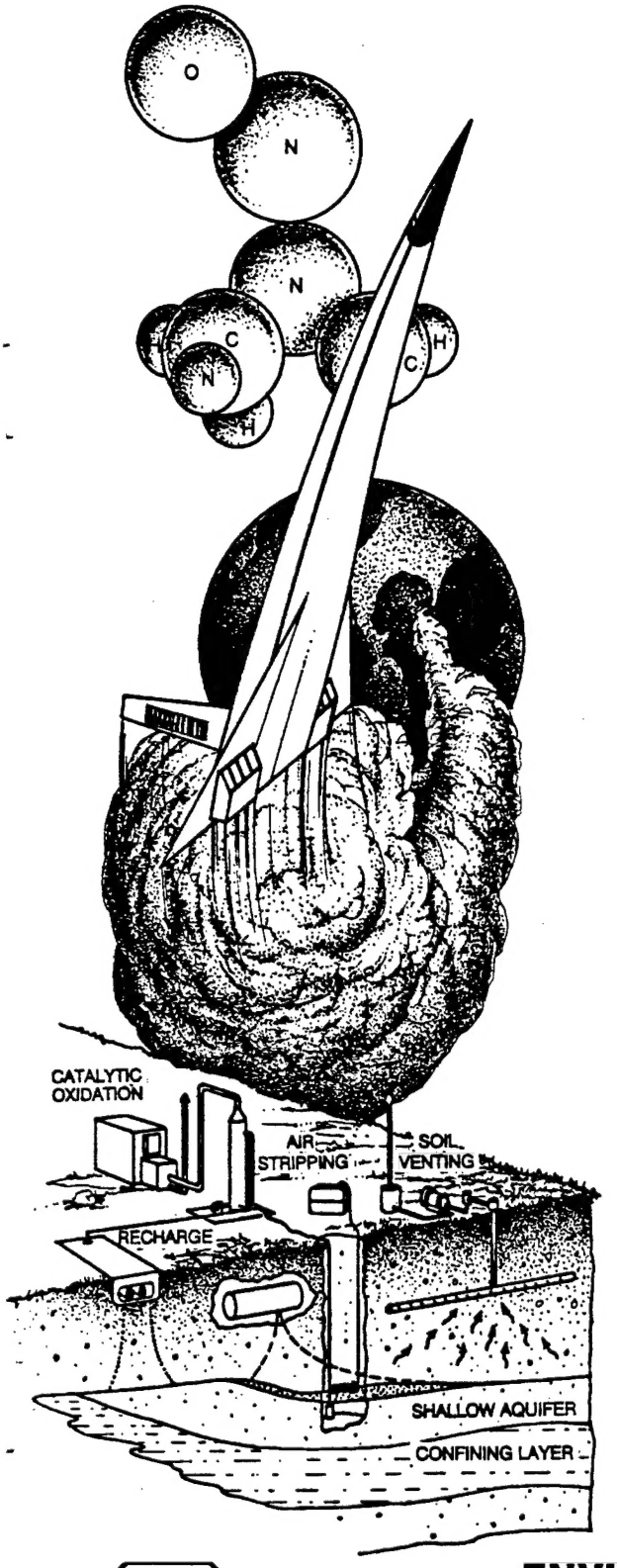

THE MICROSTRUCTURE OF COMPACTED MOIST SAND AND ITS EFFECT ON STRESS TRANSMISSION

G.E. VEYERA, PH.D.
B.J. FITZPATRICK

DEPARTMENT OF CIVIL AND ENVIRONMENTAL ENGINEERING
UNIVERSITY OF RHODE ISLAND
KINGSTON RI 02881

DECEMBER 1996

FINAL REPORT

JANUARY 1990 - DECEMBER 1991

APPROVED FOR PUBLIC RELEASE: DISTRIBUTION UNLIMITED

ENVIRONICS DIVISION
Air Force Engineering & Services Center
ENGINEERING & SERVICES LABORATORY
Tyndall Air Force Base, Florida 32403

REPORT DOCUMENTATION PAGE

Form Approved
OMB No. 074-0188

1. AGENCY USE ONLY (Leave blank)	2. REPORT DATE	3. REPORT TYPE AND DATES COVERED
	31 DECEMBER 1996	FINAL REPORT

4. TITLE AND SUBTITLE
THE MICROSTRUCTURE OF COMPACTED MOIST SAND AND ITS EFFECT ON STRESS TRANSMISSION

5. FUNDING NUMBERS
RESEARCH INITIATION GRANT PROGRAM
F49620-88-C-0053/SB5881-0378-

6. AUTHOR(S)
GEORGE E. VEYERA, Ph.D
BLAISE J. FITZPATRICK

7. PERFORMING ORGANIZATION NAME(S) AND ADDRESS(ES)
DEPARTMENT OF CIVIL AND
ENVIRONMENTAL ENGINEERING
UNIVERSITY OF RHODE ISLAND
KINGSTON, RI 02881

8. PERFORMING ORGANIZATION REPORT NUMBER

9. SPONSORING / MONITORING AGENCY NAME(S) AND ADDRESS(ES)
AIR FORCE ENGINEERING AND
SERVICES CENTER
ENGINEERING AND SERVICES
LABORATORY
TYNDALL AFB FL 32403

10. SPONSORING / MONITORING AGENCY REPORT NUMBER
ESL-TR-92-01

11. SUPPLEMENTARY NOTES
SPONSORED BY AIR FORCE OFFICE OF SCIENTIFIC RESEARCH

12a. DISTRIBUTION / AVAILABILITY STATEMENT
APPROVED FOR PUBLIC RELEASE. DISTRIBUTION UNLIMITED.

12b. DISTRIBUTION CODE
A

13. ABSTRACT *(Maximum 200 Words)*

An experimental investigation was conducted to provide a better understanding of the development of microstructure in unsaturated sand and its effect on dynamic behavior. Previous research has shown that compacting moist sands with varying amounts of water prior to dynamic loading can increase the stress transmission ratio by as much as a factor of two. The compaction method and amount of moisture have also been shown to influence static and dynamic behavior of sands In this study, sand specimens were dynamically compacted to a constant dry density at various saturations, using a standard Proctor hammer and subjected to high strain rate testing using the Split-Hopkinson Pressure Bar device. The influence of soil microstructure on compassion energy, stress transmission, and compressional wave speed for Ottawa 20-30 sand was evaluated. Experimental results suggest that the dynamic behavior of the sand depends on soil microstructure, which is a function of the initial moisture content during compaction.
An attempt was made to relate differences in dynamic soil behavior to to variations in soil microstructure formed during compaction. A two-dimensional grain orientation

14. SUBJECT TERMS
Compaction energy. High strain rate testing. Two-dimensional Grain Orientation Analysis, Vector magnitude. Stress transmission

15. NUMBER OF PAGES
224

16. PRICE CODE

17. SECURITY CLASSIFICATION OF REPORT	18. SECURITY CLASSIFICATION OF THIS PAGE	19. SECURITY CLASSIFICATION OF ABSTRACT	20. LIMITATION OF ABSTRACT
U	U	U	U

NSN 7540-01-280-5500

Standard Form 298 (Rev. 2-89)
Prescribed by ANSI Std. Z39-18
298-102

13, ABSTRACT: (Continued)

analysis was performed on epoxied specimens of compacted sand. Angular frequency histograms and orientation statistics were generated. Vector magnitude was analyzed as a function of saturation and an inverse relationship was found between vector magnitude and stress transmission ratio as a function of saturation. Results from the microstructural analysis suggest that microstructure may be a significant factor affecting the dynamic behavior of unsaturated soils. However, a clear and concise explanation of the microstructural development process is not now available.

PREFACE

This report was prepared by the Department of Civil and Environmental Engineering, he University of Rhode Island, Kingston, Rhode Island, under Contract No. F49620-88-C00523/SB5881-0378 for the Research Initiation Program (RIP) sponsored by the Air Force Office of Scientific Research (AFOSR) for the Engineering and Services Laboratory, Headquarters, Air Force Engineering and Services Center (HQ AFESC/RDCM), Tyndall Air Force Base, Florida.

This report is published by the Civil Engineering Research Division (CERD), of Research Development and Acquisition Directorate (RDAD), Air Force Civil Engineering Support Agency (AFCESA), 139 Barnes Drive, Tyndall Air Force Base, Florida 32403-5323.

This report summarizes the results of work to investigate the dynamic behavior of compacted unsaturated soil using the Split-Hopkinson Pressure (SHPB) device and represents the Master's thesis research of Mr. Blaise J. Fitzpatrick, Department of Civil and Environmental Engineering, University of Rhode Island, Kingston, Rhode Island.. A detailed microstructural analysis was performed on epoxied specimens of compacted unsaturated soil to study the relationship between microstructure and macroscale behavior. The work was initiated in January, 1990 and completed in December, 1991. Dr. George E. Veyera served as the principal investigator at The University of Rhode Island. Mr. Charles R. Bailey served as the project officer for HQ AFESC/RDCM.

(The reverse of this page is blank.)

EXECUTIVE SUMMARY

A. OBJECTIVE

The main objective of this study was to determine how the moisture content during compaction affects soil properties, including compressional wave speed, stress transmission ratio, quasi-static constrained modulus, and soil microstructure. This investigation is directed at developing a better understanding of unsaturated soil behavior and evaluates the influence of microstructure on soil behavior under dynamic and quasi-static loading conditions.

B. BACKGROUND

The ability of a soil to transmit dynamic stresses (energy) is of particular interest to the U.S. Air Force with respect to military protection construction and survivability designs. The prediction of ground motions from conventional weapons detonations and the effect on structures requires information about the response of geologic materials to intense transient loadings. The general nature of stress wave propagation and energy transmission in particulate media such as soil depends on a number of parameters, the interrelationship between which is not fully understood. The Split-Hopkinson Pressure Bar (SHPB) device provides a laboratory experimental capability for simulating the field explosive loading environment and providing insight into the dynamic behavior of soils.

Current design procedures generally assume dry soil conditions even though soils in situ are actually at a condition somewhere between dry and saturated. In addition, field compaction specifications for granular soils only require a final compacted density to be achieved without any restriction on moisture. However, for unsaturated conditions, the amount of energy traveling through a soil and transmitted to a structure can be significantly larger than for dry soil conditions, thereby having the potential for greater damage. Unsaturated soils are complex, multiphase materials the behavior of which is not well understood. Previous research has shown that compacting moist sands with varying amounts of water prior to dynamic loading can increase the stress transmission ratio by as much as a factor of two. However, at present, no theoretical, empirical or numerical methods are available for predicting large amplitude compressive stress wave transmission and compressive stress wave propagation velocity in unsaturated soils. A need exists to develop a better understanding of unsaturated soil behavior at a fundamental level for all types of loadings. Therefore, a comprehensive experimental laboratory study using the

SHPB for dynamic loading, a quasi-static uniaxial loading device, and microstructural analysis techniques was conducted on specimens of compacted unsaturated soil.

C. SCOPE

Specimens of Ottawa 20-30 sand were dynamically compacted to a constant dry density at various saturations using a standard Proctor hammer and subjected to high strain rate testing using a Split-Hopkinson Pressure Bar (SHPB) device. Saturations were varied from 0 to about 80 percent. Microstructural analyses of epoxied compacted unsaturated sands were also performed. In addition, quasi-static uniaxial compression tests were conducted to examine compacted stiffnesses. The influence of soil microstructure on compaction energy, stress transmission, and compressional wave speed for Ottawa 20-30 sand was evaluated.

D. METHODOLOGY

Specimens of Ottawa 20-30 sand were dynamically compacted to a constant dry density at different moisture conditions (saturations from 0 percent to about 80 percent) in a thick-walled stainless steel tube using a standard Proctor hammer. A series of SHPB tests was conducted on the compacted specimens to provide information about stress transmission and wave speed characteristics. In addition, a number of specimens were epoxied after compaction and after SHPB testing to preserve the microstructure and obtain data on variations in particle orientations due to the influence of moisture present during compaction to develop correlations with dynamic behavior. A series of quasi-static uniaxial confined compression tests was conducted to evaluate the stress-strain response as a function of moisture conditions.

E. TEST DESCRIPTION

The SHBP at the Air Force Engineering and Services Center (AFESC/RDCM) was used to dynamically test 50.8 mm diameter specimens of compacted, unsaturated sand in a thick-walled stainless steel specimen container at high strain rates. Specimens were compacted, epoxied and sectioned to preserve their microstructure for analysis using specialized equipment at AFESC/RDCM. Quasi-static uniaxial confined compression tests were also conducted using a Materials Testing System (MTS) ate AFESC. Photomicrographic studies and microstructural analyses were conducted at the University of Rhode Island's Geomechanics Research Laboratory in the Department of Civil and Environmental Engineering.

F. RESULTS

Previous research has shown that compaction energy, constrained modulus (a measure of soil stiffness), compressional wave speed, and stress transmission ratio have greater values at intermediate saturations (from about 20 percent to 75 percent) than for dry soil conditions. The reasons for this phenomena are not fully understood. Variations in soil microstructure developed during compaction appear to be a major factor. The experimental investigation presented herein utilized dynamic and quasi-static testing methods to evaluate the influence of soil microstructure on compaction energy, constrained modulus, wave speed, stress transmission ratio, and degree of saturation for Ottawa 20-30 sand.

In this study, unsaturated sand specimens were dynamically compacted to a constant dry density at various saturations using a standard Proctor hammer and subjected to high strain rate testing using the split-Hopkinson pressure bar device. Previous research has shown that compacting moist sands with varying amounts of water prior to dynamic loading can increase the stress transmission ratio by as much as a factor of two. The compaction method and the amount of moisture have also been shown to influence static and dynamic behavior of sands. The influence of soil microstructure on compaction energy, stress transmission, and compressional wave speed for Ottawa 20-30 sand was evaluated. Experimental results suggest that the dynamic behavior of the sand is dependent on soil microstructure which is a function of the initial moisture content during compaction.

A two-dimensional grain orientation analysis was performed on epoxied specimens of compacted unsaturated sand. Results from the analysis suggest that microstructure may be a significant factor affecting the dynamic behavior of unsaturated soils and showed vector magnitude (a measure of dispersion within a particle orientation data set) could be related to variations in saturation. At intermediate saturations, vector magnitude values were lower than that for dry soil, which indicates a stiffer soil structure. According to wave propagation theory, a stiffer material will produce greater compressional wave speed and stress transmission ratio results at intermediate saturations, as was the case for this investigation. .

Based on the results of this investigation, it was determined that soil microstructure does affect compaction energy, constrained modulus, compressional wave speed, and stress transmission ratio. However, a clear and concise explanation of the microstructural development process is not currently available. Characterization of soil microstructure is an

important first step towards establishing a better understanding of stress transmission in unsaturated soils. Relationships between vector magnitude and dynamic soil parameters may be useful in developing a model to predict stress transmission in unsaturated soils subjected to dynamic loading from conventional weapons.

G. CONCLUSIONS

The results from the SHPB tests, quasi-static uniaxial confined compression tests and microstructural analyses indicate that the amount of moisture present during compaction is probably the most significant factor influencing both the static and dynamic behavior of the Ottawa 20-30 sand.

The compactive energy required to prepare constant dry density specimens using a standard Proctor hammer was shown to be strongly dependent on the amount of moisture present during compaction. The SHPB data show that the amount of energy transmitted is greatest at saturations in the range of about 20 to 80 percent compared with values for dry sand. The microstructural analysis results suggest an inverse relationship between vector magnitude and compaction energy, wave speed, stress transmission ration and constrained modulus with variations in the degree of saturation. Preferred particle orientations were observed at saturations of 0 to about 20 percent and above 75 percent, while a random orientation was observed at saturations in the range of about 20 to 75 percent. In addition, quasi-static uniaxial confined compression test results show changes in specimen stiffness with changes in compaction moisture which are generally consistent with trends observed in the dynamic SHPB data. The variations in dynamic and static behavior observed in this investigation can be attributed to the influence of soil microstructure developed during compaction the nature of which is predominantly a function of the amount of moisture present.

H. RECOMMENDATIONS

The results of this investigation have provided important insight into the complex dynamic behavior of unsaturated soils about which very little is known. These findings are significant with regards to military protective construction design and require further detailed studies in both the laboratory and field coupled with numerical model development.

Further laboratory work using the SHPB should be conducted to study other parameters including particle size, particle shape and variations in compacted dry density

under various confinement conditions. In addition, detailed microstructural analyses should also be a part of this work.

Scaled laboratory tests should be performed in the centrifuge using explosive charges in compacted, unsaturated soils. This will allow the simulation of various field conditions in a laboratory environment and provide independent verification of the SHPB results. The centrifuge is an important research tool and has a distinct advantage over field tests in that a number of tests can be performed in a short time period. The AFESC centrifuge facility is ideally suited for this work. In addition, laboratory and numerical studies should be checked against a series of carefully controlled, fully instrumented scaled explosive field tests.

The laboratory work has progressed to the point where the development of an initial preliminary numerical model in conjunction with further experimental work is needed. The model should incorporate a mathematical approach such as the distinct element or finite element technique based on the laboratory derived results for wave speed, transmission ratio, and vector magnitude, to predict the compressional wave speed and stress transmission in unsaturated soils. This will prove to be a useful tool to help explain the intricacies of the laboratory observed behavior and also provide guidance for the direction of continued experimental work. Once centrifuge and field data are available, they can be used to further develop and improve the model.

(The reverse of this page is blank.)

TABLE OF CONTENTS

TABLE OF CONTENTS (CONTINUED)

TABLE OF CONTENTS (CONTINUED)

TABLE OF CONTENTS (CONTINUED)

TABLE OF CONTENTS (CONTINUED)

LIST OF FIGURES

LIST OF FIGURES (CONTINUED)

LIST OF FIGURES (CONTINUED)

LIST OF FIGURES (CONTINUED)

LIST OF FIGURES (CONTINUED)

LIST OF FIGURES (CONTINUED)

LIST OF TABLES

LIST OF SYMBOLS

Symbol	Definition
A	angularity
A	cross-sectional area
A_p	area of particle
A_c	area of smallest circumscribing circle
c	cohesion
cc	cubic centimeters
D	constrained modulus
E	modulus of elasticity (Youngs modulus)
e	base of natural logarithms
e	void ratio
f	number of particles in axial ratio calculation
$G_1, G_2, \ldots G_n$	constituting grain particle of sand
L	vector magnitude in terms of percent
L	specimen length
L_0	initial compacted specimen length
L_1	apparent length of long axis
L_2	apparent length of short axis
N_i	normal to the tangent plane at the contact point, P_i
n_s	axial ratio for a single particle
n_{avg}	axial ratio for a group of particles
n'	magnitude of an individual particle's long axis
n	number of components or phases
P	applied static load
P_i	contact point
p	probability of obtaining a greater amplitude by pure chance combination of random phases
r	resultant amplitude (for particle orientation analysis, it is the magnitude of the resultant vector)
R	largest inscribed radius within particle
R^2	correlation coefficient
r_i	radius of individual particle corners
S	sphericity

LIST OF SYMBOLS (CONTINUED)

Symbol	Definition
S_X ,S_Y, S_Z	summations of the projected area of contact surfaces on the YZ, ZX, and XY planes
u_a	pore air pressure
u_w	pore water pressure
V_c	compressional wave velocity
w_c	water content (based on mass)
X, Y, Z	reference axes
γ_d	dry density
ε	axial compressive strain
θ	azimuth of an individual particle's long axis
θ'	azimuth of the resultant vector
ρ	mass density of material
ρV_c	acoustic impedance
σ	axial compressive stress
σ	total stress
σ'	effective stress
σ_1	stress due to the incident stress wave
σ_2	stress due to the reflected stress wave
σ_I	stress in incident material due to incident stress wave
σ_R	stress in incident material due to reflected stress wave
σ_T	stress in transmitting material due to transmitted stress wave
σ'_T	stress transmitted into a third medium
Δ	denotes change in
Σ	denotes summation
χ	saturation parameter

SECTION I

INTRODUCTION

A. OBJECTIVES

The main objective of this study was to determine how the moisture content during compaction affects soil properties, including compressional wave speed, stress transmission ratio, quasi-static constrained modulus, and soil microstructure. This investigation is directed at developing a better understanding of unsaturated soil behavior and evaluates the influence of soil microstructure under dynamic and quasi-static loading conditions.

B. BACKGROUND

The ability of a soil to transmit dynamic stresses (energy) is of particular interest to the U.S. Air Force with respect to military protection construction and survivability designs. Field compaction specifications for granular soils only require a final compacted density to be achieved without any restrictions on moisture. In addition, design procedures generally assume dry soil conditions. However, for unsaturated conditions, the amount of energy travelling through a soil and transmitted to a structure can be significantly larger than for dry soil conditions, thereby having the potential for greater damage. Unsaturated soils are complex, multiphase materials the behavior of which is not well understood. Ross et al. (1986), state that "...there are currently no theoretical, empirical or numerical methods available for predicting large amplitude compressive stress wave velocity and stress transmission in unsaturated soils." Therefore, a need exists to develop a better understanding of unsaturated soil behavior.

Previous research has shown that compaction energy, constrained modulus (a measure of soil stiffness), compressional wave speed, and stress transmission ratio have greater values at intermediate saturations (from about 20 percent to 75 percent) than for dry soil conditions. The reasons for this phenomena are not fully understood. Variations in soil microstructure developed during compaction appear to be a major factor. The experimental investigation presented herein utilized dynamic and quasi-static testing methods to evaluate the influence of soil microstructure on compaction energy, constrained modulus, wave speed, stress transmission ratio, and degree of saturation for Ottawa 20-30 sand. A laboratory procedure was developed to prepare specimens of compacted unsaturated soil for microstructural analysis. Vertical and horizontal sections were taken

through the specimen so that a detailed microstructural analysis including axial ratio and preferred particle orientation could be performed on different planes.

Based on the results of this investigation, it was determined that soil microstructure does affect compaction energy, constrained modulus, compressional wave speed, and stress transmission ratio. Microstructural analyses showed vector magnitude (a measure of dispersion within a particle orientation data set) could be related to variations in saturation. At intermediate saturations, vector magnitude values were lower than that for dry soil, which indicates a stiffer soil structure. According to wave propagation theory, a stiffer material will produce greater compressional wave speed and stress transmission ratio results at intermediate saturations, as was the case for this investigation.

Results from this investigation may be useful in future microstructural studies of cohesionless soils. Relationships between vector magnitude and dynamic soil parameters may be used in a developing model to predict stress transmission in unsaturated soils subjected to dynamic loading from conventional weapons.

C. SCOPE

Specimens of Ottawa 20-30 sand were dynamically compacted to a constant dry density at various saturations using a standard Proctor hammer and subjected to high strain rate testing using the Split-Hopkinson Pressure Bar device. Saturations were varied from 0 to about 80 percent. Microstructural analyses of epoxied compacted unsaturated sands were also performed. In addition quasi-static uniaxial compression tests were conducted to examine compacted sdtiffnesses. The influence of soil microstructure on compaction energy, stress transmission, and compressional wave speed for Ottawa 20-30 sand was evaluated.

SECTION II

LITERATURE REVIEW

The literature review contains five sections which directly relate to the present investigation. Because the research reported here deals with granular soils, the literature review will concentrate on relevant aspects of these specific soil types. The first section defines fabric and structure in soils and explains the difference between soil fabric and soil structure. The second section deals with current methods of microstructural analysis. The third section explains sample preparation techniques and statistical analysis of two-dimensional particle orientation data. SECTION IV summarizes soil compaction principles and investigates compaction energy in unsaturated soils. The final part of SECTION II is a review of stress wave propagation theory and the effects of compressive wave propagation through unsaturated soils.

A. STRUCTURE AND FABRIC IN SOILS

The development of fabric and structure in soil is a function of natural deposition and stress history in the field and sample preparation method in the laboratory. Particle size and shape play an important role in the development of soil structure. In cohesionless soils, angularity and sphericity are used to describe particle size and shape. These two parameters are very useful in a microstructural analysis. Shear strength, compressibility, and mechanical behavior of soils are all affected by fabric/structure development and the type of applied stress, i.e., static or dynamic.

1. Definition of Fabric and Structure

The terms "soil fabric" and "soil structure" have been used interchangeably throughout the geotechnical engineering literature. When fabric was first introduced during the mid-1960s, it was used interchangeably with the terms "soil structure" and "microstructure" (Casagrande, 1932; Lambe, 1953). However, there is a significant difference between the two terms. Mitchell (1976) describes soil fabric as "...the arrangement of particles, particle groups, and pore space within a soil." In addition, he also defines soil structure as "...the combined effects of fabric, composition, geometrical and skeletal arrangement of soil particles, and the interparticle forces acting on them." In sands, soil structure includes gradation, arrangement of particles, and void ratio.

The term "fabric" has different meanings in the disciplines of geotechnical engineering and geology. Pettijohn (1963) states that geologists term fabric as "the arrangement or orientation (random or preferred) of the elements that compose a rock." In igneous or metamorphic petrology the term fabric includes "the orientation of grains as characterized by their crystal lattice," Verhoggen et al., (1970). The difference between the geotechnical engineering and geology definitions of fabric is that engineering fabric studies are concerned with the orientations of grains and pores, and geological studies are concerned with the orientations of the crystal lattice which make up the rock.

Microstructure is the level of structure that requires an optical microscope for the study of the soil structure. Structure in sands can be studied using a standard optical microscope. However, in clays, a Scanning Electron Microscope (SEM) must be used for clays. Soil microstructure as defined by Mitchell (1976) is the term being adopted for this investigation since this term refers to the skeletal arrangement (orientation) of soil particles and the forces between adjacent particles. Also, the soil structure responds to external changes in the environment such as applied loads (static or dynamic), moisture (degree of saturation), and temperature (freeze-thaw cycles) (Bowles, 1984).

Two useful subconcepts exist concerning structure in a granular soil: 1) orientation of an individual particle, and 2) the position of a particle and its mutual relationship to other particles. One of the most important structural components is the absolute position of the particle with respect to a fixed coordinate system. The importance in this concept is that the orientation of an individual particle and absolute position of the particle are used to qualitatively describe soil microstructure (Oda, 1972a).

2. Particle Size and Shape

A description of the shape or geometric form of a particle involves several separate but related geometric concepts. The larger particles in a soil, namely silt, sand, and gravel sizes may be spherical and/or angular in shape. Angularity and sphericity are two parameters used to quantitatively described the shape of soil particles. The angularity of a soil particle is a measure of the sharpness of grain surface features. For example, an angularity value of 0.1 indicates that the soil particle has sharp edges while a value of 0.9 would indicate a well-rounded particle. The sphericity of a soil particle is a measure of how closely the particle approaches a spherical shape. For example, a sphericity value of 0.1 would indicate that the soil particle is irregular in shape and does not resemble a sphere, while a value of 0.9 would indicate that the particle approaches the shape of a sphere.

Sphericity and angularity are useful in determining the origin and geological history of the material. Prior to weathering and decomposition of the parent rock, many of the soil particles produced are initially angular in shape. With time, mechanical forces acting on the soil particles tend to reduce the angularity, thereby increasing sphericity. Particles that have been weathered mechanically over a long time will be much more rounded and have high sphericity and angularity values (Brewer, 1964).

Angularity values are given by Pettijohn (1963) in Table 1, as well as a visual description of each class range. After the sphericity and angularity values have been determined, visual charts such as Figure 1 (Krumbien and Sloss, 1955) can be used as a check on the particle shape.

Particle size is determined by performing a standard mechanical sieve analysis, (ASTM D 422-90). Particle shape (angularity and sphericity) can be determined by viewing granular soils under a microscope and sketching a two-dimensional image of the individual grains. Angularity, A, is determined by constructing the largest inscribed circle within the particle and by finding the radius of individual particle corners, (Krumbien and Sloss, 1955). This is shown in Figure 2a and determined from Equation 1,

$$A = \frac{\Sigma(r_i/R)}{n} \tag{1}$$

where, r_i is the radius of individual particle corners, R is the largest inscribed radius within a particle, and n is the number of individual particles.

Sphericity, S, is determined by constructing a circumscribed circle around the entire particle. The sphericity is a measure of the ratio of projected particle area over the area of the smallest circumscribing circle (Krumbien and Sloss, 1955). This is shown in Figure 2b and determined from Equation 2,

$$S = \frac{A_p}{A_c} \tag{2}$$

where, A_p is the area of a particle and A_c is the area of the smallest circumscribing circle.

3. Characteristics of Soil Structural Elements

In general, soils consist of three components, skeleton grains, soil matrix, and pores (Lafeber, 1962). Each of these components make up the structure of the soil and differ in strength and deformation properties. Skeleton grains are the coarser particles

TABLE 1. Description of Roundness Classes (Pettijohn, 1957).

Class Name	Roundness Value[a]	Description
Angular	0 - 0.15	Strongly developed faces with sharp edges and corners; secondary corners[b] are numerous.
Subangular	0.15 - 0.25	Strongly developed faces with somewhat rounded edges and corners; secondary corners are numerous.
Subrounded	0.25 - 0.40	The edges and corners are rounded and the area of flat faces is comparatively small; secondary corners are much rounded and reduced in number (5 - 10).
Rounded	0.40 - 0.60	Flat faces are practically absent; all edges and corners are rather broad curves, and there may be broad re-entrant angles; secondary corners have disappeared.
Well-Rounded	0.60 - 1.00	There are no flat faces; the entire surface consists of broad curves.

Note: [a]Roundness value is equivalent to axial ratio.
[b]Secondary corners are the many minor convexities seen in the grain profile. Primary corners are the principal interfacial edges and are fewer in number (3-5).

which generally consist of minerals or rock fragments. The grains are moderately to highly resistant to physical and chemical weathering. The ratio of surface area to volume of the grains is relatively small. Individual grains have high strength with respect to the low to moderate stresses encountered in soil engineering practice.

The soil matrix is defined as a material that encloses other recognizable features or materials. The matrix consists of finer-grained materials (silt and clay size particles) packed between the mineral grains. Brewer (1964) states an upper size limit of 30 micrometers for soil matrix materials.

The pores are the spaces between the solid soil particles. Within the soil matrix, the pores may be filled with water, air or a combination of both. Thus, soil can be viewed as a multiphase system. The pore phase can affect soil strength and overall behavior.

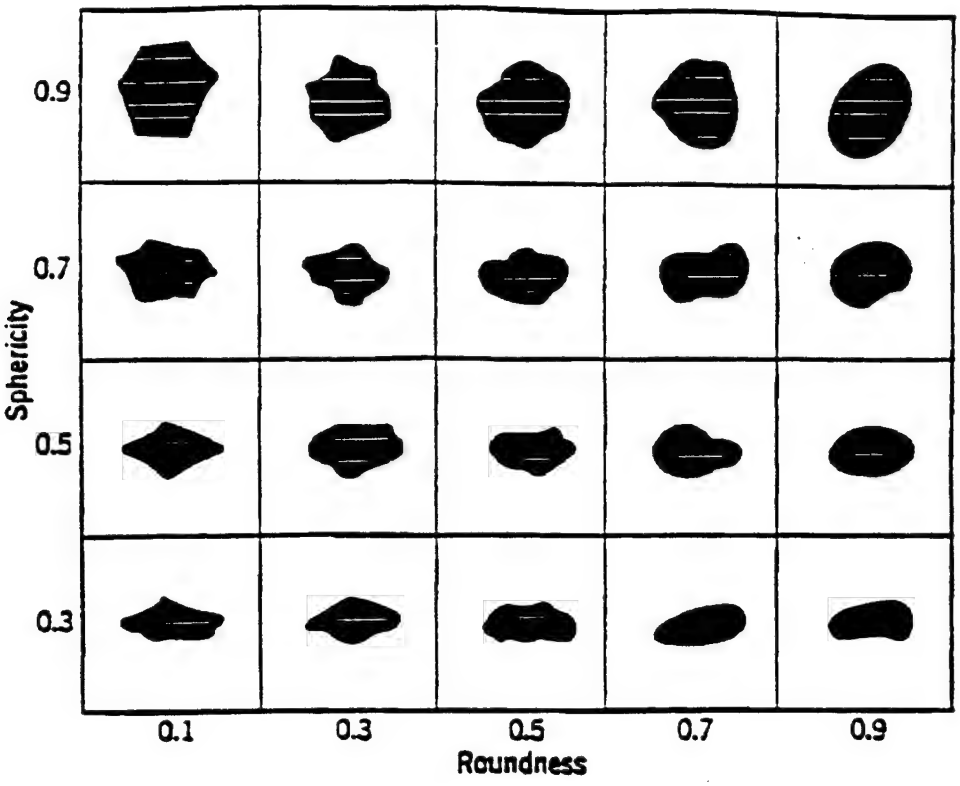

Figure 1. Sphericity and Roundness Classes (Brewer, 1964).

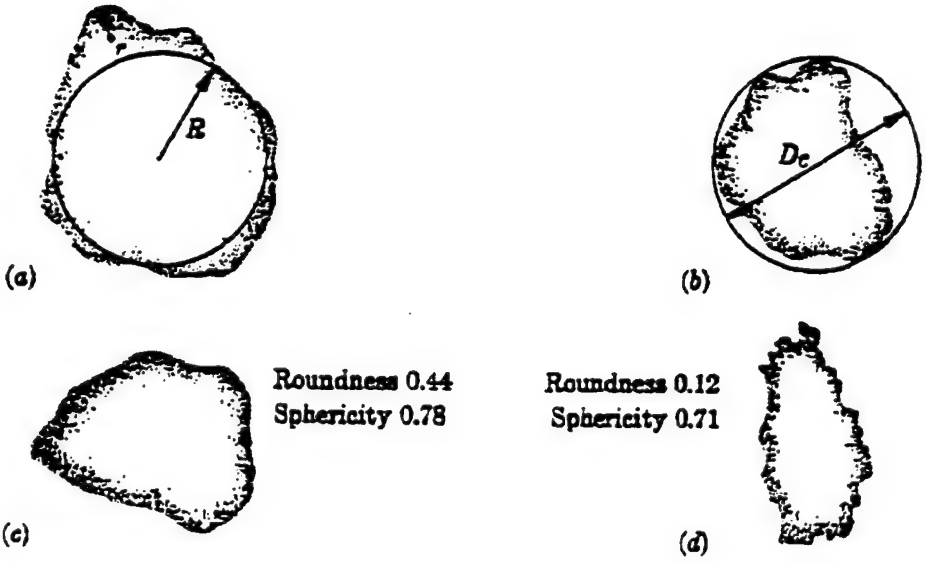

Figure 2. Particle Shapes (WU, 1966).

4. Soil Structure and Soil Mechanics

Lafeber (1966) indicates that there are two major geometrical aspects of the spatial arrangement of soil constituents: spatial distribution, and spatial orientation. Spatial distribution describes relative locations of various grains in a continuous, multicomponent, structural pattern. This pattern describes the position of grains with respect to other grains directly surrounding them and spatial orientation describes the orientation of the soil particles within the soil matrix to a given set of coordinates (Lafeber, 1963).

Australian soils analyzed by Lafeber (1963) showed that the frequency of mutual contacts between skeleton grains is only a fraction of the value which may have been expected if the grains had been in a random arrangement. Continuous subfabric or substructure was not evident in any of the soils tested by Lafeber (1966), and an open arrangement generally occurred which results in a pronounced internal geometrical anisotropy of the soil. These anisotropies can be considered to be an expression of the depositional or the previous stress-strain history of the soil, or a combination of both.

There are three problems concerning the deformation of randomly packed granular sand on the microscopic level (Oda, 1972b). They are: (1) the mechanical role of sliding and rolling of grains during deformation, (2) the mechanism to form a shear plane in the granular structure (preferred orientation of shear plane), and (3) the mechanism to control the structure reconstruction (increasing anisotropy of fabric).

The initial structure of a granular sand will change with an increase of axial strain in order to withstand a continuously increasing stress ratio (strain hardening). Relative displacement of grain particles generally occurs and particles will come into contact with each other. Newly formed contact points or surfaces will develop as existing contacts gradually decrease (Oda, 1972b).

Mahmood and Mitchell (1974) analyzed soil composed of granular materials in the silt to fine sand range and found that different microstructural arrangements developed, depending on how the soil was deposited. Mechanical properties also differed with the method of deposition which was attributed to variations in particle orientations. Characterization of the microstructure was determined by grain orientation analysis and by measurement of the pore size distribution.

Mahmood and Mitchell (1974) also used a mercury intrusion porosimetry method to determine pore size distribution and found that grains developed a strong preferred orientation in the horizontal direction when the soil was poured, forming pores between one and 30 micrometers in diameter. When the soil was compacted either by static (slow

loading with a flat piston) or dynamic (tamping) methods, near random grain arrangement and pore sizes between 0.1 and 10 micrometers in diameter resulted.

Juang and Holtz (1986) used mercury intrusion porosimetry techniques on clean Ottawa sand and a mixture of Ottawa sand and kaolinitic clay. Specimens were prepared using two packing methods, kneading and pluvial compaction. Characterization of the effects of compaction and compaction moisture content were analyzed by using a Pore Size Distribution (PSD) index. Distinct pore size distributions were observed for the different packing methods investigated.

The shear strength of crushed basalt was measured by Mahmood and Mitchell (1974). When sheared normal to the preferred orientation, the shear strength was 30 percent higher than when shearing was parallel to the orientation direction. Mahmood and Mitchell (1974) point out that this is to be expected because shearing across the preferentially oriented grains should involve breakage or reorientation of many grains.

B. MICROSTRUCTURAL ANALYSIS

A microstructural analysis can be defined as a scientific method used to quantitatively describe the arrangement of particles within a soil (Oda, 1972a). The analysis is important because relationships may be developed between the statistical results of the microstructural analysis and other relevant soil parameters.

Microstructural analyses are typically performed by determining the axial ratio (similar to sphericity) and preferred orientation of apparent particle long-axes. Oda (1972a) and Campbell (1985) developed methods for determining axial ratio and apparent particle long-axis orientations which are discussed in detail in the following two subsections. Sample preparation methods have also been related to particle long-axis orientation and to static and dynamic mechanical behavior of soils.

1. Experimental Axial Ratio Determination

Microstructural characterization of soils is closely related to particle shape, especially to the average flatness or slenderness of individual particles. Axial ratio is a shape factor used to describe the two-dimensional shape of soil particles. Oda (1972a) used the axial ratio method to measure constituting grain particles. To determine axial ratio, the apparent long-axis, L_1, and apparent short-axis, L_2, are measured on a two-dimensional section through an individual particle. The axial ratio for a group of particles, n_{avg}, is calculated from:

$$n_{avg} = (\frac{1}{f}) \sum_{i=1}^{i=f} (\frac{L_2}{L_1})_i \quad (3)$$

where, f is the number of particles in axial ratio calculation. The value of n_{avg} ranges from zero to one and may be considered as a coefficient indicating the characteristic of particle shape. As n_{avg} approaches unity, the sand grains approach the shape of a circle. This relates closely to sphericity as described in SECTION II.

2. Apparent Long-Axis Determination

Apparent long-axis determination is an important factor in microstructural analyses. Orientation of the longest axis is the main factor used to determine if a preferred orientation exists within the soil structure. Particle orientation is determined by the inclination of apparent long or short-axes of a grain with respect to a fixed reference axis. Most orientation problems require the treatment of more than one variable in a given angular measurement. Geological orientation data or vectorial structure is the spatial measurement which indicates directional properties (Pincus, 1953).

Nonspherical particle orientation is represented by the inclination of long and short-axes of each grain with respect to fixed coordinate axes. In Figure 3, grain G_1 is surrounded by grains G_2, G_3, G_4, G_5 with contact points P_1, P_2, P_3, P_4 respectfully. N_1 is the normal to the tangential plane P_1 and can be defined by the angle with the reference axes X, Y, and Z. The mutual relation of particle G_1 to particles G_2 to G_5 is defined by the number of contacts and directions of N_1 to N_4 (Oda, 1972a). Oda (1972a) points out some problems in finding a apparent long or short-axis of fine grained particles in thin sections. For particles having an axial ratio greater than 0.7, the long-axis was difficult to define because the particle approached the shape of a sphere. The state of three-dimensional grain orientations was estimated on the basis of the degree of preferred orientation of apparent long-axes by following these two steps:

a) Measure the angles θ_i between apparent long-axes of about 200 grains and the reference axis X, and
b) Develop frequency histograms of θ_i obtained from measurements.

Figure 4 shows typical frequency histograms of θ_i for sand compacted using the tamping method. The V-section, 45-section, and H-section represent vertical, 45-degree, and horizontal cut sections through the specimen, respectively. The frequency distributions show that the V-section and 45-section have a statistically preferred orientation of apparent long-axes, whereas the H-section does not have a preferred orientation. This is seen in the

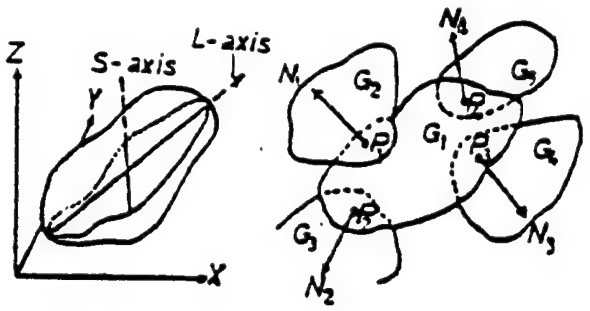

(1) Orientation (2) Relative Configuration

Figure 3. Fabric Elements of Granular Soil (Oda, 1972a).

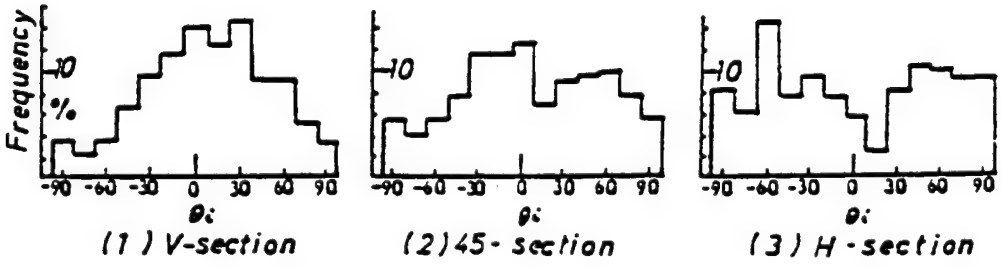

Figure 4. Frequency Histograms of in Various Sections of Sand A (Oda, 1972 a).

frequency values for each θ_i interval in which a greater number of orientations were observed from -30 to +30 degrees.

Sand A is a poorly graded sand and had an axial ratio of 0.605. The sand was compacted by the tamping method, and was characterized by the arrangement of apparent long and short-axes of particles parallel to the horizontal plane (X axis) and frequency histograms are shown in Figure 4. This sand is composed of nonspherical particles. Oda found that sands composed of relatively spherical particles have an orientation which is almost isotropic. This means that particles which are relatively spherical will tend to show the same orientation regardless of the section. The Rayleigh test of significance can be used to determine whether or not a preferred orientation is present in the soil structure (Curray, 1956). The test is widely used for particle long-axis orientation data.

3. Particle Orientation and Mechanical Behavior of Soils

Microstructural analyses of cohesionless soils can be used to relate particle orientation to the mechanical behavior. Particle orientation is characterized by investigating apparent long-axes of thin sections. The method has sufficient accuracy for three-dimensional mineral grains (Mahmood and Mitchell, 1974). When specimen sections are taken, a two-dimensional shape is obtained, which is generally ellipsoidal; therefore, the long-axes can be estimated with sufficient accuracy.

Oda (1972a, 1972b) observed that long-axis orientations in sands are a function of particle shape and method of compaction. He also noted that the initial structure is important to the mechanical properties of the soil. Oda's (1972a) research consisted of fixing the structure of sand with polyester resin in order that the spatial arrangement would not be disturbed. From viewing thin sections under an optical microscope to find preferred orientations and spatial relations, Oda (1972a) observed: (1) the characteristics of configuration relations of nonspherical particles are determined by the shape of particles and by the method of compaction, (i.e., sands which are composed of flat or elongated particles indicate strong anisotropic features of structure character), and (2) the initial structure of sand has important influences on the mechanical properties, such as mobilized stress ratio and secant deformation modulus.

Oda (1972a) has shown that "...when sand grains are deposited in a gravity field irrespective of their shape character, they tend to rest in a stable position relative to forces acting upon them." An important finding is that the nature and degree of anisotropy of sand is determined by the way in which the sand is deposited and by the shape characteristics of the sand grains. The importance of this concept comes from the type of

soil used for an experiment. A soil which is well rounded generally will not show a preferred orientation. However, angular elliptical soil grains generally shows a preferred orientation. Therefore, the type of soil used in an investigation (with regards to the shape characteristics) can greatly affect the possibility of preferred orientation within the soil.

Mitchell (1976) studied the relationship between soil structure, sample preparation methods, liquefaction, and drained compression behavior under triaxial loading for Monterey No. 0 Sand. Three methods of compaction were used: pluviation, moist tamping, and moist vibration. Characterization of microstructure was based on particle long-axis and interparticle orientations. For each method studied, a preferred orientation of long-axes developed in the horizontal direction. The degree of preferred orientation increased in the order of moist vibration (nearly random), moist tamping, and dry pluviation. Two quantitative structural elements were studied; three-dimensional distributions of normals to interparticle contact planes, and the orientations of apparent long-axes on a two-dimensional plane from a thin section. Mitchell (1976) concluded that moist vibration gave the most random orientations of particle long-axes. Dry pluviation had a distinct preferred orientation in the horizontal direction, and moist tamping gave intermediate values. Higher cyclic triaxial strengths were associated with the most random particle orientations.

Particle orientation diagrams drawn from three different compacting methods are shown in Figure 5. Mahmood and Mitchell (1974) found that when the grains were in the loosest state (pouring), a strong preferred orientation existed in the horizontal direction. In static compression, the orientation was nearly 45 degrees from the horizontal plane. When tapping the sample holder, i.e., dynamic compaction, a near random grain orientation was produced. The shear strength was observed to be greater when samples are sheared across the preferred orientation direction than when sheared parallel to the preferred orientation.

Ladd (1977) studied the cyclic structural stability of two sands using the cyclic triaxial strength test. The sands were a fine sand with a trace of silt and a coarse to fine sand with a trace of silt. Four different methods of sample preparation were used: dry vibration, moist vibration, dry tamping, and moist tamping. He found that in both sands, samples prepared using dry methods had similar cyclic shear strengths. However, similar but greater cyclic shear strengths occurred using moist preparation methods. DeGregorio (1990) used Ottawa F-70 banding sand in a study of liquefaction behavior. Samples were tested using a dead-load apparatus and a hydraulic loading system. DeGregorio observed that soil strength was influenced by sample preparation method and not by the type of loading system. Soil strength increased in order of dry pluviation, moist tamping, and moist vibration when sheared with the dead-load device. The effect of compaction method

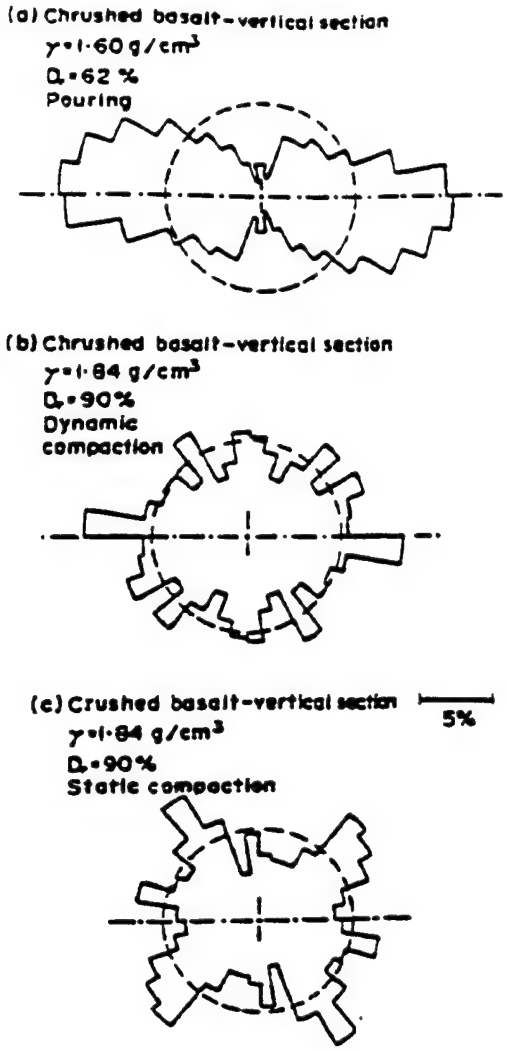

Figure 5. Particle Orientation Diagrams for Crushed Basalt: (a) pouring; (b) dynamic compaction; (c) static compaction (Mahmood and Mitchell, 1974).

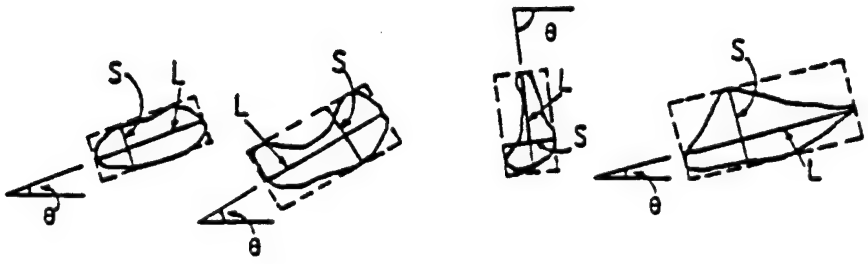

Figure 6. Technique for Marking Apparent Long- and Short-Axes of Sand Particles in Thin Sections (Campbell, 1985).

on soil behavior was demonstrated in each study. Grain orientations may have significantly influenced the results of these two studies, however, no microstructural analyses were performed.

The survey of literature, makes it apparent that structure in granular materials depends on the method of sample preparation and compaction. When soil samples are densified either by dynamic (tamping, plunging, impact, vibration) or static compaction, internal stresses are developed and grains do not maintain the initial structure as formed when the soil is initially deposited. However, structures developed using pluviation remain unchanged, since the soil is compacted during placement.

C. PARTICLE ORIENTATION AND STATISTICAL ANALYSIS

Orientations of particle long-axes in sands are determined by using microstructural analysis techniques. Microstructural analysis is an important tool used to view particles or voids in a soil which have been subjected to various preparation methods and loading conditions.

1. Specimen Preparation Techniques for Microstructural Analysis

Several sample preparation methods for microstructural analysis have evolved over the past two decades. For successful microstructural analysis of granular soils, the soil structure must be preserved so that it can withstand sectioning procedures. Some of the sample preparation methods used by various researchers are given in the following paragraphs.

Oda (1972a) prepared specimens by pouring oven-dried soil into a cylindrical mold. Compaction was performed using a tapping method in which the side of the mold was tapped with a tamper, and a plunging method in which the hand tamper was plunged directly into the sand. A polyester resin was used to fix the soil structure in the original configuration. Thin sections were prepared and photographed for microstructural analysis.

Mitchell (1976) prepared specimens of Monterey No. 0 sand using three different compaction methods, pluviation, horizontal high frequency vibrations, and moist tamping. A polyester resin was mixed with styrene (20 percent by volume) and 1 percent organic peroxide as a catalyst to reduce viscosity was used to preserve the soil structure. Thin sections (60 mm thick and 20 mm wide) were prepared for microstructural analysis.

Rein (1983) prepared samples for microstructural analysis by cutting ice-rich frozen sands with a wire saw. The research involved a study of the mechanical behavior of frozen soils. Samples were prepared by compacting a sand/snow mixture in plastic tubes.

A vacuum was applied to saturated the sample at 0° C and sections were taken with a wire saw at -10° C.

Campbell (1985) used a sugar cementation technique to preserve the soil structure. His procedure involved injecting 300 grams of granulated sugar dissolved in 1 liter of water by drawing the solution through the specimen under a low gradient until full saturation was achieved. Samples were dried by drawing a flow of dry air through the specimen under a low gradient. Thin sections were prepared by filling pore spaces with a low viscosity resin, Petropoxy 154.

Gill et al. (1986) studied the relationship between microscale physics and macroscale response of bonded soil particles. Prepared specimens were tested under uniaxial strain conditions at varying amounts of macroscopic strain. Once unloaded, the lightly cemented granular specimens were epoxied. Thin sections then were taken, permitting forensic viewing of the internal microstructural response.

2. Two-Dimensional Analysis of Orientation Data

Analyzing two-dimensional orientation data requires the use of a vector method and a statistical test of significance. The vector method is mathematically based on the same idea as vectors in engineering statics. The only difference is that the vector magnitude is taken as unity and the vector is bidirectional. The statistical test of significance is based on the work of Rayleigh (1894) in which a method for describing random phases in sound waves was developed.

a. Vector Method

Curray (1956) notes that measurements of orientation of various geological features such as fabric and structural elements can be more easily interpreted through the use of statistics. Three relevant statistical measurements can be made: (1) a preferred orientation direction, (2) the degree of preferred orientation, and (3) the probability that the preferred orientation is real and not merely due to chance.

In the past, researchers used standard linear normal distributions and computed mean and standard deviation (or variance) as descriptive statistics (Curray, 1956). Jizba (1953) and Chayes (1954) noted difficulties which arise, such as choosing an origin in order to divide a circular distribution into a linear frequency curve. By changing the choice of origin, the calculated mean and standard deviation can be considerably different.

The best method available for studying particle long-axis orientation is the vector method since the statistics used are independent of the origin chosen. Curray (1956) lists four requirements for analyzing particle orientation data: (1) a measure of the central tendency or preferred orientation direction, (2) a measure of dispersion which is independent of origin, (3) a test of the statistical significance of the results against a model randomness, and (4) a model distribution such as the circle normal or the linear normal distributions from which deviations can be tested.

Campbell (1985) developed a rapid method of directly measuring microstructure in cohesionless soils. A personal computer and digitizing tablet were used to develop a relationship between long-axis coordination and contact normal orientation data. Campbell performed analyses of thin sections photographs which involved the measurement of particle orientation information from particle shape, and orientation of the particle with respect to a fixed axis system. For the analyses, approximately 250 particles were selected for statistical review. Particle apparent long and short-axes were marked by circumscribing a rectangle around each particle. This technique permitted visualization of where the long and short-axes of each particle occur and is shown schematically in Figure 6.

A typical histogram of apparent long-axis orientation within 10-intervals is shown in Figure 7. A rose diagram (angular frequency histogram) developed from the same data is shown in Figure 8. The rose diagram is a plot of the azimuth, θ, of each particle long-axis on a 360-degree distribution graph. Figures 7 and 8 visually present the orientation of azimuths and the dashed line indicates a uniform orientation distribution. The azimuths of a group of particles (determined from the long-axes) can be detected. Equations (4) to (10) are used to analyze these data. The technique was presented by Curray (1956).

In particle orientation analysis, no distinction is made between one end of a particle and the other, i.e., the particles are bidirectional. Therefore, all measurements are made in a range of 180-degrees. A 360-degree distribution graph may be generated by plotting each grain twice, once from 0- to 180-degrees, and again in the 180- to 360-degree range. Curray (1956) presents Equations (4) to (10) which take this into account by doubling the azimuth, θ, of each particle long-axis:

$$\text{Horizontal Component} = \Sigma n' \cos 2\theta \tag{4}$$

$$\text{Vertical Component} = \Sigma n' \sin 2\theta \tag{5}$$

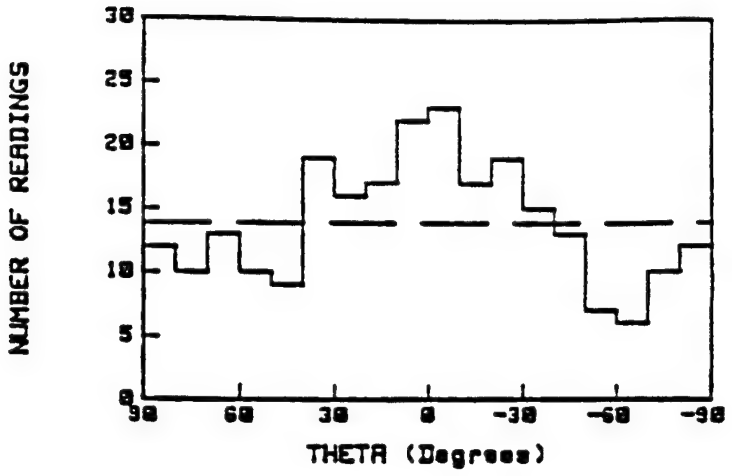

Figure 7. Example of Histogram Showing Apparent Long-Axis Orientation Data (Campbell, 1985)

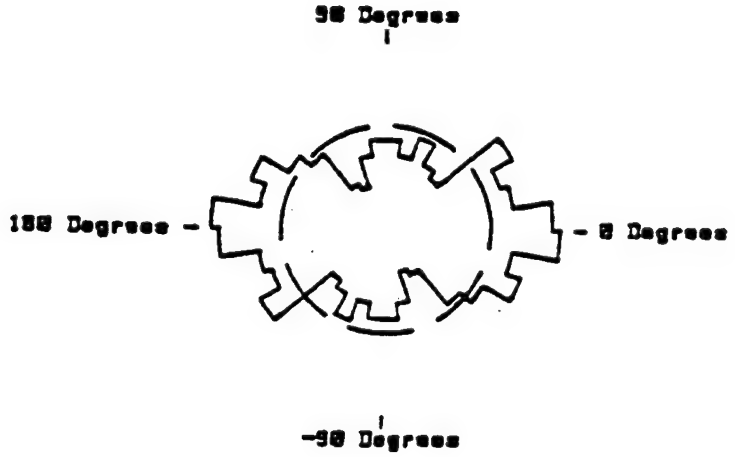

Figure 8. Example of Rose Diagram Showing Apparent-Long Axis Oreintation Data (Campbell, 1985)

$$\tan 2\theta = \frac{\Sigma n' \cos 2\theta}{\Sigma n' \sin 2\theta} \tag{6}$$

$$\theta' = \frac{1}{2} \arctan \frac{\Sigma n' \cos 2\theta}{\Sigma n' \sin 2\theta} \tag{7}$$

$$r = \sqrt{(\Sigma n' \cos 2\theta)^2 + (\Sigma n' \sin 2\theta)^2} \tag{8}$$

$$L(\%) = \frac{r}{\Sigma n'} \times 100\% \tag{9}$$

where n' is the magnitude of each particle long-axis vector (taken as unity in this case), θ is the azimuth of each particle long-axis, θ' is the azimuth of resultant vector, r is the magnitude of resultant vector, and L is the magnitude of resultant vector in terms of a percentage.

Mitchell (1976) indicates that particle orientation can be represented by its apparent long or short-axis with respect to a fixed reference axis. True orientations of long and short-axes of small particles are difficult to determine. Three-dimensional orientations are estimated from orientations observed in sections cut in different directions. Orientations were determined by measuring the angle θ_i between apparent long-axes and reference axes parallel to the long-axis of the thin section shown in Figure 9. Typical rose diagrams are shown in Figure 10 for data obtained using an azimuth class interval of θ = 10-degrees.

b. Statistical Test of Significance

A method developed by Rayleigh (1894) can be used to test the significance of a distribution of particle long-axis orientations (Campbell, 1985). The term "significance" implies that the observed data do or do not show a preferred orientation. The Rayleigh test of significance has been widely used in particle orientation analyses and is analogous to particle long-axis orientation data. This can be explained by knowing that each observation (particle long-axis) can be represented by a vector with direction and magnitude. The Rayleigh test of significance is stated as:

$$p = e^{-r^2/n} \tag{10}$$

where p is the probability of obtaining a greater amplitude by pure chance combination of random phases (for particle orientation analysis, it is the probability of obtaining a greater

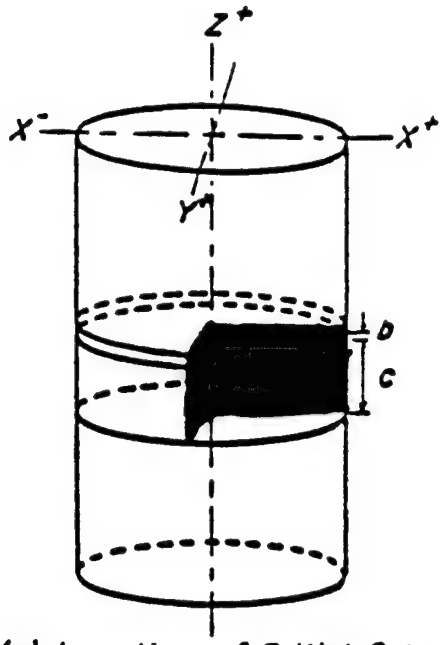

(a) Locations of Initial Cuts

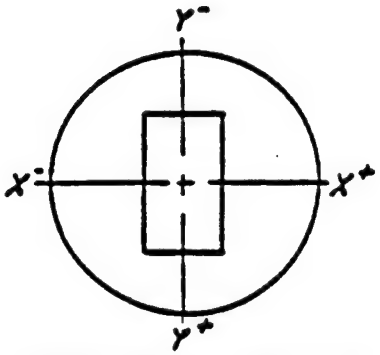

(b) Horizontal Section

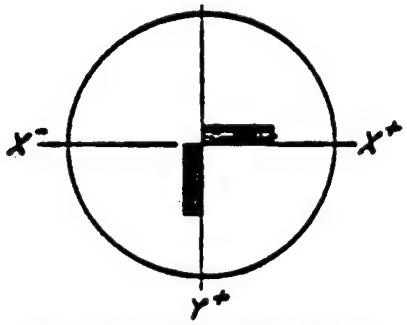

(c) Vertical Sections

Figure 9. Thin Section Locations from Within Resin-Impregnated Samples (Mitchell, 1974).

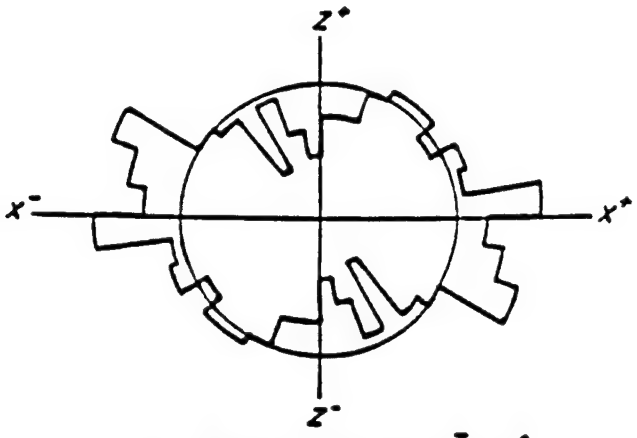

(a) Pluviated. $L = 18.3\%$, $\bar{\theta} = 86°$

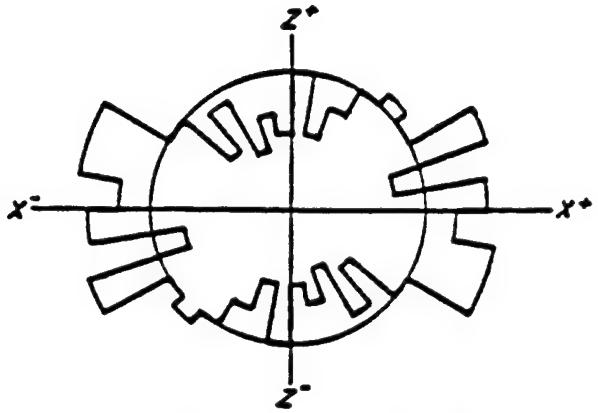

(b) Moist tamped. $L = 18.5\%$, $\bar{\theta} = 86°$

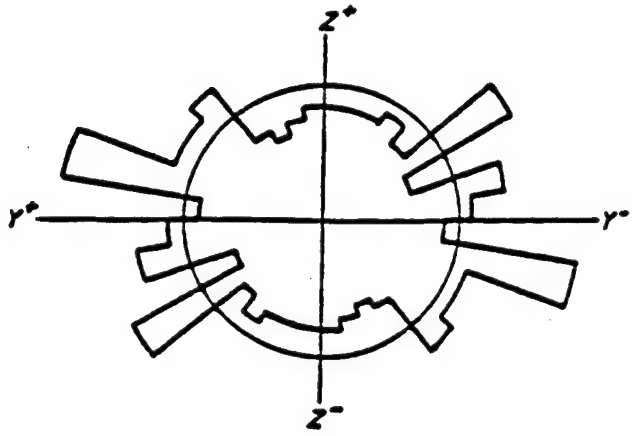

(c) Moist vibrated. $L = 13.2\%$, $\bar{\theta} = 285°$

Figure 10. Rose Diagrams of Particle Long-Axis Orientations for Samples of Monterey No. 0 Sand Prepared at 50% Relative Density by Different Methods (Mitchell, 1974).

magnitude by pure chance combinations of random orientations), r is the resultant amplitude (for particle orientation analysis, it is the magnitude of the resultant vector), n is the number of components or phases, and e is the base of natural logarithms.

A statistical analysis was performed by Campbell (1985) using the vector method and test of significance presented by Curray (1956), using Equations (4) to (10). For sand grain orientation studies, a Rayleigh significance level of 0.05 is required. If $p \geq 0.05$, additional observations should be made until $p < 0.05$. For long-axis orientation data, a minimum sample size of about 200 observations should provide an accurate measurement.

The vector mean and vector magnitude, must be determined to ensure a suitable estimation of the mean direction and variance of the frequency histograms. Vector mean is a measure of the average azimuth upon which a group of particles lie. Vector magnitude is a measure of how closely the particle long-axis distribution approaches a preferred orientation. If the vector magnitude is zero, then a completely random distribution exists. If the vector magnitude is unity, then all observations of particle long-axes have the same azimuth.

D. SOIL COMPACTION

Compaction methods are used in almost every phase of engineering construction to improve soil conditions on site. The basis of compaction theory was developed by Proctor in the late 1920s and a standard compaction test was developed in the early 1930s. Compaction energy depends on soil type and amount of moisture within the soil. Cohesionless soils differ from cohesive soils in their behavior with respect to moisture-density relationships. These topics are described in detail in the following three sections.

1. Principles and Theory of Soil Compaction

Compaction theory first came into existence through the work of R. R. Proctor who developed a controlled specification for the compaction of cohesive soils during the late 1920s. Proctor showed that soil compaction is a function of the following four variables: (1) compaction energy, (2) soil type (gradation, particle size and shape, cohesionless or cohesive soil), (3) water content, w_c, and (4) dry unit weight, γ_d. The method of soil compaction and moisture condition during compaction strongly influences both static and dynamic soil behavior. Soils which are in a loose state tend to have lower compression and shear wave speeds and shear strength, while densely compacted soils have higher compression and shear wave speeds and shear strength.

Holtz and Kovacs (1981) define compaction as "...the densification of a soil by the application of mechanical energy." Cohesionless and cohesive soils differ in their behavior when subjected to compaction energy. Cohesionless soils can be efficiently compacted in the field using vibratory techniques or by using dynamic compaction in which large weights, 10 to 40 tons, are dropped from heights of 15 to 45 meters (Hunt, 1986). Cohesive soils may be compacted in the field using sheepsfoot rollers where a kneading action occurs, statically by applying large static loads, or compacted in the lab by a falling hammer.

The influence of compaction method on engineering behavior has been demonstrated by a number of researchers. The underlying reason for compacting soils is to improve the engineering properties. Holtz and Kovacs (1981) note several advantages of soil compaction: (1) detrimental settlements can be reduced or prevented, (2) soil strength increases and slope stability can be improved, (3) bearing capacity of pavement structures can be improved, and (4) undesirable volume changes, caused by frost action, swelling, and shrinkage for example, may be controlled.

Mulilis et al. (1977) prepared samples of fine sands for cyclic liquefaction tests using 11 different compaction methods. Results showed that compaction method strongly influenced the cyclic liquefaction behavior of the sand. Of the 11 different packing methods, pluviated samples had the greatest liquefaction potential whereas samples prepared by vibration and hand tamping had the lowest liquefaction potential.

Oda (1972a) prepared specimens by pouring oven-dried soil into a cylindrical mold. Specimens were compacted using a tapping method in which the side of the mold was tapped with a tamper, and a plunging method in which a hand tamper was plunged directly into the sand. Oda found that preferred particle orientation is influenced by the method of compaction, observing that pluviated samples have a definite particle orientation and lower shear strength, whereas tamped samples showed a more random orientation with a higher shear strength.

A relationship between compaction and shear strength was observed by Olsen (1963) who studied soils containing small amounts of sands. Olsen reviewed shear strength theories and found that effective stress theories of soil compaction are based on the assumption that soil resists the compaction pressure by the development of shearing stresses on the contact surfaces between the particles. Prior to compaction, soil possesses low shear strength and an increase in the soil density can be explained by soil behavior during compaction (Olsen, 1963). As compaction energy is applied, shearing stresses developed between the soil particles reach the shearing strength of the contact surfaces, the contacts yield, particles slide over each other, and soil density increases. As the first blow

is applied, high pore water pressure weakens the soil by reducing the effective stress between particles. As more blows are applied to a soil, effective stress increases due to an increase in residual lateral total stress and pore water pressure becomes progressively smaller.

Soil strength is governed by effective stress. In saturated soils, the effective stress can be calculated with reasonable accuracy using Terzaghi's equation:

$$\sigma' = \sigma - u_w \tag{11}$$

where, σ' is the effective stress, σ is the total stress, and u_w is the pore water pressure. When a soil is unsaturated, a third phase, air, will be present with a pressure u_a. Olsen (1963) notes that Bishop (1961) suggested the effective stress in unsaturated soils could be expressed by:

$$\sigma' = \sigma - u_w(\chi) - u_a(1- \chi) \tag{12}$$

where, χ is the saturation parameter and u_a is the pore air pressure. The value of χ varies depending on the degree of saturation. For example, if the soil is saturated then χ is 1.0 and if the soil is dry then χ is zero. For unsaturated soils the value of χ is in the range between zero and 1.0. Bishop used Equation (12) to analyze the shear strength of soils with high degrees of saturation (usually over 60 percent) and found that the shear strength decreased with increasing saturation.

2. Standard Proctor Test

The standard Proctor test (ASTM D 698-90) was developed by Proctor in the late 1920's as a control specification for the compaction of cohesive soils. The research was prompted by dam construction for the Los Angeles Water District. The present standard Proctor test, designated as ASTM D 698-90, involves dropping a 25.4 N (5.5 pound) weight from a height of 0.305 m (12.0 inches) onto the soil contained in a compaction mold of volume 0.944 m^3 (1/30 ft^3). Three layers are used with 25 blows applied to each layer. The test is repeated several times using increasing water contents. A relationship between dry density, γ_d, and water content, w_c, can be developed from the data. The total compactive energy, CE, applied to a soil using the standard Proctor test is 592.7 kJ/m^3 (12,375 $ft\text{-}lbf/ft^3$). This method is considered a dynamic impact compaction test.

3. Compaction Energy in Unsaturated Soils

Relationships between dry density and moisture content can be developed for dynamically compacted cohesionless soils. The curve in Figure 11 shows that as the water content increases the dry density initially decreases. With a further increase in water content the density increases until a higher saturation level is reached. Lambe and Whitman (1969) citing Foster (1962), state that, "...this type of compaction curve occurs when the material is permeable enough to impede the development of positive pore pressures during compaction." Lambe and Whitman (1969) attribute low densities at lower water contents to bulking, a phenomena which occurs when the capillary forces of the soil resist particle rearrangement. At lower water contents (lower degrees of saturation), capillary tension in the pores inhibits the tendency of the cohesionless soil particles to be densely compacted. As the water content increases the soil particles are lubricated, and thus frictional resistance between particles decreases allowing the soil to be compressed into a denser packing.
In cohesive soils, the moisture-density curve starts at a low value of water content and dry density. The curve then rises to some peak value (optimum moisture content) after which the dry density decreases with an increase in water content as illustrated in Figure 12. A change in soil structure occurs as the moisture content increases. The soil structure below optimum moisture content tends to be flocculated, as the moisture content increases the structure of the cohesive soil becomes dispersed. The structure of cohesive soil changes as the compactive effort increases and maximum dry density increases as optimum moisture content decreases. The difference between moisture-density curves in sand and clays can be attributed to the grain size distribution, shape of the soil grains, specific gravity of soil solids, and the amount and type of clay minerals present (Das, 1985).

As the number of blows applied to a soil increases, i.e., an increase in compaction energy, the dry density and shearing strength of the soil also increase. At some point, the soil may become sufficiently strong such that no interparticle contacts yield when a blow is applied. In such a case, the soil is said to have reached its maximum density for the particular compaction method used (Olsen, 1963).

Olsen (1963) noted that prior to the second blow the soil is in a much denser condition than it was at the beginning of compaction. The denser soil produces more lateral confinement. Shearing deformations break down some of the interparticle contacts, expel pore air, and increase the dry density. The compaction effort is less for the second blow than it was for the first and the increase in dry density is smaller; this is caused by the greater lateral confinement. At low water contents the dry density increases quickly for the

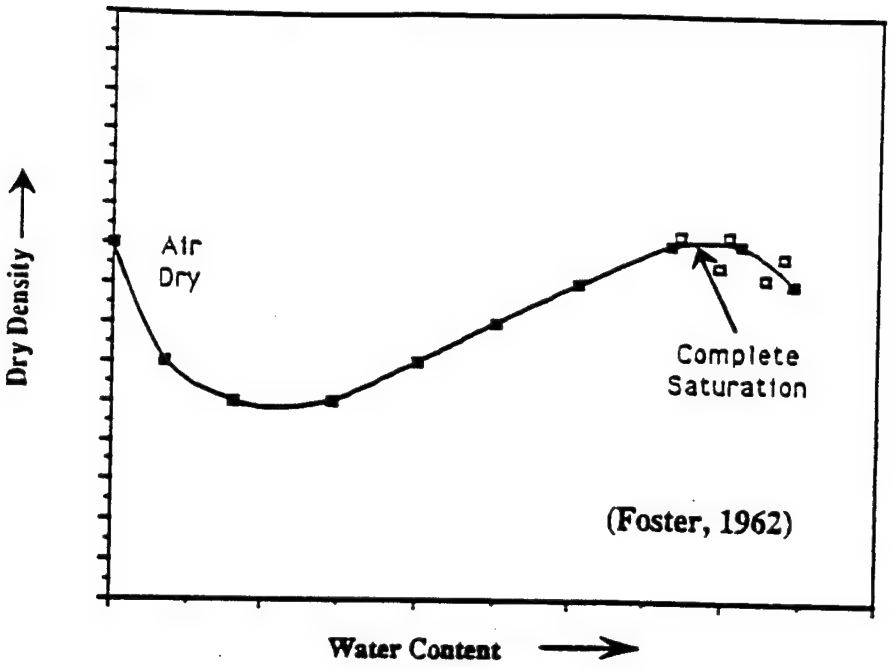

Figure 11. **Compaction Curve for Cohesionless Soils (Lambe and Whitman, 1969).**

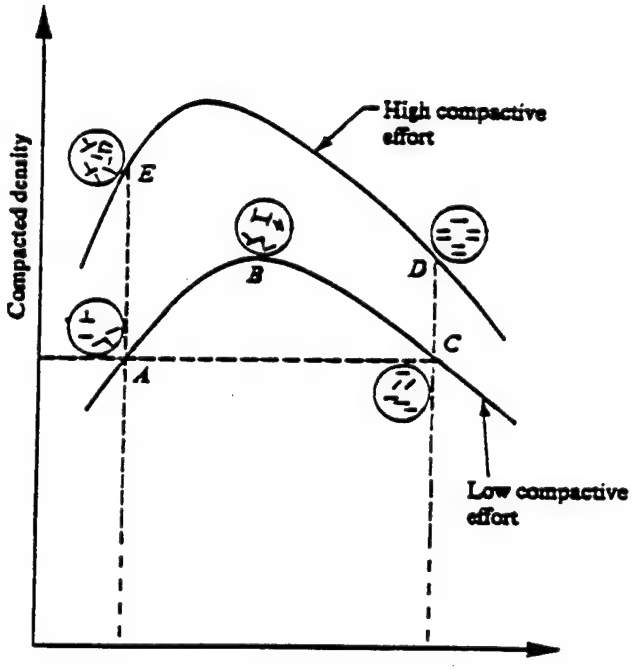

Figure 12. **Compaction Curve for Cohesive Soils (Das, 1985).**

first few blows. However, further density increases with additional compactive effort are small as shown graphically in Figure 13.

Ross (1986) and Veyera and Fitzpatrick (1990a) compacted unsaturated Ottawa 20-30 sand to a constant dry density using a standard Proctor hammer. Their findings show that the amount of energy required to compact the soil to a constant dry density changes with saturation. At saturations between 20 percent and 60 percent the amount of energy required to compact the soil to a constant dry density was much higher than at zero and 80 percent saturation. In addition, Ross (1989) also performed similar tests using Eglin sand. Figure 14 shows the relationship between saturation and energy required to compact the Eglin soil to a constant dry density. Ross found that a 22 percent increase in the amount of energy was required to compact the soil up to 40 percent saturation. From this point on the amount of energy required to compact the soil decreased. Ross (1986) states "It appears that at intermediate saturations, the capillary stress between the sand particles increases the stiffness of the sand."

E. WAVE PROPAGATION THEORY

Compression and shear waves are generated when a disturbance is introduced into a medium. Earthquakes produce motions in the ground due to stress waves (compression and shear) created by the rupture of the stressed earth mass. Compressional waves can be generated by dropping a rock being into a still body of water. The disturbance from the rock will create compressional waves which travel outward in all directions from the source (shear waves are not developed in water). Waves also may be generated by artificial means such as blasting, bombardment during war, pile driving, and aircraft landing (Prakash, 1981). The following two sections deal with wave propagation theory and specifically compressive wave velocity in unsaturated soils.

1. Wave Propagation Principles

When a dynamic load is applied to a body, the entire body is not disturbed at the time of initial loading. Regions closest to the disturbance are affected first, and deformations produced by the disturbance spread throughout the body in the form of stress waves. Wave propagation through a single material (such as a rod) can be determined from Newton's Second Law of motion and elasticity theory if the applied stresses are within the elastic limits of the material. Equation 2.13 was presented by Kolsky (1963) which determines the compressive wave propagation velocity, V_c, in a rod for an elastic material:

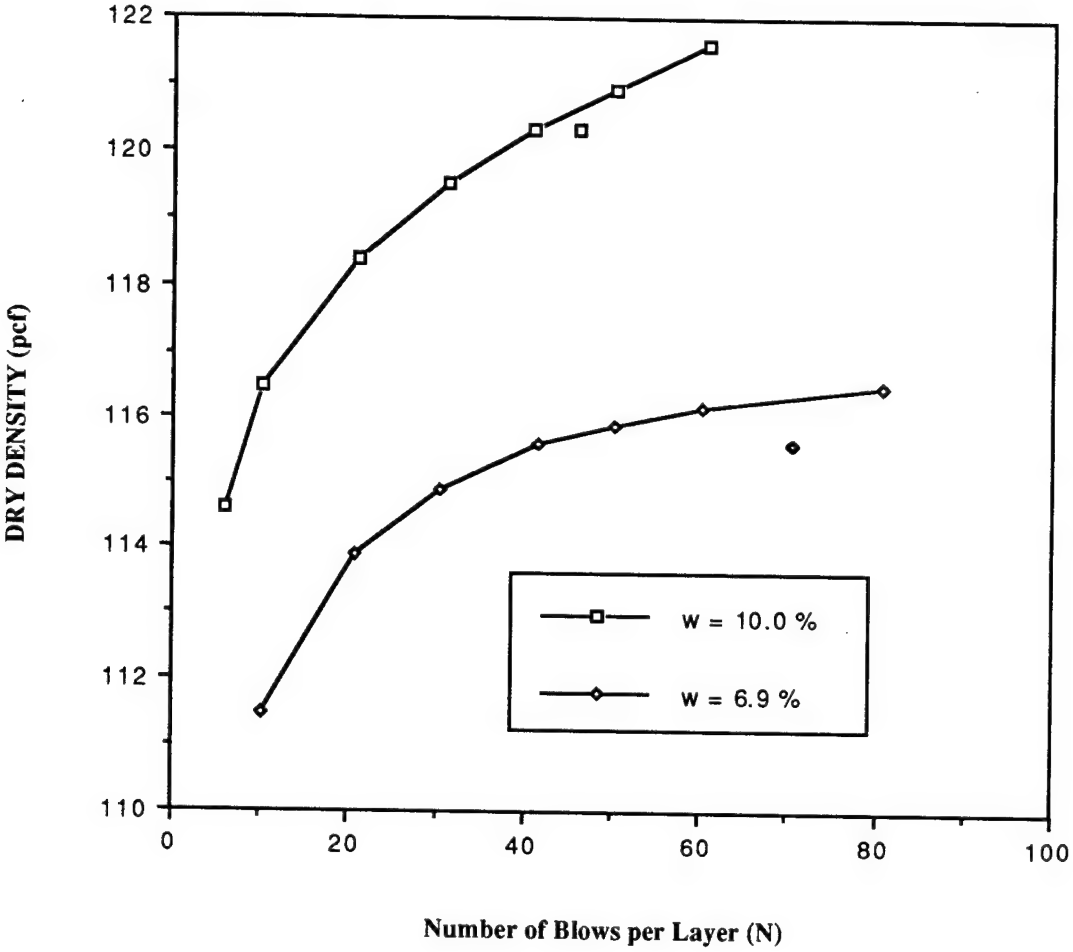

Figure 13. Effect of the Number of Stress Applications on Compacted Dry Density of a Silty Clay with an Optimum Moisture Content of 12% (Olsen, 1963).

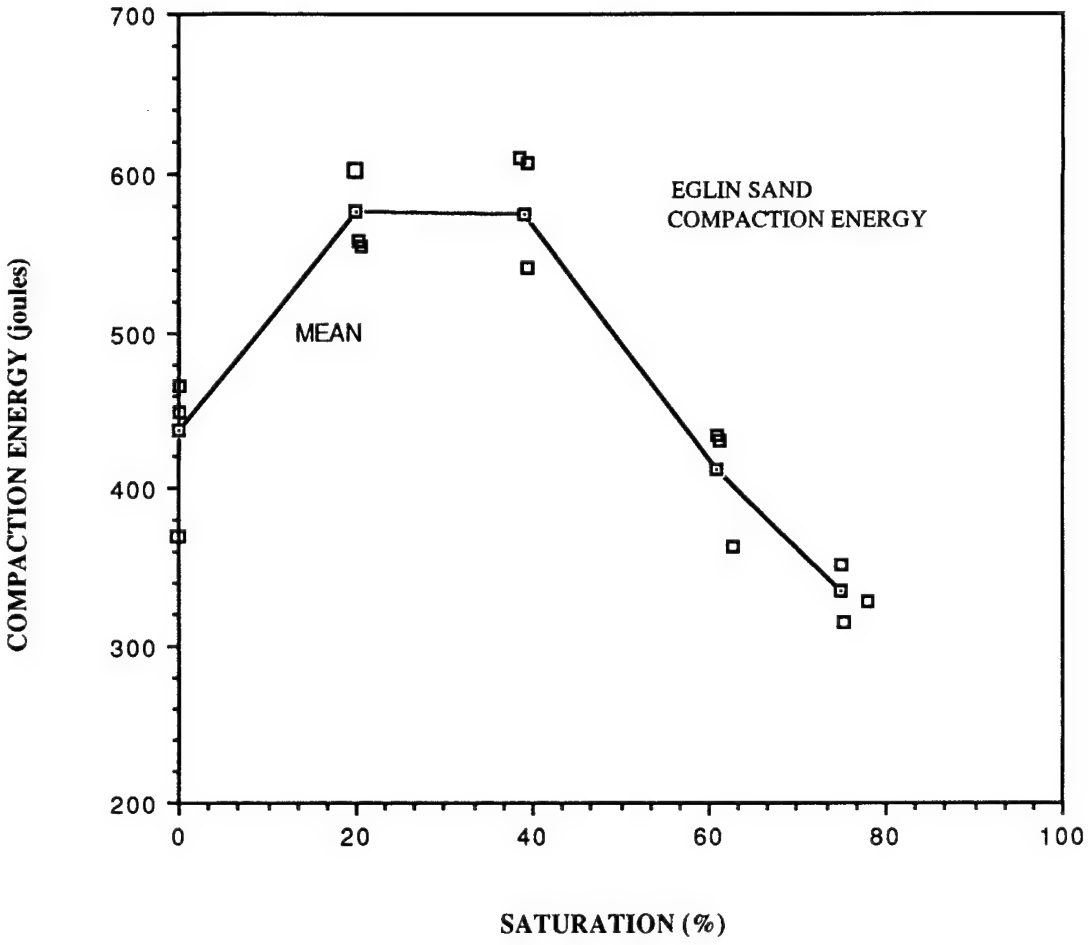

Figure 14. Compaction Energy as a Function of Saturation (Ross, 1989).

$$V_c = \sqrt{\frac{E}{\rho}} \tag{13}$$

where, E is the elastic Young's modulus and ρ is the mass density. Equation 13 gives the compressional wave speed in a bounded elastic material.

Wave propagation through several materials can also be determined from wave propagation theory. When propagating compressional waves reach a boundary between different materials, part of the wave will be reflected back into the first medium, and a part of the wave will be transmitted into the second medium. If the boundary is normal to the propagation direction, then only compressional and tensile waves will be reflected and transmitted. If the boundary is not normal to the propagation direction, then compressional, tensile and shear waves will be reflected and transmitted. Only normal boundaries will be considered here. Figure 15 shows the case where three materials are in contact with one another. The stress at each interface can be determined using Equations (14) to (17). These four equations were given by Rinehart (1975) to determine reflected and transmitted stresses between different materials.

From Figure 15, assuming normal boundaries, the amount of stress reflected back into the first material, σ_R , can be determined by:

$$\sigma_R = \left(\frac{\rho_2 V_{C2} - \rho_1 V_{C1}}{\rho_2 V_{C2} + \rho_1 V_{C1}} \right) \sigma_I \tag{14}$$

and the amount of stress being transmitted, σ_T , into the second medium is determined by:

$$\sigma_T = \left(\frac{2\rho_2 V_{C2}}{\rho_2 V_{C2} + \rho_1 V_{C1}} \right) \sigma_I \tag{15}$$

where V is the velocity, and ρ is the mass density. The subscripts T, R, and I refer to transmitted, reflected and incident stresses, respectively, and subscripts 1 and 2 refer to the first and second mediums, respectively. The product, ρV, is termed the "acoustic impedance" of the material.

The magnitude of stress transmitted into a third medium, σ'_T , can be determined by replacing the incident stress with the stress transmitted into medium 2 and by changing the values of the acoustic impedances in Equation (15):

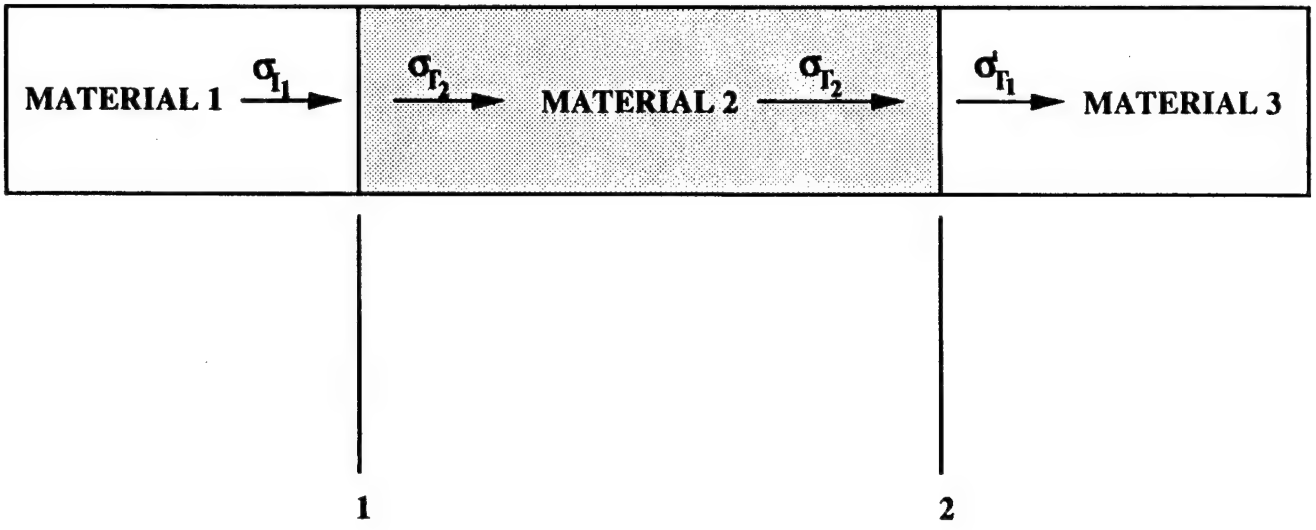

Figure 15. Stress Wave Propagation Through Dissimilar Materials (Pierce, 1989).

$$\sigma'_T = \left(\frac{\rho_3 V_{c3}}{\rho_2 V_{c2} + \rho_3 V_{c3}}\right) \sigma_T \qquad (16)$$

If the first and third mediums are the same (subscripts 1 and 3), but differ from the second medium, a relationship between the incident pulse and the pulse transmitted into the third medium can be determined. This particular case directly applies to the split-Hopkinson pressure bar where a soil sample (medium 2) is placed between two steel bars (mediums 1 and 3). By combining Equations (15) and (16) for this special condition, the following equation is obtained;

$$\frac{\sigma'_T}{\sigma_I} = (4)\left(\frac{\rho_2 V_{c2}\ \rho_1 V_{c1}}{(\rho_2 V_{c2} + \rho V_{c1})^2}\right) \qquad (17)$$

Equation 17 is referred to as the "transmission ratio." By comparing Equations (15) and (17), the magnitude of the stress transmitted into the third medium is approximately twice that in the second medium if the acoustic impedance of the second medium is considerably smaller than the first and third.

2. Compressive Wave Velocity in Unsaturated Soils

In two and three phase soil media there are several factors which affect the velocity of wave propagation. A two phase soil media consists of soil particles and water, whereas a three phase soil media consists of soil particles, air, and water. Allen et al. (1980) developed a testing program to measure the influence of void ratio and degree of saturation on compression wave propagation. Soils were tested at different void ratios, at maximum or near maximum relative density, and in the saturated and unsaturated condition. Experimental results showed that void ratio was the most influential soil parameter on wave propagation velocity in a saturated medium. For a given sand and range of void ratio, Allen et al. (1980) found that the wave velocity generally decreased as the void ratio increased. Frequency, hydrostatic pressure, temperature, specific gravity of the solid particles, and permeability had less effect on the wave propagation in saturated sands. However, in the nearly saturated state, the saturation level was the most dominant factor.

Ishihara (1967) showed that compression waves transmitted through the fluid depended primarily on the bulk compressibility of the soil-fluid system. Small amounts of air can have an appreciable influence on the bulk compressibility of water. Based on

mixture theory it can be shown that 0.10 percent of air in the mix will reduce the compression wave velocity in water to about one fourth of the value when saturated (Richart et. al., 1970).

Hughes and Kelly (1952) investigated the effects of water content on compressional wave velocity in sandstone. They found a distinct trend within the results in that small increases in saturation beyond about 95 percent caused a sharp drop in velocity as the saturation approached 100 percent. They also demonstrated that as confining pressure increases, the compressional wave velocity in the dry sandstone samples increase at a much faster rate than velocities in the saturated samples. As the saturation increases at a given pressure, the velocity at that pressure decreases. This can be seen more clearly in Figure 16. In the saturation range of 15 percent to about 90 percent, saturation has little effect on the velocity at different pressures. However, at saturations greater than 90 percent there is a considerable decrease in the velocity. Also at higher pressures the decrease in the velocity is much more dramatic.

High strain rate stress wave propagation tests using the split-Hopkinson pressure bar (SHPB) were performed by Pierce (1989). Relationships between compressional wave velocity and stress transmission with variations in saturation and confining stress were studied. Pierce compacted sands to a constant dry density using four 2.54 cm (1 inch) lifts by striking a steel rod with a rubber mallet. Samples were fully saturated, and then desaturated to a particular level by use of a pressure plate apparatus. Pierce found that saturations between zero and 80 percent do not significantly influence the values of compressive wave velocity, transmission ratio, or quasi-static stiffness for Ottawa 20-30 and Eglin sands compacted dry. However, retention curves for Ottawa 20-30 and Eglin sands show that the influence of capillary forces on effective stress is negligible. Soil microstructure developed during compaction may be influenced by the capillary stresses which affect soil behavior for static and dynamic cases.

Ross (1986, 1989), Veyera (1989), and Veyera and Fitzpatrick (1990a) performed SHPB tests on dry and unsaturated compacted sands including Ottawa 20-30 sand, Ottawa F-58 sand, Tyndall sand, and Eglin sand. Figures 17 and 18 show compressional wave speed and transmission ratio as a function of saturation in which the data have been normalized to the average value at zero saturation (dry soil). These figures show a typical behavior found in all soils tested, which is that the wave speed and transmission ratio increase up to about 20 percent saturation. At saturations of about 20 percent to 60 percent the wave speed and transmission ratio remain relatively constant. As the saturation increases past 60 percent, the wave speed and transmission ratio decrease.

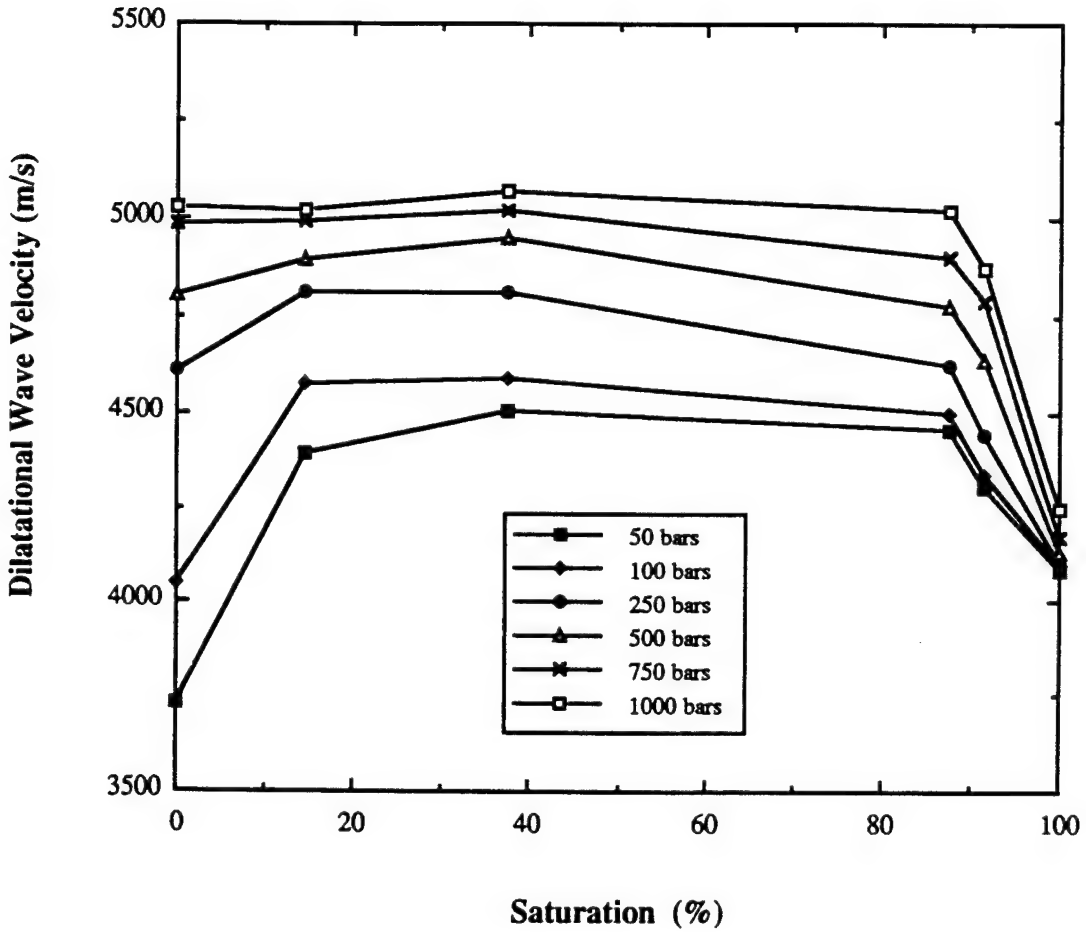

Figure 16. Dilatational Wave Propagation Velocity as a Function of Saturation and Confining Pressure (Hughes and Kelly, 1952).

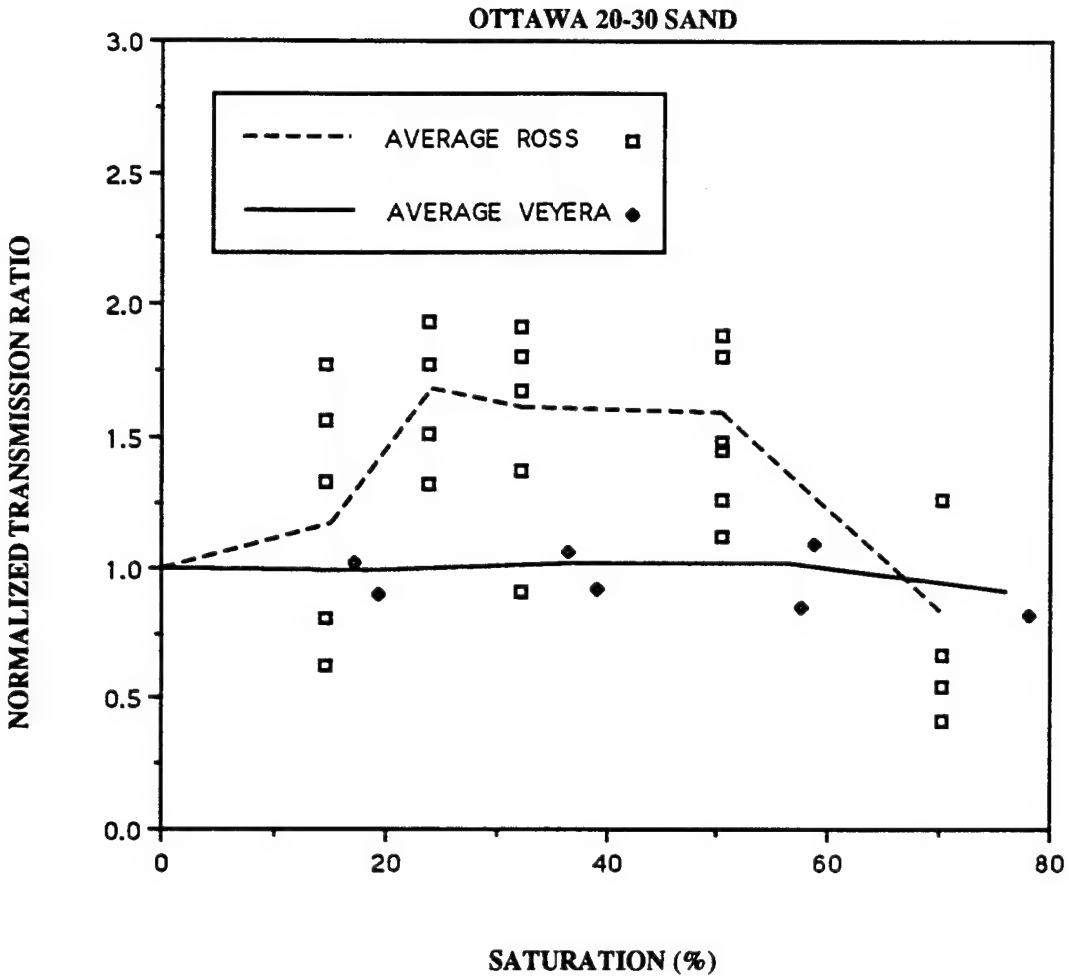

Figure 17. Normalized Transmission Ratio as a Function of Saturation for Ottawa 20-30 Sand (Veyera, 1989).

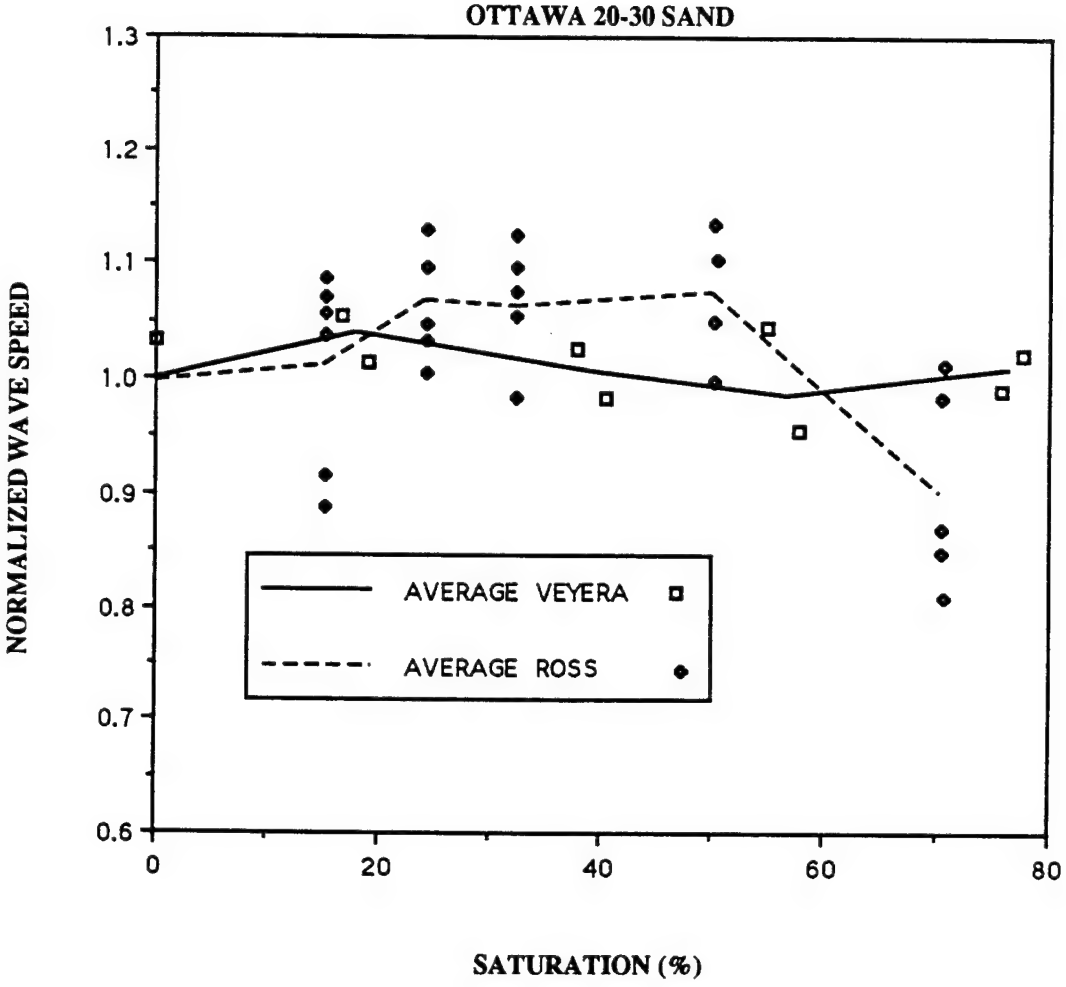

Figure 18. Normalized Wavespeed as a Function of Saturation for Ottawa 20-30 Sand (Veyera, 1989).

The stiffness of soil is dependent on the moisture present during compaction. Pierce (1989) and Ross (1986) obtained different results of wave propagation velocity and transmission ratio for the same soils using different procedures for moisture addition. The reason for the difference is probably due to the sample preparation methods. Pierce compacted sands dry and then saturated and desaturated the sands using the pressure plate apparatus, thus the effect of moisture during compaction was not present. Ross compacted sands for both dry and unsaturated conditions, thus the effect of moisture during compaction was present. Pierce concluded that soil microstructure may be influenced by the saturation level during compaction and that this difference may change the state of stress in the sand.

In reviewing previous research it is quite evident that the compressional wave speed and stress transmission ratio are both greatly affected by the amount of moisture present during compaction. The sample preparation method, void ratio, density and stiffness of the soil also produce variations in compressional wave speed and stress transmission ratio.

(The reverse of this page is blank.)

SECTION III

EXPERIMENTAL PROCEDURES

SECTION III discusses two important topics; equipment and instrumentation (including standard and specially designed items), and procedures used for this investigation. The equipment required for high strain rate testing and sample preparation of soils is located at the Air Force Engineering and Service Center, Tyndall AFB, Florida. The split-Hopkinson pressure bar (SHPB) and thin sectioning devices are specially designed equipment used to test and prepare specimens for microstructural analysis.

A. LABORATORY EQUIPMENT AND INSTRUMENTATION

1. Split-Hopkinson Pressure Bar

The split-Hopkinson pressure bar (SHPB) was used in this investigation to measure stress transmission and compressional wave propagation velocity in unsaturated Ottawa 20-30 sand. The strain rates produced by the SHPB simulate blast loadings such as those generated from conventional weapons and can be used to test materials in compression at strain rates on the order of 10/sec to 10^{+4}/sec. Strain rates for this investigation were on the order of 13/sec to 19/sec. Several researchers have used the SHPB to study dynamic stress transmission in soils (Veyera and Fitzpatrick, 1990b; Veyera, 1989; Ross, 1989; Felice et. al., 1987; Ross et. al., 1986). A schematic of a soil specimen in the SHPB device ready for testing is shown in Figure 19.

The SHPB device produces a compressive stress wave in a steel bar to load the specimen by the impact of a striker bar on an incident bar. The specimen is set between two steel bars, the incident and transmitter bar. The compressive stress wave travels through the incident bar and into the specimen. A portion of the compressive stress wave is transmitted through the specimen to the transmitter bar and a portion is reflected back into the incident bar. As the compressive stress wave travels through the incident bar, specimen, and transmitter bar the SHPB instrumentation (strain gages, signal amplifiers, and digital storage oscilloscope) records the stress pulse thus allowing the determination of the stress transmission ratio and compressional wave speed. A detailed discussion of the SHPB theory and principles is given by Ross (1989).

2. MTS Quasi-Static Loading Device

A Materials Testing System (MTS) device was used in this investigation to quasi-statically load the dry and unsaturated soil specimens. The constrained modulus, which is a measure of soil stiffness, was obtained by using this system which can be used to test materials in the quasi-static strain rate range, i.e., strain rates of 10^{-4}/sec to 10^{-2}/sec. For this investigation the maximum load was 1237 Newtons (5500 pounds) and the minimum load value was set at zero Newtons. Several cycles of loading and unloading can be achieved if so desired. For this investigation loading rates for loading cycles were on the order of 4.45 kN/min (1000 lb/min) and unloading cycles were on the order of 13.34 kN/min (3000 lb/min).

3. Specimen Container

Three different specimen containers were designed specifically for this research. Each container was 15.24 cm (6 inches) long with an inside diameter of 5.08 cm (2.00 inches). The specimen containers were designed such that they would be compatible with the SHPB. The difference between the three specimen containers was in the container wall thicknesses which were 2.54 cm (1.00 inches), 1.27 cm (0.50 inches), and 0.1588 cm (0.0625 inches). For this investigation, the 2.54 cm (1.00 inches) wall thickness specimen container was used. The other stainless steel specimen containers were used in a continuation of this work to simulate different degrees of boundary stiffness that might typically be encountered in the field, the results of which are not part of this research.

Pedestals, wafer seals, and compaction pistons were designed to fit with the specimen containers during the compaction procedure using a standard Proctor hammer ASTM D 698-90 (ASTM 1990). A pedestal was used to hold the wafer seal in place such that the top of the wafer seal was 5.08 cm (2.00 inches) up from the bottom of the specimen container. The wafer seals with Viton O-rings were used to minimize moisture leakage from the base of the specimen containers during compaction and at both ends of the specimen for containment during SHPB testing. Four compaction pistons were designed such that four individual layers each of 2.54 cm (1.00 inches) could be compacted. Figure 20 shows an assembly drawing of the specimen container.

4. Sectioning Apparatus

Two sectioning devices were used in developing specimen sections for microstructural analysis which are: a water-cooled Buehler Metaseu Powermet Automatic

(The reverse of this page is blank.)

Abrasive Cutter (AAC) used for initial rough cutting, and a Buehler Datamet Micro-Processor Grinding and Polishing unit used for grinding and polishing. A section is a cut made through the specimen which exposes the preserved soil structure. Cutting plane locations are discussed in detail in later SECTION III. The AAC is stocked with interchangeable cutting wheels and is used to make an initial rough cut through the specimen. An aluminum alignment device was fabricated such that uniform cuts through the specimen could be obtained. The alignment device had dimensions of 7.62 x 7.62 x 0.32 x 12.70 cm long (3 x 3 x 0.125 x 5 inches). Upon proper alignment, the AAC automatically makes a complete cut through the specimen.

The grinding and polishing unit is used as a final step to prepare specimens prior to the microstructural analysis and is used in conjunction with the following items: (a) a grooved cast iron polishing wheel with #600 Polishing Grit, (b) a smooth cast iron polishing wheel, (c) a polishing cloth, (d) Metadi Fluid, (e) diamond paste, and (f) Micropolish "C". The grinding and polishing procedure involves three separate steps: (1) initial grinding, (2) rough polishing, and (3) fine polishing. These three steps are briefly outlined in SECTION III of this thesis. A more detailed description of the AAC, grinding and polishing unit, and procedures is given by Veyera and Fitzpatrick (1990a).

5. Hardware and Software for Microstructural Analysis

The mathematical analysis of microstructural data is performed using Macintosh IIsi and Macintosh SE/30 personal computers. A Summagraphics (1991) digitizing tablet was interfaced with the Macintosh to perform particle orientation analyses. Two computer programs developed by Rock Ware, Inc. (1991), "Digitize" and "Rosy," were used to determine the orientation of hundreds of particles based on particle long-axis orientation. The "Digitize" program allows the user to digitize line segments which are then transformed to azimuth data and stored for statistical analysis. The program "Rosy" generates angular frequency histograms or rose plots, and performs a complete statistical analysis of the data including the number of particles measured, vector mean, confidence angle, and vector magnitude. Rosy also uses the Rayleigh test of significance to determine if a preferred particle orientation exists within the data. The output from the program is used to determine if preferred particle orientation exists in the samples as a function of saturation, compaction energy, confinement conditions, and load intensity.

B. LABORATORY PROCEDURES

1. Specimen Preparation

a. Compaction

Specimens of Ottawa 20-30 sand were dynamically compacted to a constant dry density of 1.715 g/cm^3 (107.0 pcf) at varying degrees of saturation in the 2.54 cm thick walled stainless steel specimen container using the standard Proctor hammer. An assembly drawing of a typical specimen container is shown in Figure 20.

A standard Proctor hammer, ASTM D 698-90 (ASTM 1990), was used to apply a controlled amount of compactive effort per impact to each soil specimen (7.5 Joules or 5.5 ft-lbs per impact). Prior to compaction, each specimen container and bottom steel wafer insert were sprayed with a dry Teflon® lubricating agent (TFL). All test specimens were formed using four individually compacted layers of equal weight such that a final specimen length of 10.16 cm (4.00 inches) would be obtained. Four individual lifts, each having a final thickness of 2.54 cm (1.00 inches), were used. Saturations were varied from zero (dry) to near 80 percent. At saturations of zero, each layer of dry soil was poured directly into the tube and compacted.

In preparing moist specimens, the required amount of water for a given degree of saturation (at final density when compacted) was added to the originally dry soil, thoroughly mixed in and then allowed to equilibrate before compacting. Since the specimens ranged in degree of saturation from zero to about 80 percent, the tests were conducted on unsaturated specimens. With respect to this study, the term "unsaturated" implies that both continuous air and water phases exist in the soil (e.g., there are no isolated air or water pockets in the grain structure). For most soils, this generally occurs at saturations less than about 85 percent (Corey, 1977).

After impact compaction using the standard Proctor hammer was completed, some specimens were tested in the SHPB device. The same saturation range was used for both NO SHPB (compacted only) and SHPB (compacted and tested in SHPB device) specimens in moist/moist tests (i.e., zero to about 80 percent). Upon completion of SHPB tests, specimens were dried in an oven for a minimum of 12 hours at 110° C to remove all moisture. This procedure applied to specimens dynamically compacted with the standard Proctor hammer only (NO SHPB), and to those specimens dynamically compacted with the standard Proctor hammer and tested using high strain rates (SHPB).

Other specimens were dried in an oven after impact compaction for a minimum of 12 hours at 110° C to remove all moisture and then tested in the SHPB device (moist/dry tests). The was done to determine the influence of moisture during testing.

b. Split-Hopkinson Pressure Bar Tests

For this investigation, the SHPB device was used to study dynamic stress transmission characteristics and compressional wave velocity as a function of saturation and microstructure in Ottawa 20-30 sand. The SHPB has been used by several researchers to study dynamic stress transmission in soils (e.g., Veyera and Fitzpatrick, 1990b; Veyera, 1989; Pierce, 1989; Felice et. al., 1987; Ross et. al., 1986). Dry and unsaturated specimens were compacted using the standard Proctor hammer and tested at high strain rates using the SHPB. Transmission ratio and wave speed at several saturations were measured.

The conditions of the testing program using the SHPB were as follows: (a) a 20.32 cm (8.00 inches) long, 5.08 cm (2.00 inches) diameter steel striker bar was used; (b) the average velocity of the striker bar was approximately 1305 cm/sec (514 inches/sec); (c) the diameters of the incident bar, specimen, and transmitter bar were all 5.08 cm (2.00 inches); and (d) incident stress levels were approximately 290,000 kPa (42,059 psi) in the incident bar.

c. Quasi-Static Uniaxial Compression Tests

Specimens were compacted using four layers in the 2.54 cm (1.00 inches) walled tube using the standard Proctor hammer as shown in Figure 20. The top flange plate was removed and the compaction piston used for compacting Layer 1 was placed on the soil. The specimen was placed in the MTS device and two complete load-unload cycles were applied. Maximum and minimum loads were recorded on a data sheets and analog stress-strain plots were generated by the MTS device.

For comparison purposes, constrained modulus values in uniaxial compression were determined from the analog stress-strain plots by taking a secant line at a predetermined stress level. The constrained modulus was determined for each saturation by constructing a secant line between stress levels of zero and 10,974 kPa (1,592 psi). The reason for choosing a quasi-static stress level of 10,974 kPa was that SHPB stress levels in the soil specimens were on the order of 11,000 kPa. This analysis was performed to obtain information about variation in soil stiffness with saturation. The data are useful

because the stiffness of the soil directly affects the wave speed and transmission ratio. Equation 18 defines the constrained modulus as:

$$D = \frac{\Delta\sigma}{\Delta\varepsilon} = \frac{\frac{\Delta P}{A}}{\frac{\Delta L}{L_o}} \tag{18}$$

where $\Delta\sigma$ is the change in compressive stress, $\Delta\varepsilon$ is the change in axial strain, ΔP is the change in applied static load, A is the cross sectional area, L_o is the initial compacted specimen length, and ΔL is the change in specimen length.

d. Epoxying of Compacted Specimens

A number of commercially available epoxies and bonding agents are routinely used in standard petrographic analyses of geologic materials. In this study, several criteria were set forth in selecting a suitable bonding agent, including the following requirements:

(1) strong bonding with soil grains and the ability to remain intact during cutting and polishing procedures;
(2) relatively low viscosity material;
(3) straightforward and simple preparation procedure;
(4) no shrinkage during curing;
(5) relatively rapid curing time under controlled conditions; and
(6) bonding agent can be easily colored or dyed (as necessary).

A commercially available bonding agent, "EPOTEK 301®," an epoxy produced by Epoxy Technologies, Inc., was used to preserve the structure of compacted specimens for the microstructural analysis. EPOTEK 301 is a high strength, spectrally transparent, low viscosity (100 cps), two component epoxy. Curing time takes about 1 hour in a dry, temperature controlled oven at $65 \pm 2^{\circ}C$. Specimens can also be cured at room temperature overnight. When fully cured, the epoxy is strongly bonded to the specimen grains and maintains the soil structure during cutting and polishing operations.

Since the epoxy is clear, it was necessary to introduce color to provide adequate contrast between the pores and grains. Several coloring agents and dyes were investigated and the most acceptable results were obtained using commercially available biological stains in powdered form (Sudan IV-dark red; Sudan Black-dark blue to black).

The epoxy used does not mix or cure if water is present, therefore specimens initially compacted moist at varying degrees of saturation in the specimen containers were

dried in a temperature controlled oven at 110°C for at least 12 hours. Specimens were then allowed to cool to room temperature before epoxying. Careful handling of the specimen container was essential during all phases of preparation to insure that the compacted soil structure was not disturbed (i.e., by jarring, vibration, tipping, etc.).

Material quantities of EPOTEK 301 epoxy were determined based on a calculation of the available pore space for a medium granular soil (Ottawa 20-30 sand) compacted to a void ratio of 0.545. Allowances were made for additional material required to cover particles, minor losses in handling, etc., with a minimum of waste. The mixing ratio for the epoxy component parts is 4:1 (resin to hardener) as specified by the manufacturer. Figure 21 shows a typical specimen being epoxied. Details of the laboratory procedure for epoxying compacted specimens are given by Veyera and Fitzpatrick (1990a). The general procedure is briefly outlined as follows:

(1) Specimens compacted moist are dried overnight in a temperature controlled oven. Specimens compacted dry are epoxied immediately (Step 2).

(2) EPOTEK 301 epoxy is carefully introduced into the specimen under atmospheric pressure to saturate the void spaces. The specimen is then cured in a temperature-controlled oven at $65 \pm 2^{\circ}C$ for about 1 hour.

(3) After curing, the specimen is extruded from the specimen container.

2. Specimen Sectioning

a. Extrusion

After the epoxy has fully cured, the next step is to extrude each specimen from the specimen container. For oven-cured specimens, the containers must be cooled before extrusion. The procedure uses a modified Marshall Testing machine for extruding specimens, and requires a loading piston, loading support blocks and a flange plate.

b. Initial Rough Cutting

A water-cooled Buehler Metaseu Powermet ACC was used for the initial rough cutting of epoxied specimens. A simple aluminum specimen alignment device for making uniform cuts was fabricated. Once a specimen is properly aligned, the ACC automatically makes a complete cut through the specimen. Each cut section is clearly marked to record the original orientation. Figure 22 shows the location of the various cutting planes.

Cutting the specimens for use in microstructural analysis involves several steps which are listed below;

(1) first cut removes about 0.3125 cm (0.125 inches) from each end of the specimen;
(2) second cut splits the specimen in half along its long-axis (Figure 23);
(3) third cut splits one of the specimen halves along its diameter (Figure 24).
(4) a vertical cut about 0.3125 cm (0.125 inches) in thickness is made along the long-axis of one of the halves from the initial cuts, Step 2 (Figure 25);
(5) a horizontal cut about 0.3125 cm (0.125 inches) in thickness is made along the diameter of one of the halves from the initial cuts, Step 3 (Figure 26).

c. Grinding and Polishing

The final preparation procedure for the specimens prior to microstructural analysis involves several steps and uses a Buehler Datamet Micro-Processor Grinding and Polishing Unit. Details of the laboratory procedure for the grinding and polishing of compacted specimens are given by Veyera and Fitzpatrick (1990a). The general procedure is briefly outlined as follows:

(1) Initial Grinding - This step is used to true the planar surface obtained during the rough cutting process and to prepare the specimen surface for polishing.
(2) Rough Polishing - This step is used to rough polish the specimen section surface prior to detailed finish polishing.
(3) Fine Polishing - This step is used to develop a smooth, highly polished surface finish that provides adequate contrast between the specimen grains and the expoy-filled pores.

Once the final polishing has been completed, specimens are examined under a microscope to check if the surface has been properly prepared and if adequate contrast between pore spaces and individual grains has been developed. Properly prepared specimens can then be used in microstructural analysis studies.

3. Photomicrographs of Sectioned Specimens

Photographs of sectioned specimens are used to determine axial ratio and particle long-axis orientation based on the procedure developed by Oda (1972a) and Campbell

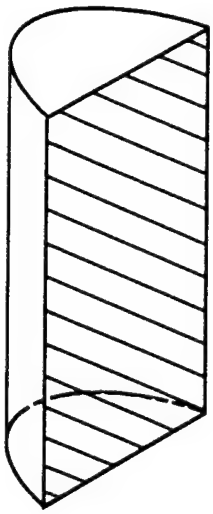

Figure 23. Initial Specimen Cut Along the Long Axis (Section A-A).

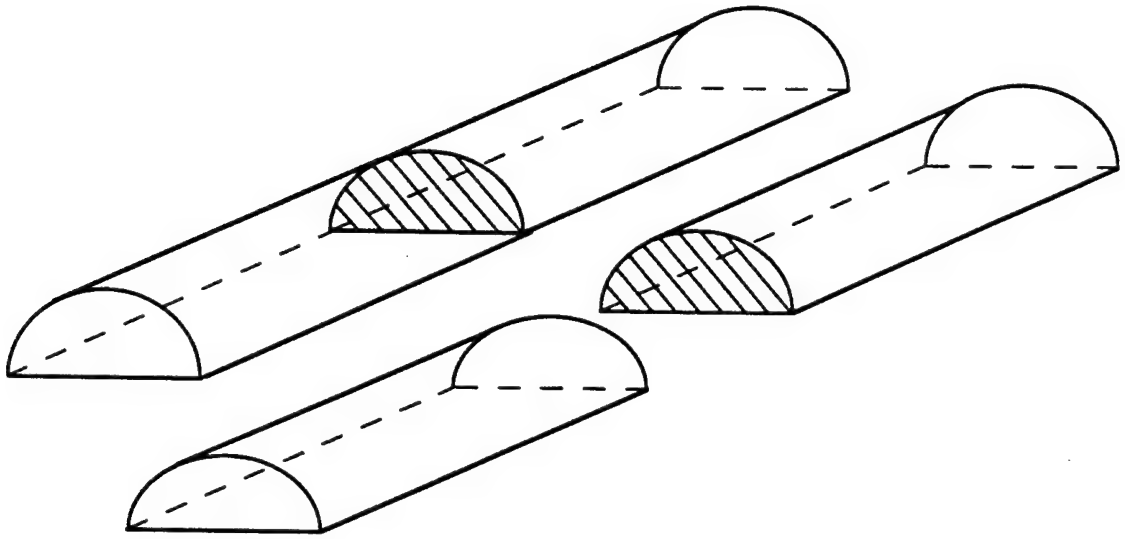

Figure 24. Initial Specimen Cut Along theDiametral Axis (Section B - B).

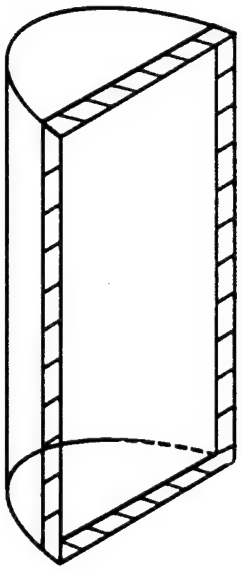

Figure 25. Final Cut of Specimen Section Along the Long Axis.

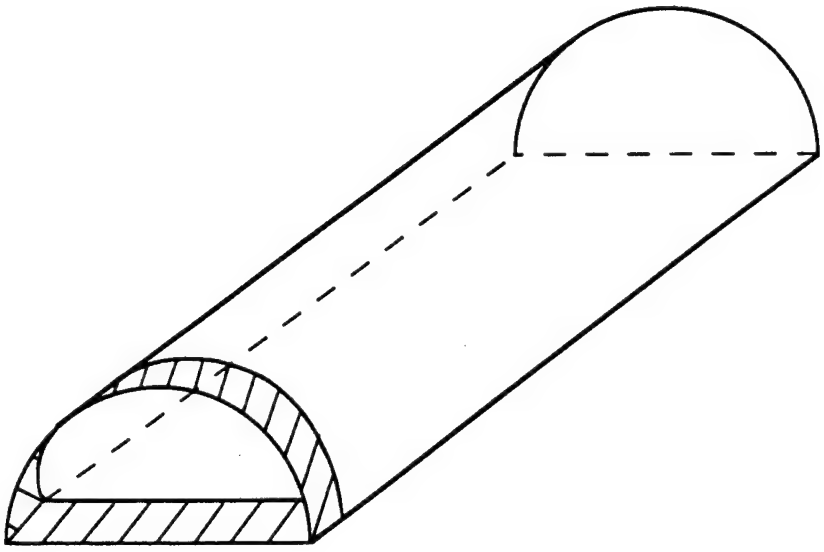

Figure 26. Final Cut of Specimen Cut Along the Diametral Axis .

(1985). A 35 mm camera with special microscope attachments was mounted on a reflected light microscope. Direct lighting was used to illuminate the cut specimen section from above. The microscope was set up such that sections of each specimen could be photographed using a magnification of 10x on all specimen sections. Standard 35 mm color slide film (ASA 100) was used to photograph specimens. The optimum shutter speed was 1/60 second, which was obtained through a careful study of photographs using various shutter speeds and provided the optimum visual contrast between sand grains and epoxy.

A series of photographs was taken in the vertical and horizontal directions. The grid layout and the identification schemes for Sections A-A and B-B are shown in Figure 27. A record of frame number and corresponding grid number was maintained for proper identification of each slide. A total of 19 grids were photographed for each specimen. Grids a-g represent the horizontal direction on Section A-A, grids h-o represent the vertical direction on Section A-A, and grids p-s represent the semicircular section. The properly identified slides are then used to analyze the microstructure of the compacted specimens.

4. Microstructural Analysis

To perform particle long-axis orientation and axial ratio analyses, a two-dimensional image of the grain and void arrangements is needed. The two-dimensional image is obtained by projecting the slides through a standard slide projector onto a 21.59 cm by 27.94 cm (8.5 in x 11 in) sheet of paper attached to the digitizing tablet (see Figure 28). Individual grains are digitized by locating the longest axis of the particle. Digitized data files are clearly identified according to degree of saturation, grid number, and whether or not the specimen was tested in the SHPB device.

a. Axial Ratio

To determine the axial ratio of an individual particle and a group of particles, the procedure suggested by Oda (1972a) was followed:

(1) Determine the length of the particle's shortest axis, L_2, by finding the largest possible circular that can be inscribed on the particle (see Figure 29a).

(2) Determine the length of the particles longest axis, L_1, by finding the smallest possible circular that can be circumscribed on the particle (see Figure 29b).

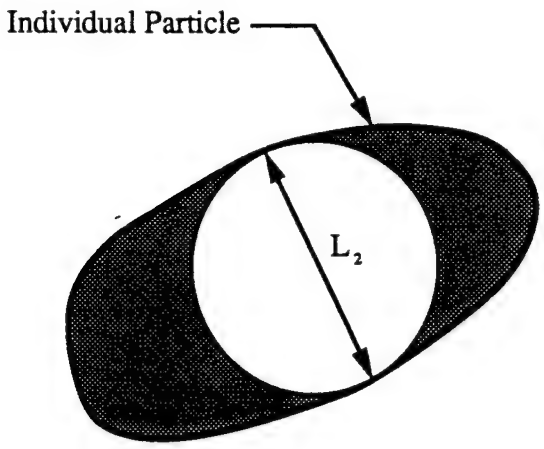

a. Short Axis (L_2) Determination.

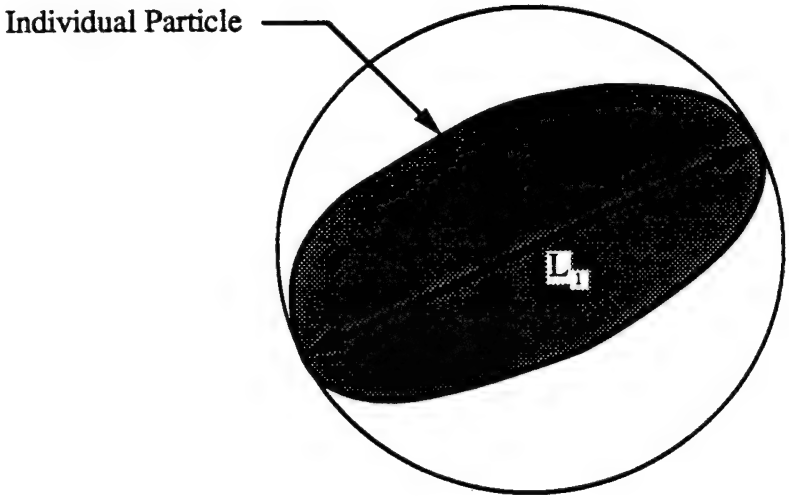

b. Long Axis (L_1) Determination.

Figure 29. Determination of Axial Ratio Parameters for an Individual Particle.

The axial ratio for a group of particles, n_{avg}, is given by Equation (5). The axial ratio for an individual particle, n_s, is given by Equation (19).

$$n_s = \frac{L_2}{L_1} \tag{19}$$

Axial ratio data are useful in classifying particle shape and also provide an indication of the potential particle arrangements that can be expected in a compacted specimen. An example would be that as particles approach a spherical shape, particle arrangement become more random. Oda (1972a) indicated that an axial ratio of 0.7 or less was required for preferred particle long-axis orientation. Table 1 provides classes and descriptions of particle shapes based on axial ratio data (roundness ratio). The Ottawa 20-30 sand used in this research would be classified as well rounded according to Table 1.

b. Particle Long-Axis Orientation

Particle long-axis orientation is a standard method used in the microstructural analysis of granular soils. The procedure used to determine long-axis orientation of individual particles was based on the method developed by Campbell (1985) which involves determining the longest axis, L_1, and the shortest axis, L_2, of a particle. Figure 30 shows the determination of particle long-axis, L_1, and orientation angle, θ, with respect to a set of Cartesian coordinate system reference axes.

The two endpoints of the longest axis are digitized and read by the "Digitize" program as line segment data. The orientation angle, θ, of an individual particle is determine by converting line segment data to azimuth data. The azimuth data is read into the "Rosy" program which then calculates the Vector Mean, Vector Magnitude, Rayleigh test of significance, and also generates angular frequency histograms (rose plots) for a group of particles. For each rose plot developed, orientation measurements (class intervals) were made at 10-degree intervals using a 95 percent confidence interval. The output from Rosy allows the user to determine if a preferred particle orientation exists in the specimen.

Particle long-axis orientation analyses were performed in the vertical and horizontal directions on Section A-A and on the semicircular Section B-B (see Figure 27). The vertical analysis was further extended to examine long-axis orientations in each compacted layer. Vertical grids (h-o), were separated into four layers: (a) Layer #1 - grids o, n, and m; (b) Layer #2 - grids m, l, and d: (c) Layer #3 - grids d, k, and j; (d)Layer #4 - grids j, i, and h. Results from the long-axis orientation analyses provide information about preferred particle orientations that may occur either locally or globally within the specimen.

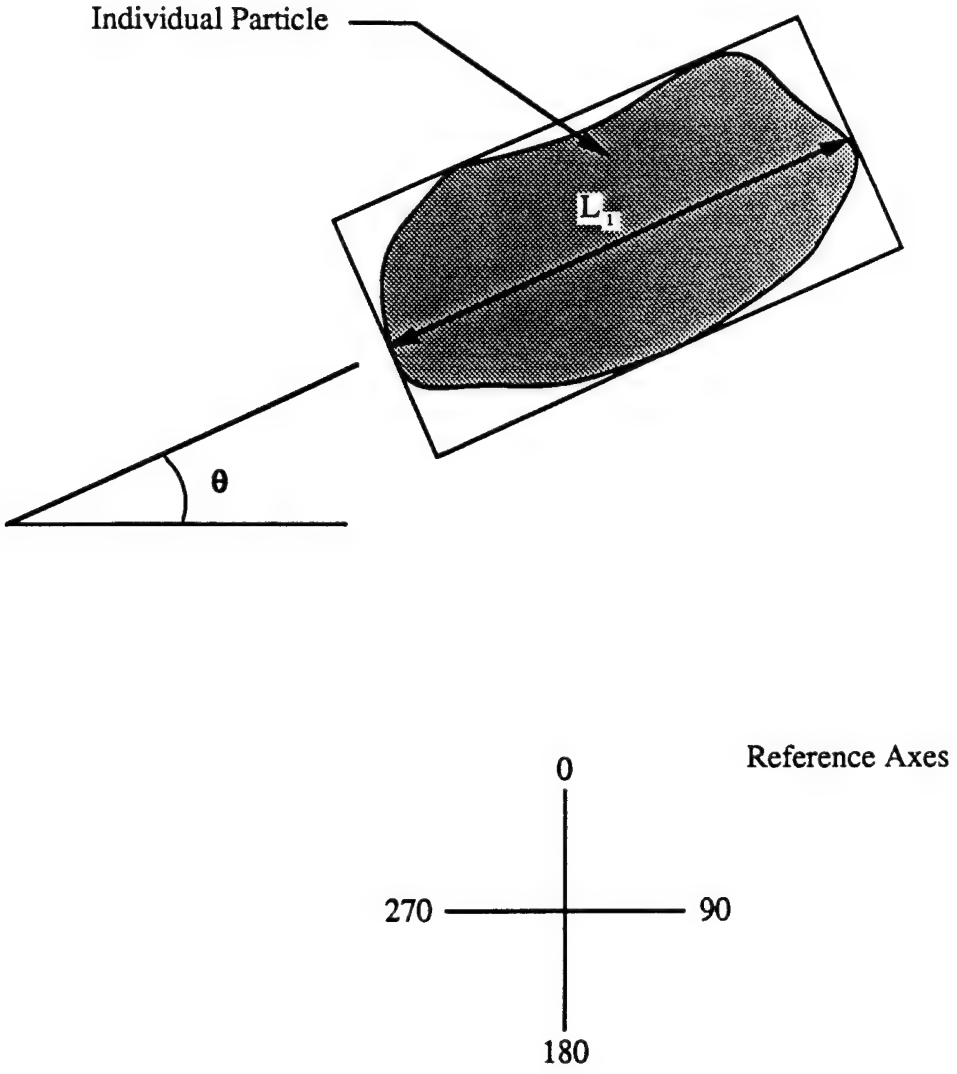

Figure 30. Determination of Particle Long Axis (L_1) Orientation Angle θ.

SECTION IV

EXPERIMENTAL RESULTS

This chapter contains five sections which show the experimental results obtained in the present investigation. The first section gives information pertaining to the physical soil properties. The second section deals with specimen compaction. The third section presents the Split-Hopkinson pressure bar results. Section four gives the results of quasi-static uniaxial compression tests, and the final section is devoted to results obtained in the microstructural analysis.

Most of the figures presented in this chapter show saturations ranging from zero to about 75 percent. Several other figures include data for saturations of about 95 percent. Specimens prepared for the microstructural analysis had saturations from zero to about 75 percent. Blow count, compressional wave speed, and stress transmission ratio data were obtained for saturations from zero to about 95 percent.

A. PHYSICAL PROPERTIES OF SOIL

A commercially available granular soil designated as "Ottawa 20-30 sand" was used in this investigation. Approximately 227 kg (500 pounds) of the sand were obtained from the Ottawa Silica Company and random samples were taken from the bulk quantity. The material is a uniformly graded, subrounded to rounded, medium sand with no fines and is classified as SP (poorly graded sand) according to the Unified Soil Classification System (USCS). Physical index properties for the Ottawa 20-30 sand are summarized in Table 2 and a grain size distribution curve is shown in Figure 31.

B. SPECIMEN COMPACTION

Each specimen of Ottawa 20-30 sand was dynamically compacted to a constant dry density of 1.715 g/cm^3 (107.0 pcf) using a standard Proctor hammer. The amount of compactive effort required to obtain to this constant dry density varied with the amount of moisture present. Records of the number of blows required to achieve this dry density for each layer and saturation were maintained. Table 3 summarizes the blow count data and Figure 32 shows the average number of blows as a function of saturation required to compact the Ottawa 20-30 sand to a constant dry density of 1.715 g/cm^3. Results are based on data collected from 56 specimens compacted in the 2.54 cm (1.00 in) thick walled

TABLE 2. Physical Properties of Ottawa 20-30 Sand.

USCS Classification	SP
Specific Gravity	2.65
D_{50} particle size	0.70 mm
[a]C_u	1.40
[b]C_c	1.03
[c]Percent passing #100 sieve	<1 %
[d]Maximum dry density	1,763 kg/m^3
[d]Minimum dry density	1,587 kg/m^3
Maximum void ratio	0.669
Minimum void ratio	0.504

Note: [a]Coefficient of Uniformity
[b]Coefficient of Curvature
[c]U.S. Standard Sieve
[d]Data from Ottawa Silica Sand Company

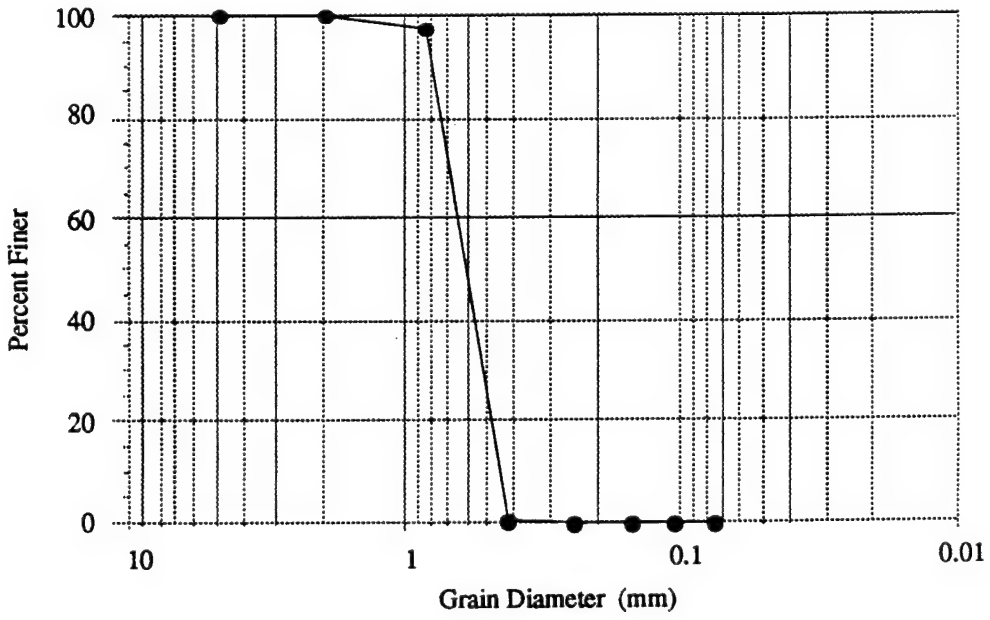

Figure 31. Grain Size Distribution for Ottawa 20-30 Sand.

specimen container. Figure 32 indicates that the total number of blows sharply increases from zero to about 20 percent saturation, then slightly increases from about 20 percent to about 40 percent saturation and decreases thereafter with increasing saturation.

Figure 33 shows the total number of blows required to compact the Ottawa 20-30 sand to a constant dry density of 1.715 g/cm^3 for each individual 2.54 cm (1.00 in) thick layer. The data show that the greatest compaction effort is required in the first layer at all saturations. The first layer shows a similar trend as that found in Figure 32. Layers 2 and 3 show a similar trend with respect to each other in that the total number of blows increases from zero to about 20 percent saturation. As the saturation increases beyond 20 percent, the total number of blows steadily decreases. In Layer 4, the total number of blows from about 20 percent to about 75 percent saturation is relatively unchanged.

C. SPLIT-HOPKINSON PRESSURE BAR TESTS

High strain rate compressive tests were conducted on Ottawa 20-30 sand using the SHPB device. Compressional wave speed and stress transmission ratio were studied as a function of saturation and microstructure. Some specimens were compacted moist and tested moist in the SHPB (moist-moist tests) and others were compacted moist and tested in the SHPB after drying (moist-dry tests).

Tables 4 and 5 give the raw data obtained from SHPB tests for compressional wave speed and stress transmission ratio for specimens which were compacted moist and tested moist (moist-moist) and specimens which were compacted moist and tested dry (moist-dry), respectively. Figures 34 through 37 show the variation within the data about the average compressional wave speed and stress transmission ratio as a function of saturation. Figures 34 and 35 show compressional wave speed and stress transmission ratio as a function of saturation from data obtained in 27 SHPB tests for specimens compacted moist and tested moist (moist-moist). Figure 34 shows that the average compressional wave speed increases from zero to about 20 percent saturation. The compressional wave speed is relatively constant from 20 percent to about 75 percent saturation, and slightly decreases thereafter. Figure 35 shows that the stress transmission ratio increases from zero to about 20 percent saturation and has a sharp increase from about 20 percent to about 40 percent saturation. The stress transmission ratio then steadily decreases from about 40 percent to about 95 percent saturation.

Figures 36 and 37 show compressional wave speed and stress transmission ratio as a function of saturation from data obtained in 25 SHPB tests for specimens compacted moist and tested dry (moist-dry). Figure 36 shows that the compressional wave speed increases

TABLE 3. BLOW COUNT TEST RESULTS FOR OTTAWA 20-30 SAND COMPACTED USING THE STANDARD PROCTOR HAMMER.

Container Wall Thickness = 2.54 cm (1.00 in)
Dry Density = 1.715 g/cc (107 pcf)
Void Ratio = 0.545
Sample Length = 10.16 cm (4.00 in)
Compacted four individual 2.54 cm (1.00 in) layers
Testing performed by Dr. George E. Veyera and Blaise J. Fitzpatrick of the University of Rhode Island.
Research performed at AFESC/RDCM, Tyndall AFB, Florida.
Date: Summer 1990

	LAYER & NUMBER OF BLOWS				TOTAL NUMBER
S%	1	2	3	4	OF BLOWS
0.0	11	6	10	4	31
0.0	9	8	8	3	28
0.0	8	7	10	5	30
0.0	11	9	6	4	30
0.0	10	4	8	4	26
0.0	18	10	12	5	45
0.0	8	7	8	4	27
0.0	16	7	8	5	36
0.0	8	5	5	6	24
0.0	18	10	12	6	46
0.0	10	5	12	4	31
0.0	15	14	18	11	58
0.0	13	12	24	5	54
0.0	19	9	12	9	49
AVERAGE	12	8	11	5	37
STD DEV	3.89	2.71	4.79	2.09	10.89

	LAYER & NUMBER OF BLOWS				TOTAL NUMBER
S%	1	2	3	4	OF BLOWS
18.7	16	21	23	10	70
18.7	25	22	34	16	97
18.7	29	25	24	12	90
18.7	34	29	20	19	102
18.7	35	29	27	11	102
18.7	40	29	37	14	120
18.7	56	27	40	13	136
18.7	55	39	24	16	134
18.7	55	40	50	13	158
18.7	40	32	38	15	125
18.7	53	34	33	13	133
AVERAGE	40	26	32	14	115
STD DEV	13.00	3.39	8.70	2.44	24.14

TABLE 3. (continued)

	LAYER & NUMBER OF BLOWS				TOTAL NUMBER
S%	1	2	3	4	OF BLOWS
37.4	43	28	26	12	109
37.4	42	30	22	15	109
37.4	37	27	37	15	116
37.4	58	25	30	10	123
37.4	53	35	24	10	122
37.4	60	30	29	15	134
37.4	72	31	31	15	149
37.4	70	30	32	20	152
37.4	45	27	30	15	117
37.4	56	31	26	17	130
AVERAGE	54	29	29	14	126
STD DEV	11.27	3.13	4.12	2.91	14.38

	LAYER & NUMBER OF BLOWS				TOTAL NUMBER
S%	1	2	3	4	OF BLOWS
56.2	35	26	25	8	94
56.2	31	22	25	9	87
56.2	41	20	22	8	91
56.2	65	26	30	10	131
56.2	36	23	27	8	94
56.2	57	27	28	13	125
56.2	50	22	34	15	121
56.2	56	25	23	9	113
56.2	41	24	27	18	110
AVERAGE	46	24	27	11	107
STD DEV	11.02	2.52	3.46	3.41	15.40

	LAYER & NUMBER OF BLOWS				TOTAL NUMBER
S%	1	2	3	4	OF BLOWS
74.9	25	21	25	8	79
74.9	54	15	21	9	99
74.9	47	16	17	12	92
74.9	70	28	10	10	118
74.9	70	17	15	12	114
74.9	62	25	26	11	124
74.9	52	16	24	8	100
74.9	60	18	15	10	103
74.9	75	19	20	11	125
74.9	55	21	18	11	105
74.9	50	20	11	10	91
74.9	45	22	27	11	105
AVERAGE	55	20	19	10	105
STD DEV	12.98	3.72	5.48	1.30	13.28

TABLE 3. (continued)

	LAYER & NUMBER OF BLOWS				TOTAL NUMBER
S%	1	2	3	4	OF BLOWS
93.6	18	11	12	10	51
93.6	12	16	15	11	54
93.6	23	16	13	12	64
AVERAGE	18	14	13	11	56
STD DEV	4.50	2.36	1.25	0.82	5.56

	LAYER & AVERAGE NUMBER OF BLOWS				AVERAGE TOTAL NUMBER
S%	1	2	3	4	OF BLOWS
0.0	12	8	11	5	37
18.7	40	30	32	14	115
37.4	54	29	29	14	126
56.2	46	24	27	11	107
74.9	55	20	19	10	105
93.6	18	14	13	11	56

	LAYER & NORMALIZED NUMBER OF BLOWS				NORMALIZED TOTAL NUMBER
S%	1	2	3	4	OF BLOWS
0.0	1.0	1.0	1.0	1.0	1.0
18.7	3.3	3.8	2.9	2.8	3.1
37.4	4.5	3.6	2.6	2.8	3.4
56.2	3.8	3.0	2.5	2.2	2.9
74.9	4.6	2.5	1.7	2.0	2.8
93.6	1.5	1.8	1.2	2.2	1.5

TABLE 4. SHPB TEST RESULTS FOR OTTAWA 20-30 SAND COMPACTED MOIST AND TESTED MOIST.

Container Wall Thickness = 2.54 cm (1.00 in)
Dry Density = 1.715 g/cc (107 pcf)
Void Ratio = 0.545
Sample Length = 10.16 cm (4.00 in)
Testing performed by Dr. George E. Veyera and Blaise J. Fitzpatrick of the University of Rhode Island.
Research performed at AFESC/RDCM, Tyndall AFB, Florida.
Date: Summer 1990

S%	Wc%	TOTAL UNIT WEIGHT g/cc	WAVE SPEED (ft/sec)	WAVE SPEED (m/sec)	TRANSMISSION RATIO
0.0	0.00	1.715	1193	363.6	0.0168
0.0	0.00	1.715	1572	479.1	0.0298
0.0	0.00	1.715	1282	390.7	0.0199
0.0	0.00	1.715	1812	552.3	0.0511
0.0	0.00	1.715	1759	536.1	0.0517
0.0	0.00	1.715	1622	494.4	0.0330
0.0	0.00	1.715	1630	496.8	0.0270
0.0	0.00	1.715	1967	599.5	0.0434
0.0	0.00	1.715	2083	634.9	0.0670
0.0	0.00	1.715	1873	570.9	0.0457
0.0	0.00	1.715	2026	617.5	0.0749
18.7	3.85	1.781	1978	602.9	0.0350
18.7	3.85	1.781	1610	490.7	0.0429
18.7	3.85	1.781	2008	612.0	0.0635
18.7	3.85	1.781	1852	564.5	0.0534
37.4	7.70	1.847	1905	580.6	0.0653
37.4	7.70	1.847	1967	599.5	0.0726
37.4	7.70	1.847	1817	553.8	0.0421
56.2	11.55	1.913	1754	534.6	0.0394
56.2	11.55	1.913	1921	585.5	0.0455
56.2	11.55	1.913	1852	564.5	0.0657
74.9	15.40	1.979	1822	555.3	0.0356
74.9	15.40	1.979	1873	570.9	0.0521
93.6	19.25	2.045	1873	570.9	0.0313
93.6	19.25	2.045	1727	526.4	0.0415
93.6	19.25	2.045	1792	546.2	0.0307

S%	AVERAGE WAVE SPEED (ft/sec)	AVERAGE WAVE SPEED (m/sec)	AVERAGE TRANSMISSION RATIO	NORMALIZED WAVE SPEED	NORMALIZED TRANSMISSION RATIO
0.0	1711	521.5	0.0418	1.000	1.000
18.7	1862	567.5	0.0487	1.088	1.165
37.4	1896	577.9	0.0600	1.108	1.435
56.2	1842	561.4	0.0502	1.077	1.201
74.9	1848	563.1	0.0439	1.080	1.049
93.6	1797	547.7	0.0345	1.050	0.825

TABLE 5. SHPB TEST RESULTS FOR OTTAWA 20-30 SAND COMPACTED MOIST AND TESTED DRY.

Container Wall Thickness = 2.54 cm (1.00 in)
Dry Density = 1.715 g/cc (107 pcf)
Void Ratio = 0.545
Sample Length = 10.16 cm (4.00 in)
Testing performed by Dr. George E. Veyera and Blaise J. Fitzpatrick of the University of Rhode Island.
Research performed at AFESC/RDCM, Tyndall AFB, Florida.
Date: Summer 1990

S%	Wc%	TOTAL UNIT WEIGHT g/cc	WAVE SPEED (ft/sec)	WAVE SPEED (m/sec)	TRANSMISSION RATIO
0.0	0.00	1.715	1193	363.6	0.0168
0.0	0.00	1.715	1572	479.1	0.0298
0.0	0.00	1.715	1282	390.7	0.0199
0.0	0.00	1.715	1812	552.3	0.0511
0.0	0.00	1.715	1759	536.1	0.0517
0.0	0.00	1.715	1622	494.4	0.0330
0.0	0.00	1.715	1630	496.8	0.0270
0.0	0.00	1.715	1967	599.5	0.0434
0.0	0.00	1.715	2083	634.9	0.0670
0.0	0.00	1.715	1873	570.9	0.0457
0.0	0.00	1.715	2026	617.5	0.0749
18.7	3.85	1.781	2002	610.2	0.0577
18.7	3.85	1.781	2110	643.1	0.0576
18.7	3.85	1.781	2090	637.0	0.0743
37.4	7.70	1.847	1705	519.7	0.0536
37.4	7.70	1.847	2144	653.5	0.0780
37.4	7.70	1.847	1899	578.8	0.0519
56.2	11.55	1.913	1569	478.2	0.0482
56.2	11.55	1.913	1684	513.3	0.0491
56.2	11.55	1.913	2110	643.1	0.0605
56.2	11.55	1.913	1990	606.5	0.0761
74.9	15.40	1.979	1495	455.7	0.0198
74.9	15.40	1.979	2008	612.0	0.0726
74.9	15.40	1.979	1889	575.7	0.0612
74.9	15.40	1.979	1910	582.1	0.0678

S%	AVERAGE WAVE SPEED (ft/sec)	AVERAGE WAVE SPEED (m/sec)	AVERAGE TRANSMISSION RATIO	NORMALIZED WAVE SPEED	NORMALIZED TRANSMISSION RATIO
0.0	1711	521.5	0.0418	1.000	1.000
18.7	2067	630.0	0.0632	1.208	1.512
37.4	1916	584.0	0.0612	1.120	1.464
56.2	1838	560.2	0.0585	1.074	1.400
74.9	1825	556.2	0.0553	1.067	1.323

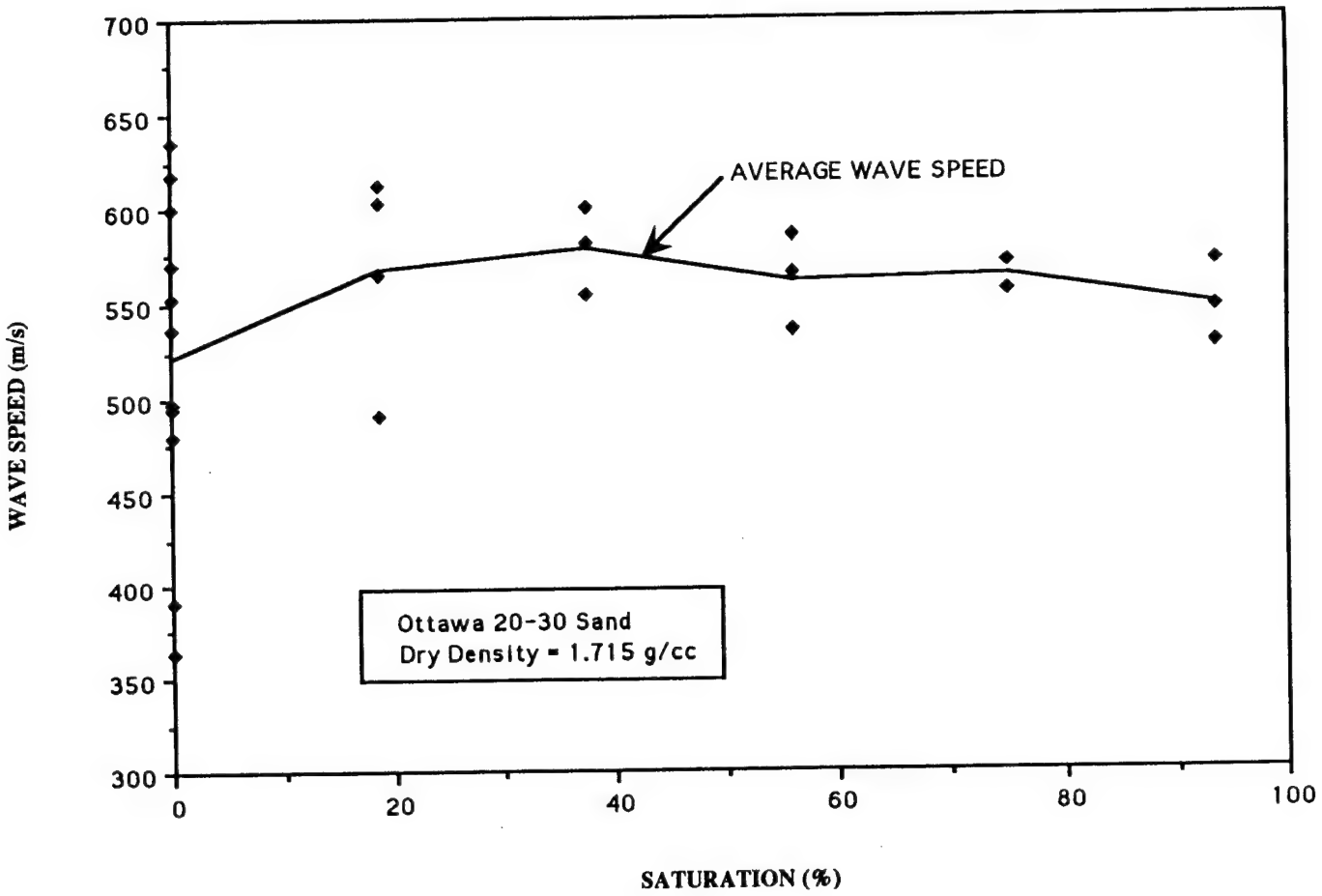

Figure 34. Wave Speed as a Function of Saturation for Ottawa 20-30 Sand Compacted Moist and Tested Moist.

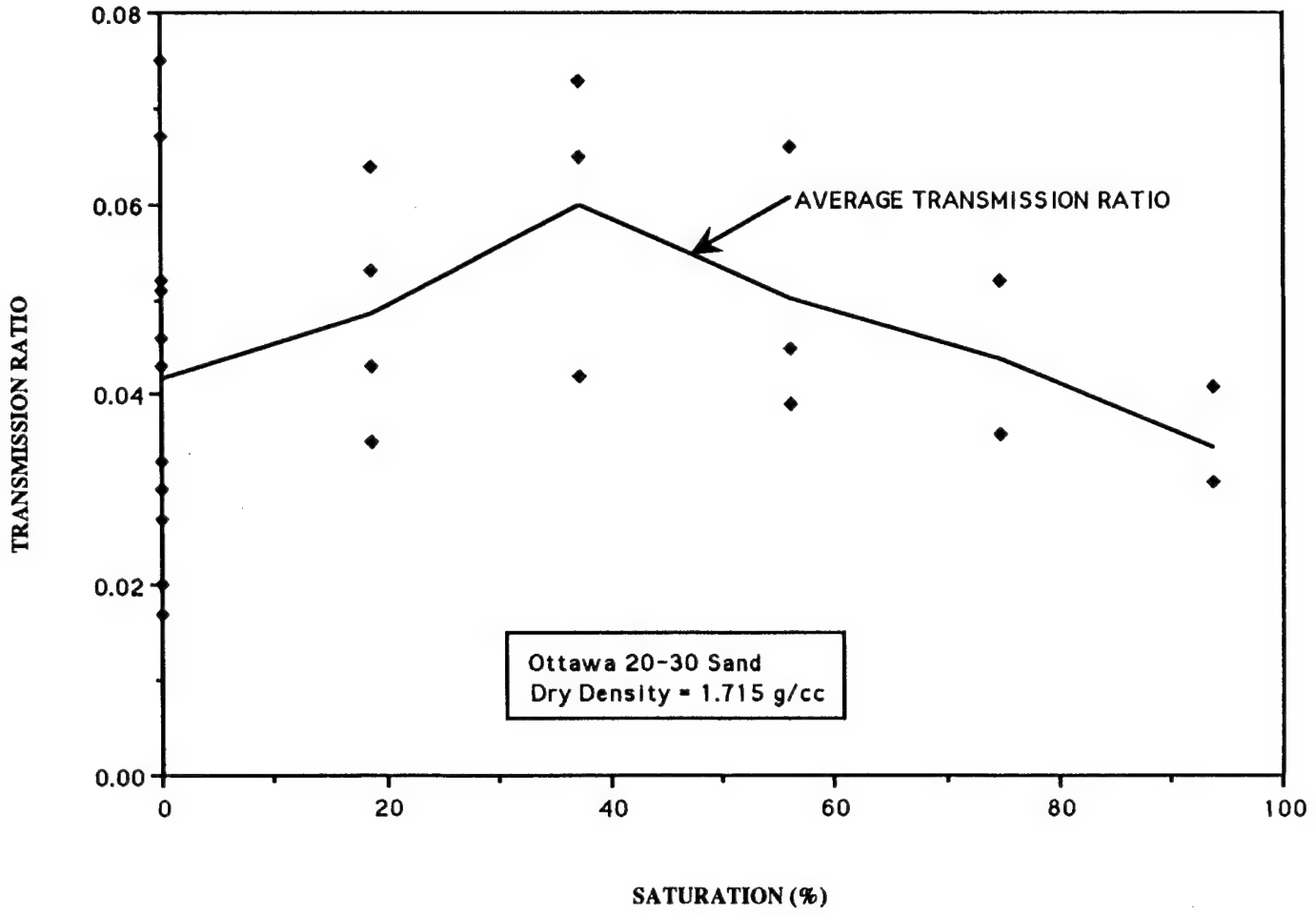

Figure 35. Transmission Ratio as a Function of Saturation for Ottawa 20-30 Sand Compacted Moist and Tested Moist.

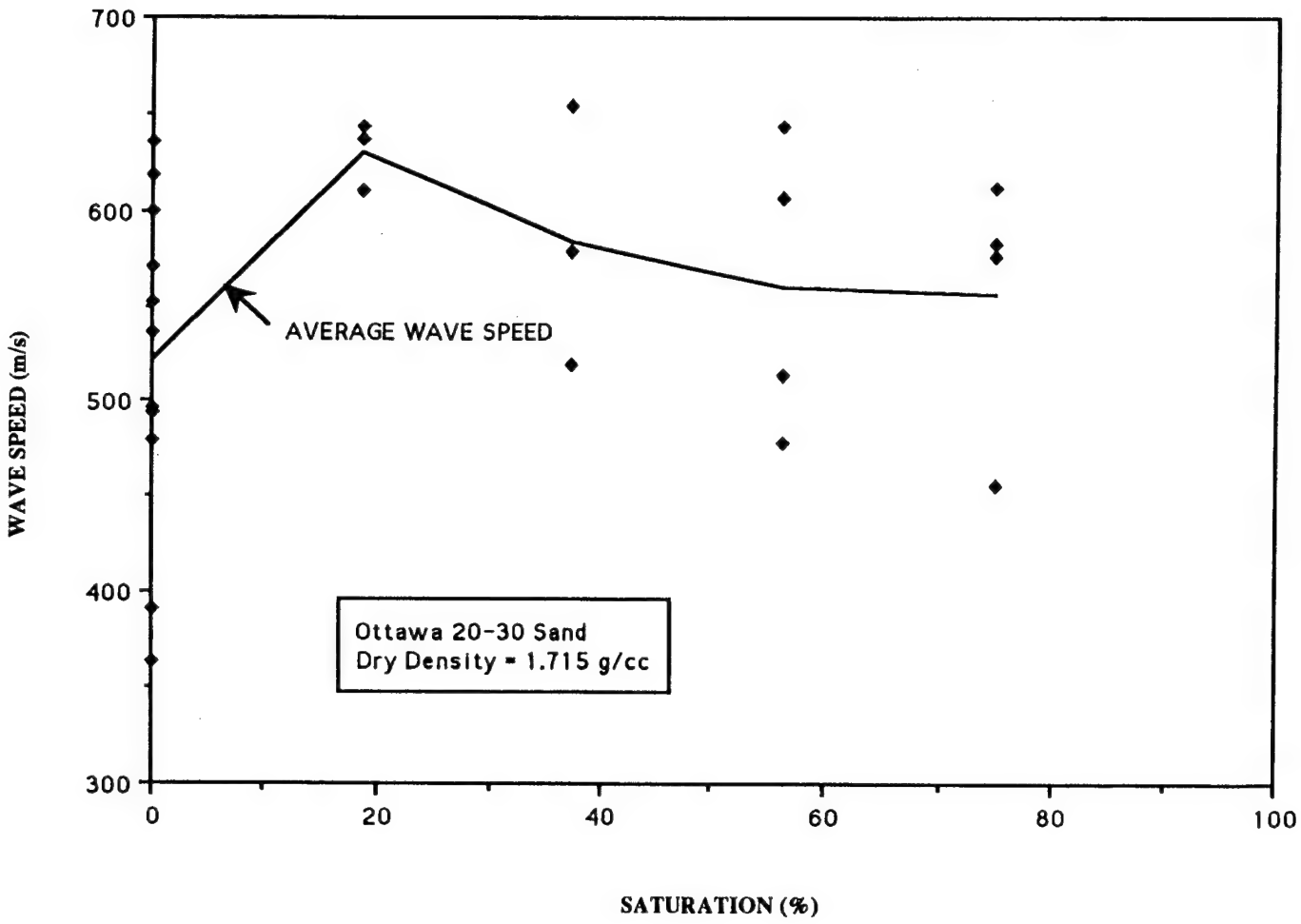

Figure 36. Wave Speed as a Function of Saturation for Ottawa 20-30 Sand Compacted Moist and Tested Dry.

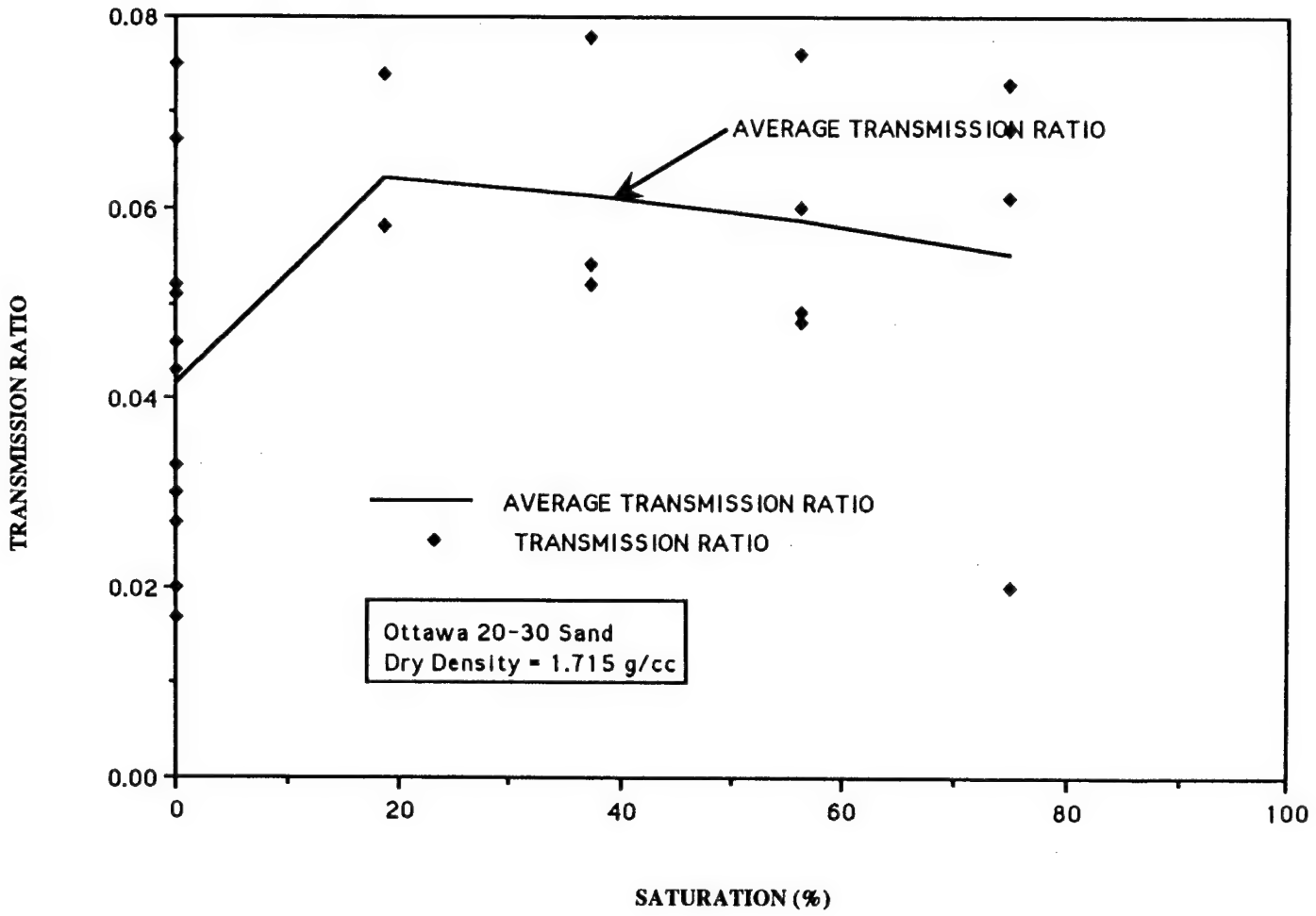

Figure 37. Transmission Ratio as a Function of Saturation for Ottawa 20-30 Sand Compacted Moist and Tested Dry.

from zero to about 20 percent saturation and gradually decreases thereafter. Figure 37 shows the stress transmission ratio increasing from zero to about 20 percent saturation and gradually decreasing thereafter.

D. QUASI-STATIC UNIAXIAL COMPRESSION TESTS

A total of 13 quasi-static uniaxial compression tests were performed on the Ottawa 20-30 sand using the MTS loading device at several saturations. The quasi-static tests were performed to obtain information about the stress-strain response and stiffness of the compacted unsaturated soils for comparison with SHPB trends. Two sets of tests were performed: the first used four compacted layers (as for SHPB tests), and the second used one compacted layer. Figures 38 through 49 show the stress-strain curves generated from each set for one loading and unloading cycle.

1. Four Compacted Layers

Figures 38 through 43 show stress-strain curves generated at different saturations using four layers compacted to a constant dry density of 1.715 g/cm^3. Each specimen was moist during testing. In all cases the unloading portion of the stress-strain curve is much steeper than the loading portion. This indicates that the soil is stiffer at the completion of the first load-unload cycle.

2. One Compacted Layer

Figures 44 through 49 show stress-strain curves generated at different saturations using one layer compacted to a constant dry density of 1.715 g/cm^3. Each specimen was moist during testing. In all cases the unloading portion of the stress-strain curve is much steeper than the loading portion. This indicates that the soil is stiffer at the completion of the first load-unload cycle.

3. Constrained Modulus

Figure 50 shows the constrained modulus as a function saturation determined from the stress-strain curves generated by the MTS loading device (see Figures 38 through 43). The constrained modulus was determined using maximum and minimum stress levels for the first loading cycle of 10,974 kPa (1,592 psi) and zero kPa and Equation (18).
Figure 50 shows that the constrained modulus sharply increases from zero to about 20 percent saturation and has a slightly increases from about 20 percent to about 40

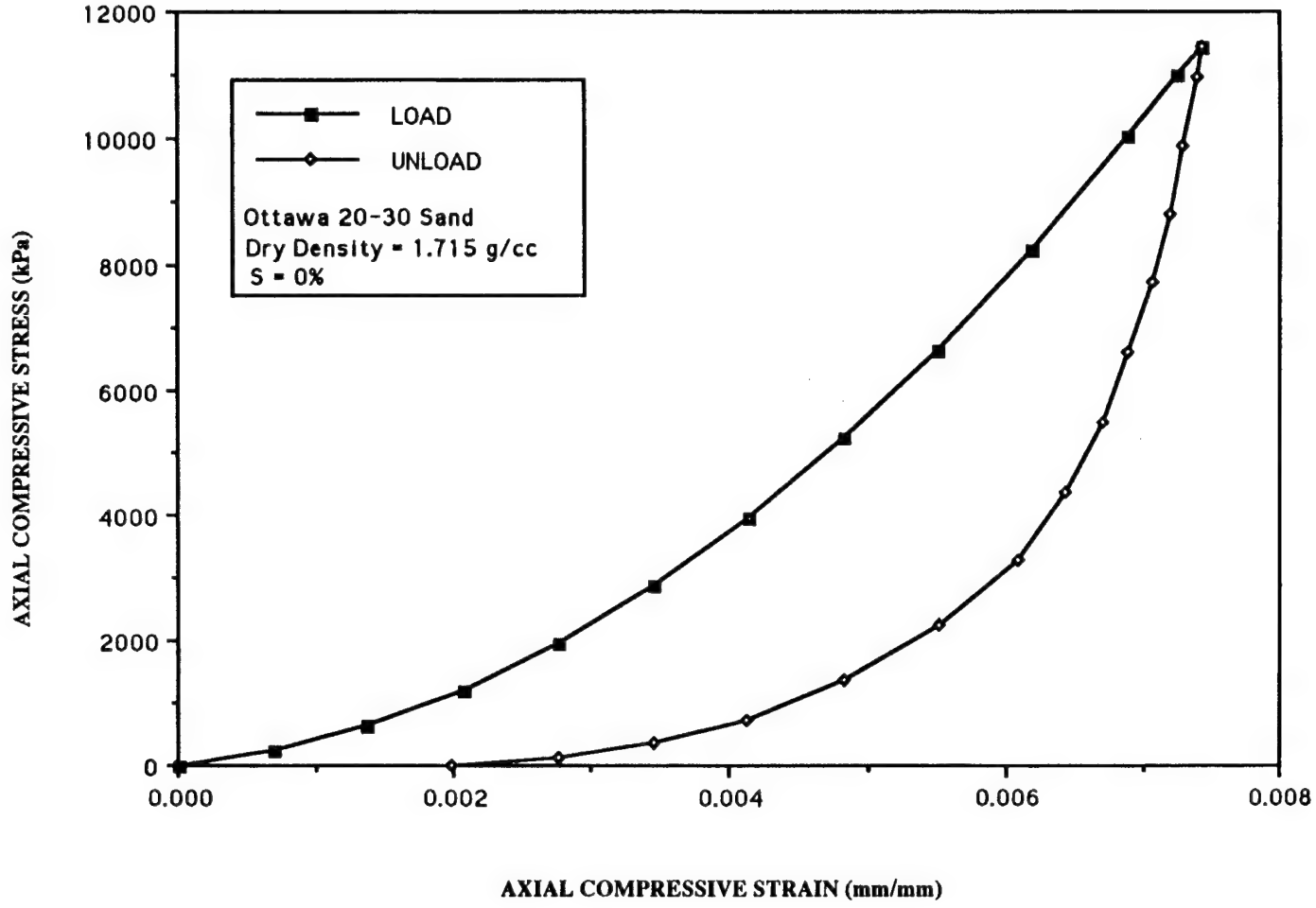

Figure 38. Quasi-Static Stress-Strain Response for Ottawa 20-30 Sand Compacted in Four Layers at S=0%.

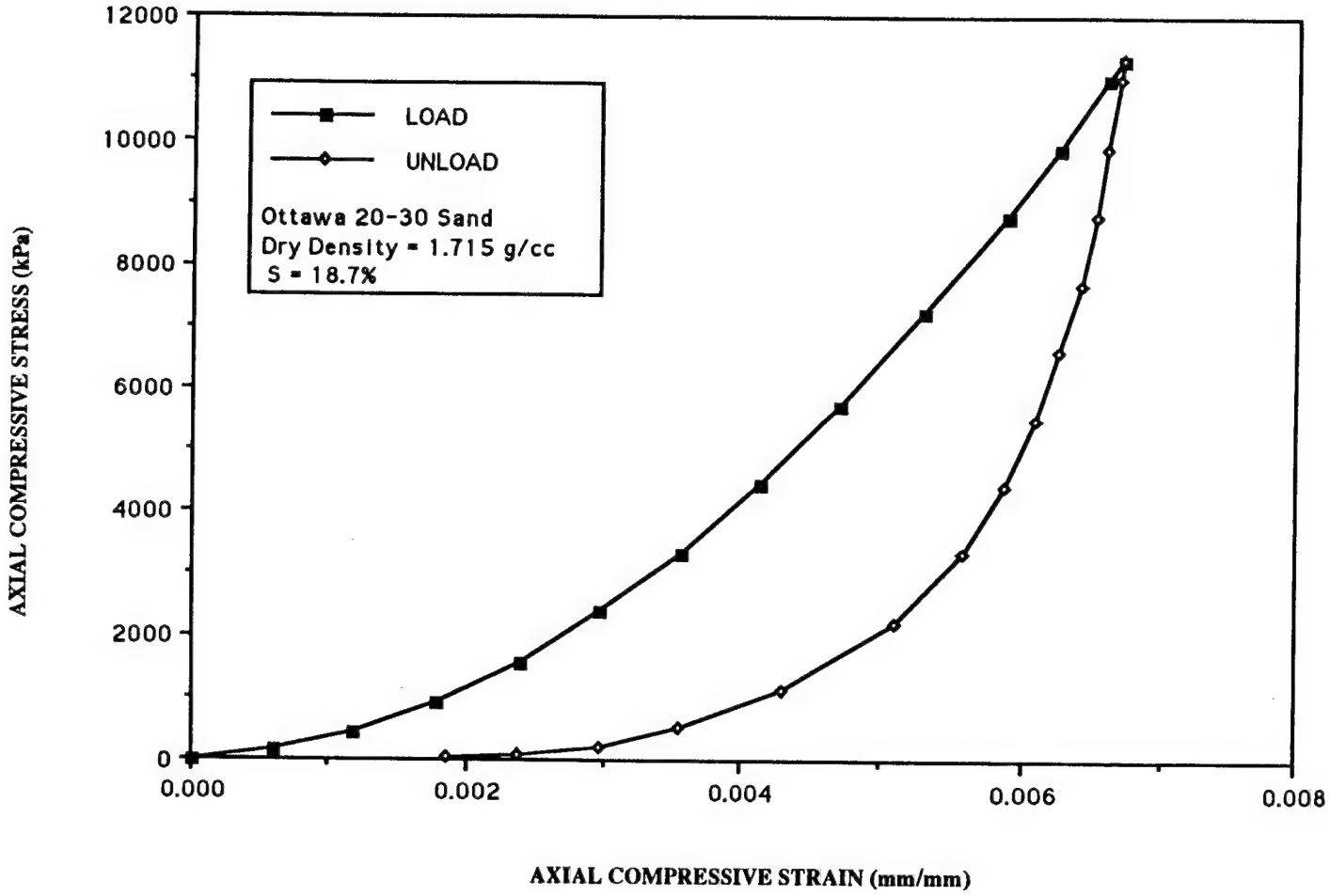

Figure 39. Quasi-Static Stress-Strain Response for Ottawa 20-30 Sand Compacted in Four Layers at S=18.7%.

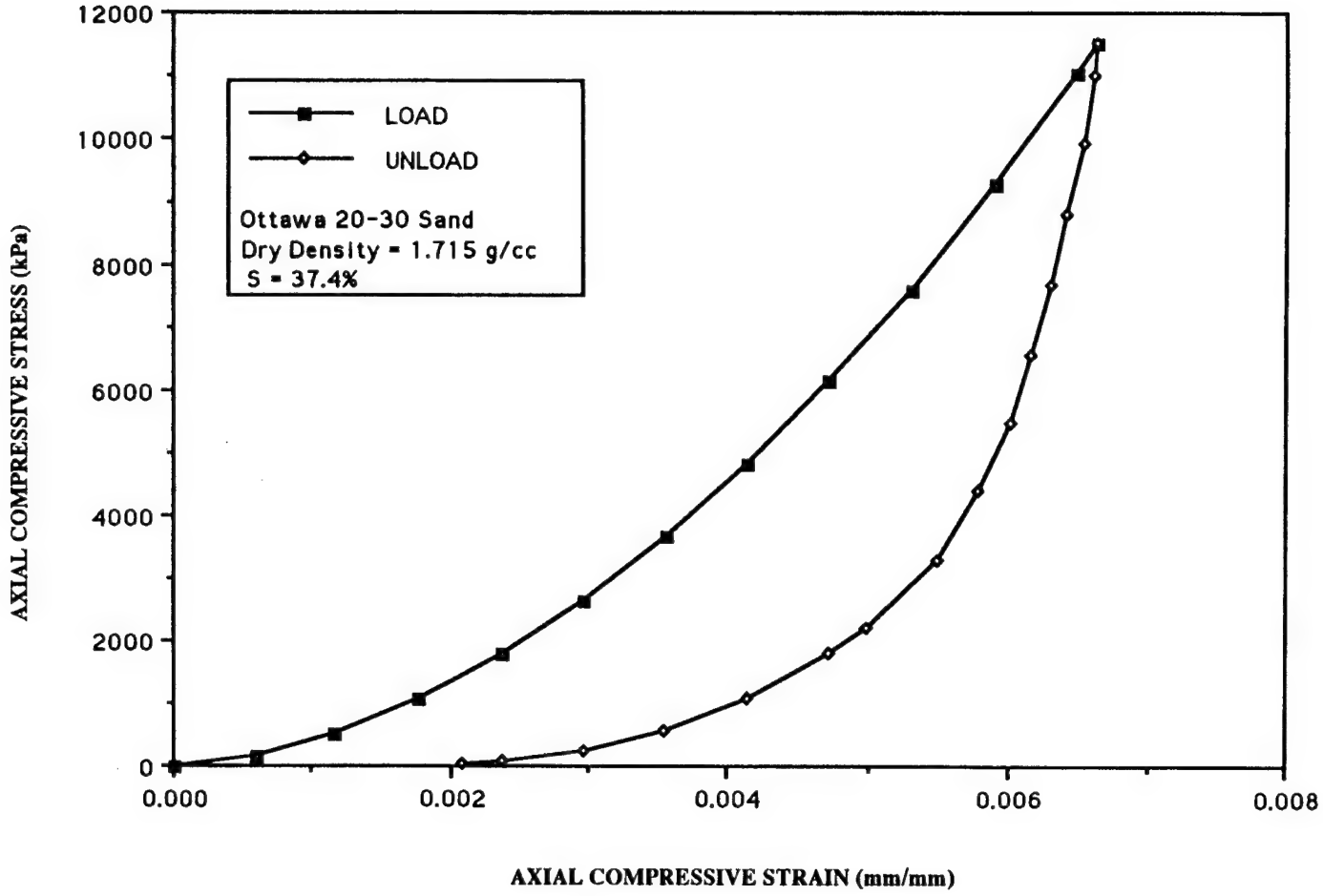

Figure 40. Quasi-Static Stress-Strain Response for Ottawa 20-30 Sand Compacted in Four Layers at S=37.4%.

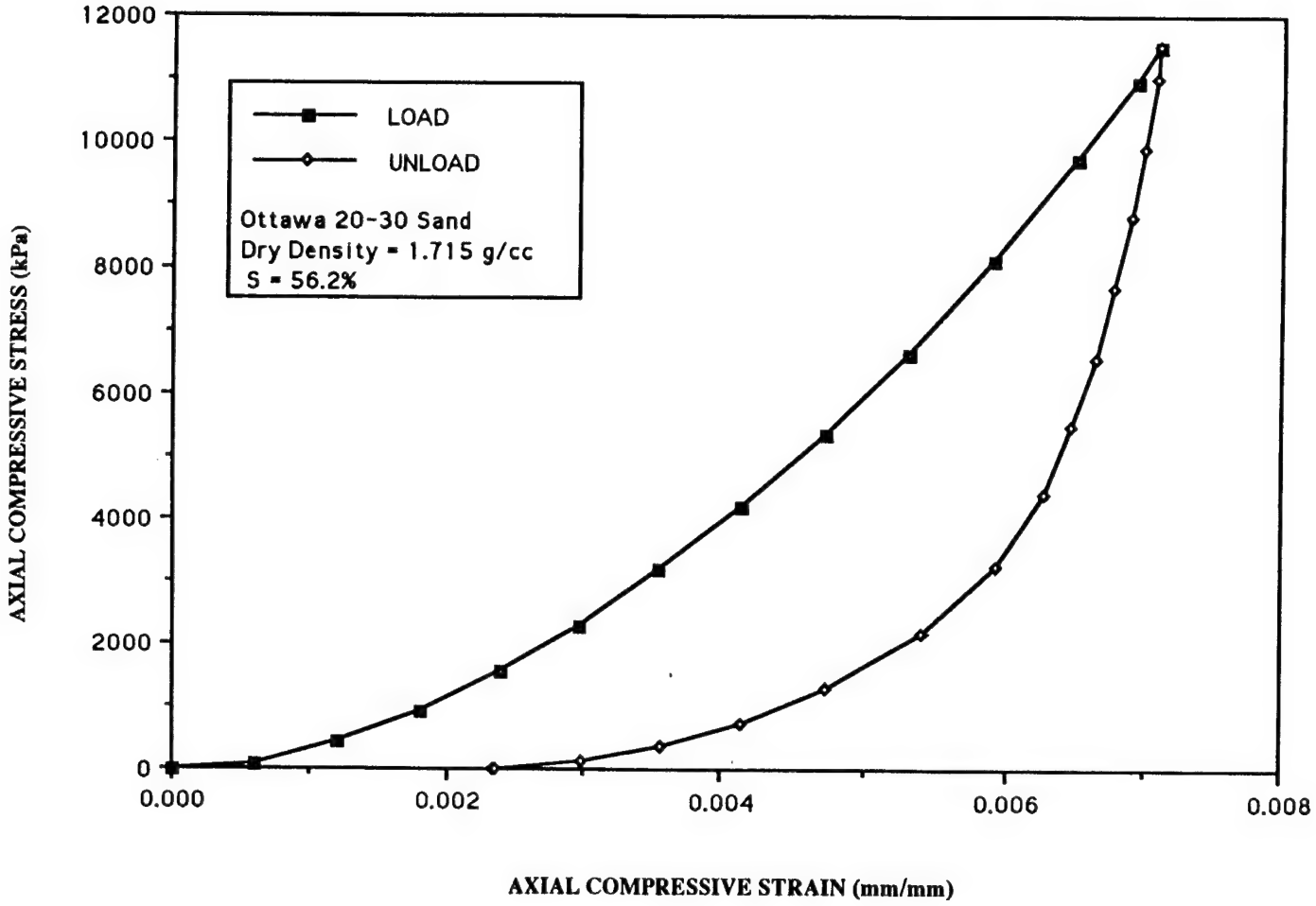

Figure 41. Quasi-Static Stress-Strain Response for Ottawa 20-30 Sand Compacted in Four Layers at S=56.2%.

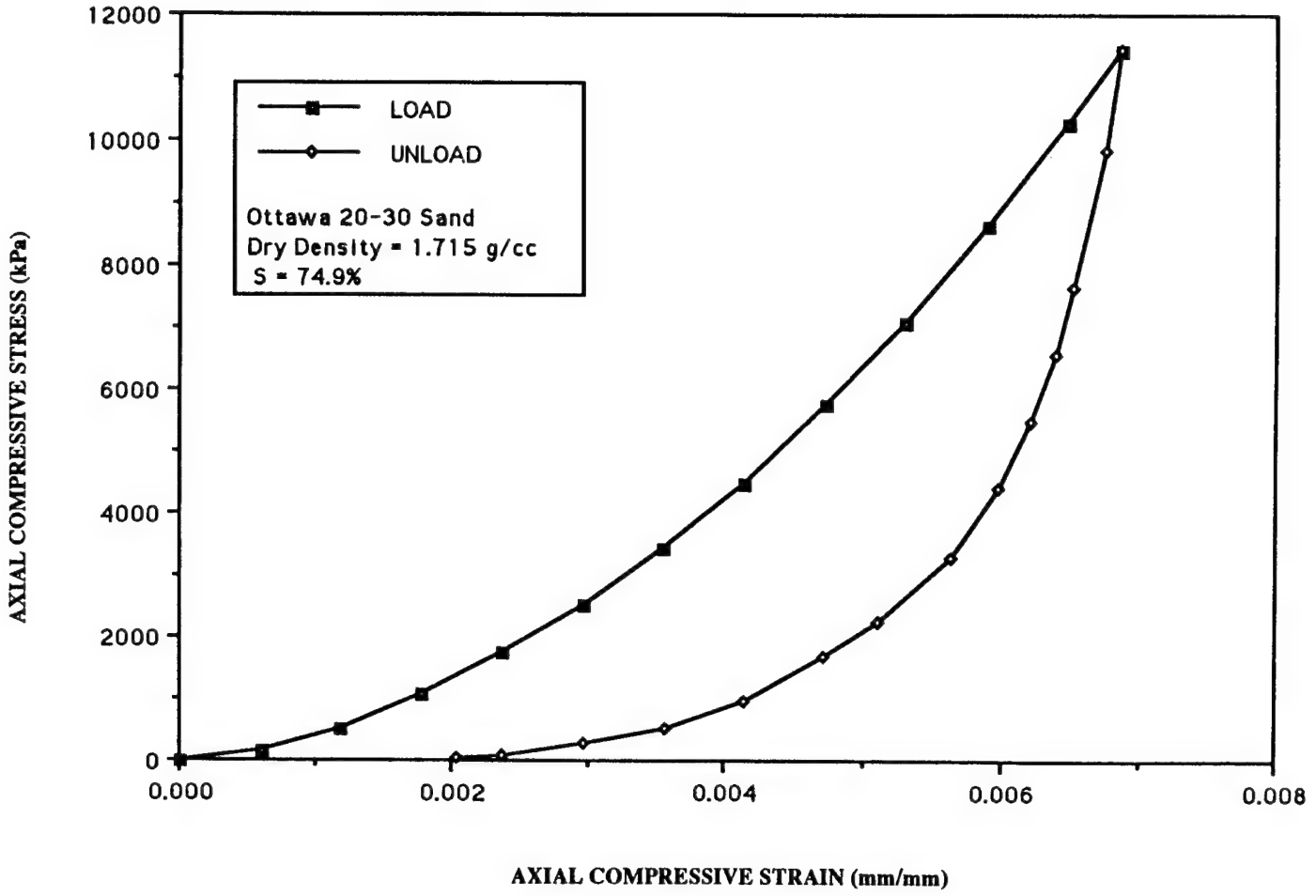

Figure 42. Quasi-Static Stress-Strain Response for Ottawa 20-30 Sand Compacted in Four Layers at S=74.9%.

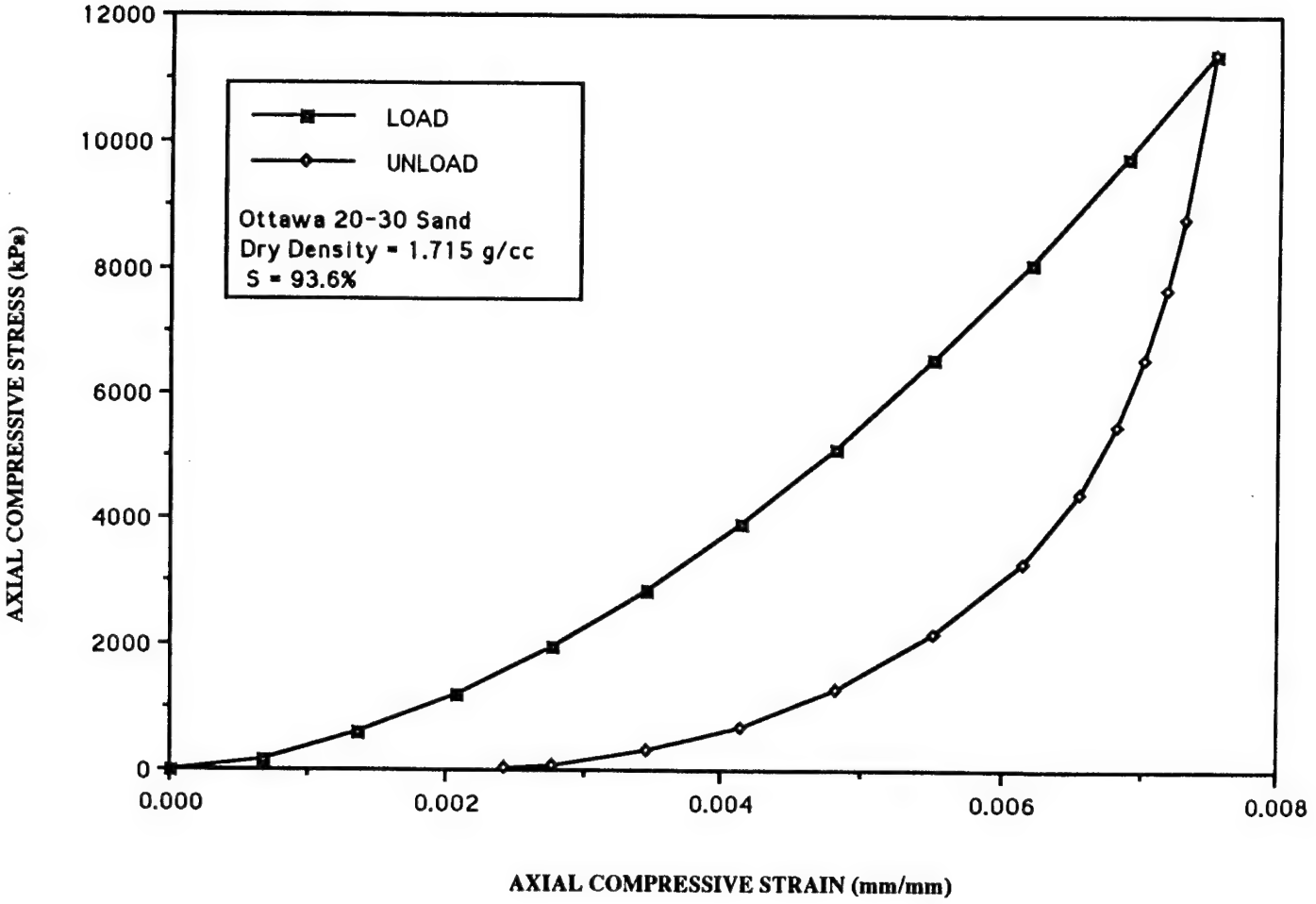

Figure 43. Quasi-Static Stress-Strain Response for Ottawa 20-30 Sand Compacted in Four Layers at S=93.6%.

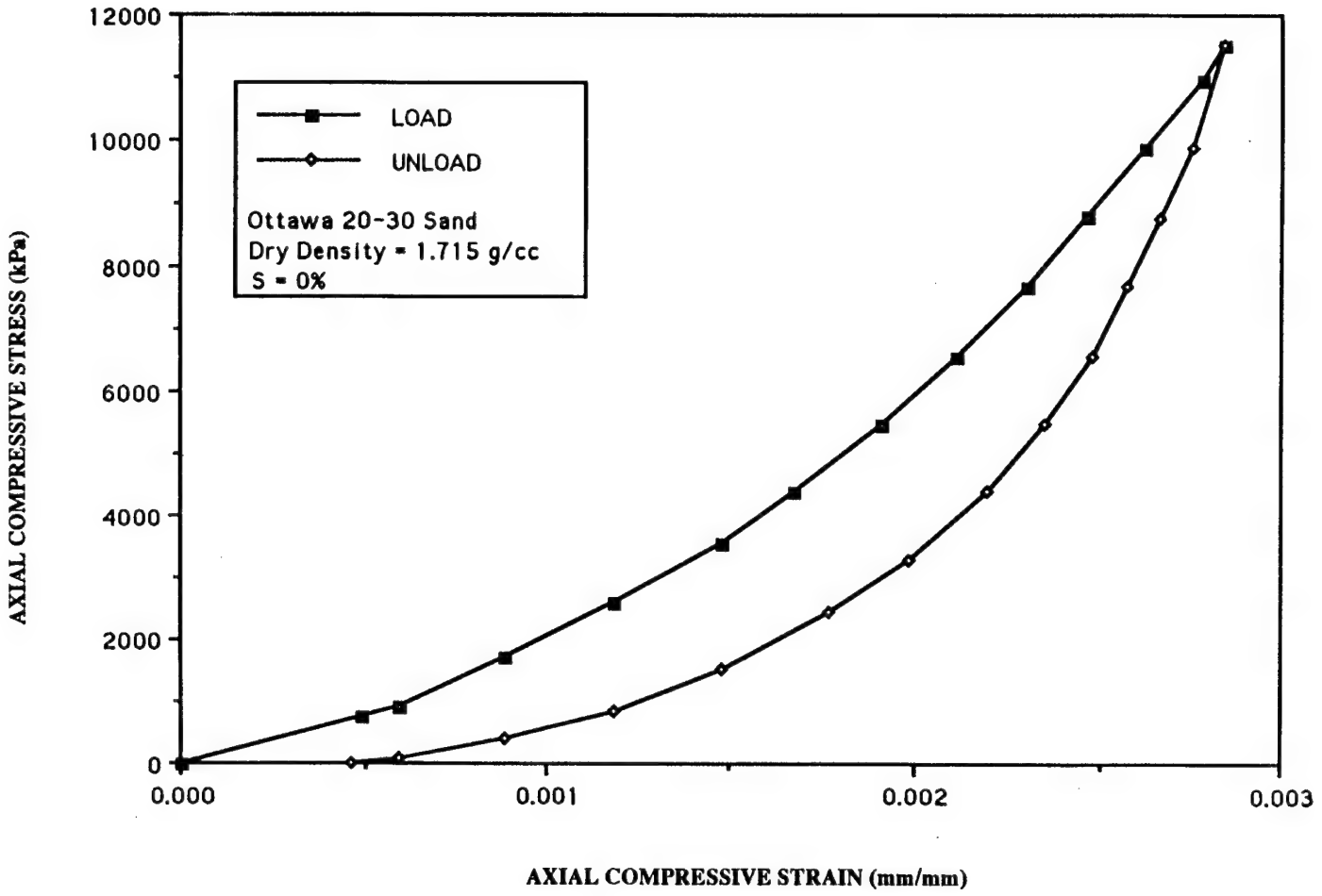

Figure 44. Quasi-Static Stress-Strain Response for Ottawa 20-30 Sand Compacted in One Layer at S=0%.

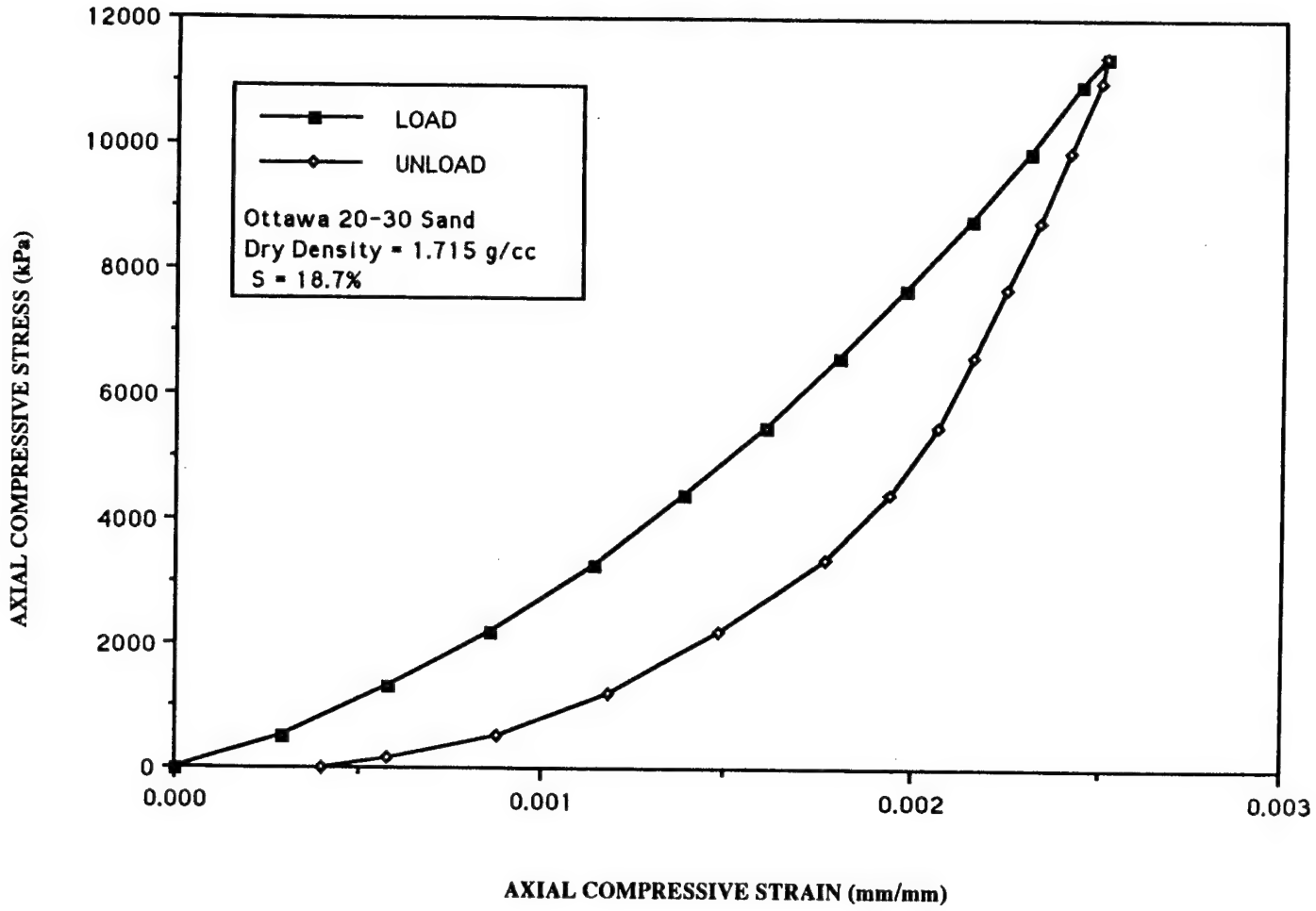

Figure 45. Quasi-Static Stress-Strain Repsonse for Ottawa 20-30 Sand Compacted in One Layer at S=18.7%.

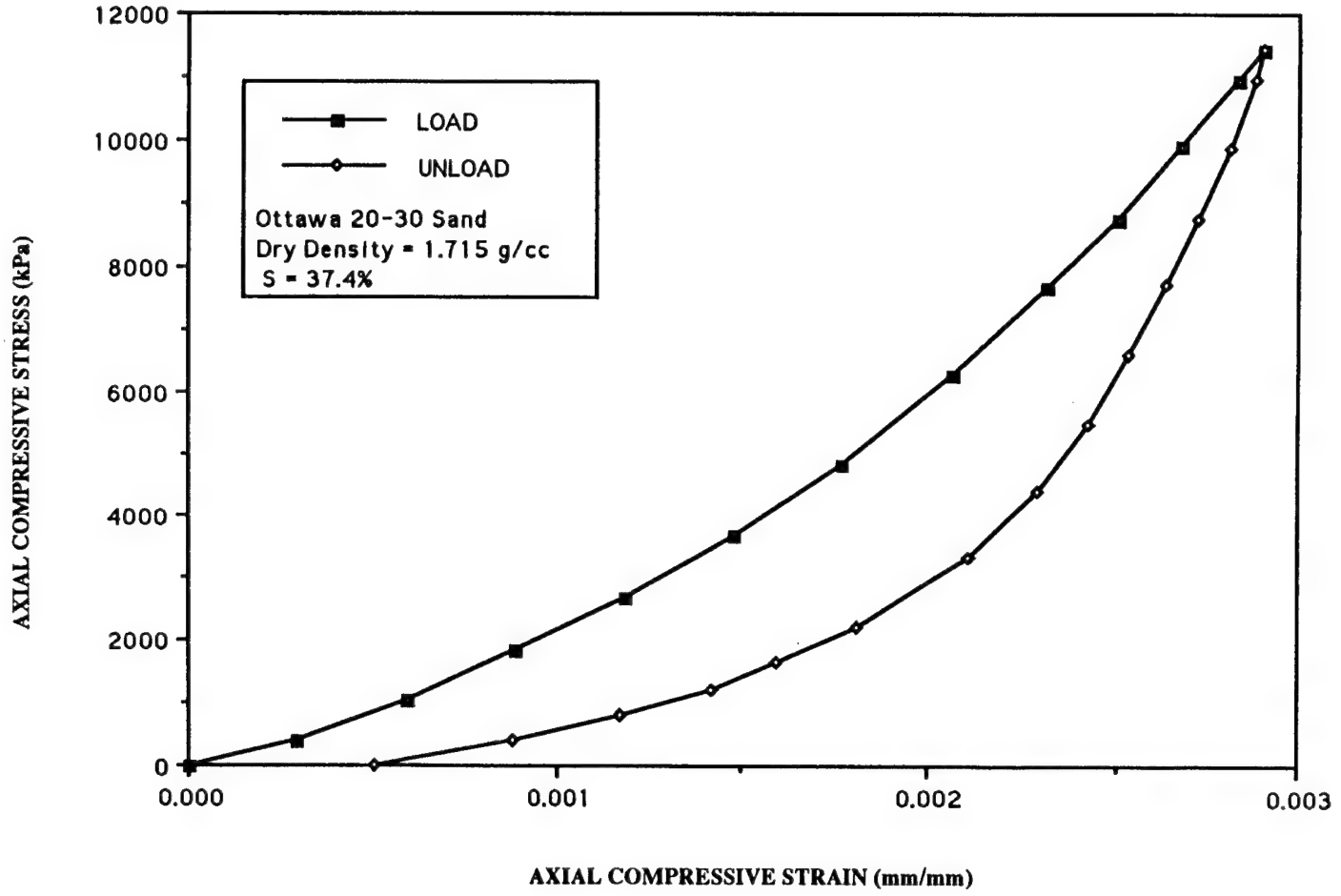

Figure 46. Quasi-Static Stress-Strain Response for Ottawa 20-30 Sand Compacted in One Layer at S=37.4%.

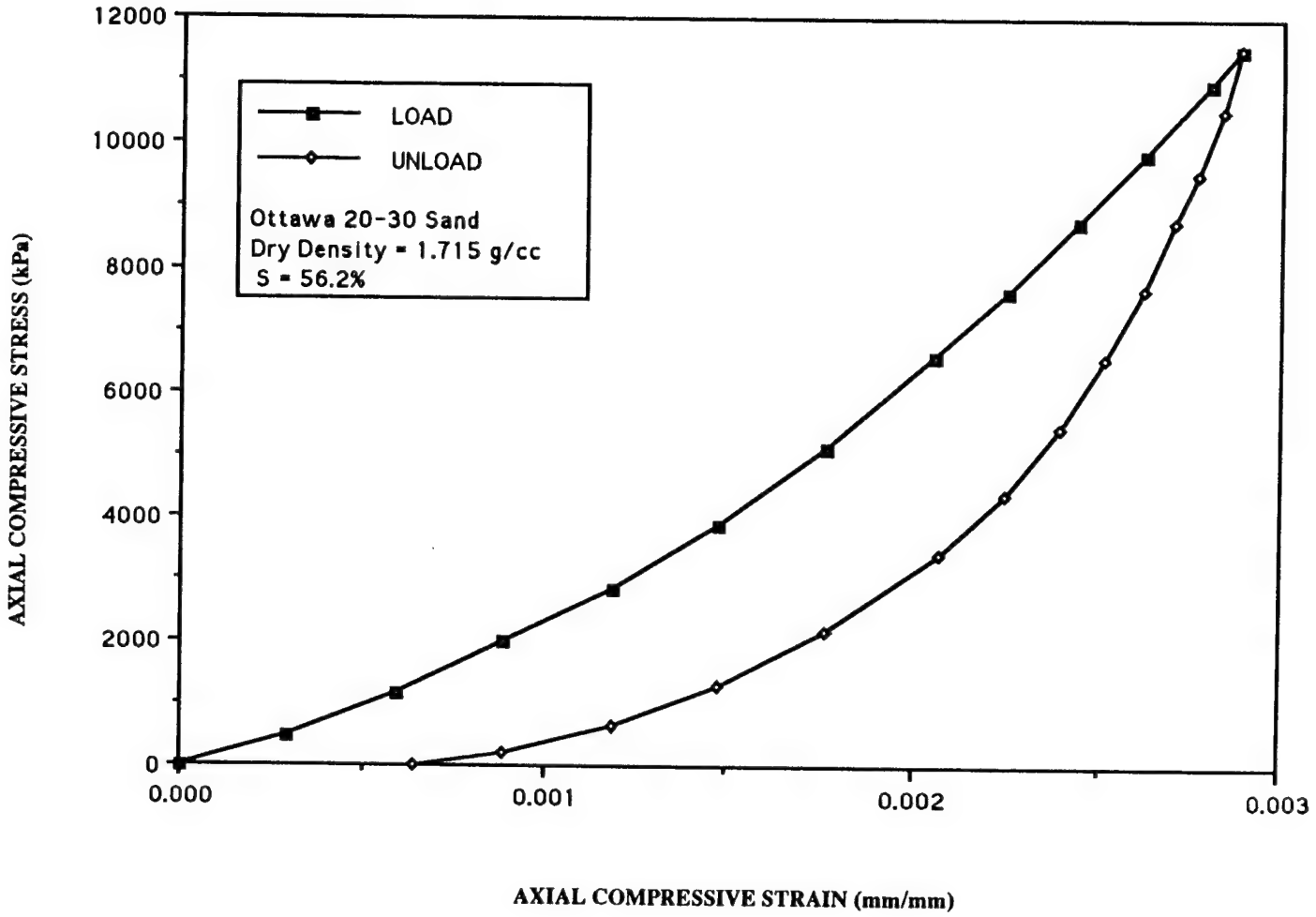

Figure 47. Quasi-Static Stress-Strain Response for Ottawa 20-30 Sand Compacted in One Layer at S=56.2%.

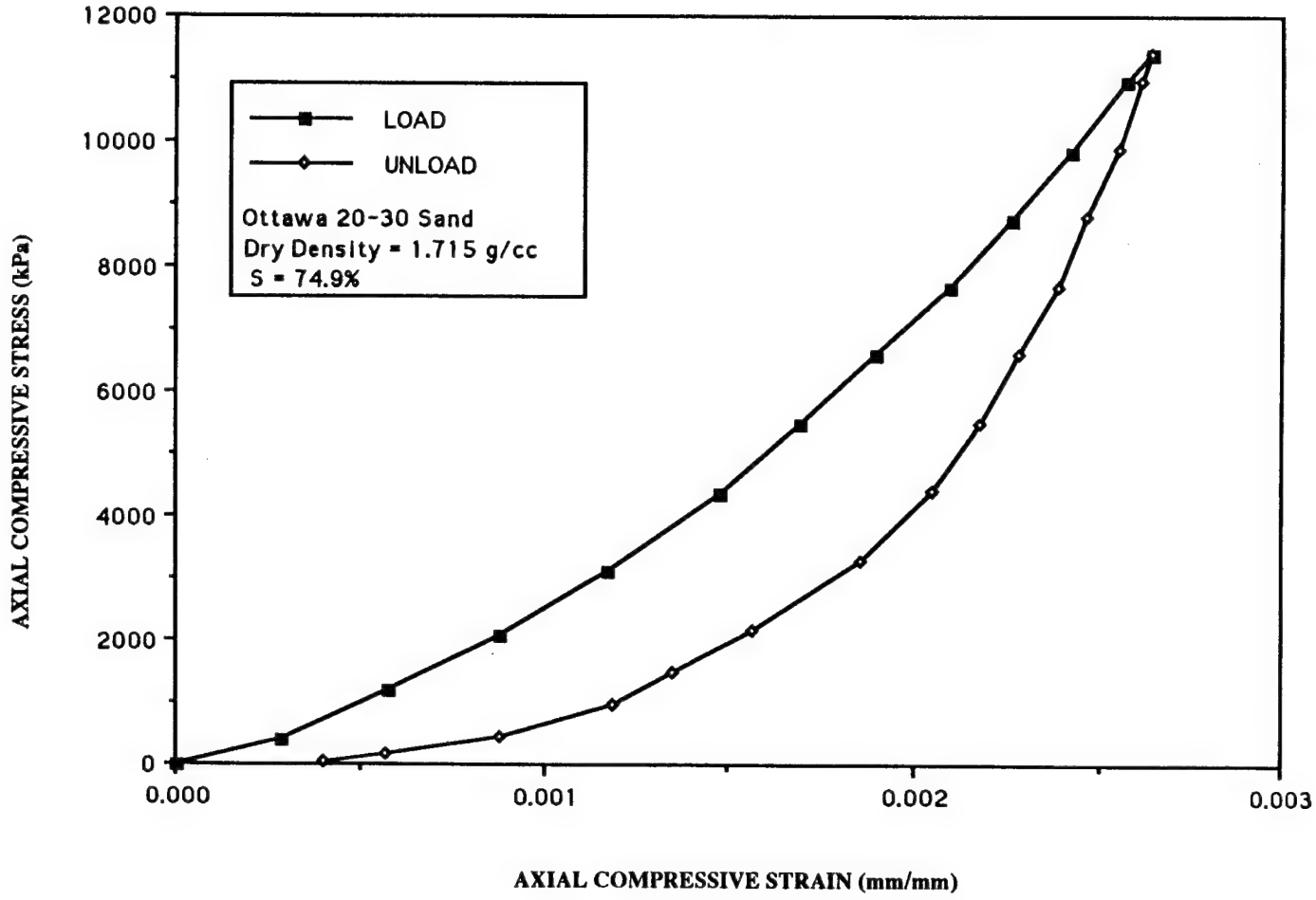

Figure 48. Quasi-Static Stress-Strain Response for Ottawa 20-30 Sand Compacted in One Layer at S=74.9%.

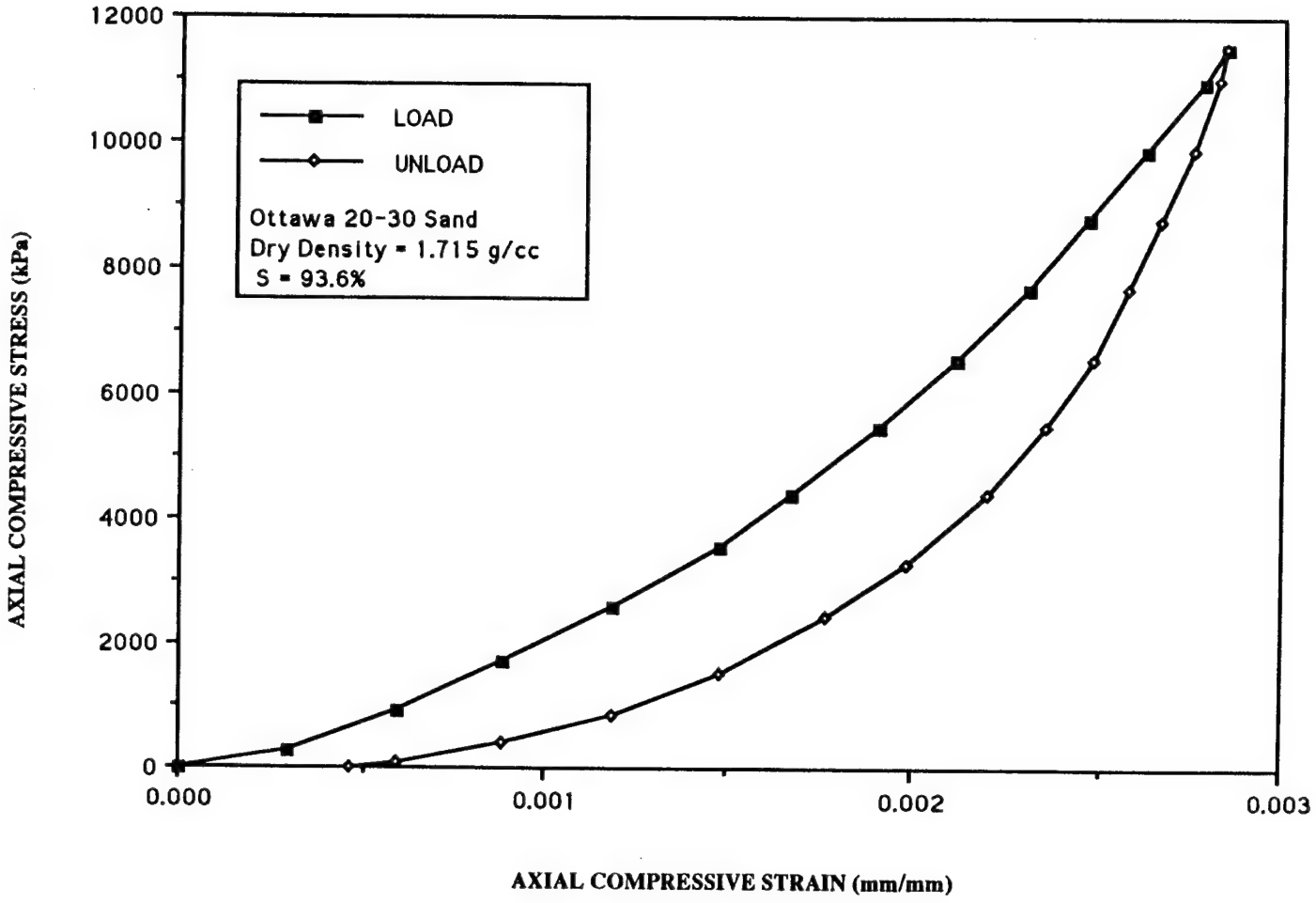

Figure 49. Quasi-Static Stress-Strain Response for Ottawa 20-30 Sand Compacted in One Layer at S=93.6%.

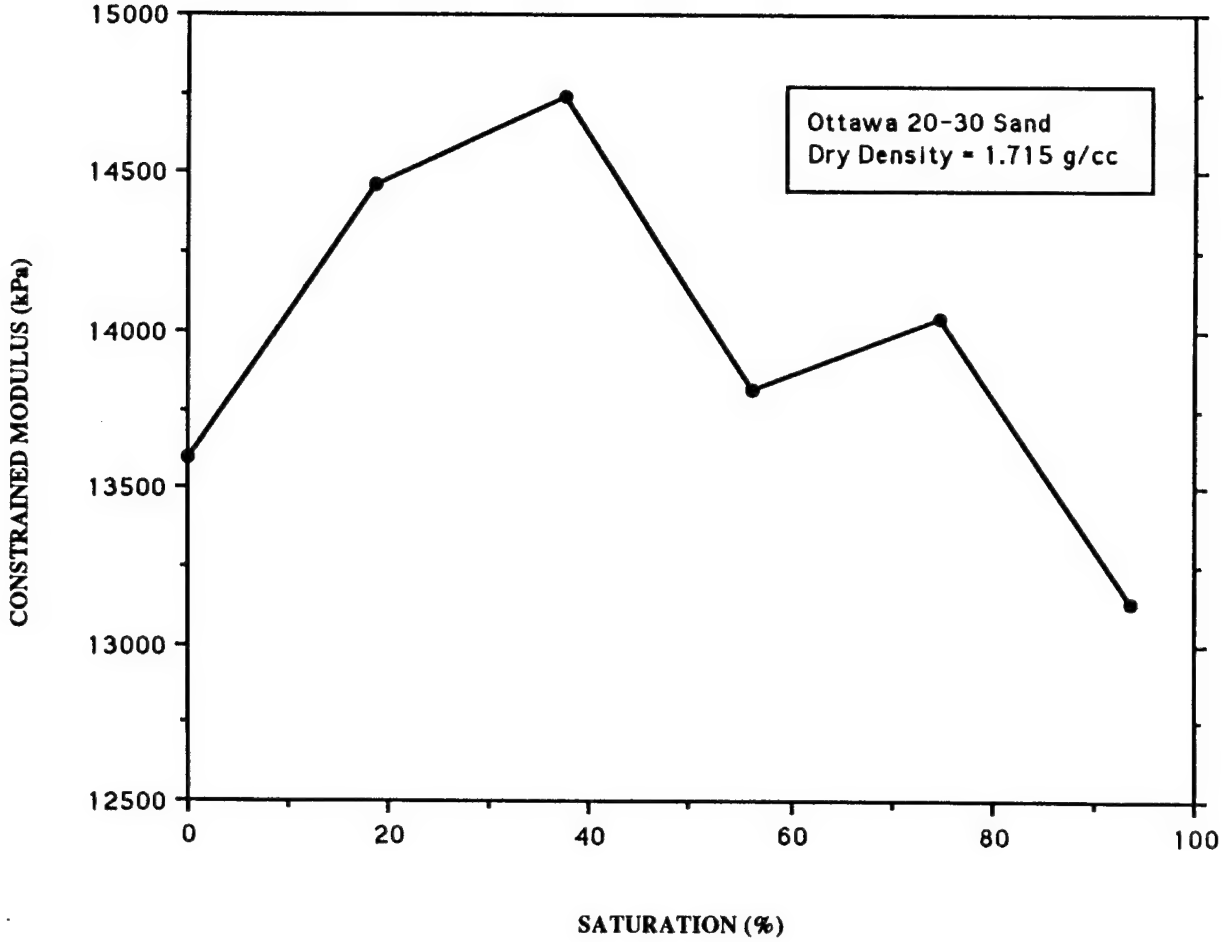

Figure 50. Constrained Modulus as a Function of Saturation for Quasi-Static Testing of Ottawa 20-30 Sand Compacted Moist and Tested Moist.

percent saturation. The constrained modulus then decreases from about 40 percent to about 60 percent saturation and slightly increases from about 60 percent to about 75 percent saturation, sharply decreasing thereafter.

E. MICROSTRUCTURAL ANALYSIS

1. Axial Ratio

Figure 51 shows the results of the axial ratio particle analysis and is a composite plot of more than 2500 individual particles which were manually analyzed using the method developed by Campbell (1985). The results for the Ottawa 20-30 sand indicate that the average axial ratio, n_{avg}, is 0.674 and the standard deviation is 0.106. This indicates that the particles are approaching a spherical shape. Axial ratio values ranged from a minimum of 0.253 to a maximum of 0.968. Based on the axial ratio data obtained, the Ottawa 20-30 sand would be classified as consisting of well rounded particles according to the criteria shown in Table 1.

2. Rose Diagrams

Particle long-axis orientations are represented by rose diagrams (angular frequency histograms). A total of 70 rose diagrams were generated from azimuth data obtained by digitizing a number of two-dimensional particle images using two main categories (see Appendix A Figures A.1 through A.70). The first set of rose diagrams includes specimens compacted using the standard Proctor hammer only (NO SHPB) and the second set of rose diagrams include specimens compacted using the standard Proctor hammer and then tested in the SHPB device (SHPB).

The two sets of rose diagrams (NO SHPB and SHPB) were further subdivided into; (a) horizontal, vertical, and semicircular rose diagrams (a total of 30 rose diagrams), and (b) Layers 1, 2, 3, and 4 in the vertical plane (a total of 40 rose diagrams). Rose diagrams for each of the four layers were developed using grids h, i, j, k, d, l, m, n, and o from Section A-A in the vertical plane (see Figure 27). Each layer consisted of two and one-quarter grids, (eg. Layer 1 used grids o, n, and one-fourth of grid m). The complete set of rose diagrams can be found in Appendix A.

Statistics provided within the "ROSY" software provide the following data: the number of particles measured, the maximum percentage of particles that fall within a given class interval, the mean and standard deviation of this percentage, vector mean, confidence angle, vector magnitude, and Rayleigh test of significance. A summary of the statistical

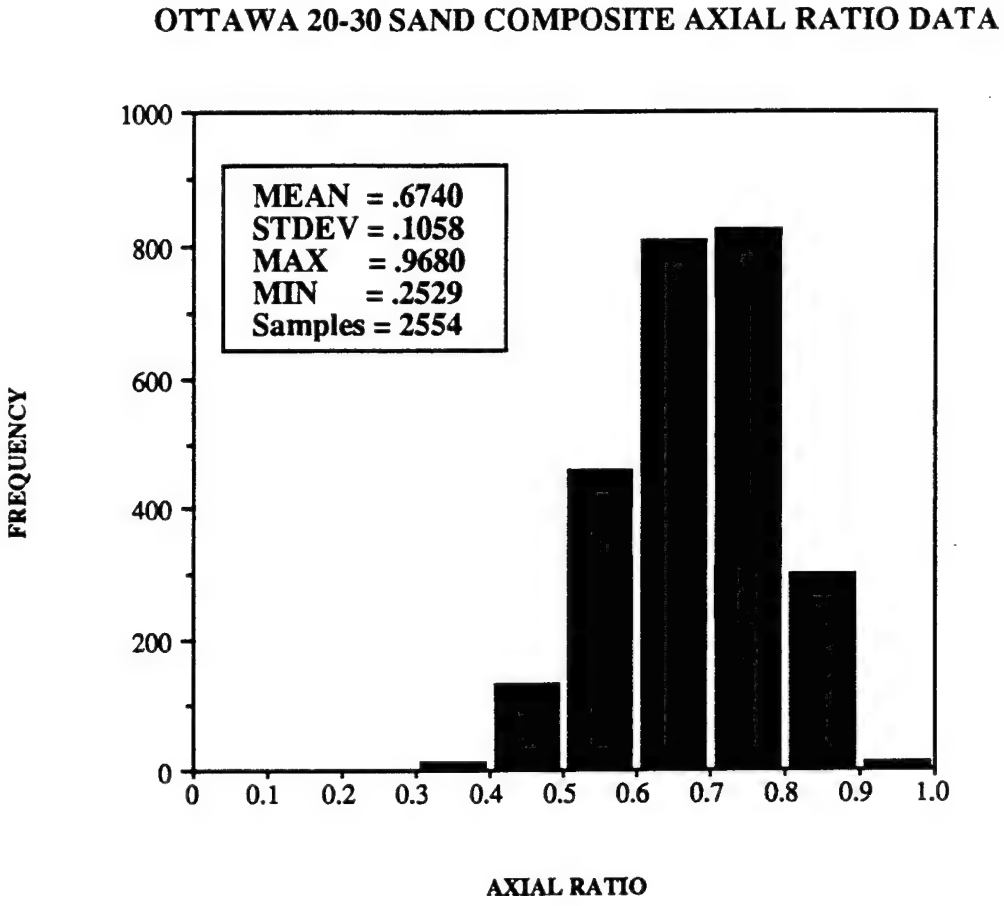

Figure 51. Axial Ratio Histogram for Ottawa 20-30 Sand Particles.

data generated by ROSY for each rose diagram has been compiled in Tables 6 and 7. A description of each heading used in rose diagrams and in Tables 6 and 7 is given in Table 8. A typical rose diagram is presented in Figure 52. This figure shows how to interpret the rose diagram statistics output by Rosy. Comparisons of the results from the statistical analysis of all 70 rose diagrams will be discussed in SECTION V.

Table 6 shows the final results of the number of particles measured for each rose diagram, N, maximum percentage, vector mean, confidence angle, vector magnitude, and Rayleigh test of significance as a function of saturation for the horizontal, vertical, and semicircular sections, and Layers 1, 2, 3, and 4 in the vertical plane on Section A-A (see Figure 27), for NO SHPB specimens. Table 7 shows the final results as a function of saturation for the horizontal, vertical, and semicircular sections, and Layers 1, 2, 3, and 4 in the vertical plane on Section A-A (see Figure 27), for SHPB specimens. All data were collected from rose diagrams generated by the ROSY program.

The Rosy data given in Tables 6 and 7 show that the semicircular plane has the highest Rayleigh values and lowest vector magnitude values. This indicates that there is no preferred particle orientation in any semicircular plane. The number of particles measured in the semicircular plane (150 to 310) are much lower than those measured in the horizontal or vertical planes (280 to 760). Only 4 grids (p through s) were available for measurement in the semicircular plane, whereas the horizontal plane had 7 grids (a through g), the vertical plane had and 9 grids (h through o, including d). Oda (1972a) and Campbell (1985) stated that a minimum of 200 to 300 particles need to be measured for a particle orientation analysis. Therefore, due to the limited amount of data for the semicircular plane, those results will not be analyzed in SECTION V. However, data for the vertical and horizontal planes show Rayleigh values less than 0.05 and high vector magnitude values which indicates there is a preferred particle orientation in these planes. Therefore, the microstructural analysis presented in SECTION V will focus on results for the vertical and horizontal planes.

3. Particle Long-Axis Orientation

Figure 53 shows vector magnitude as a function of saturation in the horizontal (upper portion of Layer 2 and lower portion of Layer 3), vertical (Layers 1 through 4), and semicircular planes for NO SHPB specimens (see Figure 25). In the horizontal and vertical planes the vector magnitude tends to be lower at intermediate saturations and higher at zero percent and about 75 percent saturation. In the semicircular plane, the vector magnitude tends to be higher at intermediate saturations and lower at 0 percent and 80 percent

TABLE 6. STATISTICAL RESULTS FOR MICROSTRUCTURAL ANALYSIS OF NO SHPB SPECIMENS.

S%	N	Max. %	V.M.	Conf Angle	R. Mag.	Rayleigh	Section
0.0	615	8.6	277.8	17.54	0.182	0.0000	horizontal
18.7	487	9.7	280.8	23.68	0.152	0.0000	horizontal
37.4	618	9.5	274.4	17.73	0.177	0.0000	horizontal
56.2	636	9.6	88.3	22.62	0.137	0.0000	horizontal
74.9	672	9.5	270.0	12.69	0.236	0.0000	horizontal

S%	N	Max. %	V.M.	Conf Angle	R. Mag.	Rayleigh	Section
0.0	607	9.1	275.0	13.22	0.240	0.0000	vertical
18.7	287	10.1	85.6	52.26	0.089	0.1028	vertical
37.4	626	10.1	276.8	17.39	0.182	0.0000	vertical
56.2	729	11.7	87.9	13.21	0.220	0.0000	vertical
74.9	764	9.8	89.1	12.44	0.226	0.0000	vertical

S%	N	Max. %	V.M.	Conf Angle	R. Mag.	Rayleigh	Section
0.0	245	9.4	79.4	227.13	0.025	0.8587	semi-circular
18.7	250	9.2	272.9	63.29	0.078	0.2146	semi-circular
37.4	310	8.7	25.3	87.98	0.052	0.4256	semi-circular
56.2	265	9.8	291.9	53.65	0.091	0.1089	semi-circular
74.9	237	8.4	38.5	85.43	0.061	0.4183	semi-circular

S%	N	Max. %	V.M.	Conf Angle	R. Mag.	Rayleigh	Layer #
0.0	69	21.7	290.0	25.52	0.363	0.0001	1
18.7	147	13.6	279.2	18.22	0.245	0.0000	1
37.4	160	11.2	78.5	21.34	0.285	0.0000	1
56.2	164	12.8	82.8	22.66	0.267	0.0000	1
74.9	177	10.7	86.4	31.15	0.190	0.0017	1

S%	N	Max. %	V.M.	Conf Angle	R. Mag.	Rayleigh	Layer #
0.0	197	11.2	270.3	29.54	0.190	0.0008	2
18.7	151	9.9	73.3	39.64	0.164	0.0173	2
37.4	179	12.3	276.2	27.80	0.212	0.0003	2
56.2	181	13.8	88.3	19.97	0.288	0.0000	2
74.9	189	10.1	81.7	24.54	0.234	0.0000	2

S%	N	Max. %	V.M.	Conf Angle	R. Mag.	Rayleigh	Layer #
0.0	213	8.9	89.1	33.28	0.165	0.0030	3
18.7	90	8.9	299.2	60.07	0.137	0.1833	3
37.4	186	11.8	296.4	31.96	0.181	0.0022	3
56.2	202	9.9	89.7	40.17	0.137	0.0228	3
74.9	218	12.4	275.0	19.54	0.270	0.0000	3

S%	N	Max. %	V.M.	Conf Angle	R. Mag.	Rayleigh	Layer #
0.0	128	12.5	275.5	16.26	0.414	0.0000	4
18.7	15	20.0	336.9	84.43	0.238	0.4261	4
37.4	101	12.9	290.3	53.17	0.146	0.1176	4
56.2	181	12.7	271.4	28.07	0.206	0.0005	4
74.9	179	11.2	270.2	27.85	0.211	0.0003	4

TABLE 7. STATISTICAL RESULTS FOR MICROSTRUCTURAL ANALYSIS OF SHPB SPECIMENS.

S%	N	Max. %	V.M.	Conf Angle	R. Mag.	Rayleigh	Section
0.0	420	14.3	279.4	9.05	0.407	0.0000	horizontal
18.7	742	12.4	274.0	12.38	0.234	0.0000	horizontal
37.4	556	10.4	271.6	13.79	0.241	0.0000	horizontal
56.2	554	10.3	273.2	16.62	0.202	0.0000	horizontal
74.9	510	10.4	275.8	20.29	0.174	0.0000	horizontal

S%	N	Max. %	V.M.	Conf Angle	R. Mag.	Rayleigh	Section
0.0	544	13.6	279.6	9.43	0.348	0.0000	vertical
18.7	738	10.8	88.8	10.70	0.266	0.0000	vertical
37.4	455	14.5	278.6	11.25	0.324	0.0000	vertical
56.2	632	10.4	272.1	13.67	0.226	0.0000	vertical
74.9	607	11.9	281.2	12.07	0.265	0.0000	vertical

S%	N	Max. %	V.M.	Conf Angle	R. Mag.	Rayleigh	Section
0.0	159	10.7	312.0	158.58	0.039	0.7813	semi-circular
18.7	320	9.7	270.7	40.76	0.107	0.0253	semi-circular
37.4	218	11.5	278.9	135.59	0.039	0.7141	semi-circular
56.2	229	9.2	291.5	52.73	0.099	0.1083	semi-circular
74.9	191	8.4	293.7	72.28	0.079	0.3060	semi-circular

S%	N	Max. %	V.M.	Conf Angle	R. Mag.	Rayleigh	Layer #
0.0	113	14.2	275.4	21.31	0.340	0.0000	1
18.7	182	11.0	87.1	21.49	0.267	0.0000	1
37.4	87	13.8	276.2	18.23	0.444	0.0000	1
56.2	239	11.7	83.3	17.33	0.290	0.0000	1
74.9	145	12.4	88.3	29.73	0.218	0.0010	1

S%	N	Max. %	V.M.	Conf Angle	R. Mag.	Rayleigh	Layer #
0.0	129	13.2	274.9	19.93	0.348	0.0000	2
18.7	205	13.2	271.4	16.96	0.317	0.0000	2
37.4	114	16.7	209.4	17.39	0.406	0.0000	2
56.2	139	13.7	84.8	37.38	0.177	0.0126	2
74.9	170	12.9	275.3	15.06	0.386	0.0000	2

S%	N	Max. %	V.M.	Conf Angle	R. Mag.	Rayleigh	Layer #
0.0	174	14.9	285.1	16.22	0.357	0.0000	3
18.7	179	11.7	274.9	23.37	0.250	0.0000	3
37.4	137	10.9	88.4	29.12	0.230	0.0007	3
56.2	177	10.2	284.1	22.69	0.257	0.0000	3
74.9	145	15.2	281.8	18.33	0.346	0.0000	3

S%	N	Max. %	V.M.	Conf Angle	R. Mag.	Rayleigh	Layer #
0.0	128	12.5	280.3	18.74	0.363	0.0000	4
18.7	172	13.4	80.1	24.81	0.241	0.0000	4
37.4	117	18.8	275.4	22.42	0.317	0.0000	4
56.2	161	11.2	277.7	26.92	0.229	0.0000	4
74.9	147	9.5	307.6	31.18	0.205	0.0020	4

saturation. Figure 54 shows vector magnitude as a function of saturation in the horizontal, vertical, and semicircular planes for SHPB specimens. In the horizontal and vertical planes the vector magnitude tends to be lower at all saturations and higher at zero percent saturation. In the semicircular plane the vector magnitude tends to be higher at intermediate saturations and lower at zero percent and about 75 percent saturation. SHPB specimens should have higher vector magnitudes since they were tested in the split-Hopkinson pressure bar device after compaction.

TABLE 8. DESCRIPTION OF STATISTICS USED IN ROSY PROGRAM.

N - The number of particles measured for each rose diagram.

Class Interval - The width of each petal on the rose diagram (10-degree intervals for this investigation).

Max. % - The maximum percentage of particles that occur on a given cell (or petal of the rose diagram).

Mean % - Mean percentage of the average percent of all data.

Standard Deviation - Standard deviation of the mean percentage.

Vector Mean - the average azimuth of all particles measured.

Conf. Angle - Confidence angle. For a confidence interval of 95 percent, this shows that 95 percent of the particles measured lie within some angle ± of the vector mean.

R. Magnitude. - Vector magnitude, values range from 0.0 to 1.0, data sets which have large dispersion will have R. Mag. values near 0.0, data sets with very small dispersions will have R. Mag. values near 1.0.

Rayleigh - Rayleigh test of significance, if a value of 0.05 or greater occurs, then the data is said to be no good and no preferred particle orientation exists. If a value < 0.05 is encountered, then a preferred particle orientation exists within the sample.

Figures 55 through 58 compare vector magnitude as a function of saturation for each individual compacted layer (NO SHPB or SHPB). In nearly all cases, the vector magnitude is higher for SHPB specimens as compared to NO SHPB specimens. For SHPB specimens the vector magnitude tends to be higher at zero percent saturation and lower at all other saturations. For NO SHPB specimens a general trend occurs throughout most of the four layers in that the vector magnitude tends to be lower at intermediate saturations and higher at zero percent and about 75 percent saturation.

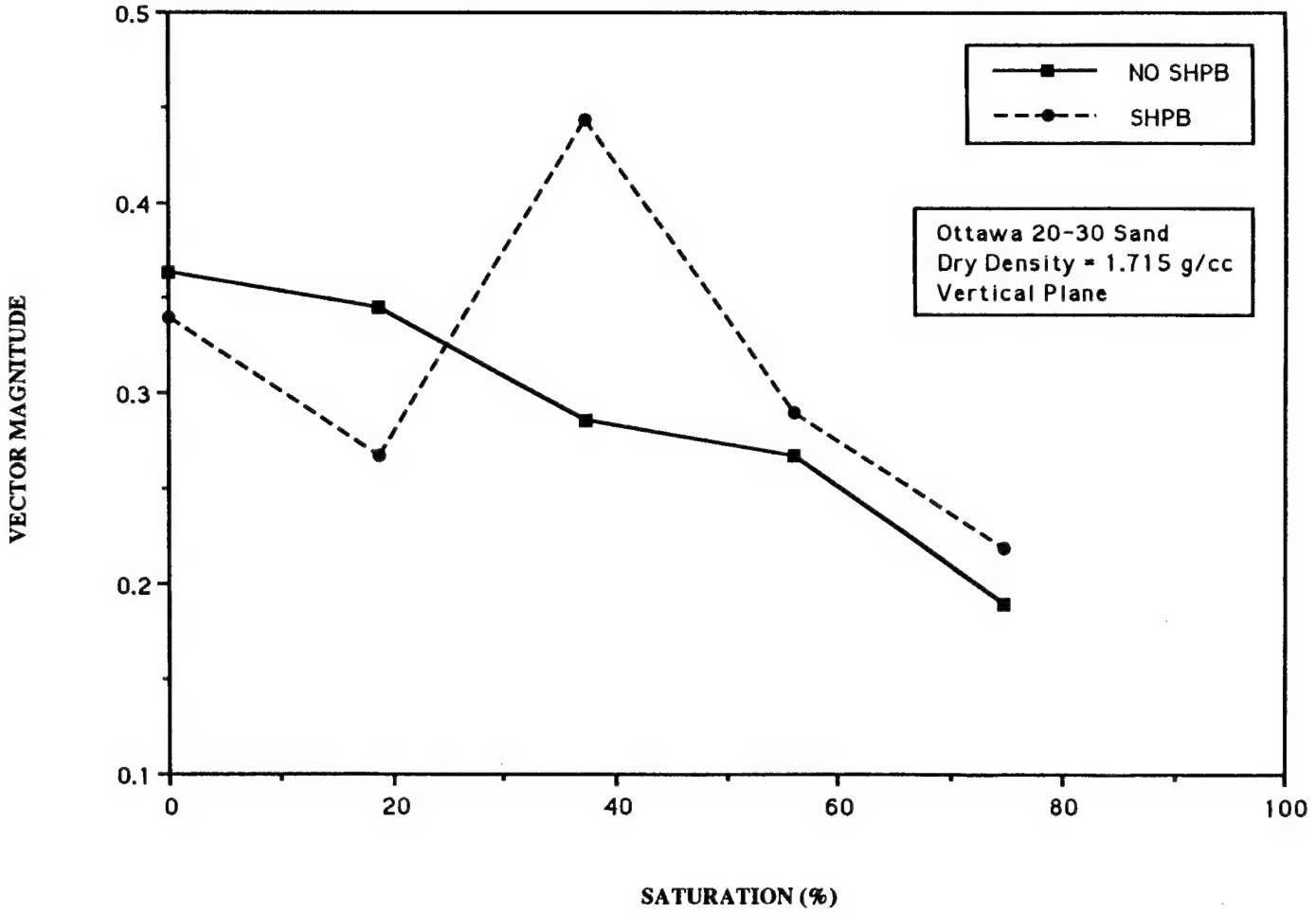

Figure 55. Vector Magnitude as a Function of Saturation for Layer #1.

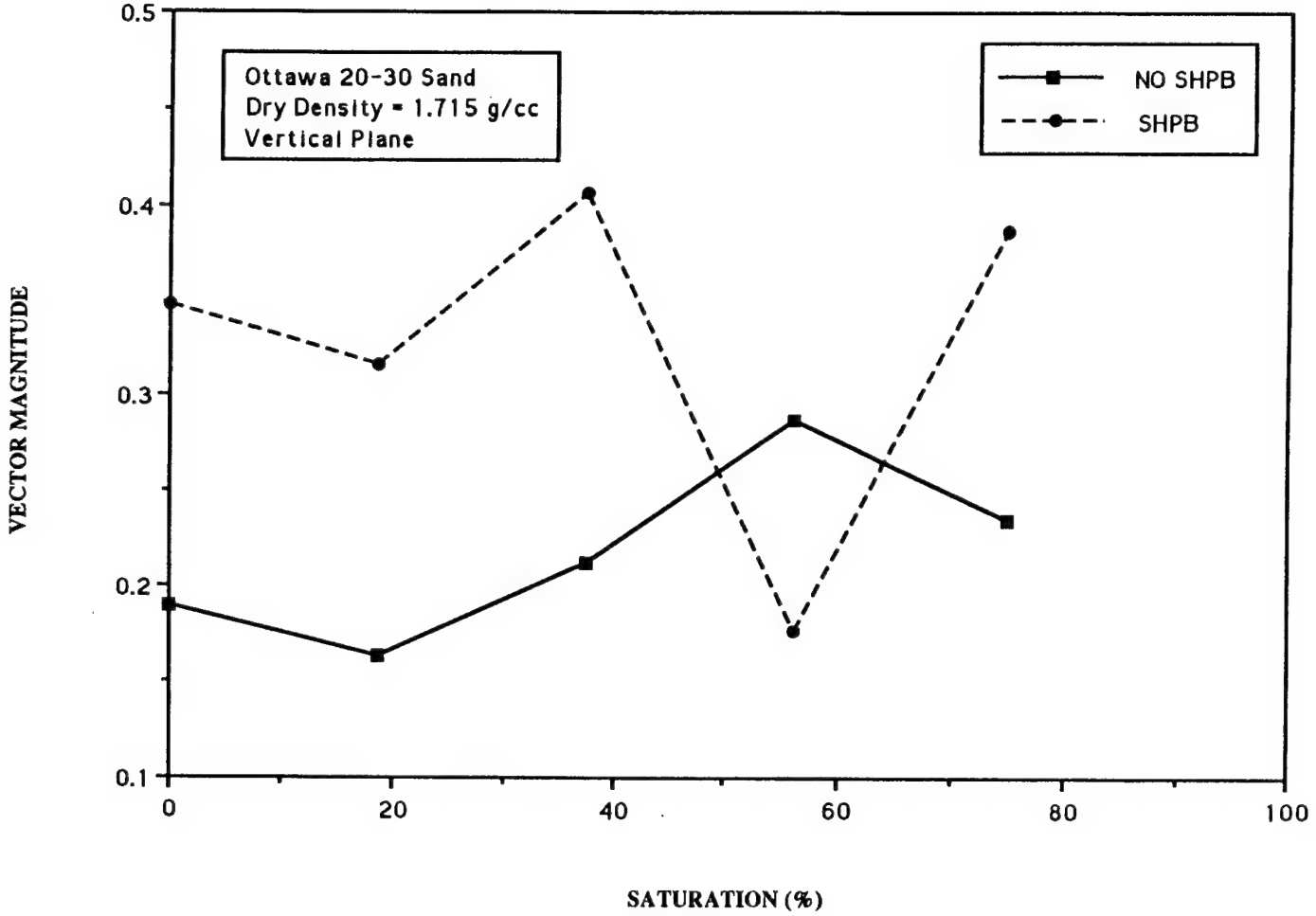

Figure 56. Vector Magnitude as a Function of Saturation for Layer #2.

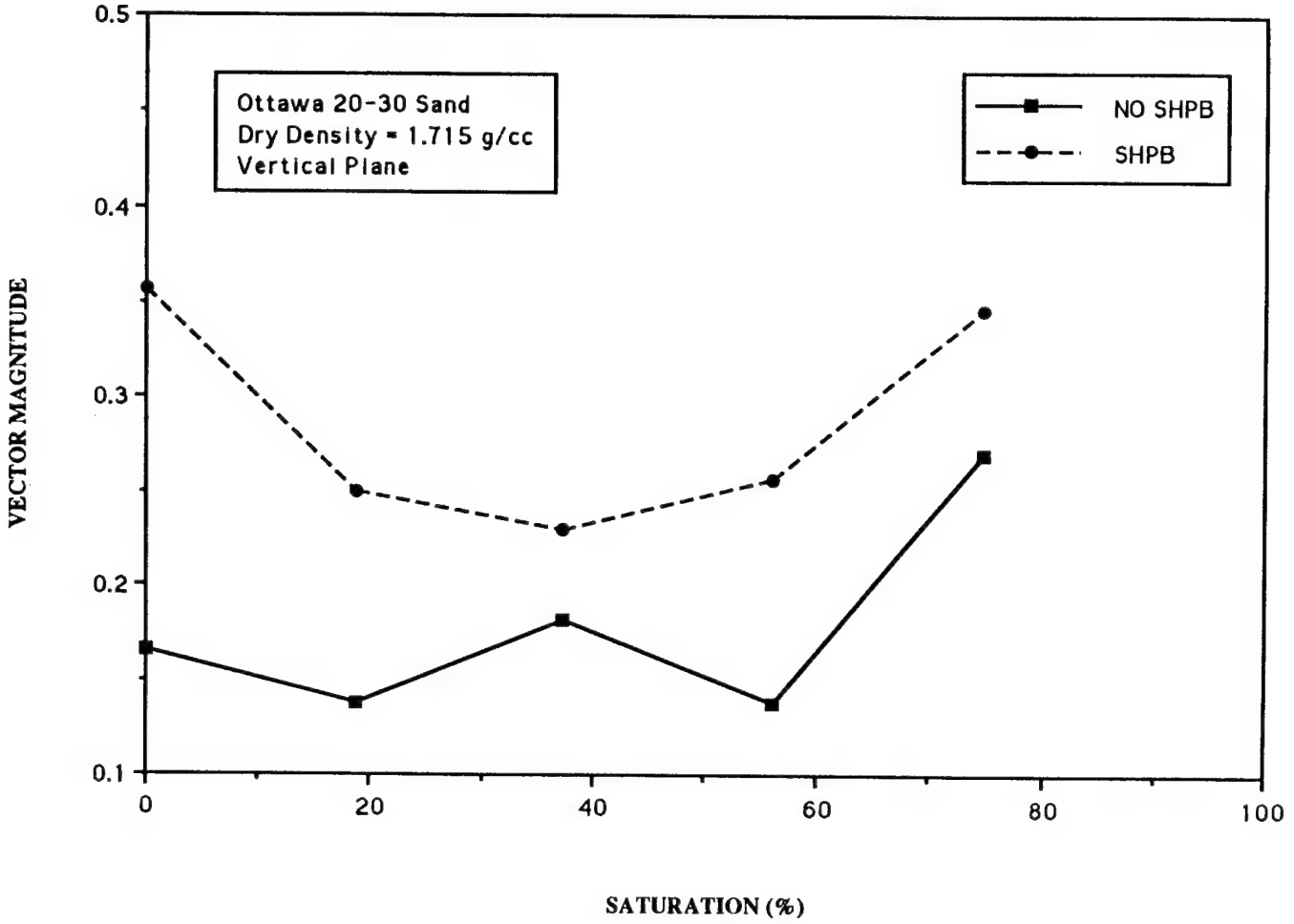

Figure 57. Vector Magnitude as a Function of Saturation for Layer #3.

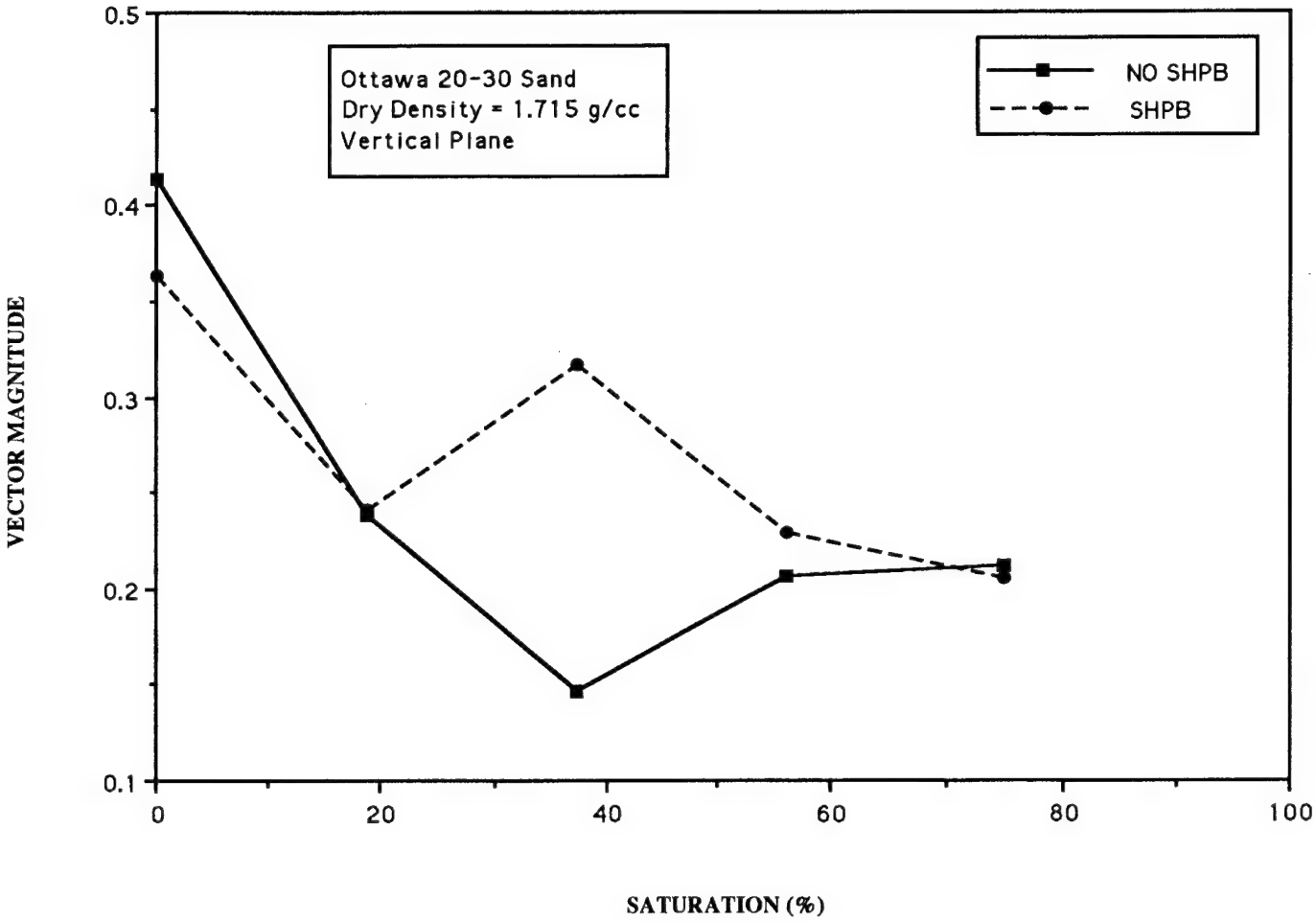

Figure 58. Vector Magnitude as a Function of Saturation for Layer #4.

SECTION V

ANALYSIS OF RESULTS

A. COMPACTION ENERGY

A summary of the compaction energy results using the standard Proctor hammer is presented in Figure 59, which shows normalized total compactive energy as a function of saturation. As can be seen, the amount of energy required to compact the Ottawa 20-30 sand to a constant dry density of 1.715 g/cm^3 varied with saturation. This trend has been observed by several other researchers for Ottawa 20-30 sand and other sands (Ross et al.,1986; Pierce, 1989; Veyera, 1989). The results from Figure 59 show that the amount of required compactive energy sharply increases from zero to about 20 percent saturation, then slightly increases from about 20 percent to about 40 percent saturation and decreases thereafter.

There appears to be an increase in soil stiffness at intermediate saturations which is most likely due to capillary tension forces present during compaction. The particles are most resistant to rearrangement at saturations between about 20 percent and 40 percent. The higher compaction energy required at these saturations may be due to the particles resisting rearrangement, thus requiring more energy for compaction. At higher saturations (greater than about 60 percent), the moisture may somewhat "lubricate" the soil particles as surface tension forces are reduced. This would allow the particles to slide past one another during compaction with less resistance, therefore decreasing the amount of compactive energy necessary.

Figure 60 shows compactive energy results for each individual 2.54 cm (1.00 inches) thick layer. The data have been normalized to the average compactive energy required for the first layer at zero saturation. As shown, more compactive energy was required to compact the first layer at all saturations as compared with Layers 2, 3, and 4. This may be explained as follows: prior to the first blow for Layer 1, the soil is in its loosest state from initial placement. After the first blow is applied, the density of the soil increases because during the first blow the particles are forced to rearrange themselves into a much denser packing. A compressional stress wave generated by the standard Proctor hammer is transmitted through the soil and into the steel pedestal below. As the energy from this wave propagates through the soil, it compacts and increases the density of the soil. When the compressional stress wave encounters the steel pedestal it is reflected back as a tensile wave which may loosen the layer being compacted.

Each of the four layers show the same general trend as that found in Figure 59, i.e., the amount of energy required to compact the soil to a constant dry density sharply increases from zero to about 20 percent saturation and decreases thereafter. The trend is similar yet less pronounced in Layers 2, 3, and 4 than it is in Layer 1 (Figure 60). Different stiffnesses and densities exist between the compacted soil and steel pedestal. Differences in compaction energy between the four layers may be due the magnitude of the reflected tensile wave being reduced as the specimen is compacted to final height, creating less disturbance in Layers 2, 3, and 4. Also, the amount of energy needed to compact the soil to the required dry density decreases with each layer.

Figure 61 shows cumulative compactive energy results (total blows applied to each layer including those of succeeding layers) for each individual 2.54 cm (1.00 inches) thick layer. The cumulative energy applied to Layer 1 represents the total amount of compaction energy (see Figure 32) applied to the sample. Each of the four curves in Figure 61 show the same general trend, i.e., less energy was required to compact each layer to a constant dry density at zero percent saturation and more energy was required to compact each layer to a constant dry density at intermediate saturations (20 percent to 60 percent). Similar behavior is expected between the four layers because the same soil was compacted to the same constant dry density. Thus, it seems that the effect of moisture (capillary tension forces) during compaction on each individual layer may be significant.

B. SPLIT-HOPKINSON PRESSURE BAR RESULTS

1. Compressional Wave Speed and Transmission Ratio

The split-Hopkinson pressure bar was used to measure compressional wave speed and stress transmission ratio as a function of saturation for Ottawa 20-30 sand. Figures 62 and 63 show results for specimens compacted moist and tested moist (moist-moist), and Figures 64 and 65 show results for specimens compacted moist and tested dry (moist-dry). Specimens were tested under moist-moist and moist-dry conditions to determine if the presence of water during SHPB testing significantly affected the compressional wave speed and stress transmission ratio, or if the observed behavior was more strongly influenced by microstructure alone.

a. Moist-Moist Results

Results obtained from moist-moist tests in this investigation are shown in Figures 62 and 63 and indicate trends similar to those observed in previous research

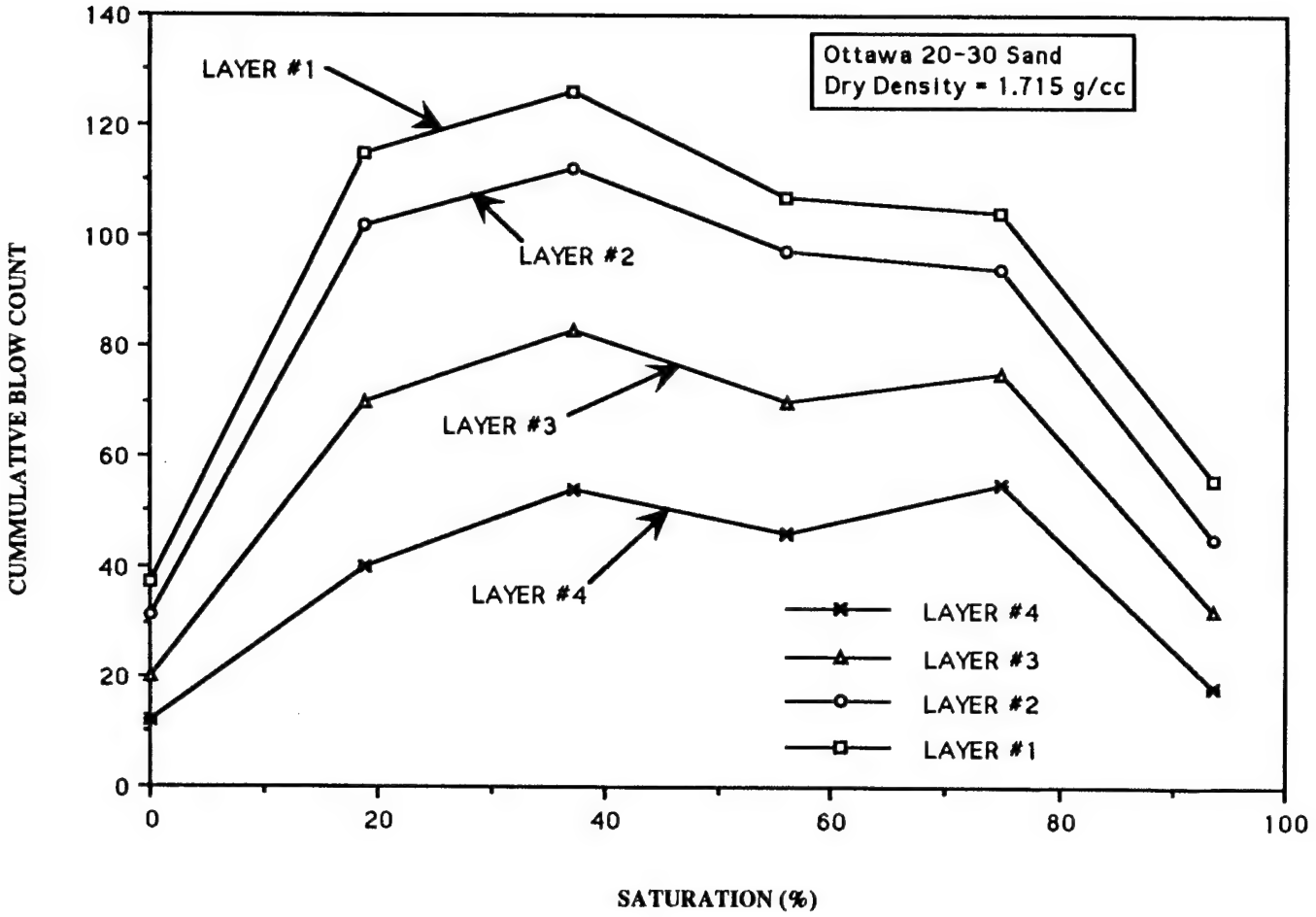

Figure 61. Cummulative Blow Count as a Function of Saturation for Ottawa 20-30 Sand for Layers 1 to 4.

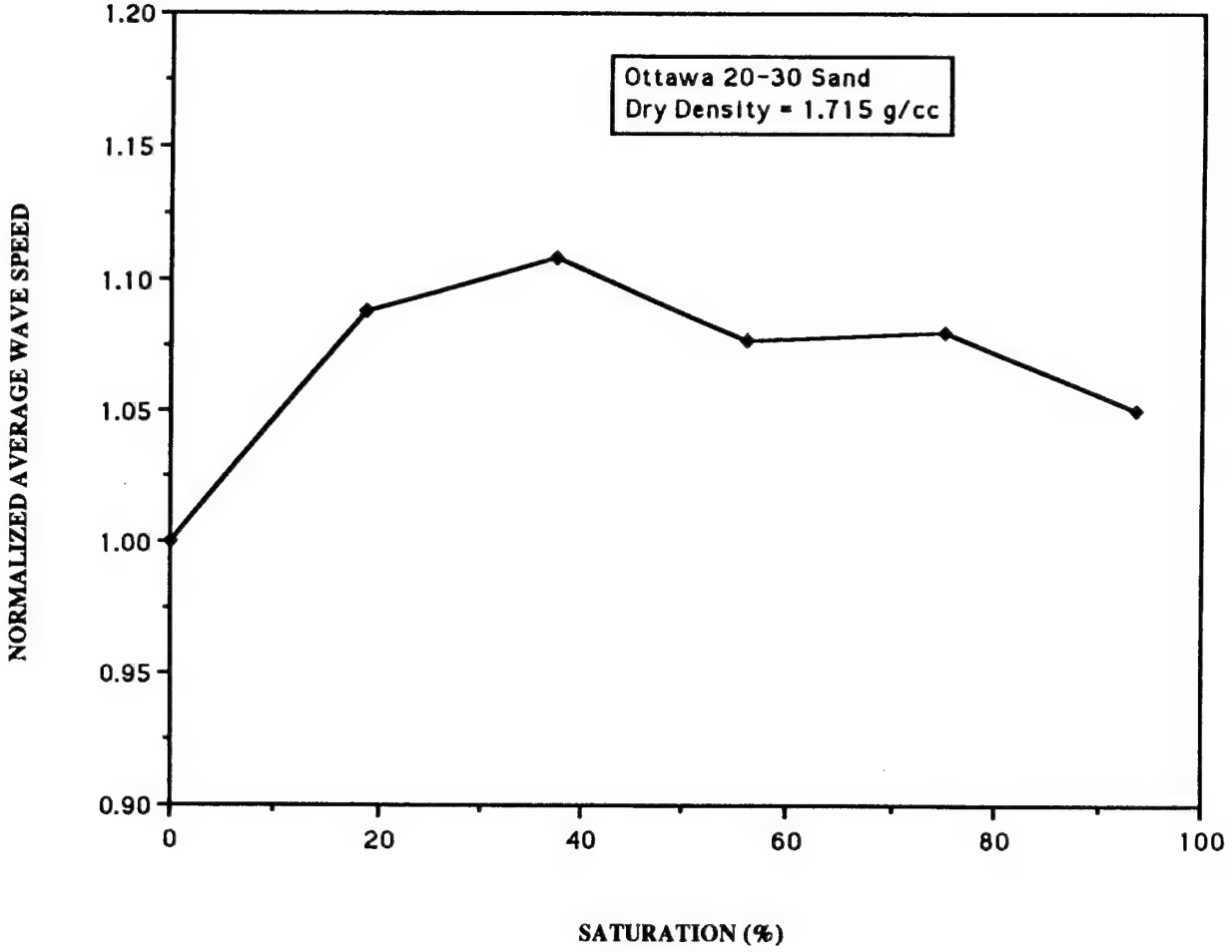

Figure 62. Normalized Average Wave Speed as a Function of Saturation for Ottawa 20-30 Sand Compacted Moist and Tested Moist.

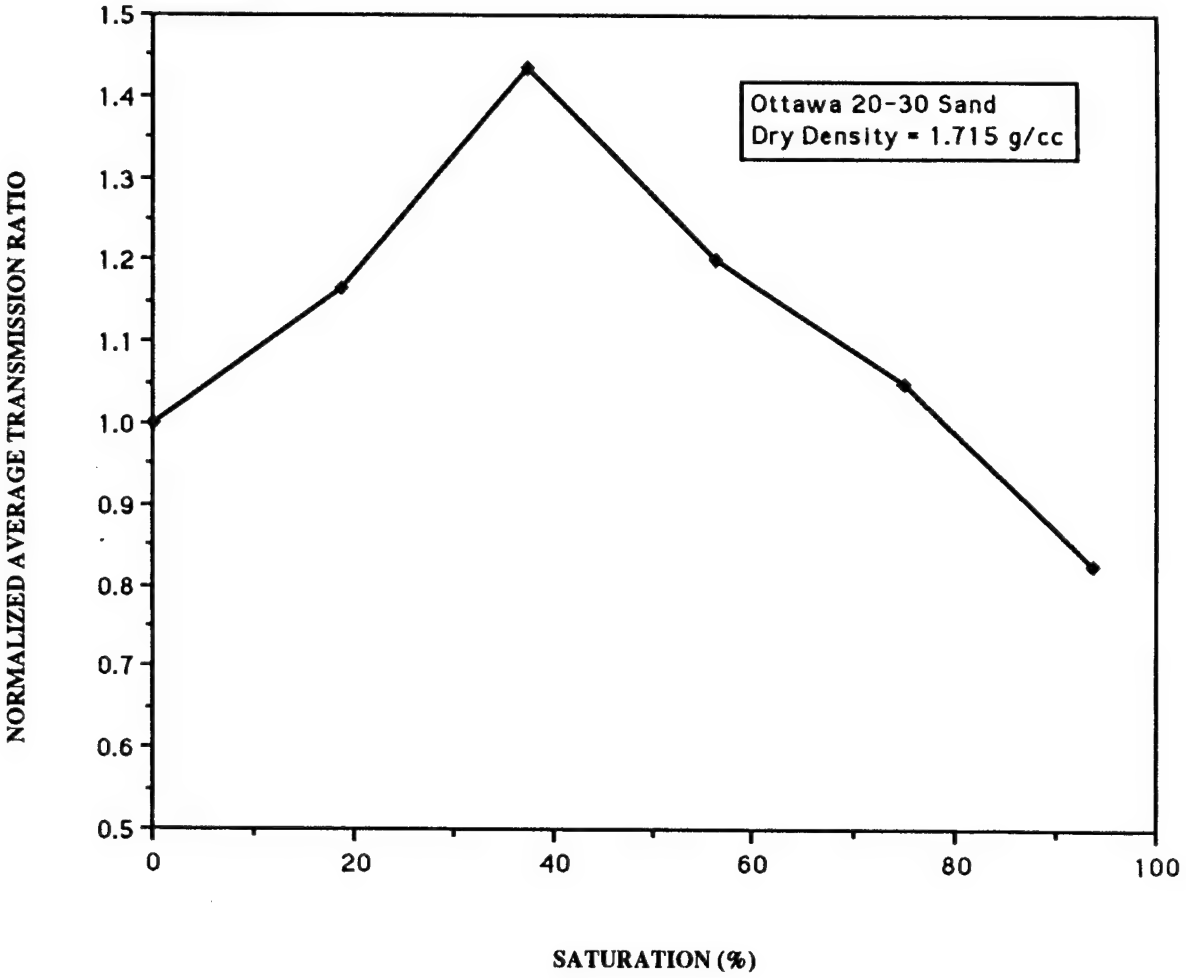

Figure 63. Normalized Average Transmission Ratio as a Function of Saturation for Ottawa 20-30 Sand Compacted Moist and Tested Moist.

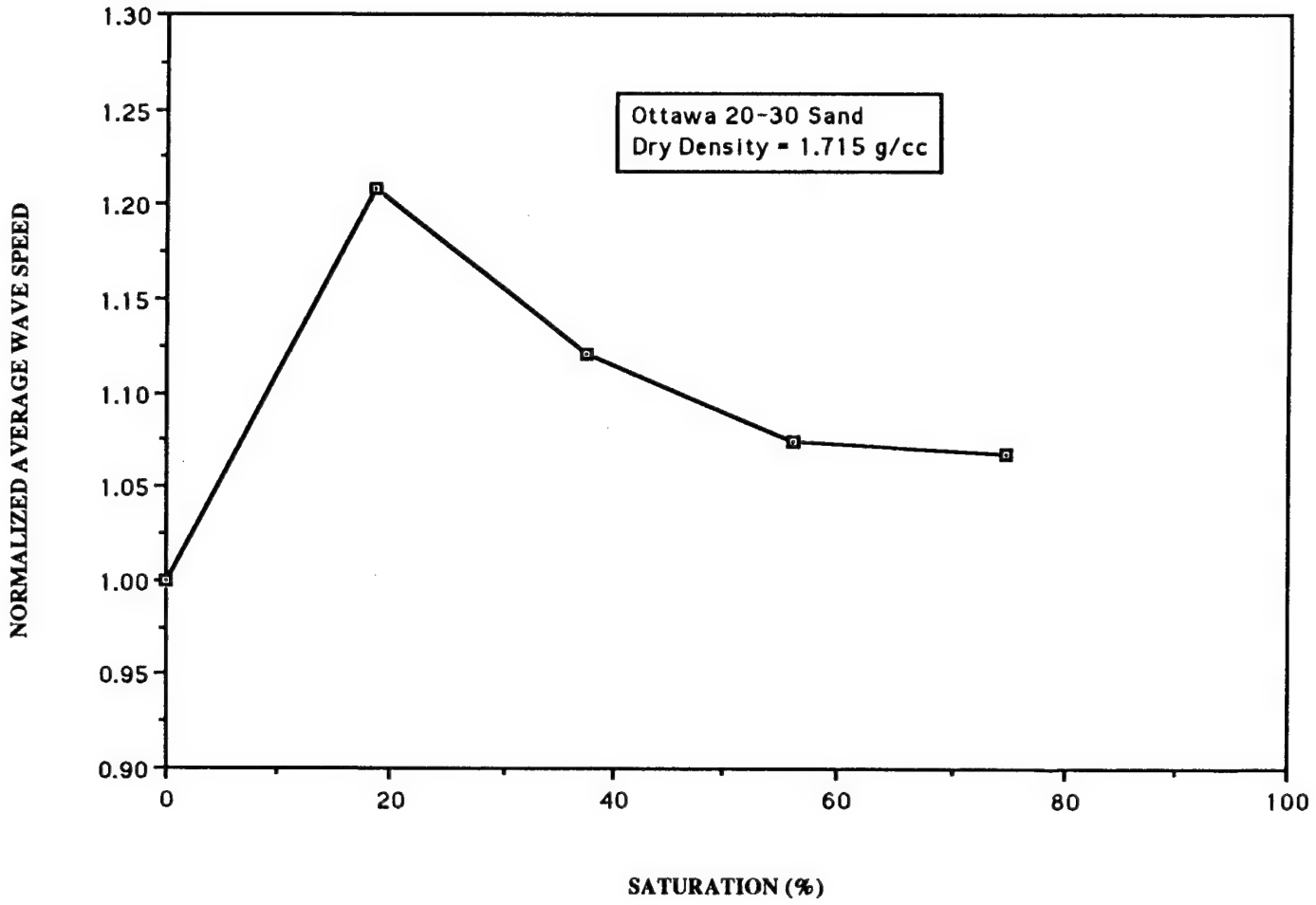

Figure 64. Normalized AverageWave Speed as a Function of Saturation for Ottawa 20-30 Sand Compacted Moist and Tested Dry.

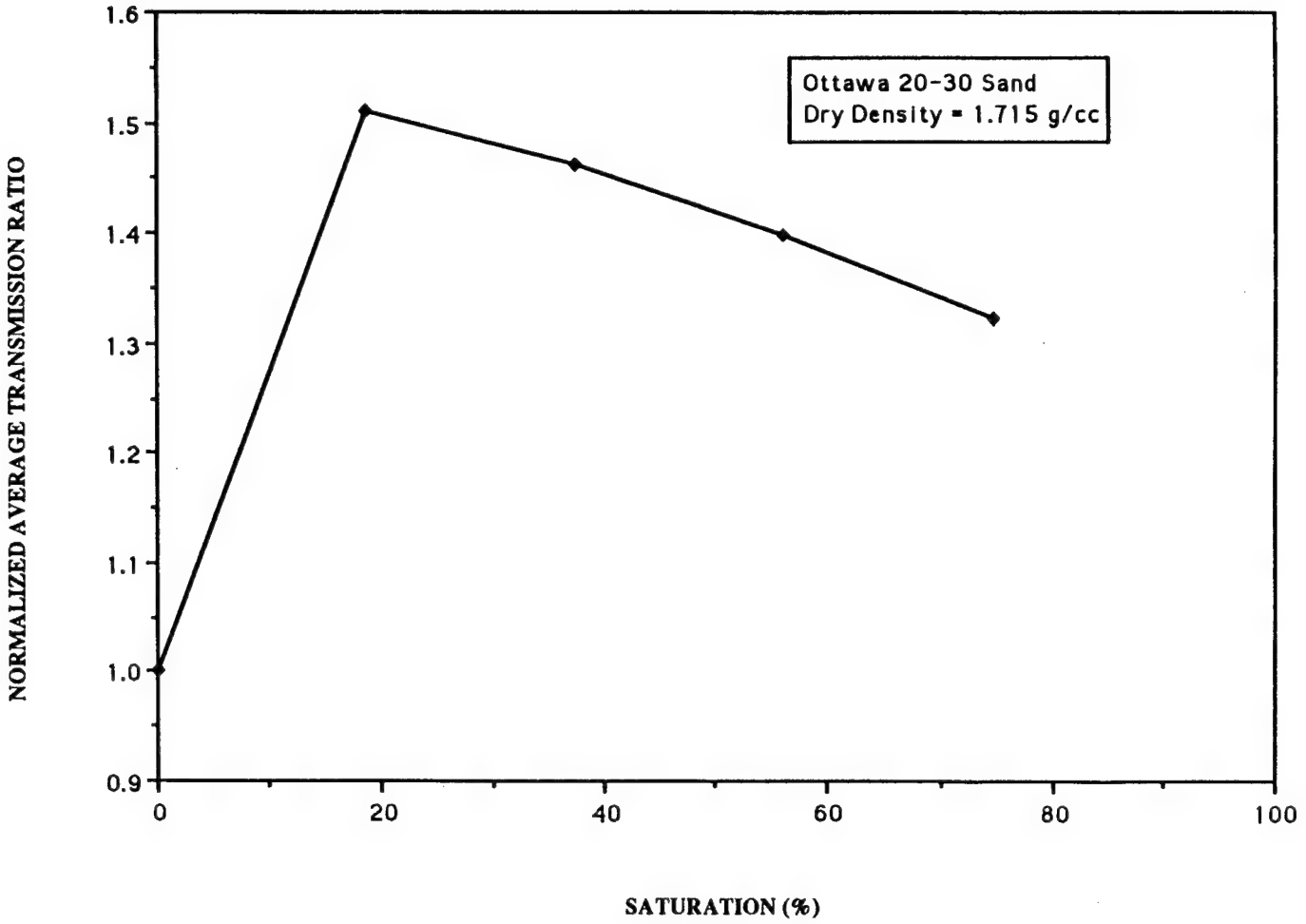

Figure 65. Normalized Average Transmission Ratio as a Function of Saturation for Ottawa 20-30 Sand Compacted Moist and Tested Dry.

(Ross, 1989) using the same SHPB. The data have been normalized to the compressional wave speed and stress transmission ratio at zero saturation (dry soil). Figures 62 and 63 show that at intermediate saturations (20 percent to 75 percent), compressional wave speed and stress transmission ratio are approximately 1.11 and 1.44 times greater in magnitude, respectively, than for dry soil. As saturations increase to about 75 percent, both the compressional wave speed and stress transmission ratio are roughly 1.08 and 1.05 times greater in magnitude, respectively, than for dry soil. Beyond 75 percent saturation, compressional wave speed and stress transmission ratio decrease, however they will increase as the soil approaches a saturated condition (i.e., S = 100 percent). Saturated soil will have a slightly greater value of compressional wave speed than the theoretical compressional wave speed in water due to a higher stiffness and total density of the soil-water mixture. The theoretical compressional wave speed in water is 1433 meters/sec (4700 feet/sec) at atmospheric pressure and at a temperature of 20° C (68° F).

The results for compressional wave speed and stress transmission ratio as a function of saturation obtained in this study are similar to those obtained by other researchers who also performed SHPB tests on the Ottawa 20-30 sand compacted moist and tested moist (Veyera, 1989; Ross, 1989; Felice et. al., 1987; and Ross et. al., 1986). At intermediate saturations (20 percent to 75 percent) these values were greater than those at zero percent saturation, and may be due to an increase in soil stiffness from capillary forces (see SECTION V). This applies to SHPB specimens which were compacted moist and tested moist and to those compacted moist and tested dry.

Results of compressional wave speed and stress transmission ratio as a function of saturation in this investigation differed from results presented by Pierce (1989) who compacted specimens dry and saturated them to the desired level by means of a pressure plate apparatus, thus the influence of moisture during compaction was not present. Pierce did not observe any changes in transmission ratio or wave speed for specimens prepared as stated. His results were not replicated in this study, and this can be attributed to different sample preparation techniques. In this investigation specimens were compacted moist, thus the influence of moisture during compaction is present. Differences between results obtained by Pierce (1989), Ross (1986), Veyera (1989), and the present investigation show that when moisture is present during compaction, the compressional wave speed, stress transmission ratio, and constrained modulus are greatly influenced. Therefore, it is evident that the specimen preparation method can significantly affect test results.

b. Moist-Dry Results

Results obtained from moist-dry tests in Figures 64 and 65 show that at a saturation of about 20 percent, compressional wave speed and stress transmission ratio are approximately 1.21 and 1.52 times greater in magnitude, respectively, than for dry soil. The data have been normalized to the compressional wave speed and stress transmission ratio at zero saturation. As the saturation increases beyond about 20 percent to about 75 percent in both Figures 64 and 65, the compressional wave speed and stress transmission ratio steadily decrease to approximately 1.07 and 1.34 times the magnitude of that for dry soil, respectively.

2. Comparison Between Moist-Moist and Moist-Dry Results

A comparison between the results obtained from moist-moist and moist-dry tests is shown in Figures 66 and 67. Both test series produced similar results in that at intermediate saturations (20 percent to 60 percent), compressional wave speed and stress transmission ratio had greater values than at zero saturation. This further reinforces the hypothesis that soil microstructure developed during compaction may be the primary phenomenon affecting the compressional wave speed and stress transmission ratio.

The results obtained in moist-dry testing conditions showed higher values of compressional wave speed and stress transmission ratio at all compacted saturations over moist-moist results (Figures 66 and 67). This suggests that moisture present during SHPB testing also affects the compressional wave speed and stress transmission ratio. Moist-moist tests were conducted on a three phase material exists, i.e., soil, water, and air, whereas moist-dry tests were conducted on a two phase material, i.e., soil and air. Therefore, if water is present, frictional resistance between particles may be lower and the compressional wave speed transmission ratio will have lower values during SHPB testing.

Capillary tension forces are present during moist-moist tests, however their effect on compressional wave speed and stress transmission ratio is negligible. Pierce (1989) studied capillary stresses in unsaturated Ottawa 20-30 sand and found that they are extremely small (on the order of 7 kPa (1 psi)) as compared to stress levels encountered in split-Hopkinson pressure bar testing (on the order of 15,000 kPa (2,175 psi)). Therefore, they have little effect on dynamic testing. However, the influence of these capillary tension forces in the development of soil microstructure during compaction appears to be a significant factor which affects both the static and dynamic soil behavior.

C. QUASI-STATIC COMPRESSION TESTS AND CONSTRAINED MODULUS

Figures 68 and 69 show comparison stress-strain curves generated from the MTS device using four compacted layers and one compacted layer, respectively, at each saturation. The stress-strain curve at zero percent saturation is compared to stress-strain curves at saturations of 18.7 percent, 37.4 percent, 56.2 percent, 74.9 percent, and 93.6 percent. Dry soil values (S = 0 percent) are used as a basis for comparison in normalizing the results.

Figure 68 shows that the slope of the stress-strain curve for zero percent saturation was steeper than 93.6 percent, whereas the slopes of the stress-strain curves for saturations of 18.7 percent, 37.4 percent, 56.2 percent and 74.9 percent were generally steeper than zero percent saturation, for specimens with four compacted layers. Figure 69 shows that the slope of the stress-strain curve for zero percent was steeper than 37.4 percent and 93.6 percent, whereas the slope of the stress-strain curve for saturations of 18.7 percent, 56.2 percent and 74.9 percent was steeper than zero percent saturation, for specimens with one compacted layer. The general trend in Figures 68 and 69 is an increase in overall stiffness with increasing saturation.

In Figures 68 and 69, the stress-strain curves which have the steepest slope indicate a stiffer soil. In comparing stress-strain results for four layers and one layer it can be seen that specimens with one layer were much stiffer than those with four layers. This may be due to the initial length of the specimen. For one layer, the initial specimen length was 2.54 cm (1.0 inches). Thus the amount of strain (deformation) produced is smaller and the specimen behaves as a stiffer material. Both specimens were subjected to the same uniaxial compressive load. In general, as saturations are increased to about 75 percent, the soil becomes stiffer as compared with zero percent saturation. As saturations increase past 75 percent, the soil becomes less stiff. This compares well with SHPB test results for compressional wave speed and stress transmission ratio in that a stiffer material is present to saturations of about 75 percent.

Figure 70 shows that the constrained modulus (normalized to results at S = 0 percent) was found to be approximately 1.08 times greater at saturations to about 40 percent and was approximately 1.03 times greater at saturations between about 60 percent and 75 percent. A further increase in saturation showed that the constrained modulus was approximately 0.97 times the constrained modulus at zero percent saturation. This trend (higher values at intermediate saturations) was also observed in the compaction data (Figure 59), compressional wave speed data (Figure 62), and stress transmission ratio data (Figure63) as a function of saturation. The behavior may be due to the resistance of

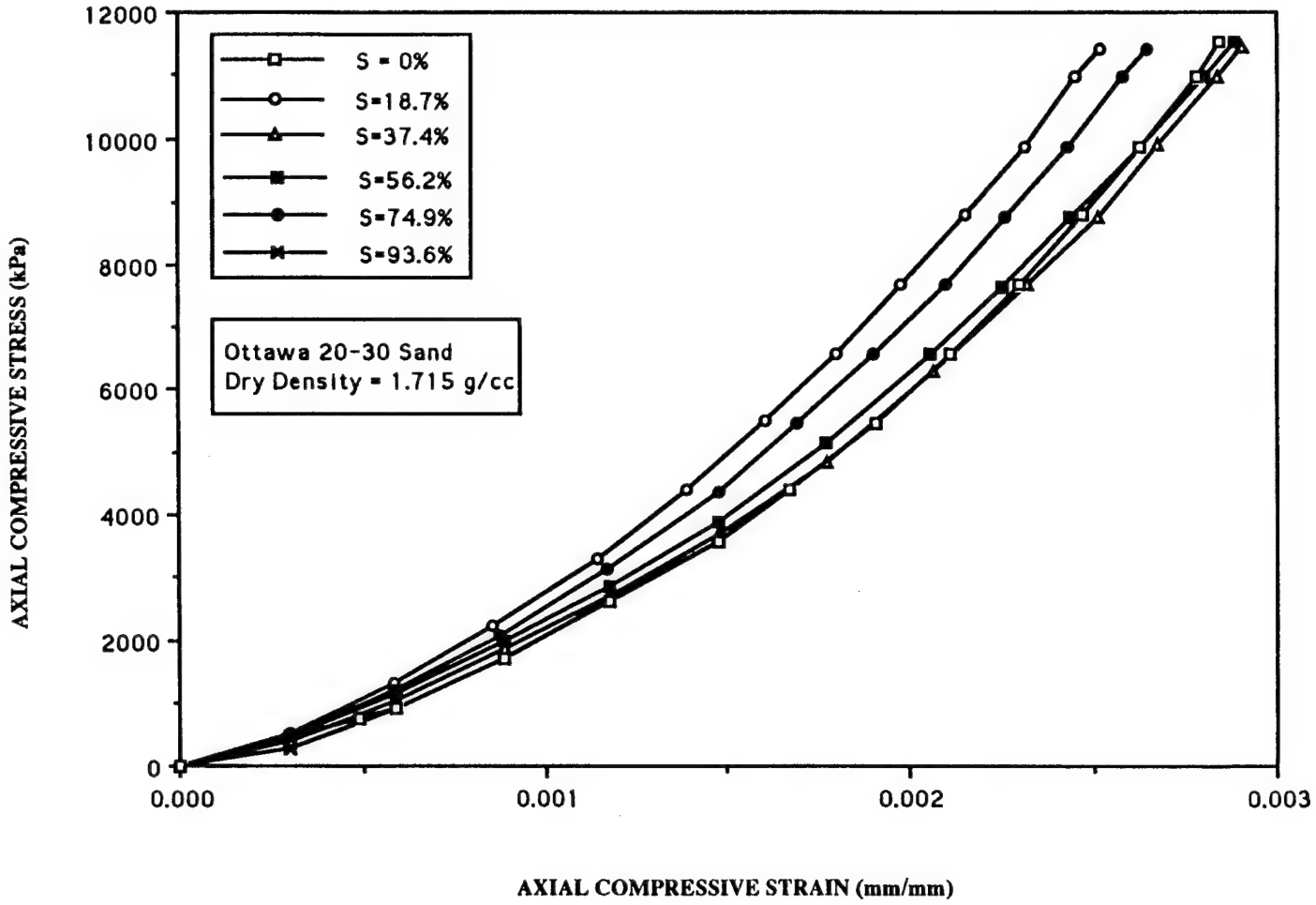

Figure 69. Comparison of Stress-Strain Curves at All Saturations, for One Compacted Layer During Loading Cycle.

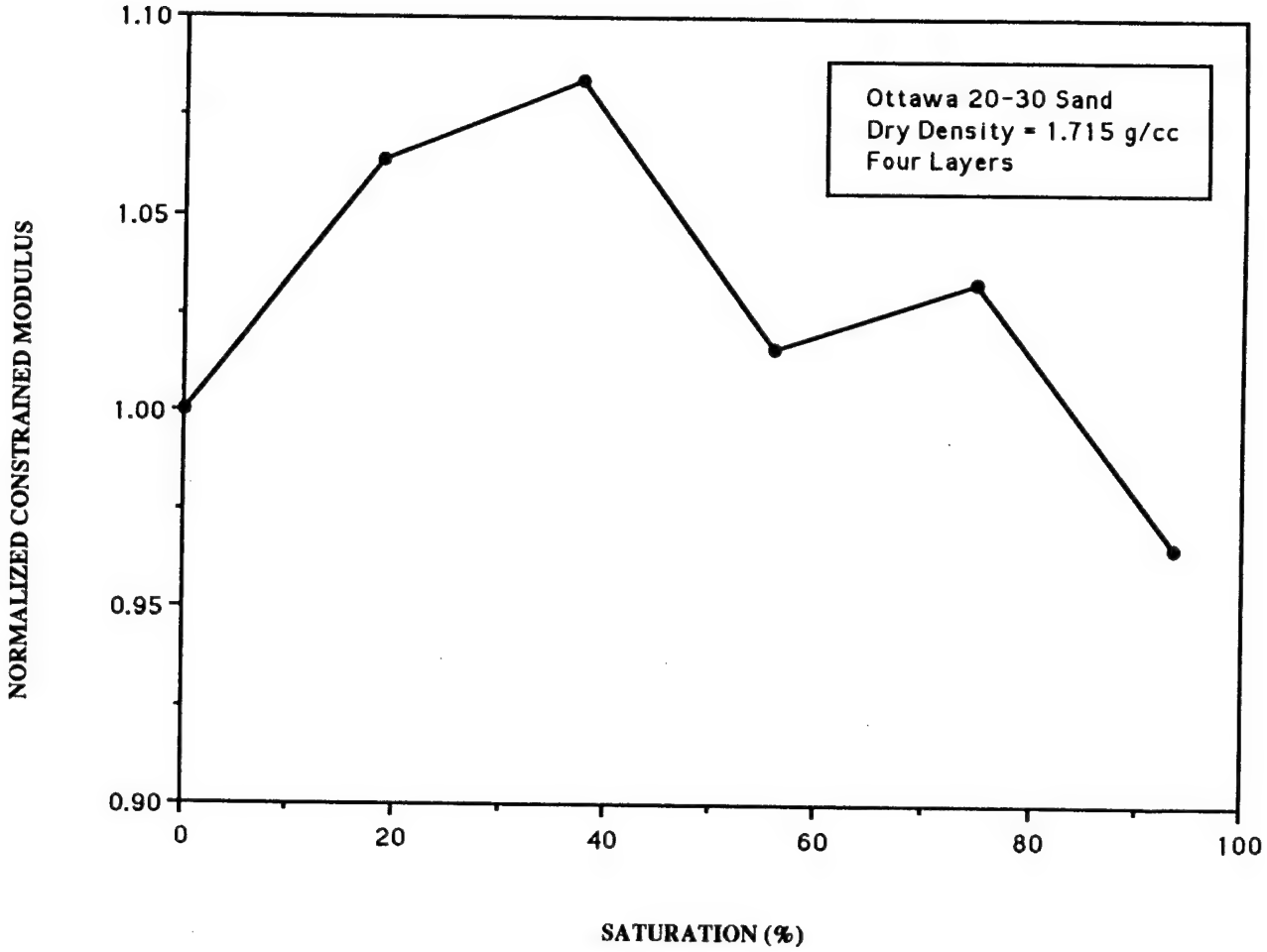

Figure 70. Normalized Constained Modulus as a Function of Saturationfor Ottawa 20-30 Sand Compacted Moist and Tested Moist.

particles to relative movements at intermediate saturations. By applying a quasi-static loading, the soil is compressed into a packing greater than that from the initial compaction procedure. As in the impact compaction process using the standard Proctor hammer, capillary forces probably tend to resist particle rearrangements at lower saturations in these tests. Capillary forces decrease with increasing saturation, thereby reducing the frictional resistance between soil particles which may allow particles to move relative to one another with greater ease.

Figure 71 shows the normalized constrained modulus and normalized total blow count (normalized to results at S = 0 percent) as a function of saturation. The same trend is noticeable for constrained modulus and total blow count, i.e., high values are obtained at intermediate saturations. The constrained modulus and total blow count can be related to soil stiffness. A stiffer material will produce a higher constrained modulus and more energy will be required to compact a stiffer material to a constant dry density. Therefore, the relationships shown in Figure 71 are further evidence that moisture present during compaction affects soil stiffness and, in turn, the constrained modulus and required compaction energy.

D. AXIAL RATIO

More than 2,500 particles were measured to determine the axial ratio of the Ottawa 20-30 sand used in this investigation. The average axial ratio, n_{avg}, was found to be 0.674 with a standard deviation of 0.106. Axial ratio values ranged from 0.253 to 0.968. Ottawa 20-30 sand is classified as a well rounded sand according to Table 1.

Oda (1972a) proposed that the minimum axial ratio required for preferred particle orientation is 0.7. An important note is that axial ratio is a "shape parameter" and is not a function of saturation within a soil. However, particle shape does affect the probability of obtaining a preferred particle orientation. With an average axial ratio of 0.674 the particles are well-rounded and there is a low resistance to movements from applied loads. In other words, well rounded particles will have less resistance to movement due to either static or dynamic loading than would angular particles. From the two-dimensional images of sections through the specimen, most of the particles were elliptical in shape.

E. COMPARISONS OF PARTICLE ORIENTATION ANALYSIS RESULTS

Rose plots generated from the two-dimensional particle orientation analyses are given in Appendix A. A detailed description of the statistics used in the Rosy program has been given in SECTION IV. From an in-depth review of all statistical parameters generated by

the Rosy program, it was determined that the vector magnitude was the only parameter that related compressional wave speed, transmission ratio, microstructure, and saturation together.

Vector magnitude is a measure of the dispersion of azimuths in a data set and values range from zero to one. Vector magnitude values near zero indicate that there is no preferred particle orientation. The data obtained in this study implies that low values of vector magnitude may be related to higher values of soil stiffness, compaction energy, compressional wave speed, and transmission ratio, i.e., an inverse relationship may exist between the soil parameters. As previously explained in SECTION V, at intermediate saturations (20 percent to 60 percent) the soil is stiffer and resists rearrangement of soil particles. Thus, a lower degree of preferred particle orientation would be expected and vector magnitude values are expected to be lower at intermediate saturations which may be attributable to the resistance of particle movements at intermediate saturations.

1. Vector Magnitude Results

Two separate categories were analyzed from the two-dimensional orientation data: NO SHPB results, and SHPB results, respectively. The reason for performing the different analyses is to observe the differences in soil microstructure in compacted specimens before and after testing in the split-Hopkinson pressure bar.

a. Horizontal and Vertical Planes

Figures 53 and 54 show the vector magnitude as a function of saturation in the horizontal and vertical planes for NO SHPB and SHPB specimens, respectively. As expected, SHPB specimens had higher values of vector magnitude at all saturations for each plane. Since more energy is applied to the soil, the particles are forced to develop a higher degree of preferred orientation.

The Ottawa 20-30 sand used in this investigation has been classified as a poorly-graded, well-rounded sand. The mean axial ratio of the sand is 0.647 and most of the particles are somewhat elliptical in shape, having smooth surfaces. For this shape, most of the soil particles would tend to have a vector mean in the range of 80- to 110-degrees or 260- to 280-degrees from initial deposition for dry soil conditions only (note that vector mean values are bidirectional). The principle behind this idea is that an elliptical shaped particle falling through the air will tend to rest on its longest axis parallel to the plane of deposition. This was confirmed by Mitchell (1976) in which dry pluviated samples showed a strong degree of preferred particle orientation parallel to the plane of

deposition. As energy is applied, the sand is forced to rearrange itself into a denser packing and develop high vector magnitude values.

It was expected that the vector magnitude as a function of saturation would exhibit an inverse relationship as compared to compaction energy, compressional wave speed and stress transmission ratio as a function of saturation. In the cases of compaction energy, compressional wave speed and stress transmission ratio as a function of saturation, each of these exhibited a typical trend in that at intermediate saturations (20 percent to 60 percent) higher values were observed. Data for vector magnitude as a function of saturation imply that lower values are encountered at intermediate saturations (20 percent to 60 percent). In general, this trend was observed in both the horizontal and vertical planes, as shown in Figures 53 and 54. SHPB specimens exhibited greater vector magnitude values for both the horizontal and vertical planes.

b. Layers 1 Through 4

Figures 72 and 73 show the vector magnitude as a function of saturation and layer number (developed from vertical plane data) for NO SHPB and SHPB specimens, respectively. The data have been normalized to the vector magnitude at zero saturation for Layer 1. Vector magnitude values for each layer were assumed to decrease with successive layers, i.e., Layer 1 should have the highest vector magnitude and Layer 4 should have the lowest vector magnitude. Since Layer 1 has had much more energy applied to it from the total number of blows, the particles probably have a higher degree of preferred orientation, i.e., a higher vector magnitude.

Figures 55 through 58 show the vector magnitude as a function of saturation for each layer and compare vector magnitude values for NO SHPB and SHPB specimens. As the amount of energy applied to a soil increases the degree of preferred particle orientation should increase. This is seen in each of the four layers and saturations in that the SHPB specimens generally had higher vector magnitude values.

2. Correlation of Vector Magnitude with Average Total Blow Count

The next step in the analysis was to take the product of vector magnitude and compaction energy as a function of saturation and to note any distinct trends that may be occurring in the data. These products as a function of saturation may constitute a first order or second order function on a best fit curve which may be of use in future studies. This comes from the inverse relationship between vector magnitude and compaction energy, compressional wave speed, and transmission ratio as a function of saturation.

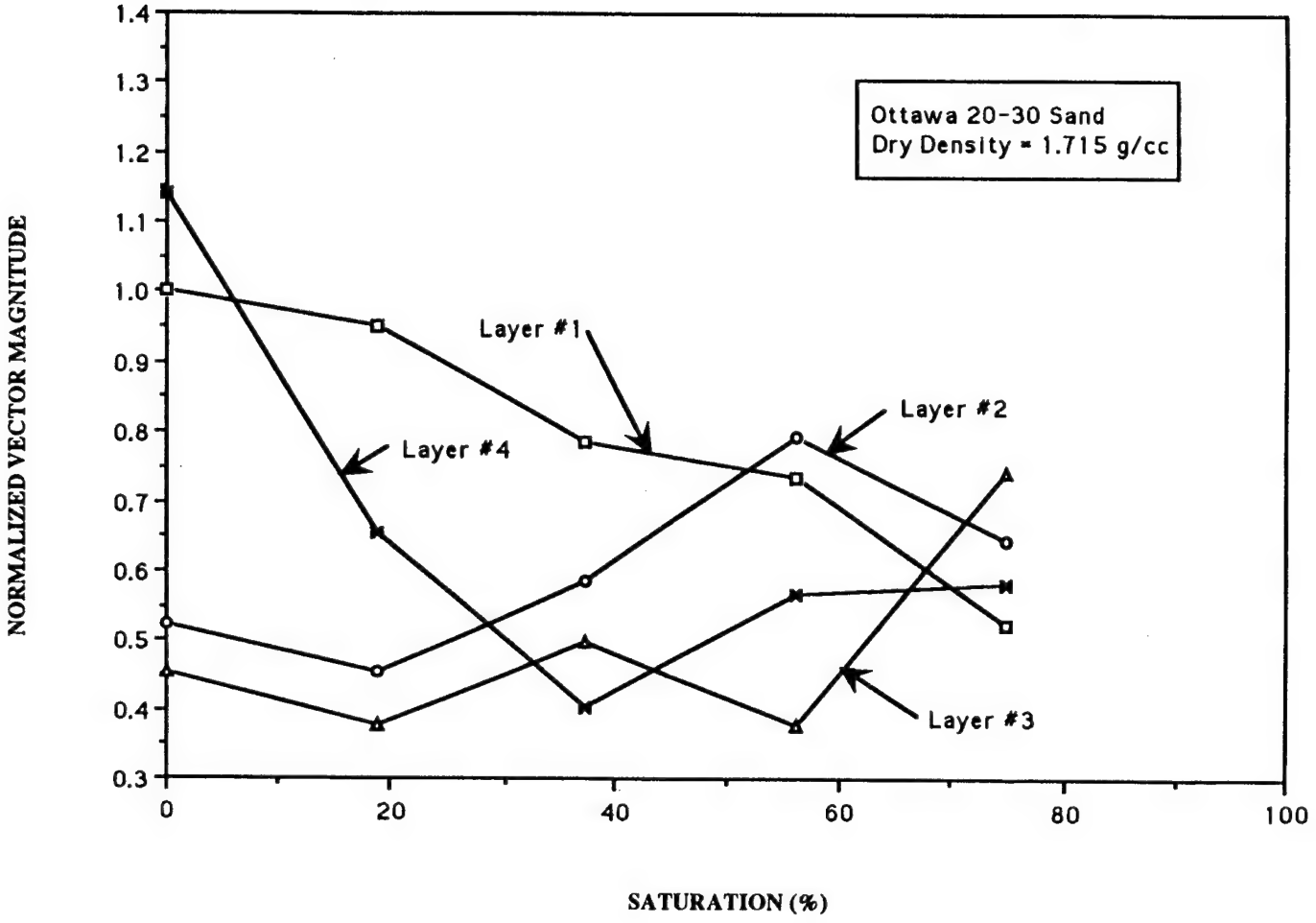

Figure 72. Vector Magnitude Normalized to 0% at Layer #1 as a Function of Saturation for Ottawa 20-30 Sand (NO SHPB).

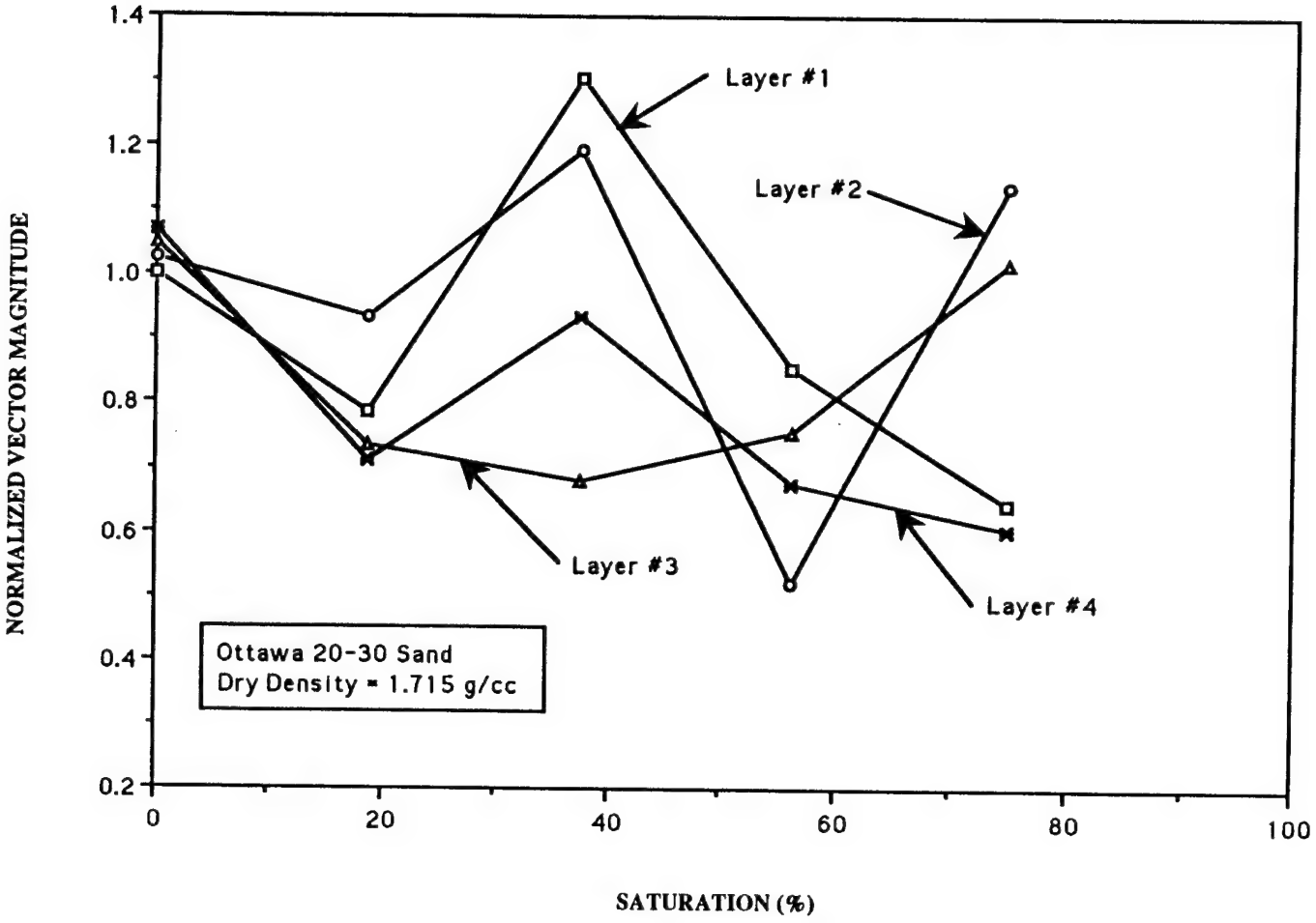

Figure 73. Vector Magnitude Normalized to 0% at Layer #1 as a Function of Saturation for Ottawa 20-30 Sand (SHPB).

a. Horizontal and Vertical Planes

Figures 74 and 75 show the product of vector magnitude and average total blow count as a function of saturation for the horizontal and vertical planes for NO SHPB and SHPB specimens, respectively. Both the horizontal and vertical plane results in Figure 74 show that as saturation increases the product steadily increases. In Figure 75 the product for both the horizontal and vertical planes increases to about 40 percent higher saturation and decreases thereafter. The values for blow count used in both NO SHPB and SHPB specimens are the same. However, values for vector magnitude are greater for SHPB specimens than for NO SHPB specimens. Therefore, the curves developed in Figures 74 and 75 are dependent on the vector magnitude values.

Overall, the NO SHPB specimens showed an increase in the product as saturations increased, whereas the product in the SHPB specimens reached a peak value and decreased thereafter. This seems to correlate with compaction energy, compressional wave speed, and stress transmission ratio as a function of saturation which generally had maximum values at intermediate saturations (see Figures 59, 62, and 63). Both the vertical and horizontal plane exhibited a similar trend for both NO SHPB and SHPB specimens. Overall, the product of vector magnitude and average total blow count presented in this analysis shows small variations in the results between the horizontal and vertical plane. This suggests that soil microstructure throughout the specimen may be similar.

Figures 76 and 77 show normalized vector magnitude and normalized average total blow count as a function of saturation (normalized to results at S = 0 percent) for NO SHPB and SHPB specimens, respectively. Normalizing vector magnitude and average total blow count (plotted using the same scales on both axes) allows for direct comparison of trends. Both figures show an inverse relationship between vector magnitude and average total blow count. At intermediate saturations, vector magnitude values are lower while average total blow count values are higher. The lower vector magnitude values indicate a more random orientation within the soil structure. This random orientation can be attributed to particles resisting movement relative to one another during the compaction process when moisture is present. The results shown in Figures 76 and 77 suggest that a random orientation may create a stiffer soil, and thus more energy is required to compact the moist soil to a constant dry density.

b. Layers 1 Through 4

Figures 78 and 79 show the product of vector magnitude and average blow count as a function of saturation for Layers 1 through 4 for NO SHPB and SHPB

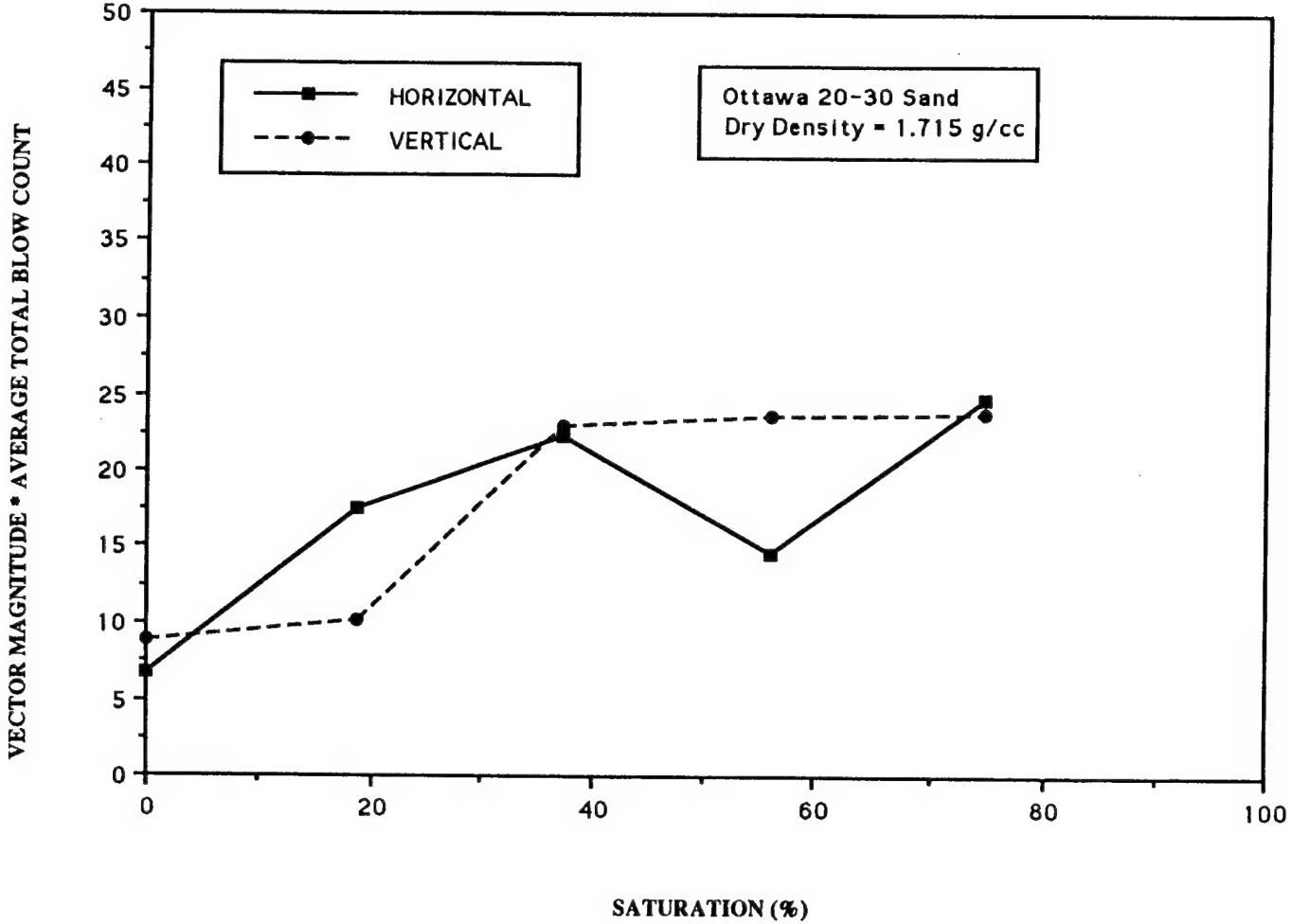

Figure 74. Product of Vector Magnitude and Average Total Blow Count as a Function of Saturation for Ottawa 20-30 Sand (NO SHPB).

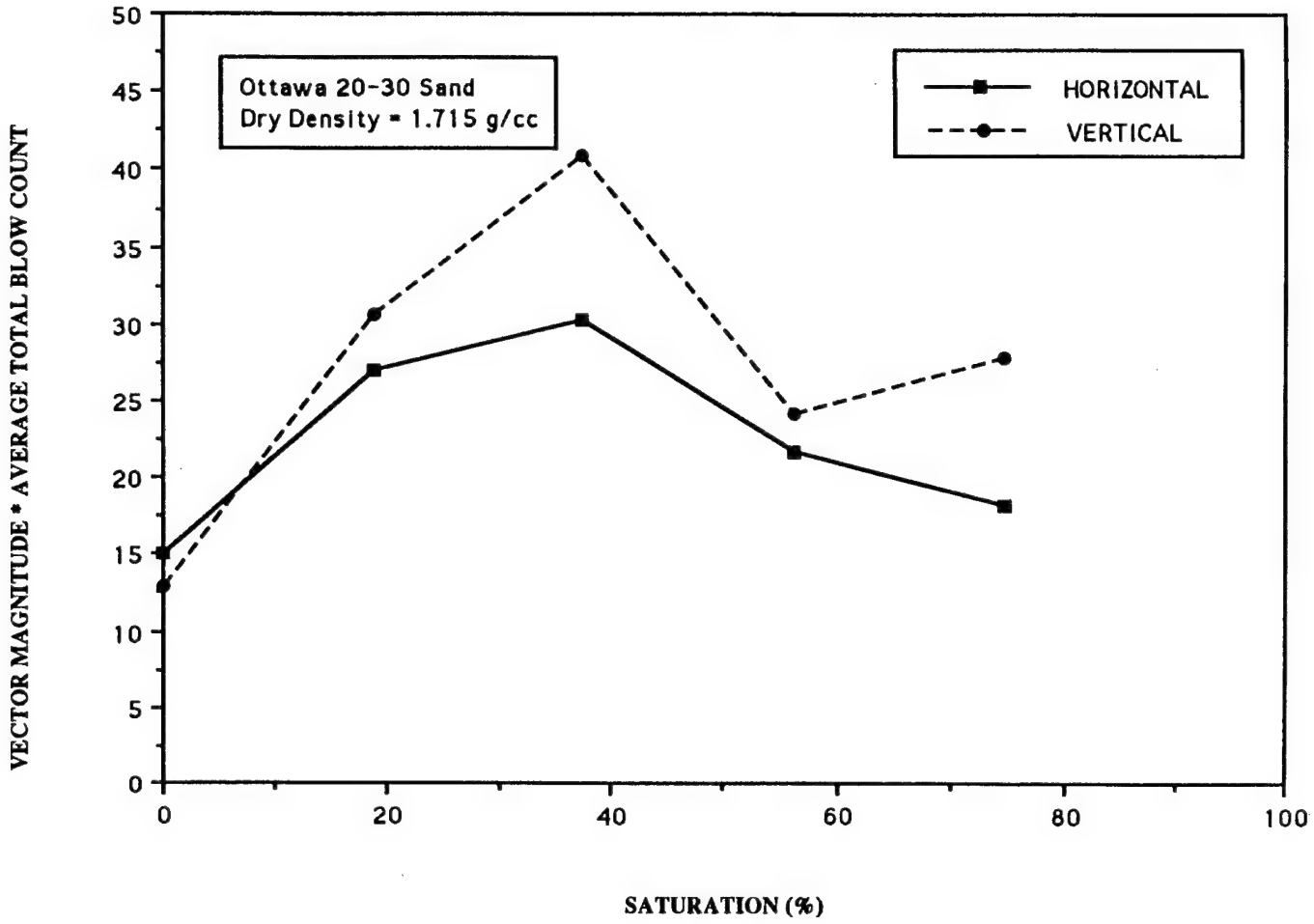

Figure 75. Product of Vector Magnitude and Average Total Blow Count as a Function of Saturation for Ottawa 20-30 Sand (SHPB).

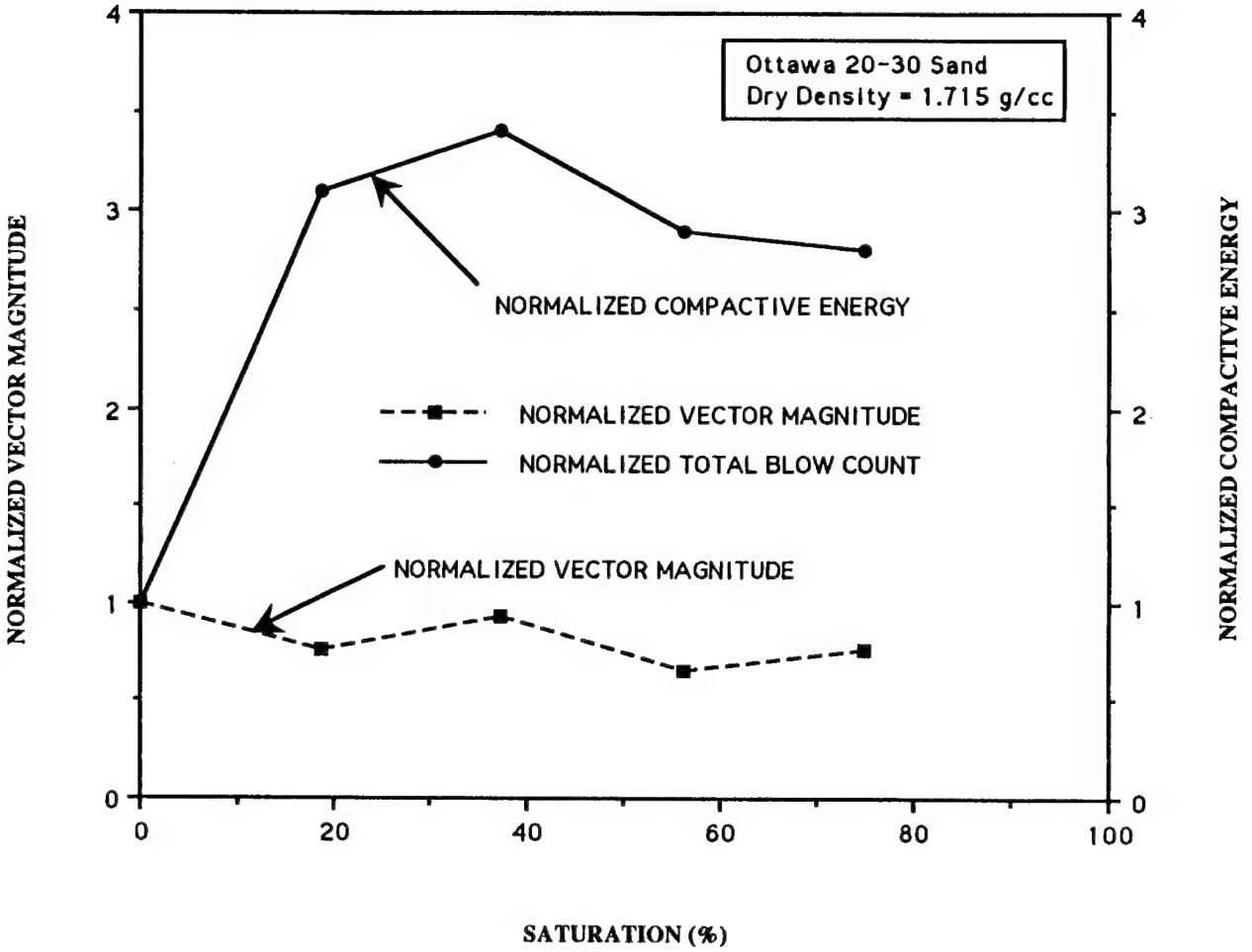

Figure 77. Normalized Vector Magnitude in the Vertical Plane and Normalized Compactive Energy as a Function of Saturation (SHPB).

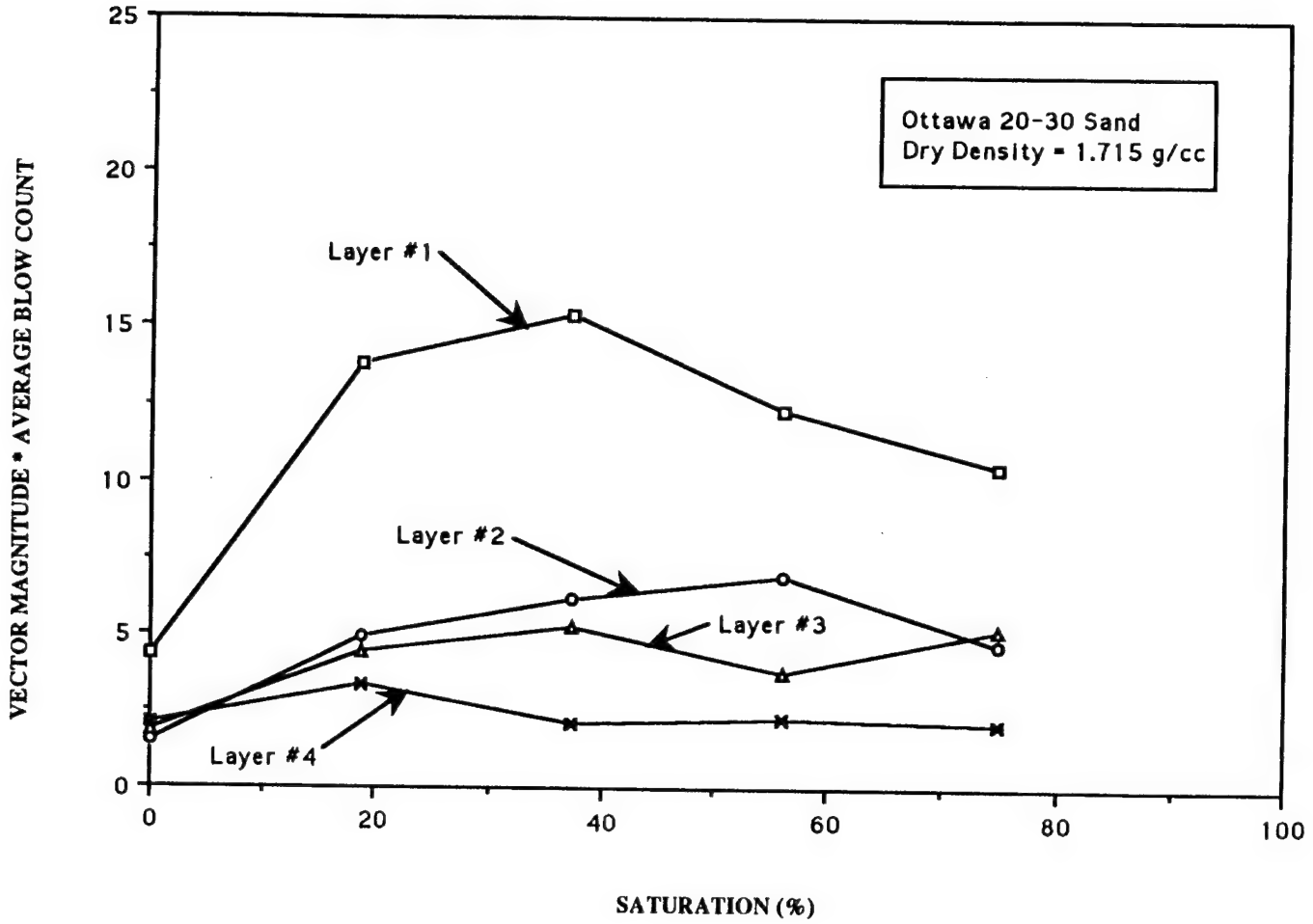

Figure 78. Product of Vector Magnitude and Average Blow Count as a Function of Saturation for Ottawa 20-30 Sand (NO SHPB).

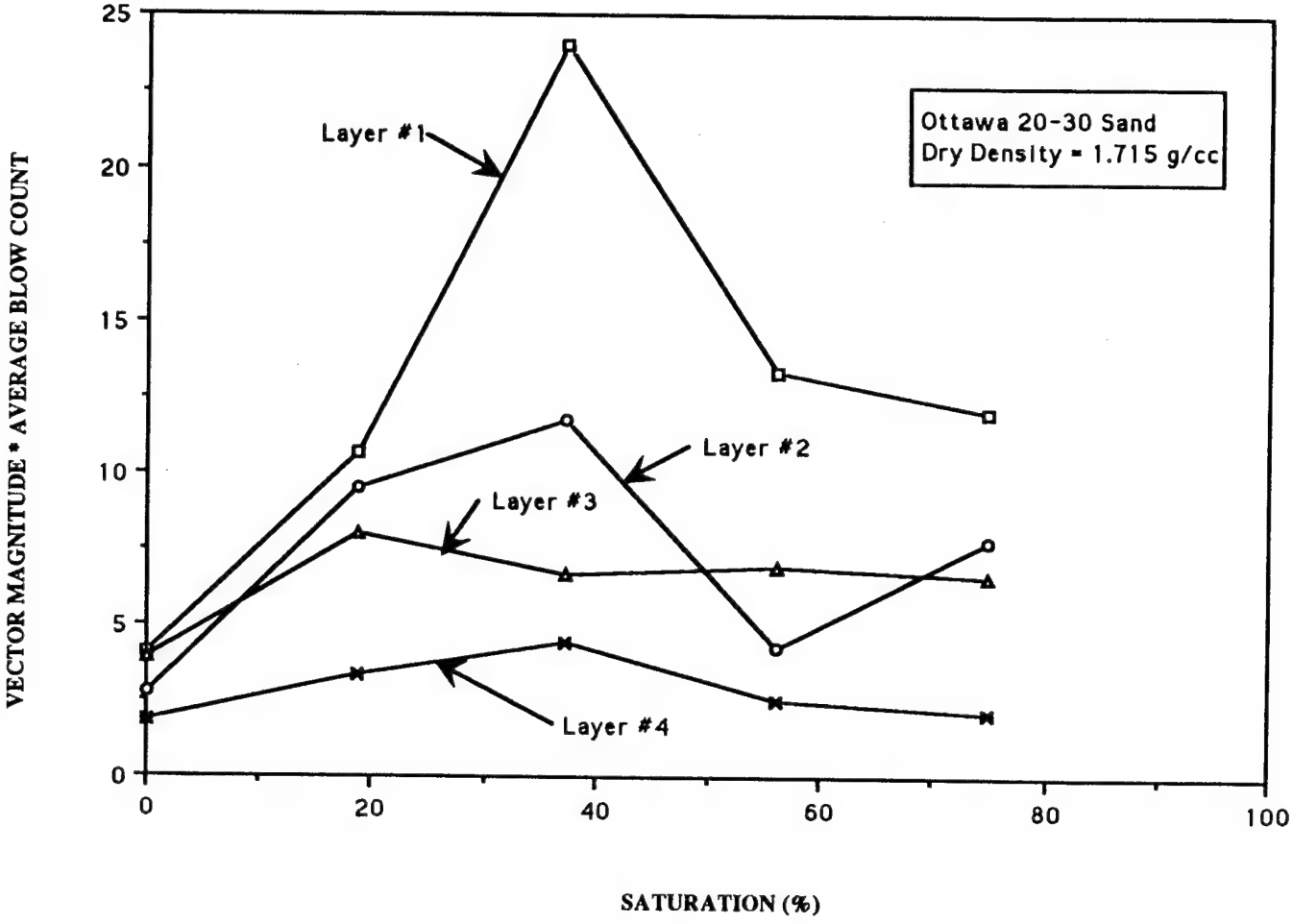

Figure 79. Product of Vector Magnitude and Average Blow Count as a Funtion of Saturation for Ottawa 20-30 Sand (SHPB).

specimens, respectively. In each figure, the product of vector magnitude and total blow count indicates that Layer 1 has the greatest value at all saturations. In Layers 2, 3, and 4, the product of vector magnitude and total compaction energy decrease with respect to saturation. However, in most cases values for vector magnitude are greater for SHPB specimens than for NO SHPB specimens and therefore, the curves developed in Figures 78 and 79 are dependent on the vector magnitude values.

Overall, the NO SHPB specimens showed a more uniform increase in the product of vector magnitude and average blow count as saturations increased, whereas the product for the SHPB specimens varied in that there was more dispersion within each layer. This relates to compaction energy, compressional wave speed, and stress transmission ratio as a function of saturation which generally had maximum values at intermediate saturations.

3. Product of Vector Magnitude and Normalized Compressional Wave Speed and Stress Transmission Ratio

Figures 80 and 81 show the product of vector magnitude and normalized wave speed, and the product of vector magnitude and transmission ratio as a function of saturation, respectively, for SHPB specimen sections in the horizontal and vertical planes. Results in the horizontal and vertical planes for Figures 80 and 81 show a similar trend in that the product generally decreases with increasing saturation. Figures 82 and 83 show the product of normalized vector magnitude and normalized wave speed and transmission ratio normalized to unity at zero percent saturation as a function of saturation, respectively, for SHPB specimen sections in the horizontal and vertical planes.

The products of normalized products in Figures 82 and 83 for the vertical and horizontal planes show similar results to those shown in Figures 80 and 81. Figures 82 and 83 show a similar trend in that the product generally decreases with increasing saturation. The behavior in the vertical and horizontal planes of Figure 83 is a bit more pronounced than that of Figure 82. Overall, the product of vector magnitude and normalized wave speed and transmission ratio presented in this analysis show small variations in the results between the horizontal and vertical planes. This suggests that soil microstructure throughout the specimen may be similar.

Figures 84 and 85 show normalized vector magnitude for NO SHPB and SHPB specimens as a function of saturation (normalized to the results at S = 0 percent) in the vertical and horizontal planes, respectively. For SHPB specimens, vertical and horizontal planes exhibit the same general trend in that the normalized vector magnitude decreases as

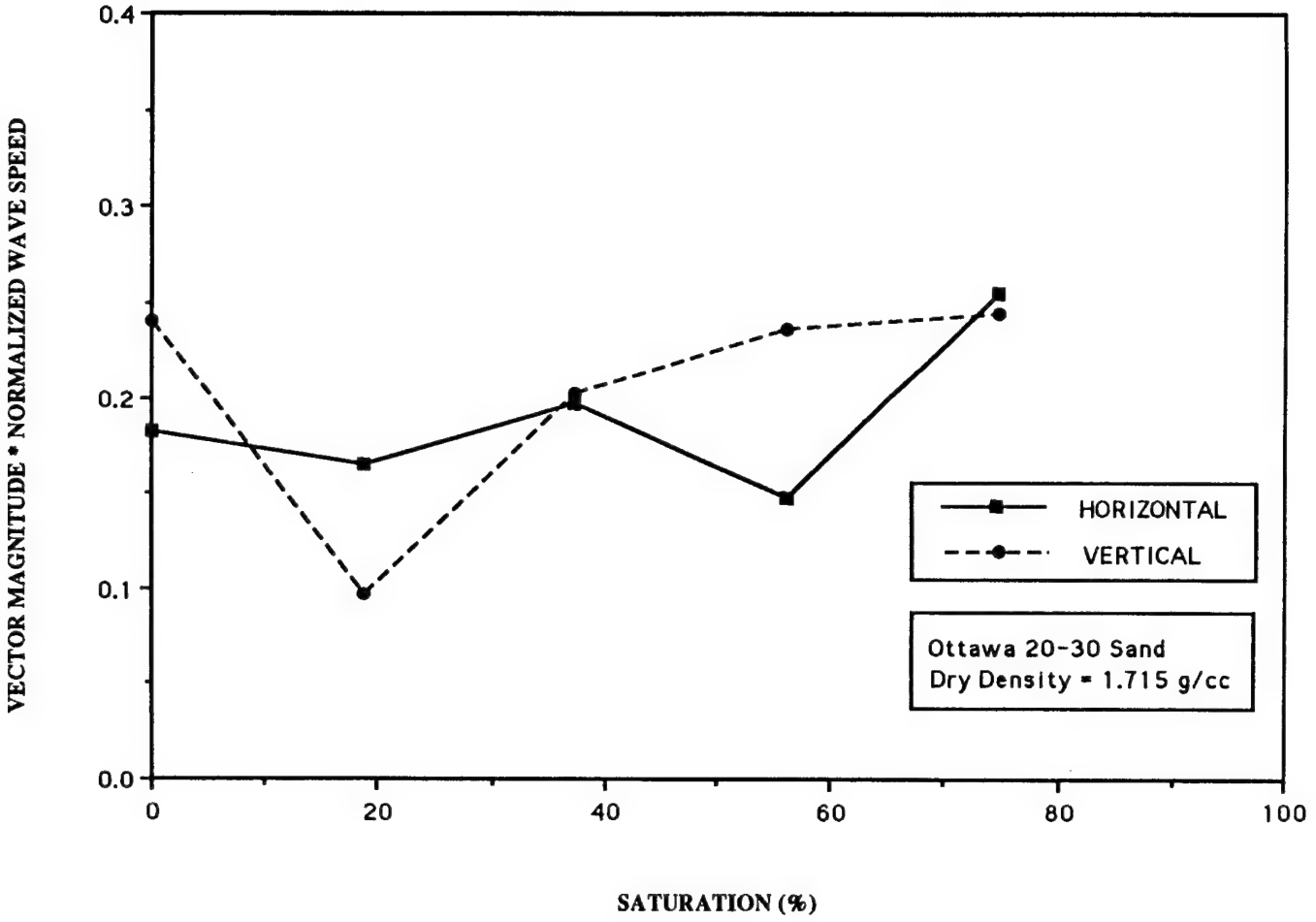

Figure 80. Product of Vector Magnitude and Normalized Wave Speed as a Function of Saturation Ottawa 20-30 Sand (SHPB).

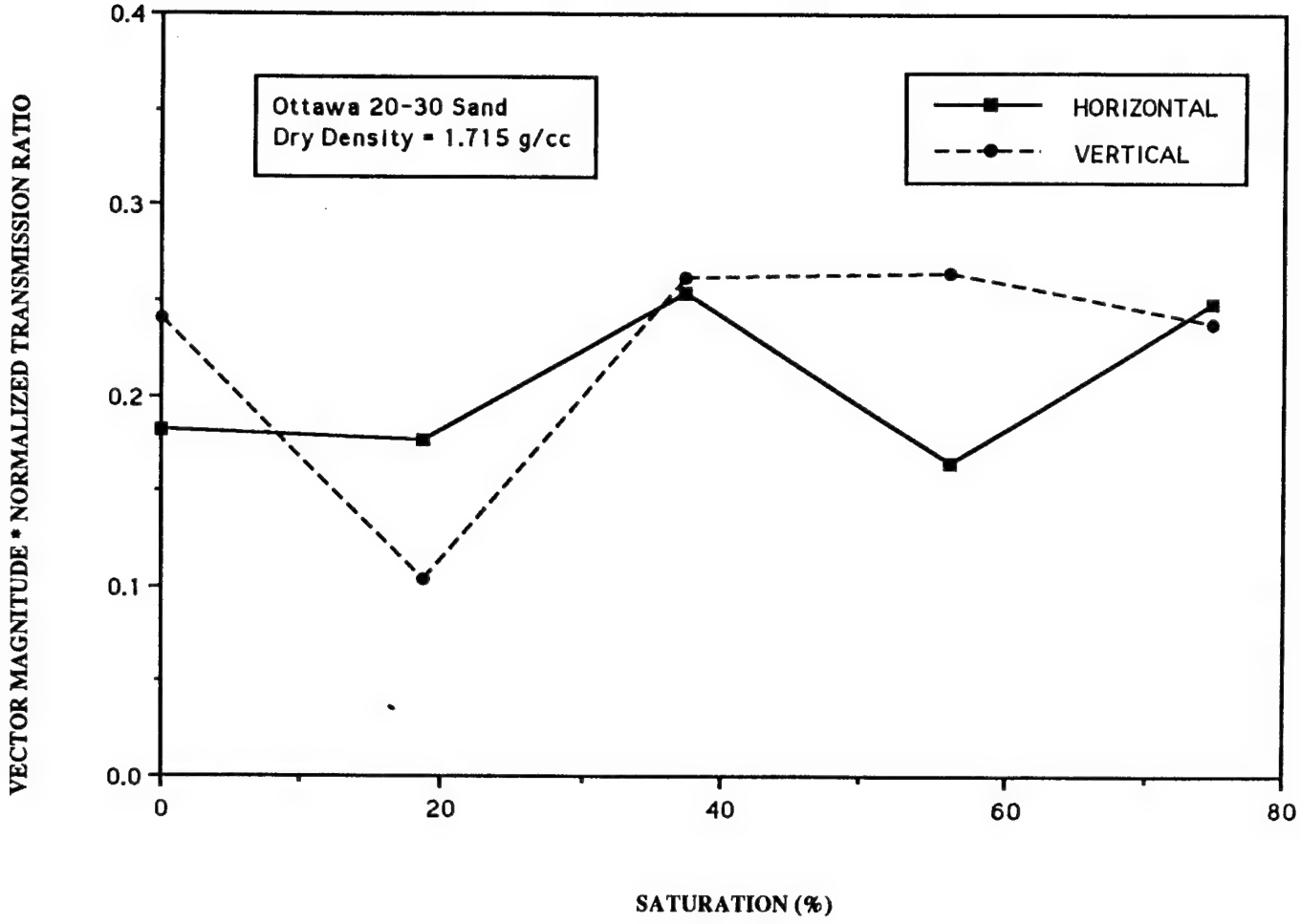

Figure 81. Product of Vector Magnitude and Normalized Transmission Ratio as a Function of Saturation Ottawa 20-30 Sand (SHPB).

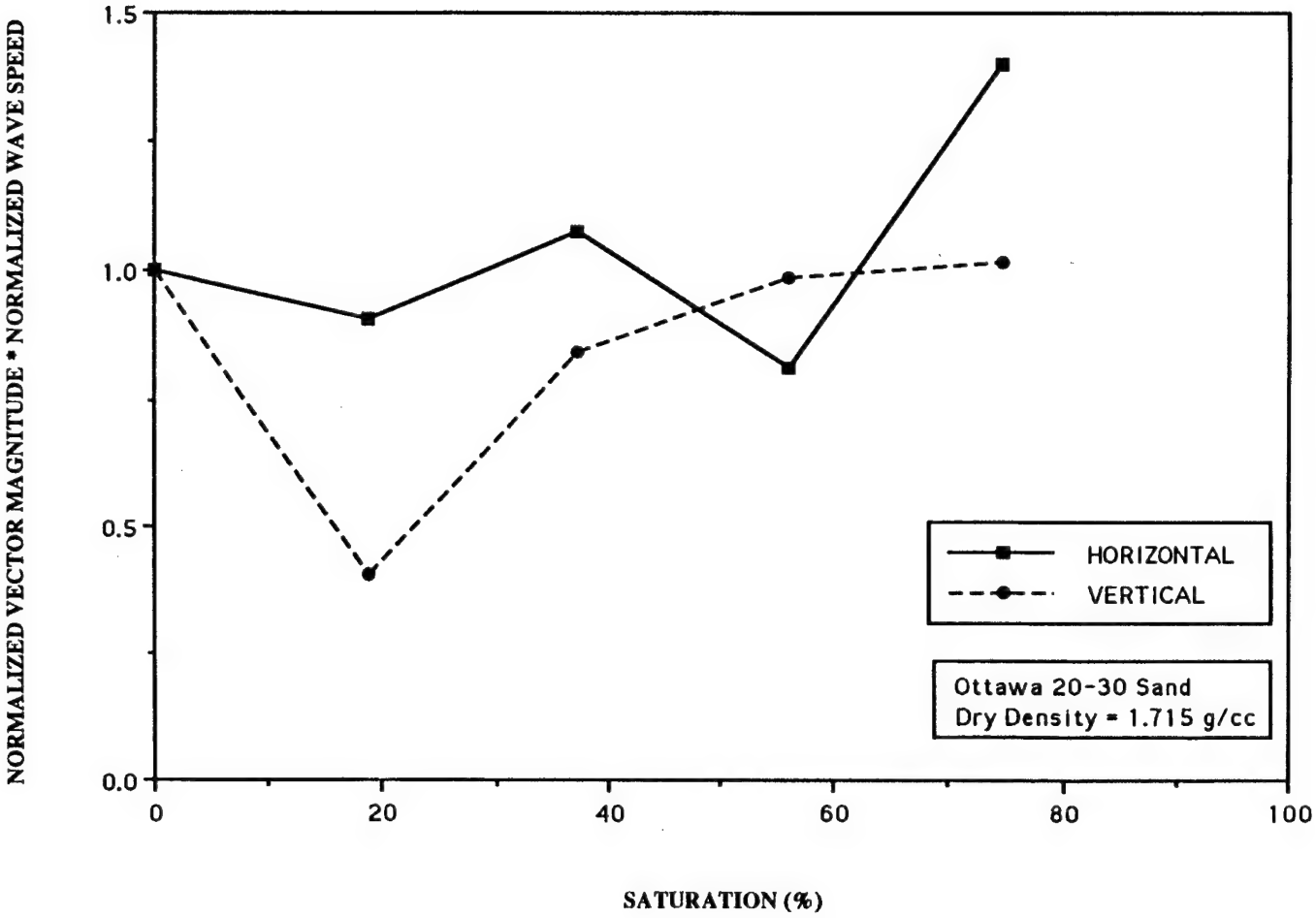

Figure 82. Product of Normalized Vector Magnitude and Normalized Wave Speed as a Function of Saturation for Ottawa 20-30 Sand (SHPB).

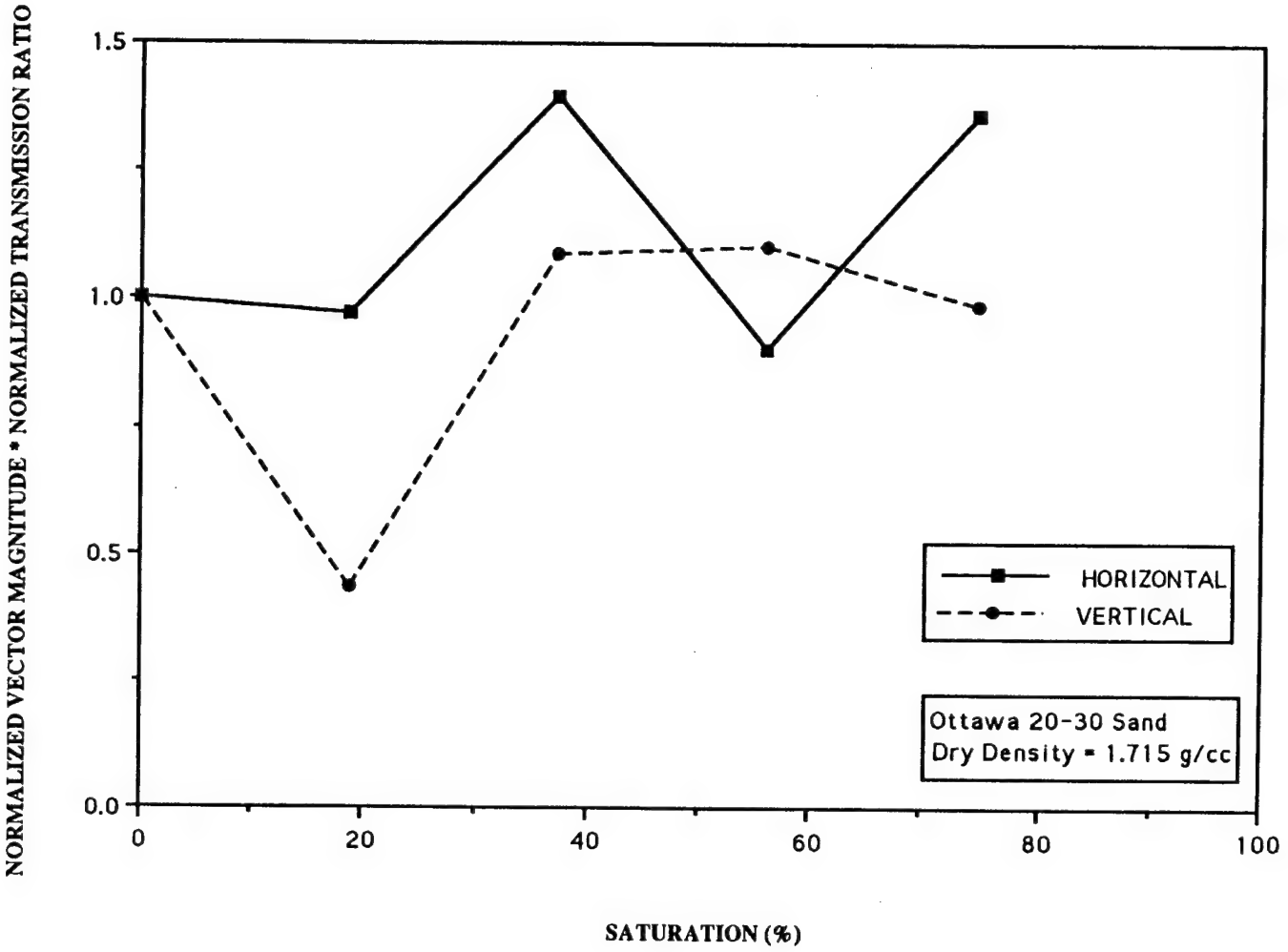

Figure 83. Product of Normalized Vector Magnitude and Normalized Transmission Ratio as Function of Saturation for Ottawa 20-30 Sand (SHPB).

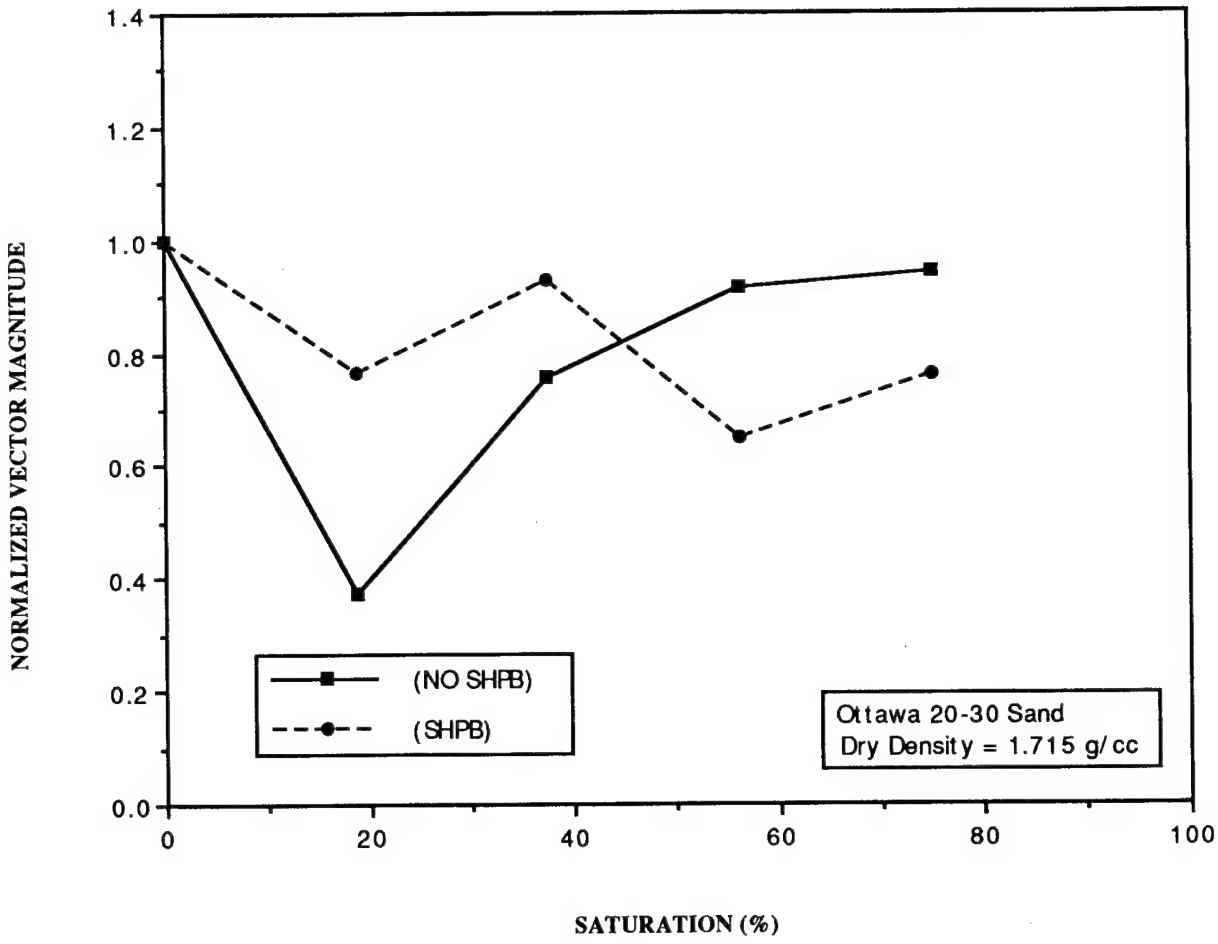

Figure 84. Normalized Vector Magnitude in the Vertical Plane as a Function of Saturation for Ottawa 20-30 Sand Compacted Moist and Tested Moist.

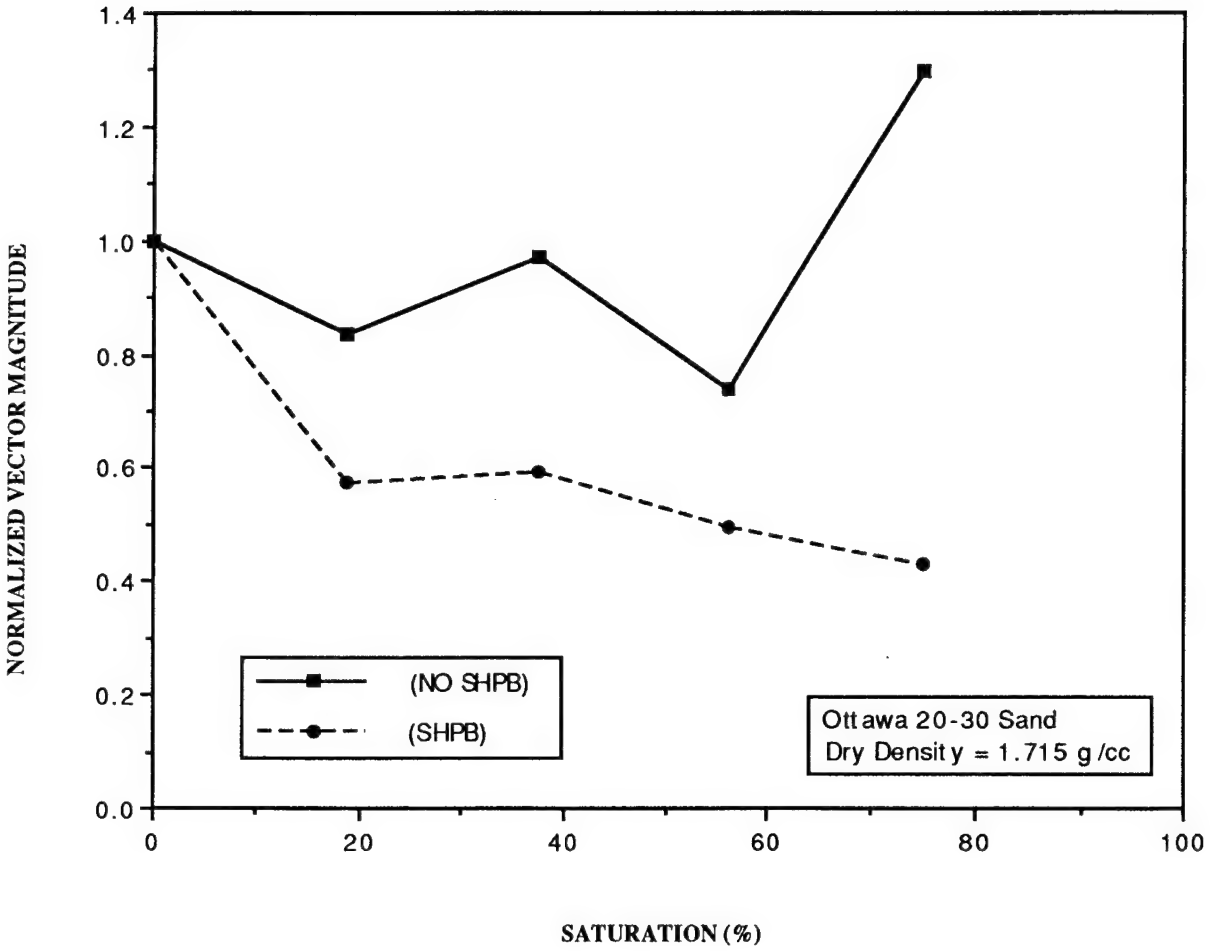

Figure 85. Normalized Vector Magnitude in the Horizontal Plane as a Function of Saturation for Ottawa 20-30 Sand Compacted Moist and Tested Moist.

saturation increases. However, for NO SHPB specimens, the normalized vector magnitude in the vertical and horizontal planes initially decrease to about 20 percent saturation and increase thereafter.

Figures 86 and 87 show normalized vector magnitude (NO SHPB) and normalized compressional wave speed (moist-moist) as a function of saturation, respectively, (normalized to results at S = 0 percent) for the vertical and horizontal planes. Both figures show an inverse relationship between vector magnitude and compressional wave speed. At intermediate saturations, vector magnitude values are lower while compressional wave speed values are higher. Figures 88 and 89 show normalized vector magnitude (NO SHPB) and normalized transmission ratio (moist-moist) as a function of saturation (normalized to the results at S = 0 percent) for the vertical and horizontal planes, respectively. Both figures show an inverse relationship between vector magnitude and transmission ratio. At intermediate saturations, vector magnitude values are lower while transmission ratio values are higher.

Figures 90 and 91 show normalized vector magnitude (NO SHPB) and normalized compressional wave speed (moist-dry) as a function of saturation (normalized at zero percent saturation) for the vertical and horizontal planes, respectively. Both figures show an inverse relationship between vector magnitude and compressional wave speed. At intermediate saturations, vector magnitude values are lower while compressional wave speed values are higher. Figures 92 and 93 show normalized vector magnitude (NO SHPB) and normalized transmission ratio (moist-dry) as a function of saturation (normalized at zero percent saturation) for the vertical and horizontal planes, respectively. Both figures show an inverse relationship between vector magnitude and transmission ratio. At intermediate saturations, vector magnitude values are lower while transmission ratio values are higher.

The results shown in Figures 86 through 93 suggest that the lower vector magnitude values indicate a more random particle orientation within the soil structure. This random orientation can be attributed to particles resisting movement relative to one another during the compaction process when moisture is present. This implies that a random orientation creates a stiffer soil, thus producing higher values of wave speed and transmission ratio at intermediate saturations for Ottawa 20-30 sand compacted to a constant dry density.

Figure 94 shows a comparison of compressional wave speed values obtained from in the split-Hopkinson pressure bar tests and theoretical calculations using constrained modulus values obtained from the quasi-static compression test results (Figures 38 through 43). Theoretical values of compressional wave speed were calculated using Equation (13)

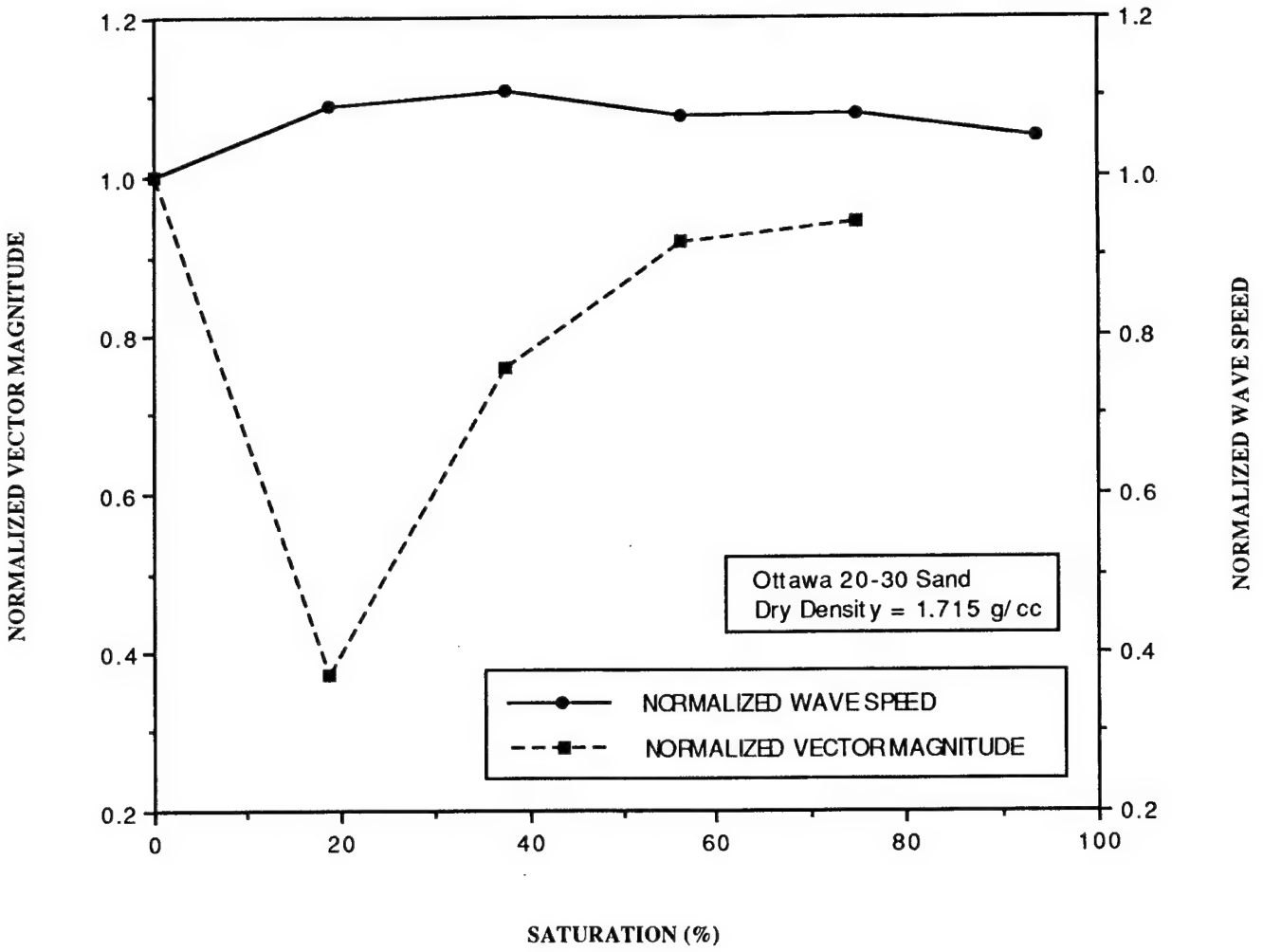

Figure 86. Normalized Vector Magnitude (NO SHPB) in the Vertical Plane and Normalized Wave Speed (moist-moist) as a Function of Saturation.

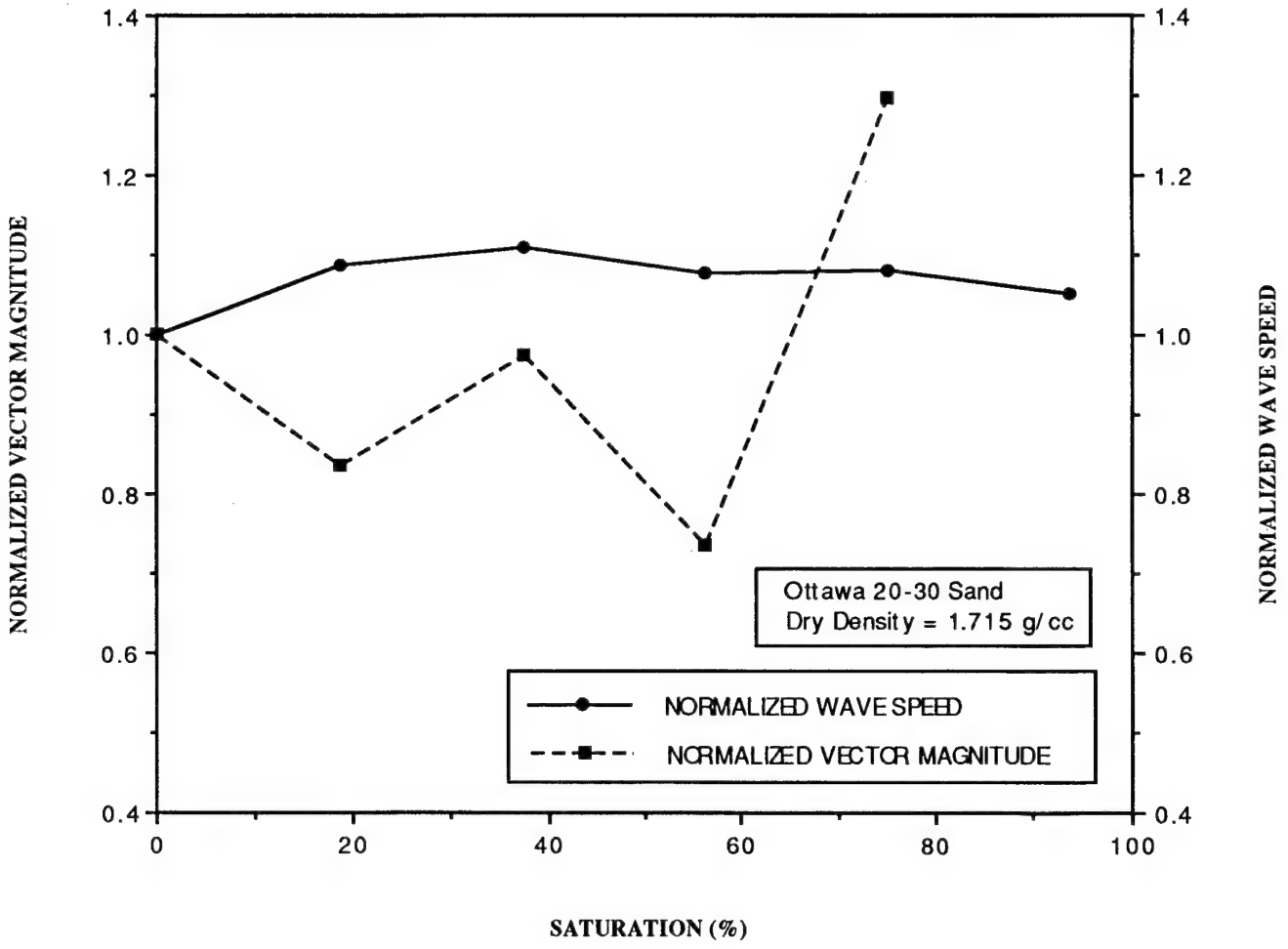

Figure 87. Normalized Vector Magnitude (NO SHPB) in the Horizontal Plane and Normalized Wave Speed (moist-moist) as a Function of Saturation.

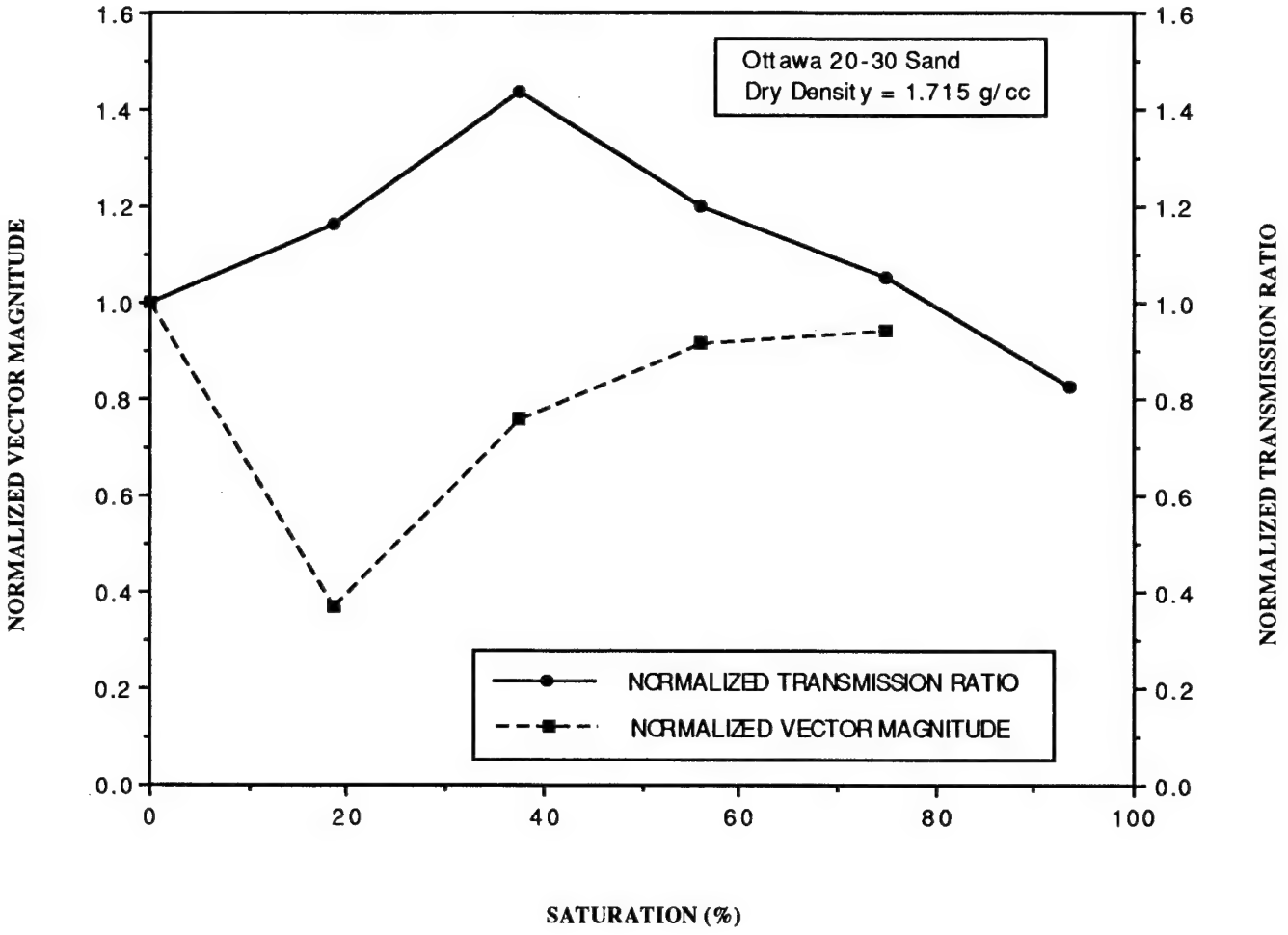

Figure 88. Normalized Vector Magnitude (NO SHPB) in the Vertical Plane and Normalized Transmission Ratio (moist-moist) as a Function of Saturation.

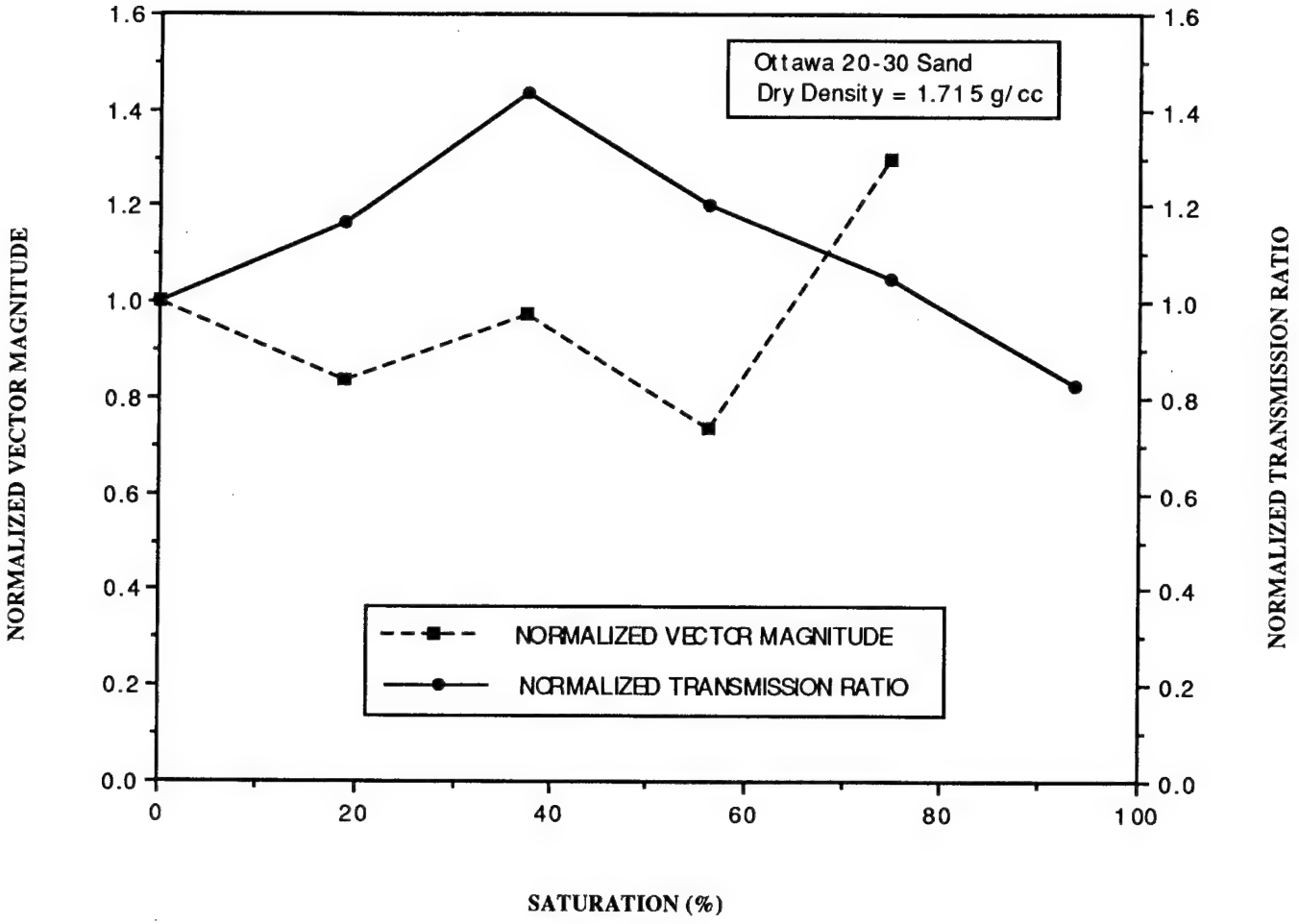

Figure 89. Normalized Vector Magnitude (NO SHPB) in the Horizontal Plane and Normalized Transmission Ratio (moist-moist) as a Function of Saturation.

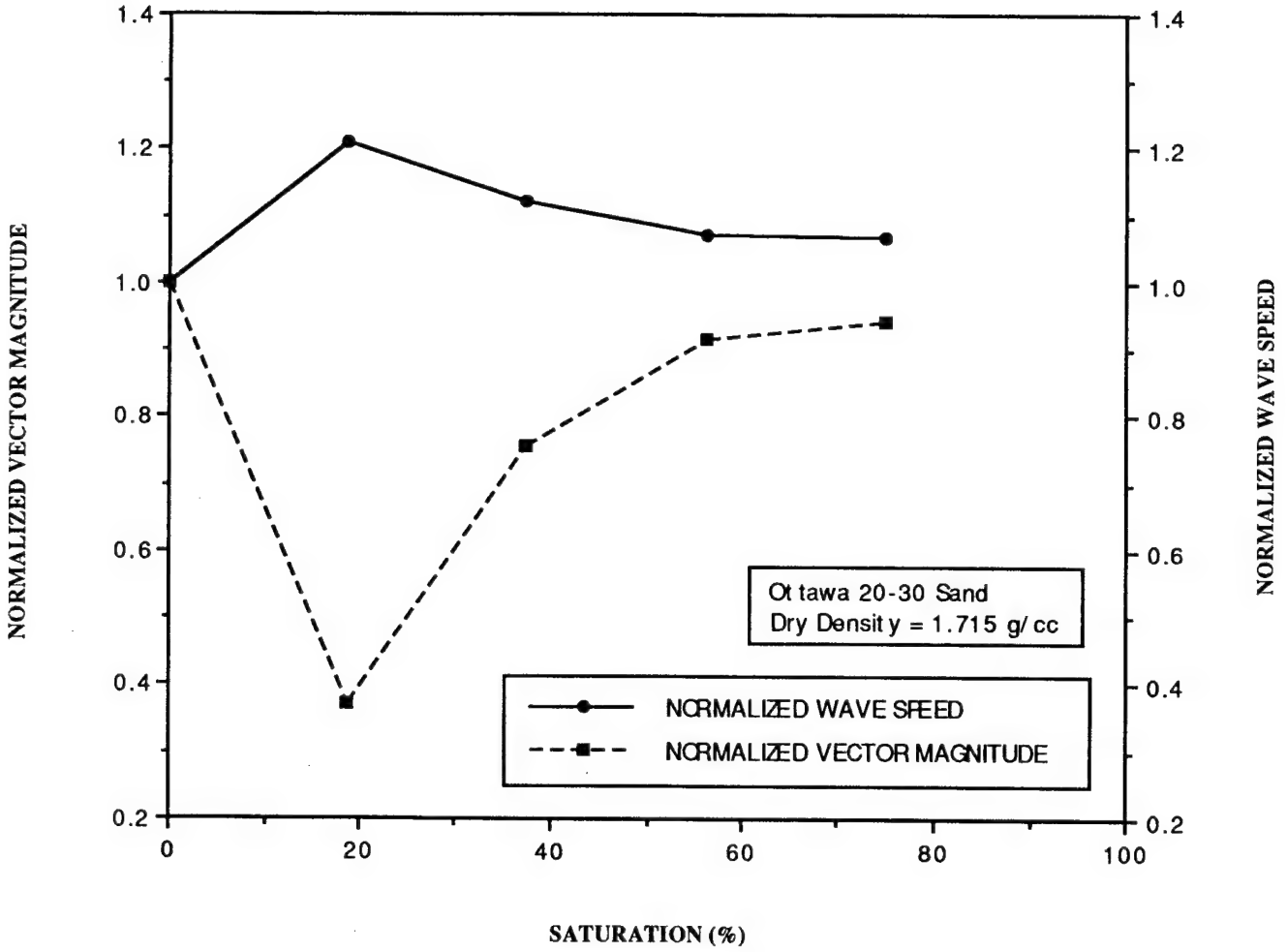

Figure 90. Normalized Vector Magnitude (NO SHPB) in the Vertical Plane and Normalized Wave Speed (moist-dry) as a Function of Saturation.

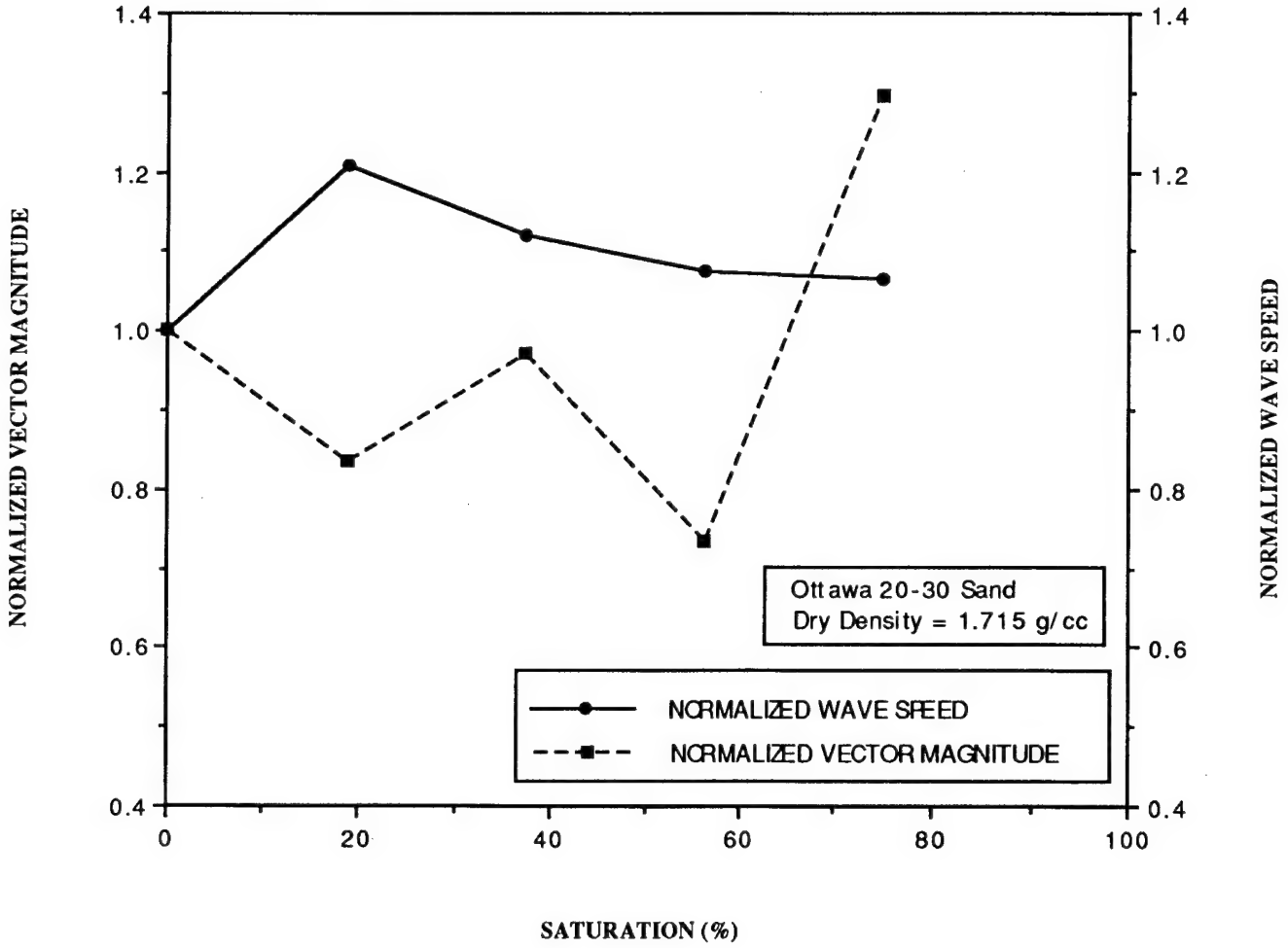

Figure 91. Normalized Vector Magnitude (NO SHPB) in the Horizontal Plane and Normalized Wave Speed (moist-dry) as a Function of Saturation.

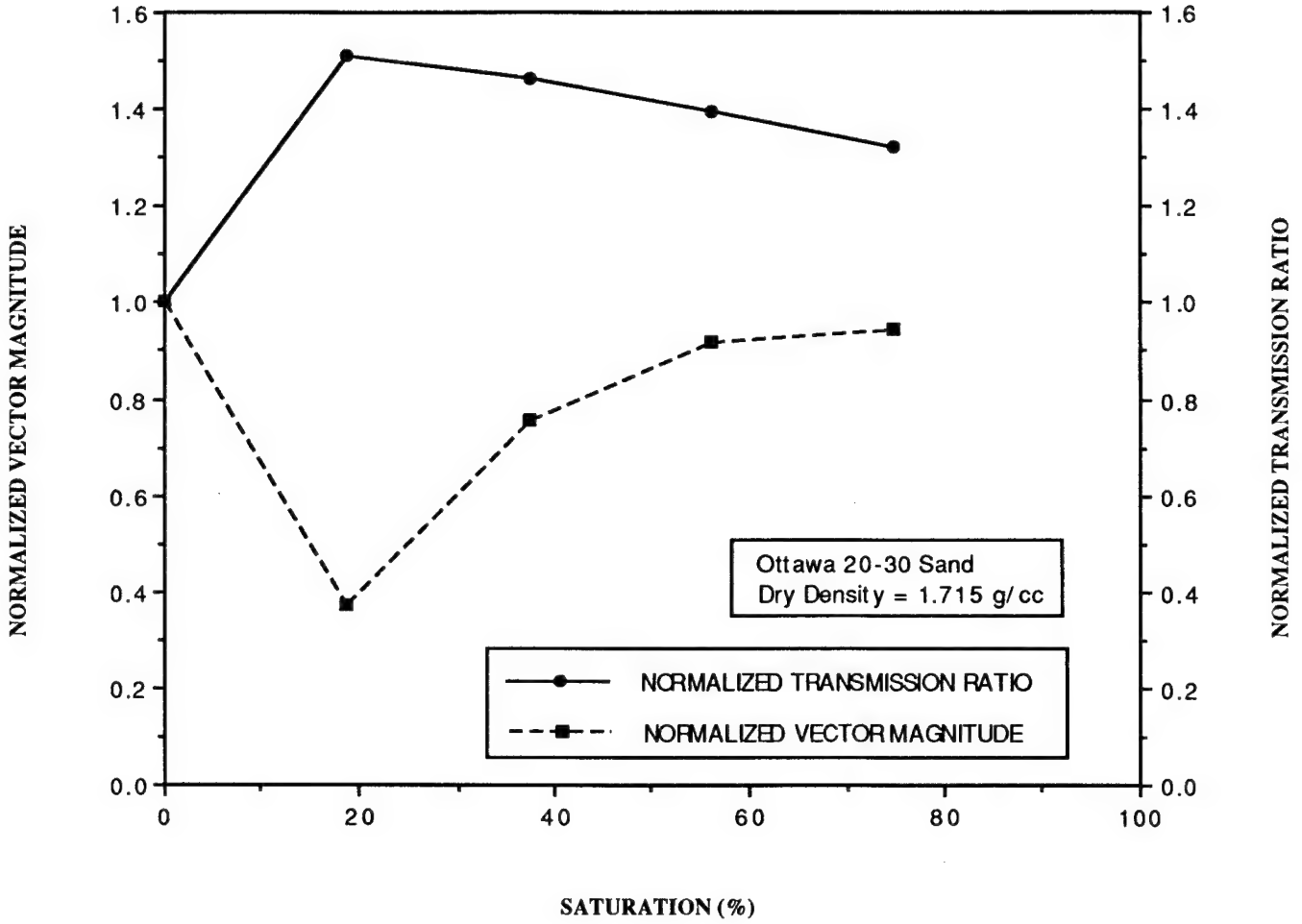

Figure 92. Normalized Vector Magnitude (NO SHPB) in the Vertical Plane and Normalized Transmission Ratio (moist-dry) as a Function of Saturation.

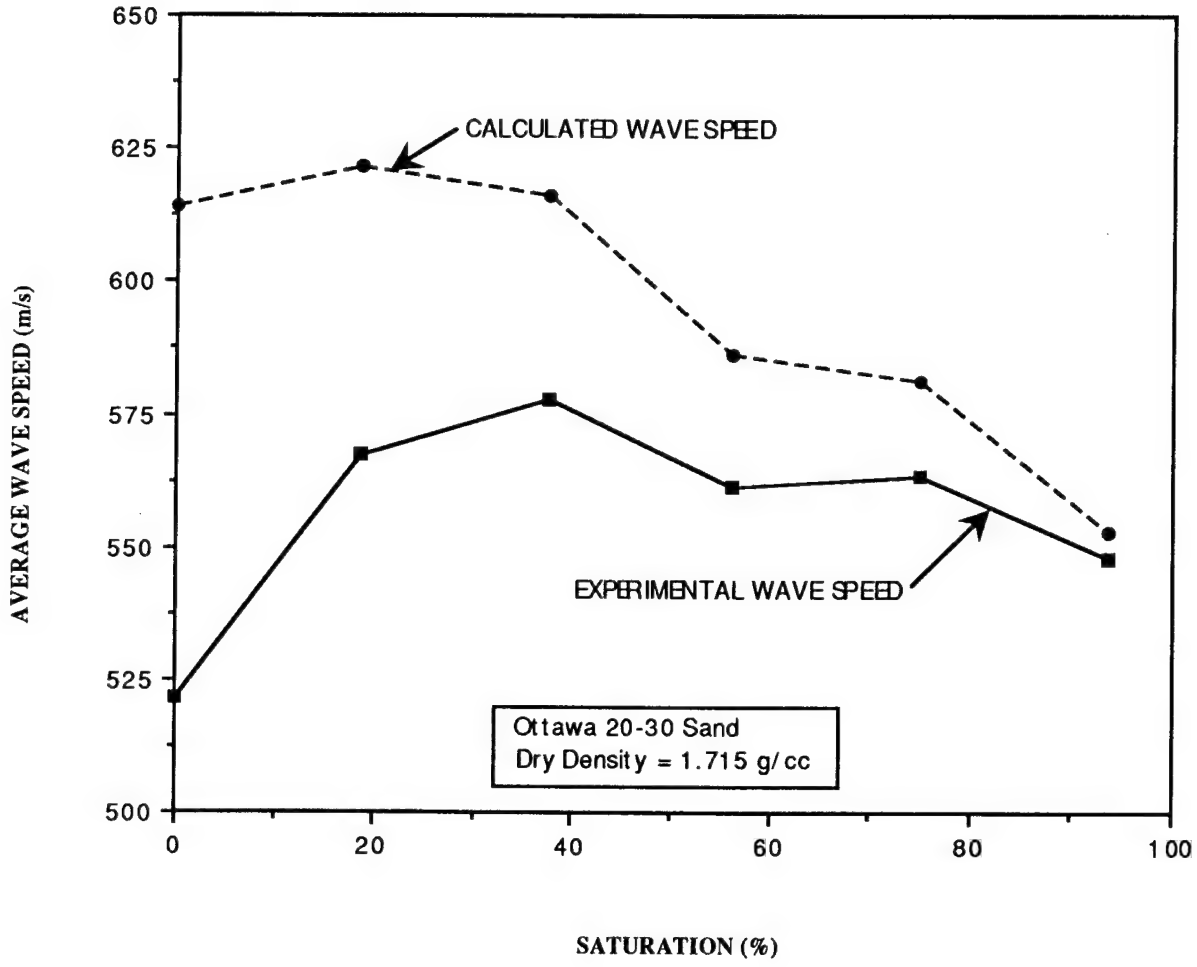

Figure 94. Comparison of Average Experimental and Calculated Wave Speed as a Function of Saturation for Moist/Moist Tests.

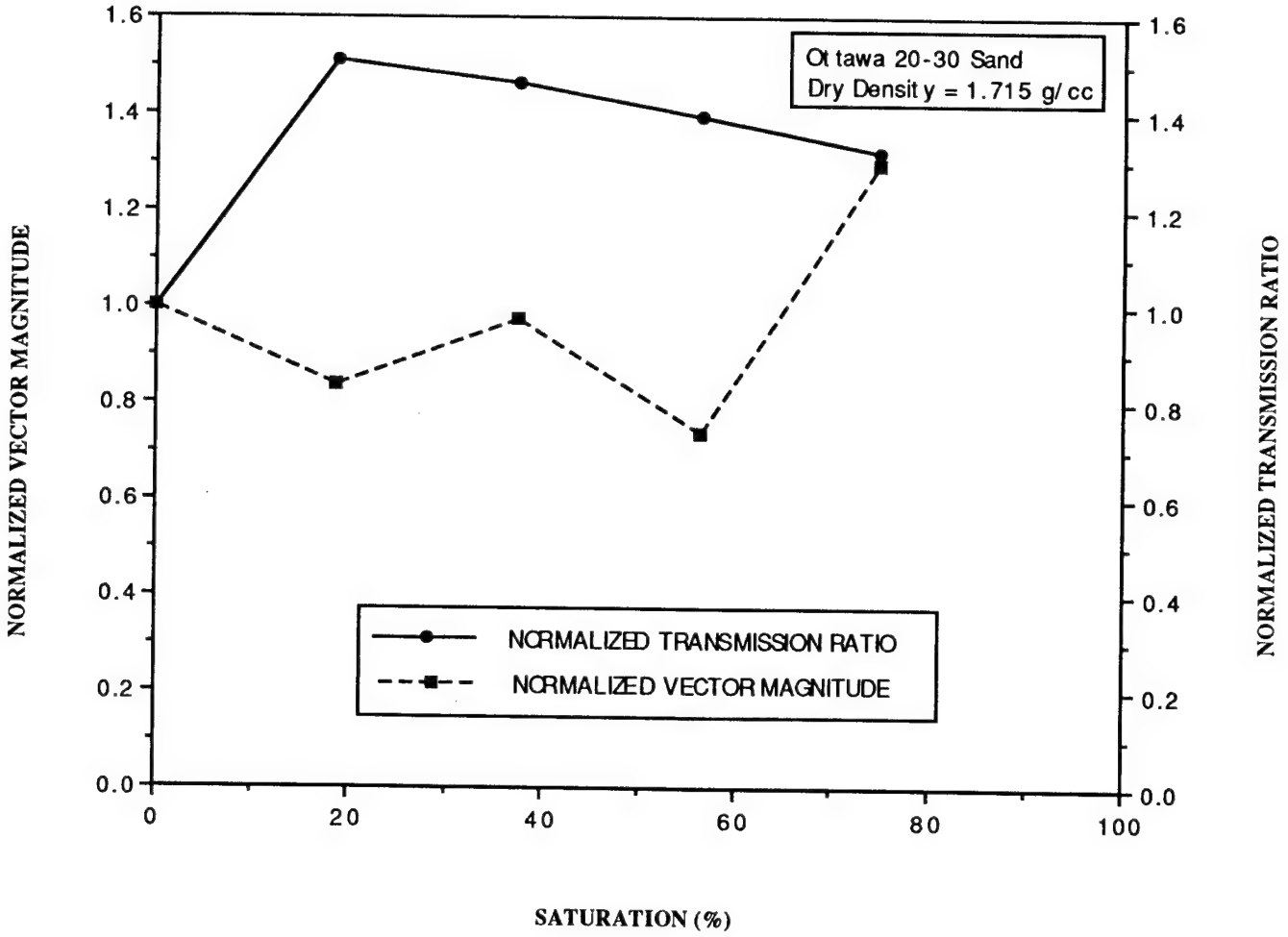

Figure 93. Normalized Vector Magnitude (NO SHPB) in the Horizontal Plane and Normalized Transmission Ratio (moist-dry) as a Function of Saturation.

and replacing the modulus of elasticity, E, with the constrained modulus, D. At all saturations, the theoretical wave speeds are greater than experimental values. The theoretical wave speed slightly increases from zero to about 20 percent saturation and gradually decreases thereafter. At saturations greater than about 40 percent both experimental and theoretical wave speed curves exhibit the same general trend. Table 9 shows results of constrained modulus and theoretical compressional wave speed.

TABLE 9. RESULTS OF CONSTRAINED MODULUS AND CALCULATED WAVE SPEED FOR OTTAWA 20-30 SAND COMPACTED MOIST AND TESTED MOIST

S (%)	Total Unit Weight (g/cc)	Constrained Modulus (kPa)	Normalized Constrained Modulus	Calculated Wave Speed (m/sec)	Normalized Wave Speed
0.0	1.715	13595	1.000	614.3	1.000
18.7	1.781	14463	1.064	621.7	1.012
37.4	1.847	14740	1.084	616.3	1.003
56.2	1.913	13814	1.016	586.3	0.954
74.9	1.979	14041	1.033	581.1	0.946
93.6	2.045	13131	0.966	552.8	0.900

4. Comparison of Vector Magnitude and Rayleigh Values

Vector magnitude and Rayleigh test of significance values can be related as follows. A preferred particle orientation exists in a soil when the Rayleigh value, p, is less than 0.05 (see Equation (10)). The corresponding vector magnitude value was generally in the range of 0.1 to 0.5 for this investigation; however the highest obtainable value is 1.0. A correlation between the confidence angle and Rayleigh value can also be observed such that a smaller confidence angle is present when the Rayleigh value is below 0.05. This implies that the dispersion within the azimuth readings is small at lower Rayleigh values.

a. Horizontal and Vertical Planes

Similar vector magnitude and Rayleigh values were obtained in the horizontal and vertical planes. All Rayleigh values were less than 0.05 for NO SHPB and SHPB specimens. The only exception was the Rayleigh value at saturations of 18.7 percent for

NO SHPB specimens in the vertical plane. One possible reason for this is that the number of particles measured were less than those measured at other saturations, or that no preferred particle orientations exist for that section. The number of particles measured, N, does affect the Rayleigh value. In comparing the vertical and horizontal planes, the sections that showed a preferred particle orientation had a number of particle measurements greater than or equal to 320. This coincides with the findings from other researchers such as Oda (1972b) and Campbell (1985) who said that a minimum of 200 to 300 particles need to be measured in an orientation analysis.

The lower Rayleigh values and higher vector magnitude values obtained in the horizontal and vertical planes may be attributed to the location of Section A-A (see Figures 22 and 23). Ottawa 20-30 sand is well rounded and elliptically shaped in two dimensions, thus particles will tend to rest on the longest axis parallel to the plane of deposition (90 or 270-degrees) for dry conditions only (see previous discussion in SECTION V). If a majority of the particles follow this trend then it is expected that lower Rayleigh values and higher vector magnitude values will be obtained.

Stresses developed during compaction using the standard Proctor hammer force the sand to rearrange itself into a denser packing after initial placement. During SHPB testing the density increases further and the soil particles are forced into a higher degree of preferred orientation by rotating a majority of the particles from their original orientation back along the plane of deposition plus or minus a few degrees for dry and unsaturated conditions. This may explain why lower Rayleigh values and higher vector magnitude values are obtained in the horizontal and vertical planes for SHPB specimens when compared with the NO SHPB results.

Overall, the vertical plane results had the highest vector magnitude values for both NO SHPB and SHPB specimens. The vertical plane on Section A-A (Figures 22 and 23) is at the centerline of the specimen and at a constant distance from the boundary, i.e., the wall of the specimen container. Therefore, any boundary condition effects should be uniform over the entire vertical plane since the specimen is cylindrical in shape. The horizontal plane on Section A-A is not at a constant distance from the boundary and boundary condition effects would not be expected to be uniform over the entire horizontal plane. This may be the reason for lower vector magnitude values in the horizontal plane. However, the trends for both the vertical and horizontal directions are similar (see Figures 80 through 83).

b. Layers 1 Through 4

The vector magnitude and Rayleigh values obtained in Layers 1 through 4 were typically higher than those for the horizontal and vertical planes. The data can be seen in Tables 6 and 7 for NO SHPB and SHPB specimens, respectively. In each layer the Rayleigh values were less than 0.05 for NO SHPB and SHPB specimens. The only exceptions were the Rayleigh values at a saturation of 18.7 percent for NO SHPB results for Layer 3, and at saturation of 18.7 percent and 37.4 percent for NO SHPB results for Layer 4. The number of particles measured for each individual layer was not very large, typically on the order of 120 to 220 particles. This does not coincide with the findings of Oda (1972b) and Campbell (1985), who stated that 200 to 300 particles need to be measured for particle orientation analysis. A possible reason for higher vector magnitude values and lower Rayleigh values for Layers 1 through 4 can be attributed to the location of Section A-A (see Figures 22 and 23). Orientation data for Layers 1 through 4 were obtained from the vertical plane, developed from Section A-A (see Figure 27), and a preferred particle orientation was evident in both NO SHPB and SHPB specimens along the vertical plane (see Figure 72, 73, 78, and 79).

In each specimen, the first layer was subjected to the greatest amount of compaction energy (see Figure 61). Therefore, it was expected that Layer 1 would have low Rayleigh values and higher vector magnitude values than Layers 2, 3, and 4 due to the increased number of blows (i.e., higher compaction energy). Even though Layer 1 received the greatest amount of compaction energy it was also the layer closest to the steel pedestal. The effect of the reflected tensile wave may have been greatest in this layer and may have rearranged the particles, thereby reducing the vector magnitude value. However, a preferred particle orientation does exist within this layer for both the NO SHPB and SHPB specimens.

Layers 2 and 3 were subjected to an intermediate amount of compaction energy (see Figure 61). Therefore, it was expected that these layers would have similar Rayleigh values and lower vector magnitude values than Layer 1. As the total amount of compaction energy decreases (compared to Layer 1), there would be less rearrangement of the particles leading to lower vector magnitude values. However, even though Layers 2 and 3 received an intermediate amount of compaction energy they are further away from the steel pedestal, thus the effect of the reflected tensile wave may be lower in these two layers. Therefore, the particles may have less rearrangement and the vector magnitude values would be lower. A preferred particle orientation does, however, exist within both layers for both the NO SHPB and SHPB specimens.

Layer 4 was subjected to the least amount of compaction energy (as compared to Layers 1, 2, and 3, see Figure 61). It was expected that Layer 4 would have higher Rayleigh values and the lowest vector magnitude values. Layer 4 is the furthest away from the steel pedestal and the effect of the reflected tensile wave may be the least in this layer and due to this, particles may have less rearrangement, therefore vector magnitude values would be lower. However, a preferred particle orientation does exist within this layer for both the NO SHPB and SHPB specimens.

SECTION VI

SUMMARY

This study has investigated the effects of saturation on soil microstructure, compaction energy, compressional wave speed, and stress transmission ratio in unsaturated soils. Soils are generally in an unsaturated state in the field, therefore a better understanding of their behavior during dynamic loading is useful.

Specimens of Ottawa 20-30 sand were compacted to a constant dry density of 1.715 g/cm^3 in a 2.54 cm (1.0 inches) wall specimen container in four layers using a standard Proctor hammer. Saturations varied from zero to about 94 percent. Some specimens were tested under quasi-static loading conditions using a Material Testing System (MTS) device to evaluate the soil's constrained modulus. Dynamic wave propagation tests were performed using a split-Hopkinson pressure bar (SHPB) which applies an intense, transient compressive loading to the specimen. Compressional wave speed and stress transmission ratio can be evaluated through the use of the SHPB.

The amount of compaction energy required to compact the Ottawa 20-30 sand to a constant dry density of 1.715 g/cm^3 varied with saturation. This trend has been observed by several other researchers for Ottawa 20-30 sand and other sands (Ross et al., 1986; Pierce, 1989; Veyera, 1989). There appears to be an increase in soil stiffness at intermediate saturations which is most likely due to capillary tension forces present during compaction. Capillary tension forces may resist particle rearrangement, thus requiring more compaction energy. As saturations increase beyond about 60 percent, the additional moisture may "lubricate" the soil particles as surface tension forces are reduced which would allow particles to move relative to one another with less resistance decreasing the amount of compactive energy required to obtain a constant dry density.

More compaction energy was required to compact the first layer at all saturations as compared with Layers 2, 3, and 4. In all four layers, less energy was required to compact the soil to a constant dry density at zero percent saturation (dry soil). More energy was required to compact each layer to a constant dry density at intermediate saturations (20 percent to 60 percent). The effect of moisture (capillary tension forces) during compaction for each individual layer is also evident (see Figure 61).

Dynamic split-Hopkinson pressure bar (SHPB) tests were performed on specimens compacted moist and tested moist (moist-moist), and also on specimens compacted moist and tested dry (moist-dry) to evaluate the influence of moisture during SHPB testing. Results showed that specimens compacted moist and tested moist had lower values of

compressional wave speed and stress transmission ratio at all saturations. Thus, the presence of moisture during SHPB testing does influence the compressional wave speed and stress transmission ratio.

The results presented herein are similar to those obtained by previous researchers who performed SHPB tests on the same and similar soils compacted moist and tested moist (Veyera, 1989; Ross, 1989; Felice et. al., 1987; and Ross et. al., 1986). Results of compaction energy, compressional wave speed, stress transmission ratio, and constrained modulus as a function of saturation all show a similar trend. At intermediate saturations (20 percent to 75 percent) these values were greater than those at zero percent saturation, and may be due to an increase in soil stiffness from capillary tension forces. However, Pierce (1989) noted that capillary stresses are negligible compared to stress levels during in SHPB testing and therefore probably do not influence the dynamic response.

Results of compressional wave speed and stress transmission ratio as a function of saturation in this investigation differed from results presented by Pierce (1989) who compacted specimens dry and saturated and desaturated them to the desired level by means of a pressure plate apparatus, thus the influence of moisture during compaction was not present. In this investigation specimens were compacted moist, thus the influence of moisture was present during compaction. Differences between results obtained by Pierce (1989), Ross (1986), Veyera (1989), and this investigation can be attributed to differences in sample preparation techniques particularly the presence of moisture during compaction.

Specimens were compacted using the standard Proctor hammer only (NO SHPB) and also compacted using the standard Proctor hammer and tested using high strain rates in the split-Hopkinson pressure bar (SHPB). The microstructure from both NO SHPB and SHPB specimens was preserved by the use of a two-part epoxy resin. Sections were taken through the cylindrical specimen to view the microstructure along different planes. Photomicrographs of each specimen were subdivided into three different planes, i.e., the horizontal, vertical, and semicircular directions. The vertical plane was further subdivided into four 2.54 cm (1.0 in) layers such that the microstructure of each compacted layer could be analyzed. A complete microstructural analysis was performed including an axial ratio and particle long-axis orientation study. A total of 70 rose plots were generated by digitizing the two-dimensional photomicrographs. A relationship between the vector magnitude (a result of the statistical analysis from the Rosy program) and saturation was analyzed. The product of vector magnitude and compaction energy, vector magnitude and compressional wave speed, and vector magnitude and transmission ratio was also analyzed as a function of saturation.

The microstructural analysis produced several important findings. The horizontal section, vertical section, and Layers 1 through 4 showed that a preferred orientation exists for both NO SHPB and SHPB specimens. Most of the specimens had vector mean values in the range of 260- to 280-degrees. The semicircular section showed no preferred orientation for both NO SHPB and SHPB specimens which is most likely due to the small number of particles measured. An inverse relationship exists between compaction energy, compressional wave speed, and stress transmission ratio, and vector magnitude as a function of saturation (i.e., at intermediate saturations lower values of vector magnitude were observed).

Soil microstructure developed during compaction is influenced by the moisture present during compaction. This can be seen in vector magnitude values obtained from the particle orientation analysis in that lower values are obtained at intermediate saturations for all parameters investigated. The lower vector magnitude values can be related to soil stiffness and the data implies that if a more random orientation of particles exists within the grain structure, a stiffer soil may be present. Therefore, it appears that the presence of moisture during compaction significantly affects the resultant soil microstructure which in turn influences compaction energy, compressional wave speed, and stress transmission ratio.

Results from quasi-static compression tests and constrained modulus data were developed from stress-strain curves generated by the MTS device using four compacted layers and one compacted layer at each saturation level. Stress-strain curves at zero percent saturation were compared to stress-strain curves at all other saturations. There were some noticeable differences between the slopes of the stress-strain curves with variations in saturation. Stress-strain curves which have the steepest slope indicate a stiffer soil structure. In general, as saturations are increased to about 60 percent, the soil became stiffer as compared with zero percent saturation. As saturations increase beyond 60 percent, the soil became less stiff. This compares well with SHPB test results for compressional wave speed and stress transmission ratio, in that a stiffer material is present to saturations of about 60 percent.

Values of constrained modulus at intermediate saturations (20 percent to 60 percent) were higher than at all other saturations. This trend was also observed in data for compaction energy (Figure 59), compressional wave speed (Figure 62, and stress transmission ratio (Figure 63) as a function of saturation. The behavior may be due to the resistance of particle movements relative to one another at intermediate saturations. By applying a quasi-static loading, the soil is compressed into a denser packing than that produced in the compaction procedure. At lower saturations, capillary forces resist particle

movements relative to one another. As saturation increases, capillary forces decrease, thereby reducing the frictional resistance between soil particles which may allow particles to move relative to one another with greater ease.

SECTION VII

CONCLUSIONS

Based on the results of this study and the discussions presented in previous chapters, the following conclusions were drawn. These conclusions pertain to the laboratory investigation of Ottawa 20-30 sand evaluated under the experimental conditions previously stated in this thesis.

- The results from dynamic SHPB tests, quasi-static compression tests and microstructural analyses indicate that the amount of moisture present during compaction is probably the most significant factor influencing both the dynamic and static behavior of Ottawa 20-30 sand.

- The compactive energy required to produce a constant dry density specimen by dynamic impact compaction is strongly dependent on the moisture present during compaction. The greatest amount of effort was necessary when compacting specimens at intermediate saturations (from about 20 percent to 60 percent). This is most probably due to the influence of capillary tension forces which affect the ease with which grains can reorient during compaction.

- The microstructural analysis results suggest that an inverse relationship exists between vector magnitude and compaction energy, compressional wave speed, stress transmission ratio and constrained modulus with variations in the degree of saturation. Lower vector magnitude values indicate a more random particle orientation and higher specimen stiffness at intermediate saturations. Higher vector magnitude values indicate a more preferred particle orientation and lower stiffness for dry soil (zero saturation) and at saturations above about 75 percent.

- For SHPB specimens compacted moist and tested moist, the transmission ratio increases from zero percent to about 40 percent saturation, and then decreases with increasing saturation. The wave speed increases from zero percent to about 20 percent saturation, and remains relatively constant thereafter. This implies that the presence of moisture during testing may have a lubricating effect, allowing the particles to move somewhat relative to each other during loading. However, the

influence of microstructure formed during compaction is a significant contributing factor.

- For SHPB specimens compacted moist and tested dry, increases in transmission ratio and wave speed are generally larger than for specimens compacted moist and tested moist, particularly at about 20 percent saturation, after which they decrease with increasing saturation. No plateau region exists at intermediate saturations and it appears that the microstructural characteristics developed during compaction which affect the dynamic properties, remain intact even after the moisture in the pores has been removed.

- Quasi-static uniaxial compression test results show changes in specimen stiffness with changes in compaction moisture which are generally consistent with trends observed in the SHPB dynamic test data.

SECTION VIII

RECOMMENDATIONS

After a thorough review of the results obtained in this investigation and those from previous work, the following recommendations for further research are made:

- The influence of specimen preparation techniques on stress transmission ratio, wave speed and vector magnitude results should be examined. Other possible compaction methods include pluviation, vibration and static densification.

- A model to predict compressional wave speed and stress transmission in unsaturated soils using laboratory results for wave speed, stress transmission ratio, and vector magnitude should be developed. The model should be verified and improved through a series of carefully controlled explosive field tests.

- Scaled tests should be performed in the centrifuge using actual explosive charges in compacted, unsaturated soils. This would have the benefit of being able to simulate a variety of field conditions in a laboratory environment and would also to provide an independent verification of the SHPB results reported herein.

- Microstructural analyses should be conducted to study the effects of particle shape and size compacted to varying degrees of dry density. These analyses may show that soil type and dry density affect wave speed, stress transmission ratio, and vector magnitude results.

- Analyses of two-dimensional particle preferred orientations developed under different confinement conditions (i.e., different specimen container wall thicknesses) should be performed.

- An analysis of the preferred orientation of pores within the soil should be considered. The orientation of pores which contains both water and air may influence stress transmission in an unsaturated soil.

- Three-dimensional characterization of soil microstructure should be undertaken. This will require developing new techniques and could use such devices as a CAT scanner or MRI. Results would be very useful in model development.

THIS PAGE INTENTIONALLY LEFT BLANK

APPENDIX A: Rose Diagrams

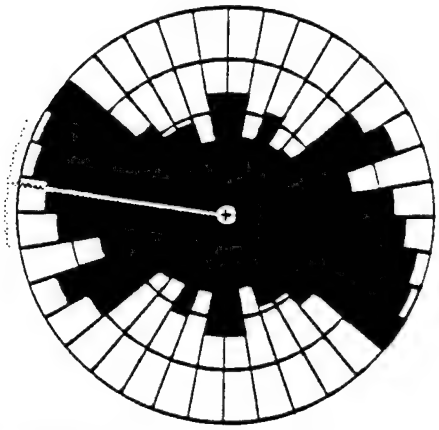

W=2.54 cm S=0% HORIZONTAL (NO SHPB)	Statistics
N = 615 Class Interval = 10 degrees Maximum Percentage = 8.8 Mean Percentage = 5.56 Standard Deviation = 1.88	Vector Mean = 277.8 Conf. Angle = 17.54 R Magnitude = 0.182 Rayleigh = 0.0000

Figure A.1. Results from statistical analysis using Rosy for W=2.54 cm (1.00 inch) and S=0% in the horizontal plane (NO SHPB).

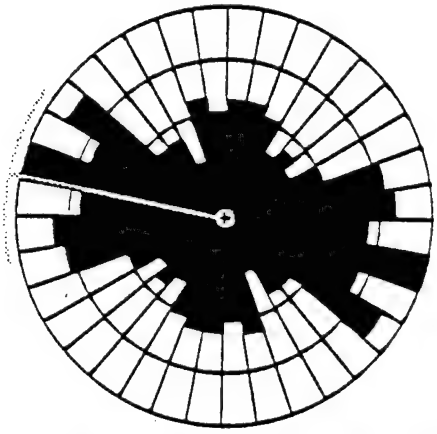

W=2.54 cm S=18.7% HORIZONTAL (NO SHPB)	Statistics
N = 487 Class Interval = 10 degrees Maximum Percentage = 9.7 Mean Percentage = 5.56 Standard Deviation = 1.92	Vector Mean = 280.8 Conf. Angle = 23.68 R Magnitude = 0.152 Rayleigh = 0.0000

Figure A.2. Results from statistical analysis using Rosy for W=2.54 cm (1.00 inch) and S=18.7% in the horizontal plane (NO SHPB).

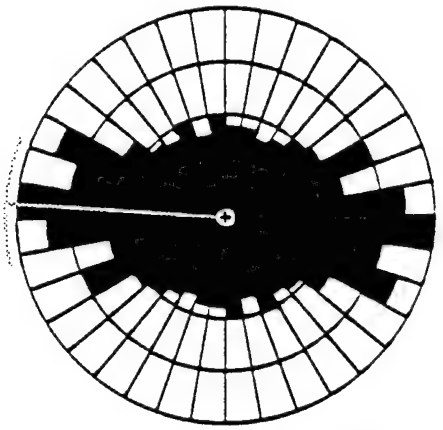

W=2.54 cm S=37.4% HORIZONTAL (NO SHPB)	Statistics
N = 618	Vector Mean = 274.4
Class Interval = 10 degrees	Conf. Angle = 17.73
Maximum Percentage = 9.5	R Magnitude = 0.177
Mean Percentage = 5.56 Standard Deviation = 1.74	Rayleigh = 0.0000

Figure A.3. Results from statistical analysis using Rosy for W=2.54 cm (1.00 inch) and S=37.4% in the horizontal plane (NO SHPB).

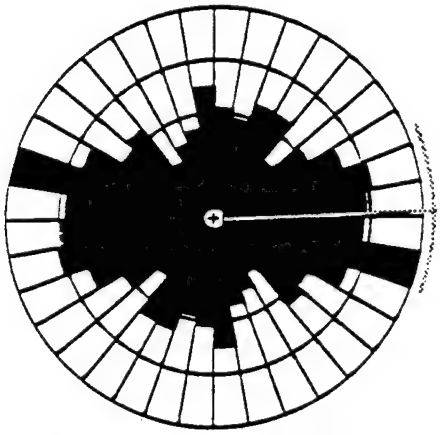

W=2.54 cm S=56.2% HORIZONTAL (NO SHPB)	Statistics
N = 636	Vector Mean = 88.3
Class Interval = 10 degrees	Conf. Angle = 22.62
Maximum Percentage = 9.6	R Magnitude = 0.137
Mean Percentage = 5.56 Standard Deviation = 1.58	Rayleigh = 0.0000

Figure A.4. Results from statistical analysis using Rosy for W=2.54 cm (1.00 inch) and S=56.2% in the horizontal plane (NO SHPB).

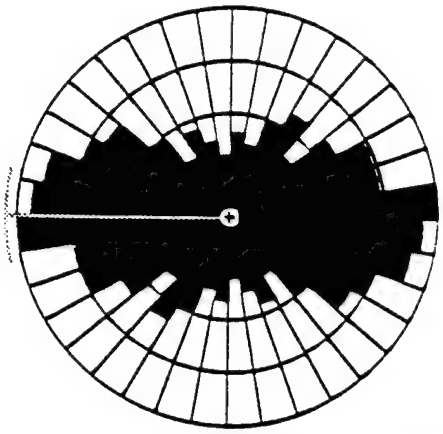

W=2.54 cm S=74.9% HORIZONTAL (NO SHPB)	Statistics
N = 672	Vector Mean = 270.0
Class Interval = 10 degrees	Conf. Angle = 12.69
Maximum Percentage = 9.5	R Magnitude = 0.236
Mean Percentage = 5.56 Standard Deviation = 2.08	Rayleigh = 0.0000

Figure A.5. Results from statistical analysis using Rosy for W=2.54 cm (1.00 inch) and S=74.9% in the horizontal plane (NO SHPB).

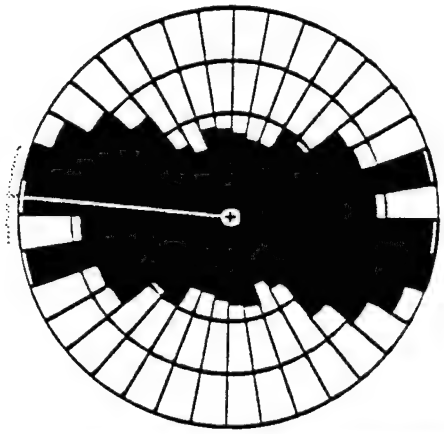

W=2.54 cm S=0% VERTICAL (NO SHPB)	Statistics
N = 607	Vector Mean = 275.0
Class Interval = 10 degrees	Conf. Angle = 13.22
Maximum Percentage = 9.1	R Magnitude = 0.240
Mean Percentage = 5.56 Standard Deviation = 2.08	Rayleigh = 0.0000

Figure A.6. Results from statistical analysis using Rosy for W=2.54 cm (1.00 inch) and S=0% in the vertical plane (NO SHPB).

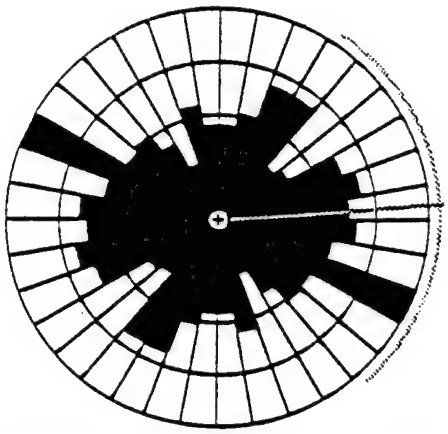

W=2.54 cm S=18.7% VERTCAL (NO SHPB)	Statistics
N = 287	Vector Mean = 85.6
Class Interval = 10 degrees	Conf. Angle = 52.28
Maximum Percentage = 10.1	R Magnitude = 0.089
Mean Percentage = 5.56 Standard Deviation = 1.68	Rayleigh = 0.1028

Figure A.7. Results from statistical analysis using Rosy for W=2.54 cm (1.00 inch) and S=18.7% in the vertical plane (NO SHPB).

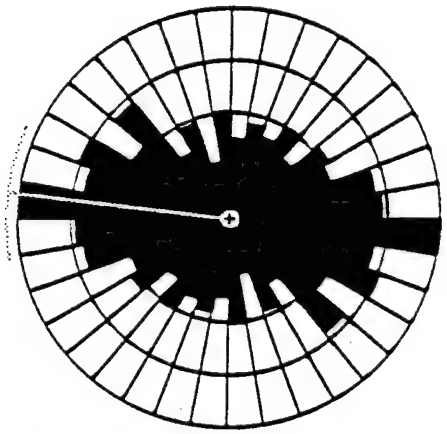

W=2.54 cm S=37.4% VERTICAL (NO SHPB)	Statistics
N = 626	Vector Mean = 276.8
Class Interval = 10 degrees	Conf. Angle = 17.39
Maximum Percentage = 10.1	R Magnitude = 0.182
Mean Percentage = 5.56 Standard Deviation = 1.80	Rayleigh = 0.0000

Figure A.8. Results from statistical analysis using Rosy for W=2.54 cm (1.00 inch) and S=37.4% in the vertical plane (NO SHPB).

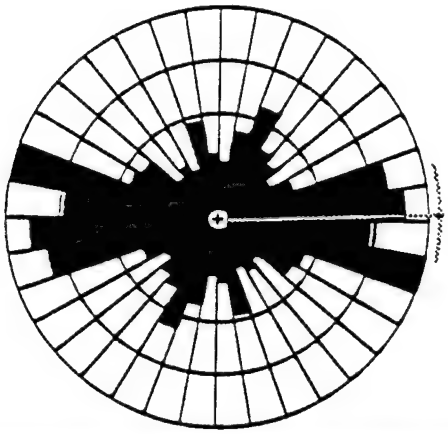

W=2.54 cm S=56.2% VERTICAL (NO SHPB)	Statistics
N = 729	Vector Mean = 87.9
Class Interval = 10 degrees	Conf. Angle = 13.21
Maximum Percentage = 11.7	R Magnitude = 0.220
Mean Percentage = 5.56 Standard Deviation = 2.67	Rayleigh = 0.0000

Figure A.9. Results from statistical analysis using Rosy for W=2.54 cm (1.00 inch) and S=56.2% in the vertical plane (NO SHPB).

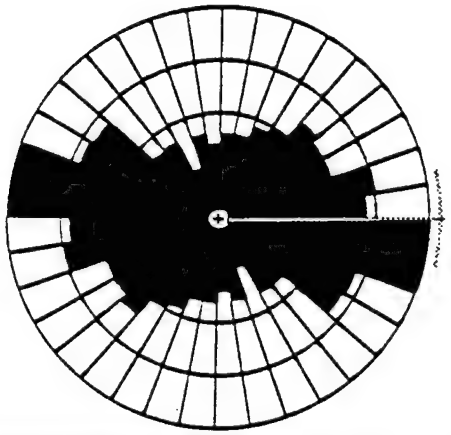

W=2.54 cm S=74.9% VERTICAL (NO SHPB)	Statistics
N = 784	Vector Mean = 89.1
Class Interval = 10 degrees	Conf. Angle = 12.44
Maximum Percentage = 9.8	R Magnitude = 0.226
Mean Percentage = 5.56 Standard Deviation = 2.04	Rayleigh = 0.0000

Figure A.10. Results from statistical analysis using Rosy for W=2.54 cm (1.00 inch) and S=74.9% in the vertical plane (NO SHPB).

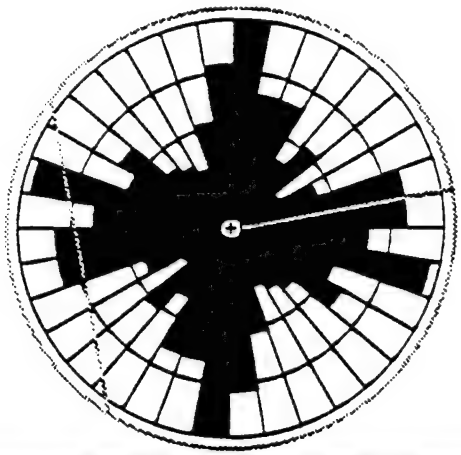

W=2.54 cm S=0% SEMI-CIRCULAR (NO SHPB)	Statistics
N = 245	Vector Mean = 79.4
Class Interval = 10 degrees	Conf. Angle = 227.13
Maximum Percentage = 9.4	R Magnitude = 0.025
Mean Percentage = 5.56 Standard Deviation = 2.04	Rayleigh = 0.8587

Figure A.11. Results from statistical analysis using Rosy for W=2.54 cm (1.00 inch) and S=0% in the semi-circular plane (NO SHPB).

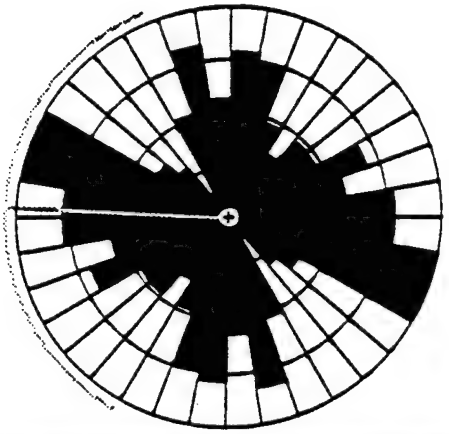

W=2.54 cm S=18.7% SEMI-CIRCULAR (NO SHPB)	Statistics
N = 250	Vector Mean = 272.9
Class Interval = 10 degrees	Conf. Angle = 63.29
Maximum Percentage = 9.2	R Magnitude = 0.078
Mean Percentage = 5.56 Standard Deviation = 2.16	Rayleigh = 0.2148

Figure A.12. Results from statistical analysis using Rosy for W=2.54 cm (1.00 inch) and S=18.7% in the semi-circular plane (NO SHPB).

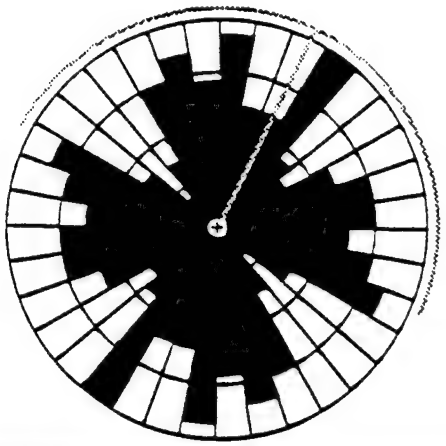

W=2.54 cm S=37.4% SEMI-CIRCULAR (NO SHPB)	Statistics
N = 310 Class Interval = 10 degrees Maximum Percentage = 8.7 Mean Percentage = 5.56 Standard Deviation = 1.88	Vector Mean = 25.3 Conf. Angle = 87.98 R Magnitude = 0.052 Rayleigh = 0.4256

Figure A.13. Results from statistical analysis using Rosy for W=2.54 cm (1.00 inch) and S=37.4% in the semi-circular plane (NO SHPB).

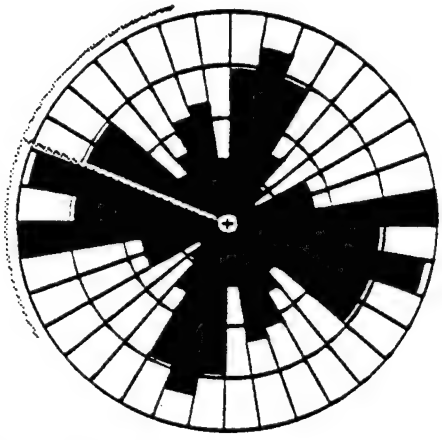

W=2.54 cm S=56.2% SEMI-CIRCULAR (NO SHPB)	Statistics
N = 265 Class Interval = 10 degrees Maximum Percentage = 9.8 Mean Percentage = 5.56 Standard Deviation = 2.44	Vector Mean = 291.9 Conf. Angle = 53.65 R Magnitude = 0.091 Rayleigh = 0.1089

Figure A.14. Results from statistical analysis using Rosy for W=2.54 cm (1.00 inch) and S=56.2% in the semi-circular plane (NO SHPB).

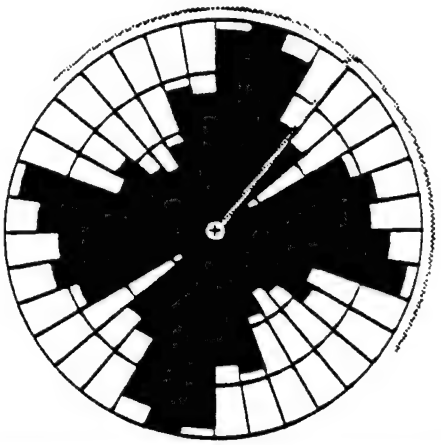

W=2.54 cm S=74.9% SEMI-CIRCULAR (NO SHPB)	Statistics
N = 237	Vector Mean = 38.5
Class Interval = 10 degrees	Conf. Angle = 85.43
Maximum Percentage = 8.4	R Magnitude = 0.061
Mean Percentage = 5.56 Standard Deviation = 1.99	Rayleigh = 0.4163

Figure A.15. Results from statistical analysis using Rosy for W=2.54 cm (1.00 inch) and S=74.9% in the semi-circular plane (NO SHPB).

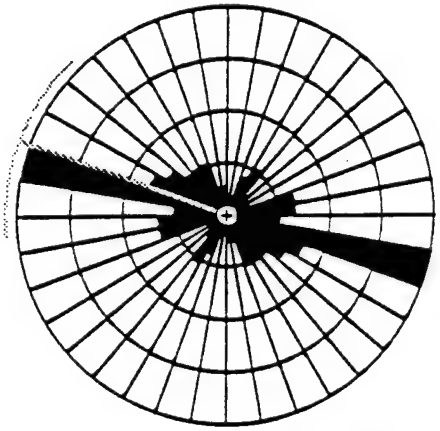

W=2.54 cm S=0% LAYER #1 (NO SHPB)	Statistics
N = 69	Vector Mean = 290.0
Class Interval = 10 degrees	Conf. Angle = 25.52
Maximum Percentage = 21.7	R Magnitude = 0.363
Mean Percentage = 5.56 Standard Deviation = 4.60	Rayleigh = 0.0001

Figure A.16. Results from statistical analysis using Rosy for W=2.54 cm (1.00 inch) and S=0% in layer #1 (NO SHPB).

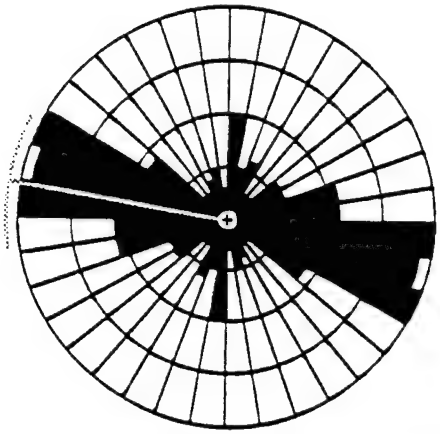

W=2.54 cm S=18.7% LAYER #1 (NO SHPB)	Statistics
N = 147	Vector Mean = 279.2
Class Interval = 10 degrees	Conf. Angle = 18.22
Maximum Percentage = 13.6	R Magnitude = 0.345
Mean Percentage = 5.56 Standard Deviation = 3.99	Rayleigh = 0.0000

Figure A.17. Results from statistical analysis using Rosy for W=2.54 cm (1.00 inch) and S=18.7% in layer #1 (NO SHPB).

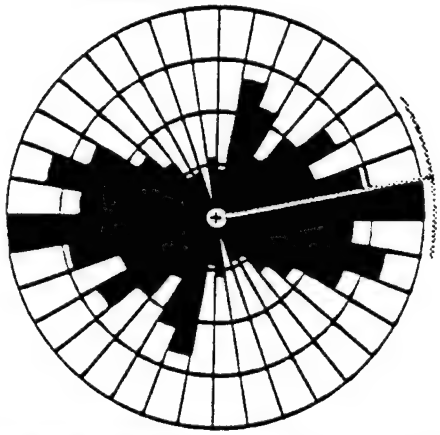

W=2.54 cm S=37.4% LAYER #1 (NO SHPB)	Statistics
N = 160	Vector Mean = 78.5
Class Interval = 10 degrees	Conf. Angle = 21.34
Maximum Percentage = 11.2	R Magnitude = 0.286
Mean Percentage = 5.56 Standard Deviation = 2.77	Rayleigh = 0.0000

Figure A.18. Results from statistical analysis using Rosy for W=2.54 cm (1.00 inch) and S=37.4% in layer #1 (NO SHPB).

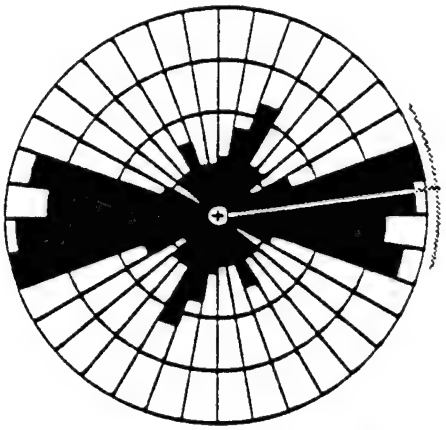

W=2.54 cm S=56.2% LAYER #1 (NO SHPB)	Statistics
N = 164	Vector Mean = 82.8
Class Interval = 10 degrees	Conf. Angle = 22.66
Maximum Percentage = 12.8	R Magnitude = 0.287
Mean Percentage = 5.56 Standard Deviation = 3.81	Rayleigh = 0.0000

Figure A.19. Results from statistical analysis using Rosy for W=2.54 cm (1.00 inch) and S=56.2% in layer #1 (NO SHPB).

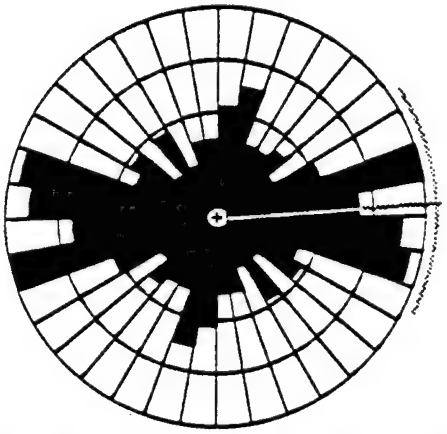

W=2.54 cm S=74.9% LAYER #1 (NO SHPB)	Statistics
N = 177	Vector Mean = 86.4
Class Interval = 10 degrees	Conf. Angle = 31.15
Maximum Percentage = 10.7	R Magnitude = 0.190
Mean Percentage = 5.56 Standard Deviation = 2.41	Rayleigh = 0.0017

Figure A.20. Results from statistical analysis using Rosy for W=2.54 cm (1.00 inch) and S=74.9% in layer #1 (NO SHPB).

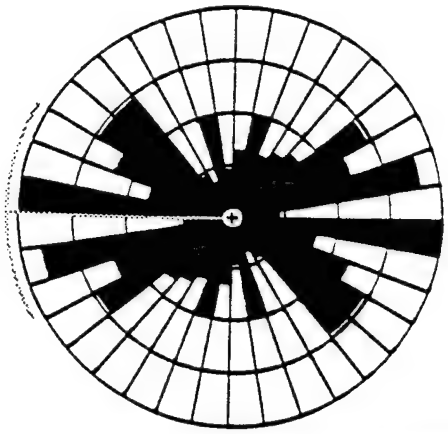

W=2.54 cm S=0% LAYER #2 (NO SHPB)	Statistics
N = 197 Class Interval = 10 degrees Maximum Percentage = 11.2 Mean Percentage = 5.56 Standard Deviation = 2.69	Vector Mean = 270.3 Conf. Angle = 29.54 R Magnitude = 0.190 Rayleigh = 0.0008

Figure A.21. Results from statistical analysis using Rosy for W=2.54 cm (1.00 inch) and S=0% in layer #2 (NO SHPB).

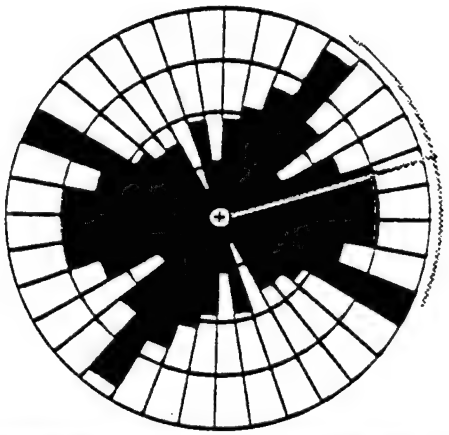

W=2.54 cm S=18.7% LAYER #2 (NO SHPB)	Statistics
N = 151 Class Interval = 10 degrees Maximum Percentage = 9.9 Mean Percentage = 5.56 Standard Deviation = 2.17	Vector Mean = 73.3 Conf. Angle = 39.64 R Magnitude = 0.164 Rayleigh = 0.0173

Figure A.22. Results from statistical analysis using Rosy for W=2.54 cm (1.00 inch) and S=18.7% in layer #2 (NO SHPB).

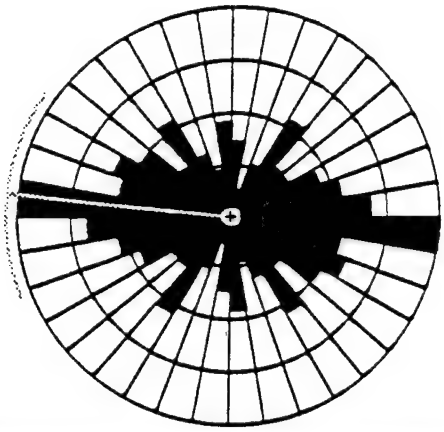

W=2.54 cm S=37.4% LAYER #2 (NO SHPB)	Statistics
N = 179	Vector Mean = 276.2
Class Interval = 10 degrees	Conf. Angle = 27.80
Maximum Percentage = 12.3	R Magnitude = 0.212
Mean Percentage = 5.56 Standard Deviation = 2.41	Rayleigh = 0.0003

Figure A.23. Results from statistical analysis using Rosy for W=2.54 cm (1.00 inch) and S=37.4% in layer #2 (NO SHPB).

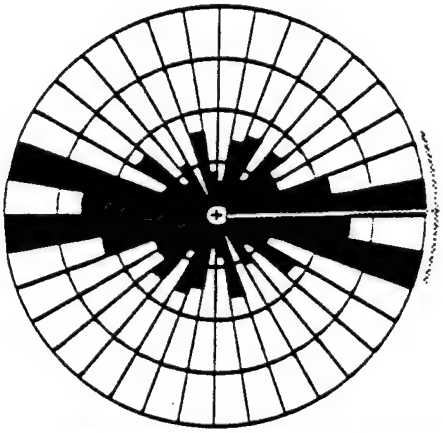

W=2.54 cm S=56.2% % LAYER #2 (NO SHPB)	Statistics
N = 181	Vector Mean = 88.3
Class Interval = 10 degrees	Conf. Angle = 19.97
Maximum Percentage = 13.8	R Magnitude = 0.288
Mean Percentage = 5.56 Standard Deviation = 3.51	Rayleigh = 0.0000

Figure A.24. Results from statistical analysis using Rosy for W=2.54 cm (1.00 inch) and S=56.2% in layer #2 (NO SHPB).

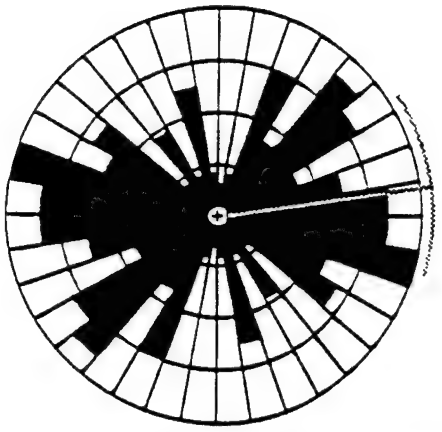

W=2.54 cm S=74.9% LAYER #2 (NO SHPB)	Statistics
N = 189	Vector Mean = 81.7
Class Interval = 10 degrees	Conf. Angle = 24.54
Maximum Percentage = 10.1	R Magnitude = 0.234
Mean Percentage = 5.56 Standard Deviation = 2.71	Rayleigh = 0.0000

Figure A.25. Results from statistical analysis using Rosy for W=2.54 cm (1.00 inch) and S=74.9% in layer #2 (NO SHPB).

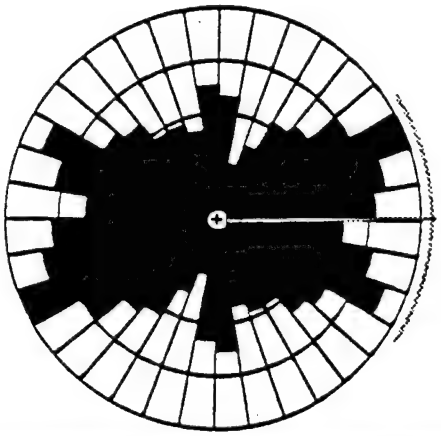

W=2.54 cm S=0% LAYER #3 (NO SHPB)	Statistics
N = 213	Vector Mean = 89.1
Class Interval = 10 degrees	Conf. Angle = 33.28
Maximum Percentage = 8.9	R Magnitude = 0.185
Mean Percentage = 5.56 Standard Deviation = 1.69	Rayleigh = 0.0030

Figure A.26. Results from statistical analysis using Rosy for W=2.54 cm (1.00 inch) and S=0% in layer #3 (NO SHPB).

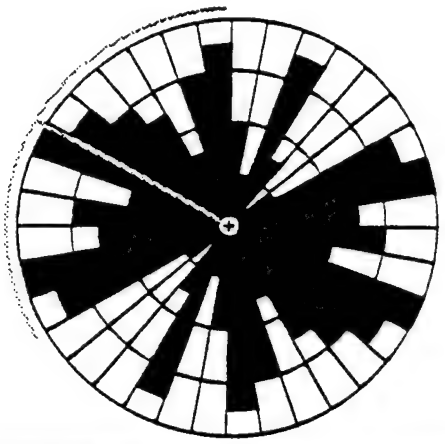

W=2.54 cm S=18.7% LAYER #3 (NO SHPB)	Statistics
N = 90	Vector Mean = 299.2
Class Interval = 10 degrees	Conf. Angle = 60.07
Maximum Percentage = 8.9	R Magnitude = 0.137
Mean Percentage = 5.88 Standard Deviation = 2.18	Rayleigh = 0.1833

Figure A.27. Results from statistical analysis using Rosy for W=2.54 cm (1.00 inch) and S=18.7% in layer #3 (NO SHPB).

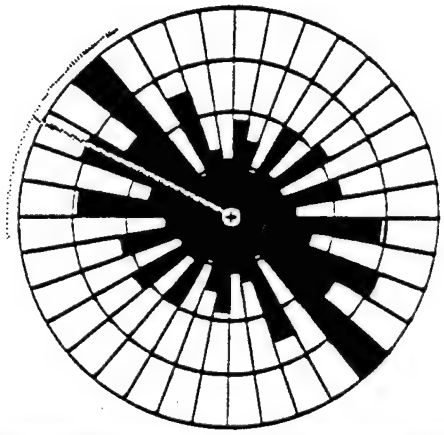

W=2.54 cm S=37.4% LAYER #3 (NO SHPB)	Statistics
N = 186	Vector Mean = 298.4
Class Interval = 10 degrees	Conf. Angle = 31.98
Maximum Percentage = 11.8	R Magnitude = 0.181
Mean Percentage = 5.56 Standard Deviation = 2.51	Rayleigh = 0.0022

Figure A.28. Results from statistical analysis using Rosy for W=2.54 cm (1.00 inch) and S=37.4% in layer #3 (NO SHPB).

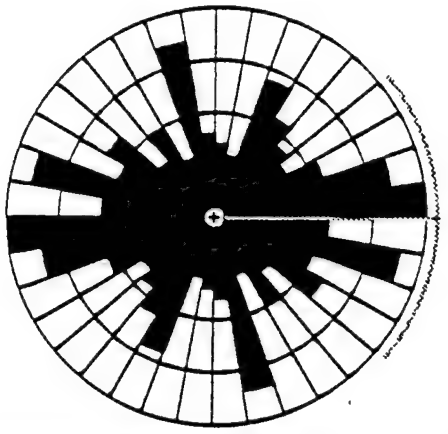

W=2.54 cm S=56.2% LAYER #3 (NO SHPB)	Statistics
N = 202	Vector Mean = 89.7
Class Interval = 10 degrees	Conf. Angle = 40.17
Maximum Percentage = 9.9	R Magnitude = 0.137
Mean Percentage = 5.56 Standard Deviation = 2.11	Rayleigh = 0.0228

Figure A.29. Results from statistical analysis using Rosy for W=2.54 cm (1.00 inch) and S=56.2% in layer #3 (NO SHPB).

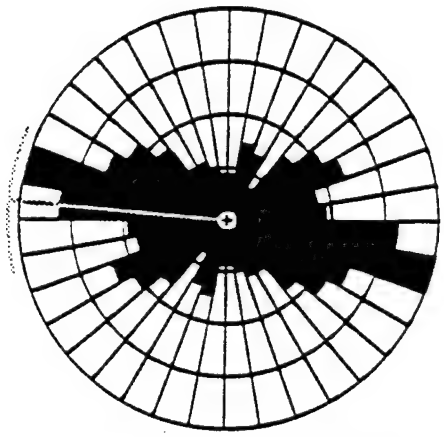

W=2.54 cm S=74.9% LAYER #3 (NO SHPB)	Statistics
N = 218	Vector Mean = 275.0
Class Interval = 10 degrees	Conf. Angle = 19.54
Maximum Percentage = 12.4	R Magnitude = 0.270
Mean Percentage = 5.56 Standard Deviation = 2.62	Rayleigh = 0.0000

Figure A.30. Results from statistical analysis using Rosy for W=2.54 cm (1.00 inch) and S=74.9% in layer #3 (NO SHPB).

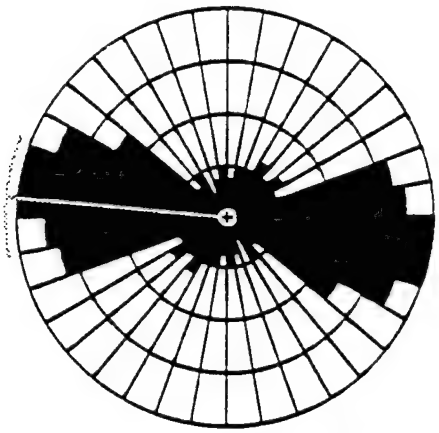

W=2.54 cm S=0% LAYER #4 (NO SHPB)	Statistics
N = 128	Vector Mean = 275.5
Class Interval = 10 degrees	Conf. Angle = 16.28
Maximum Percentage = 12.5	R Magnitude = 0.414
Mean Percentage = 5.56 Standard Deviation = 3.92	Rayleigh = 0.0000

Figure A.31. Results from statistical analysis using Rosy for W=2.54 cm (1.00 inch) and S=0% in layer #4 (NO SHPB).

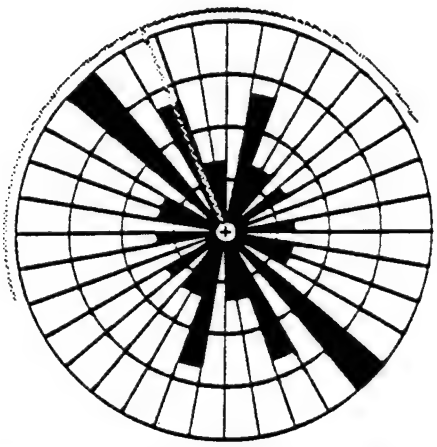

W=2.54 cm S=18.7% LAYER #4 (NO SHPB)	Statistics
N = 15	Vector Mean = 338.9
Class Interval = 10 degrees	Conf. Angle = 84.43
Maximum Percentage = 20.0	R Magnitude = 0.238
Mean Percentage = 9.09 Standard Deviation = 4.39	Rayleigh = 0.4281

Figure A.32. Results from statistical analysis using Rosy for W=2.54 cm (1.00 inch) and S=18.7% in layer #4 (NO SHPB).

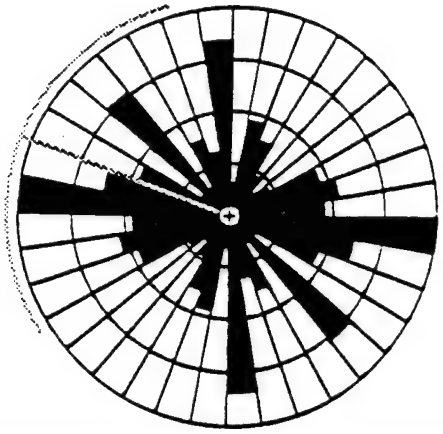

W=2.54 cm S=37.4% LAYER #4 (NO SHPB)	Statistics
N = 101	Vector Mean = 290.3
Class Interval = 10 degrees	Conf. Angle = 53.17
Maximum Percentage = 12.9	R Magnitude = 0.146
Mean Percentage = 5.56 Standard Deviation = 3.18	Rayleigh = 0.1176

Figure A.33. Results from statistical analysis using Rosy for W=2.54 cm (1.00 inch) and S=37.4% in layer #4 (NO SHPB).

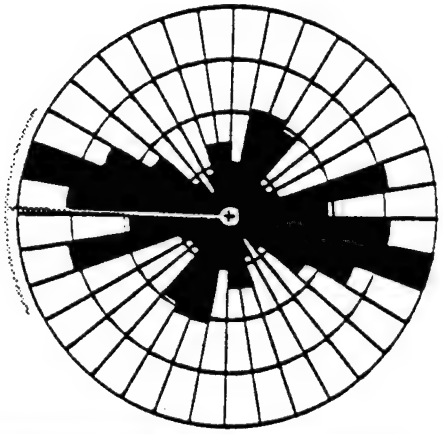

W=2.54 cm S=56.2% LAYER #4 (NO SHPB)	Statistics
N = 181	Vector Mean = 271.4
Class Interval = 10 degrees	Conf. Angle = 28.07
Maximum Percentage = 12.7	R Magnitude = 0.206
Mean Percentage = 5.56 Standard Deviation = 3.01	Rayleigh = 0.0005

Figure A.34. Results from statistical analysis using Rosy for W=2.54 cm (1.00 inch) and S=56.2% in layer #4 (NO SHPB).

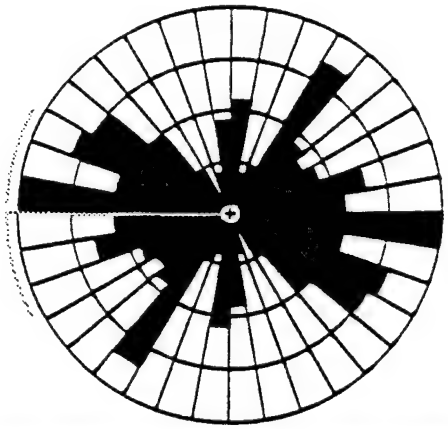

W=2.54 cm S=74.9% LAYER #4 (NO SHPB)	Statistics
N = 179	Vector Mean = 270.2
Class Interval = 10 degrees	Conf. Angle = 27.86
Maximum Percentage = 11.2	R Magnitude = 0.211
Mean Percentage = 5.56 Standard Deviation = 2.72	Rayleigh = 0.0003

Figure A.35. Results from statistical analysis using Rosy for W=2.54 cm (1.00 inch) and S=74.9% in layer #4 (NO SHPB).

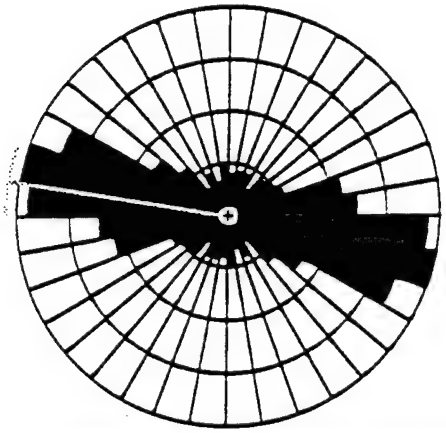

W=2.54 cm S=0% HORIZONTAL (SHPB)	Statistics
N = 420	Vector Mean = 279.4
Class Interval = 10 degrees	Conf. Angle = 9.05
Maximum Percentage = 14.3	R Magnitude = 0.407
Mean Percentage = 5.56 Standard Deviation = 3.97	Rayleigh = 0.0000

Figure A.36. Results from statistical analysis using Rosy for W=2.54 cm (1.00 inch) and S=0% in the horizontal plane (SHPB).

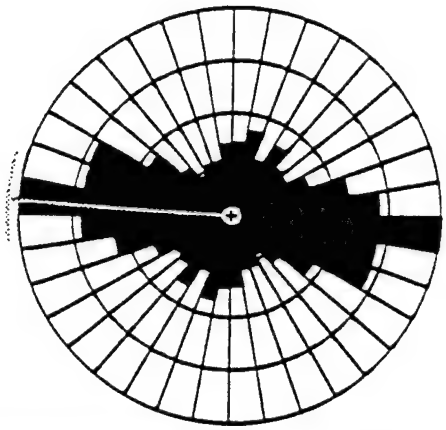

W=2.54 cm S=18.7% HORIZONTAL (SHPB)	Statistics
N = 742	Vector Mean = 274.0
Class Interval = 10 degrees	Conf. Angle = 12.38
Maximum Percentage = 12.4	R Magnitude = 0.234
Mean Percentage = 5.56 Standard Deviation = 2.55	Rayleigh = 0.0000

Figure A.37. Results from statistical analysis using Rosy for W=2.54 cm (1.00 inch) and S=18.7% in the horizontal plane (SHPB).

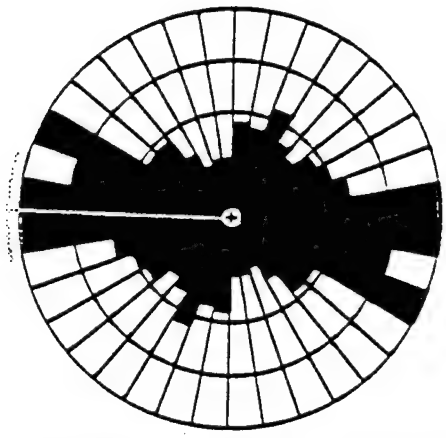

W=2.54 cm S=37.4% HORIZONTAL (SHPB)	Statistics
N = 556	Vector Mean = 271.6
Class Interval = 10 degrees	Conf. Angle = 13.79
Maximum Percentage = 10.4	R Magnitude = 0.241
Mean Percentage = 5.56 Standard Deviation = 2.49	Rayleigh = 0.0000

Figure A.38. Results from statistical analysis using Rosy for W=2.54 cm (1.00 inch) and S=37.4% in the horizontal plane (SHPB).

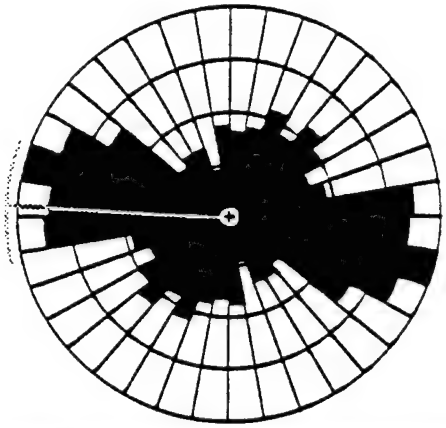

W=2.54 cm S=56.2% HORIZONTAL (SHPB)	Statistics
N = 554	Vector Mean = 273.2
Class Interval = 10 degrees	Conf. Angle = 16.62
Maximum Percentage = 10.3	R Magnitude = 0.202
Mean Percentage = 5.56 Standard Deviation = 2.25	Rayleigh = 0.0000

Figure A.39. Results from statistical analysis using Rosy for W=2.54 cm (1.00 inch) and S=56.2% in the horizontal plane (SHPB).

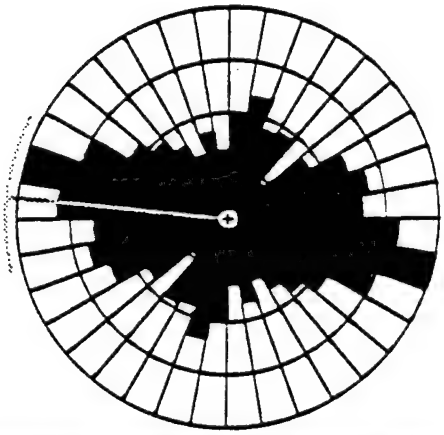

W=2.54 cm S=74.9% HORIZONTAL (SHPB)	Statistics
N = 510	Vector Mean = 275.8
Class Interval = 10 degrees	Conf. Angle = 20.29
Maximum Percentage = 10.4	R Magnitude = 0.174
Mean Percentage = 5.56 Standard Deviation = 1.95	Rayleigh = 0.0000

Figure A.40. Results from statistical analysis using Rosy for W=2.54 cm (1.00 inch) and S=74.9% in the horizontal plane (SHPB).

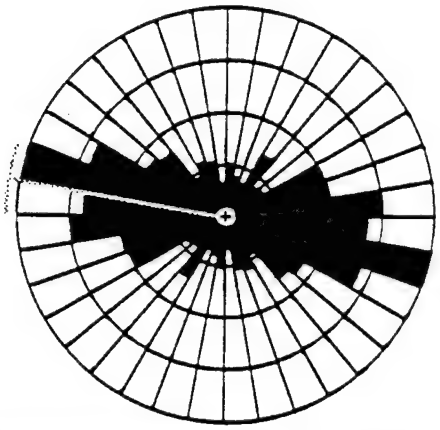

W=2.54 cm S=0% VERTICAL (SHPB)	Statistics
N = 544	Vector Mean = 279.6
Class Interval = 10 degrees	Conf. Angle = 9.43
Maximum Percentage = 13.6	R Magnitude = 0.348
Mean Percentage = 5.56 Standard Deviation = 3.22	Rayleigh = 0.0000

Figure A.41. Results from statistical analysis using Rosy for W=2.54 cm (1.00 inch) and S=0% in the vertical plane (SHPB).

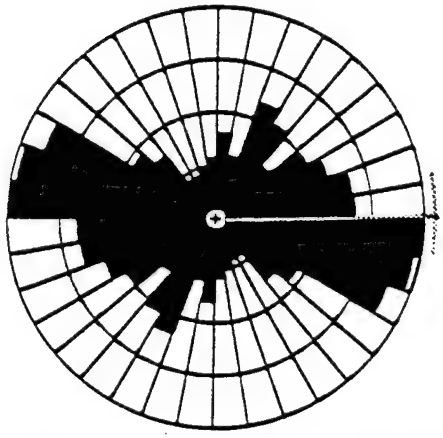

W=2.54 cm S=18.7% VERTICAL (SHPB)	Statistics
N = 738	Vector Mean = 88.8
Class Interval = 10 degrees	Conf. Angle = 10.70
Maximum Percentage = 10.8	R Magnitude = 0.266
Mean Percentage = 5.56 Standard Deviation = 2.68	Rayleigh = 0.0000

Figure A.42. Results from statistical analysis using Rosy for W=2.54 cm (1.00 inch) and S=18.7% in the vertical plane (SHPB).

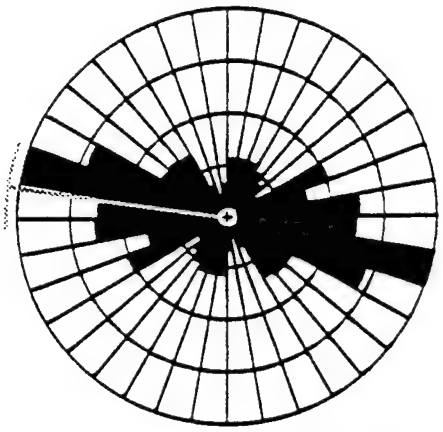

W=2.54 cm S=37.4% VERTICAL (SHPB)	Statistics
N = 455	Vector Mean = 278.6
Class Interval = 10 degrees	Conf. Angle = 11.25
Maximum Percentage = 14.5	R Magnitude = 0.334
Mean Percentage = 5.56 Standard Deviation = 3.32	Rayleigh = 0.0000

Figure A.43. Results from statistical analysis using Rosy for W=2.54 cm (1.00 inch) and S=37.4% in the vertical plane (SHPB).

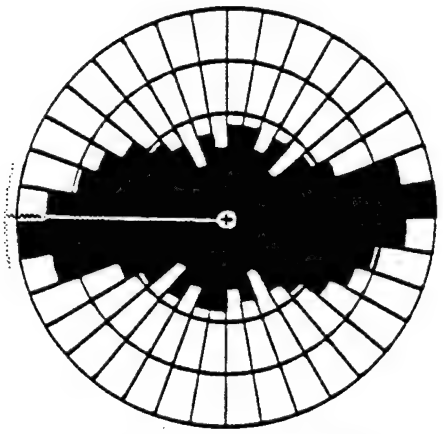

W=2.54 cm S=56.2% VERTICAL (SHPB)	Statistics
N = 632	Vector Mean = 272.1
Class Interval = 10 degrees	Conf. Angle = 13.67
Maximum Percentage = 10.4	R Magnitude = 0.228
Mean Percentage = 5.56 Standard Deviation = 2.15	Rayleigh = 0.0000

Figure A.44. Results from statistical analysis using Rosy for W=2.54 cm (1.00 inch) and S=56.2% in the vertical plane (SHPB).

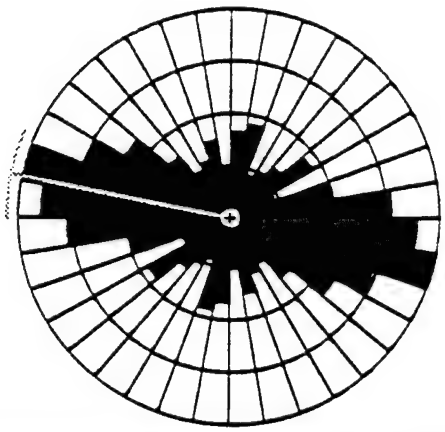

W=2.54 cm S=74.9% VERTICAL (SHPB)	Statistics
N = 607	Vector Mean = 281.2
Class Interval = 10 degrees	Conf. Angle = 12.07
Maximum Percentage = 11.9	R Magnitude = 0.266
Mean Percentage = 5.56 Standard Deviation = 2.80	Rayleigh = 0.0000

Figure A.45. Results from statistical analysis using Rosy for W=2.54 cm (1.00 inch) and S=74.9% in the vertical plane (SHPB).

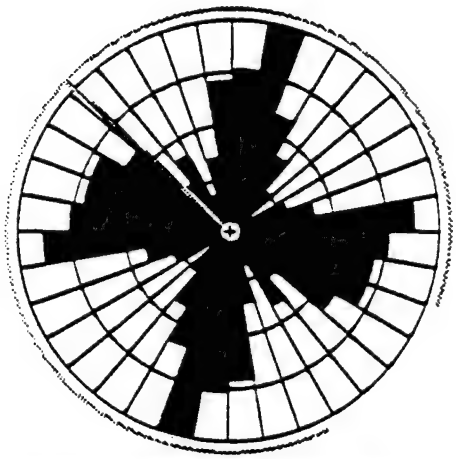

W=2.54 cm S=0% SEMI-CIRCULAR (SHPB)	Statistics
N = 159	Vector Mean = 312.0
Class Interval = 10 degrees	Conf. Angle = 158.58
Maximum Percentage = 10.7	R Magnitude = 0.039
Mean Percentage = 5.56 Standard Deviation = 2.77	Rayleigh = 0.7813

Figure A.46. Results from statistical analysis using Rosy for W=2.54 cm (1.00 inch) and S=0% in the semi-circular plane (SHPB).

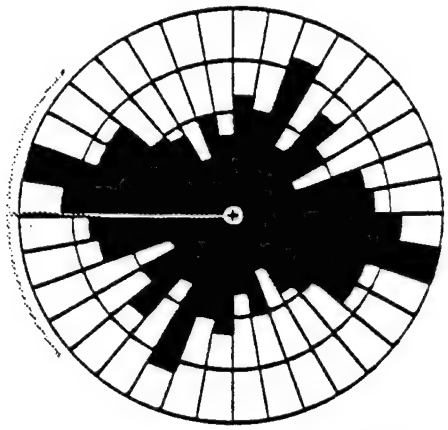

W=2.54 cm S=18.7% SEMI-CIRCULAR (NO SHPB)	Statistics
N = 320	Vector Mean = 270.7
Class Interval = 10 degrees	Conf. Angle = 40.76
Maximum Percentage = 9.7	R Magnitude = 0.107
Mean Percentage = 5.56 Standard Deviation = 1.78	Rayleigh = 0.0253

Figure A.47. Results from statistical analysis using Rosy for W=2.54 cm (1.00 inch) and S=18.7% in the semi-circular plane (SHPB).

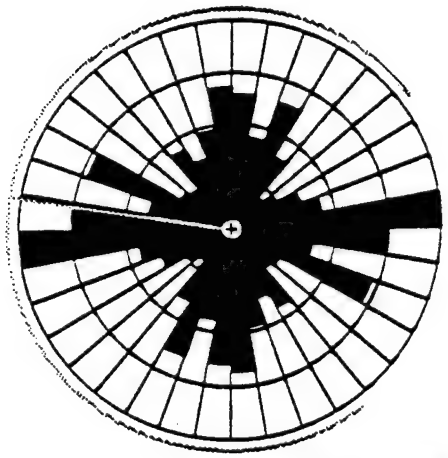

W=2.54 cm S=37.4% SEMI-CIRCULAR (SHPB)	Statistics
N = 218	Vector Mean = 278.9
Class Interval = 10 degrees	Conf. Angle = 135.59
Maximum Percentage = 11.5	R Magnitude = 0.039
Mean Percentage = 5.56 Standard Deviation = 2.42	Rayleigh = 0.7141

Figure A.48. Results from statistical analysis using Rosy for W=2.54 cm (1.00 inch) and S=37.4% in the semi-circular plane (SHPB).

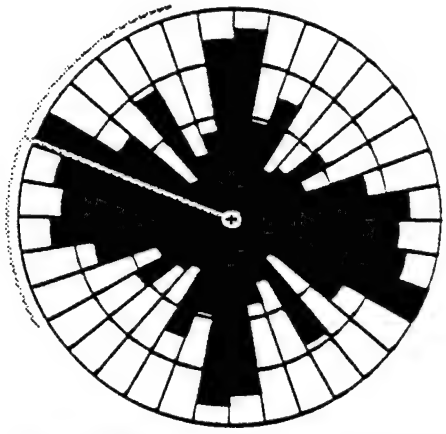

W=2.54 cm S=56.2% SEMI-CIRCULAR (SHPB)	Statistics
N = 229	Vector Mean = 291.5
Class Interval = 10 degrees	Conf. Angle = 52.73
Maximum Percentage = 9.2	R Magnitude = 0.099
Mean Percentage = 5.56 Standard Deviation = 2.17	Rayleigh = 0.1083

Figure A.49. Results from statistical analysis using Rosy for W=2.54 cm (1.00 inch) and S=56.2% in the semi-circular plane (SHPB).

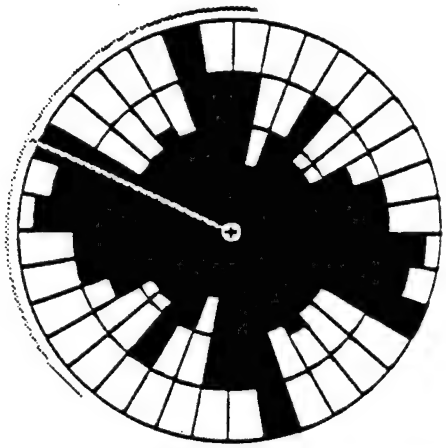

W=2.54 cm S=74.9% SEMI-CIRCULAR (SHPB)	Statistics
N = 191	Vector Mean = 293.7
Class Interval = 10 degrees	Conf. Angle = 72.28
Maximum Percentage = 8.4	R Magnitude = 0.079
Mean Percentage = 5.56 Standard Deviation = 1.71	Rayleigh = 0.3060

Figure A.50. Results from statistical analysis using Rosy for W=2.54 cm (1.00 inch) and S=74.9% in the semi-circular plane (SHPB).

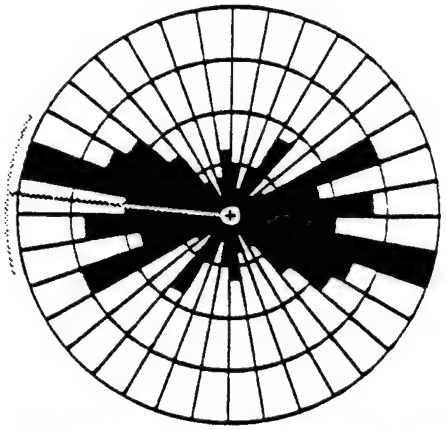

W=2.54 cm S=0% LAYER #1 (SHPB)	Statistics
N = 113	Vector Mean = 275.4
Class Interval = 10 degrees	Conf. Angle = 21.31
Maximum Percentage = 14.2	R Magnitude = 0.340
Mean Percentage = 5.56 Standard Deviation = 3.58	Rayleigh = 0.0000

Figure A.51. Results from statistical analysis using Rosy for W=2.54 cm (1.00 inch) and S=0% in layer #1 (SHPB).

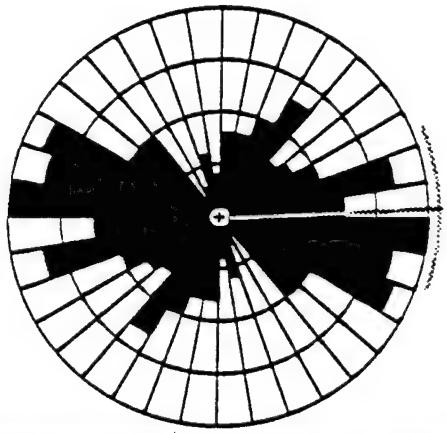

W=2.54 cm S=18.7% LAYER #1 (SHPB)	Statistics
N = 182	Vector Mean = 87.1
Class Interval = 10 degrees	Conf. Angle = 21.48
Maximum Percentage = 11.0	R Magnitude = 0.287
Mean Percentage = 5.56 Standard Deviation = 2.87	Rayleigh = 0.0000

Figure A.52. Results from statistical analysis using Rosy for W=2.54 cm (1.00 inch) and S=18.7% in layer #1 (SHPB).

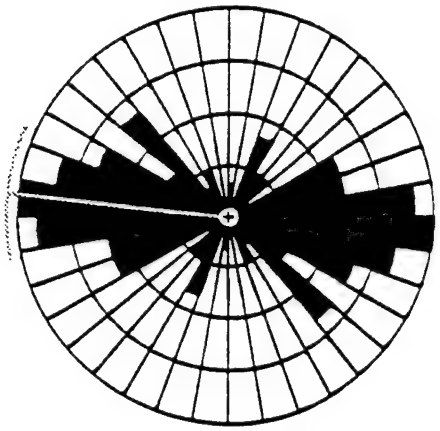

W=2.54 cm S=37.4% LAYER #1 (SHPB)	Statistics
N = 87	Vector Mean = 276.2
Class Interval = 10 degrees	Conf. Angle = 18.23
Maximum Percentage = 13.8	R Magnitude = 0.444
Mean Percentage = 8.25 Standard Deviation = 4.08	Rayleigh = 0.0000

Figure A.53. Results from statistical analysis using Rosy for W=2.54 cm (1.00 inch) and S=37.4% in layer #1 (SHPB).

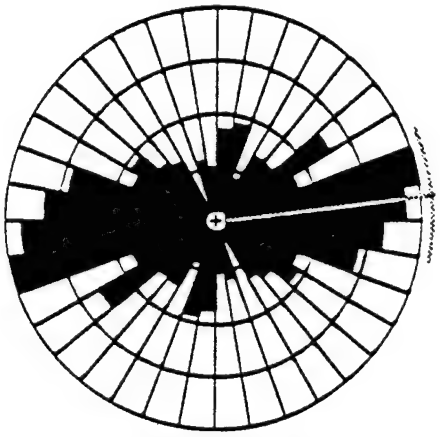

W=2.54 cm S=56.2% LAYER #1 (SHPB)	Statistics
N = 239	Vector Mean = 83.3
Class Interval = 10 degrees	Conf. Angle = 17.33
Maximum Percentage = 11.7	R Magnitude = 0.290
Mean Percentage = 5.56 Standard Deviation = 2.91	Rayleigh = 0.0000

Figure A.54. Results from statistical analysis using Rosy for W=2.54 cm (1.00 inch) and S=56.2% in layer #1 (SHPB).

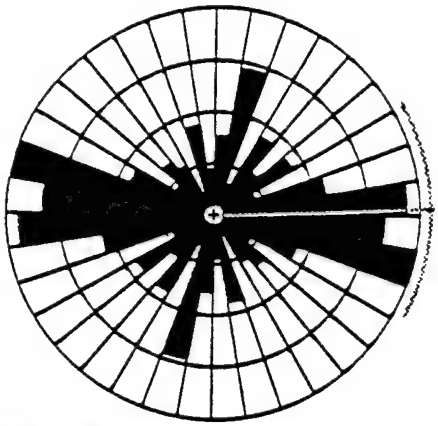

W=2.54 cm S=74.9% LAYER #1 (SHPB)	Statistics
N = 145	Vector Mean = 88.3
Class Interval = 10 degrees	Conf. Angle = 29.73
Maximum Percentage = 12.4	R Magnitude = 0.218
Mean Percentage = 5.56 Standard Deviation = 3.28	Rayleigh = 0.0010

Figure A.55. Results from statistical analysis using Rosy for W=2.54 cm (1.00 inch) and S=74.9% in layer #1 (SHPB).

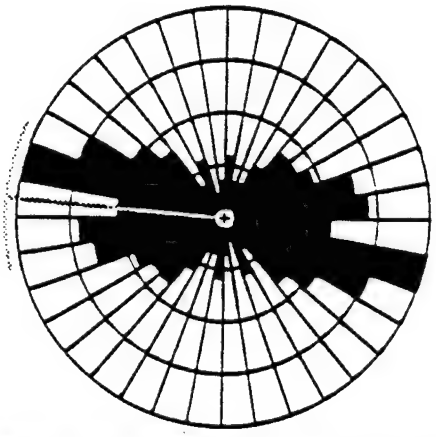

W=2.54 cm S=0% LAYER #2 (SHPB)	Statistics
N = 129	Vector Mean = 274.9
Class Interval = 10 degrees	Conf. Angle = 19.39
Maximum Percentage = 13.2	R Magnitude = 0.348
Mean Percentage = 5.56 Standard Deviation = 3.14	Rayleigh = 0.0000

Figure A.56. Results from statistical analysis using Rosy for W=2.54 cm (1.00 inch) and S=0% in layer #2 (SHPB).

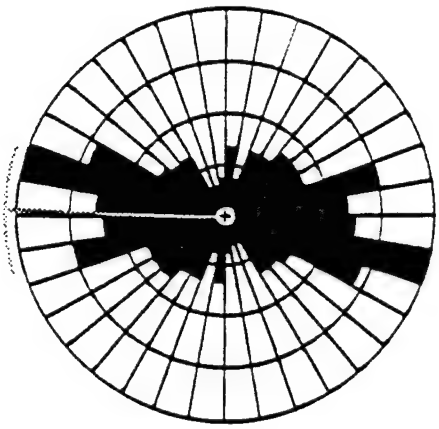

W=2.54 cm S=18.7% LAYER #2 SHPB	Statistics
N = 205	Vector Mean = 271.4
Class Interval = 10 degrees	Conf. Angle = 18.98
Maximum Percentage = 13.2	R Magnitude = 0.317
Mean Percentage = 5.56 Standard Deviation = 2.97	Rayleigh = 0.0000

Figure A.57. Results from statistical analysis using Rosy for W=2.54 cm (1.00 inch) and S=18.7% in layer #2 (SHPB).

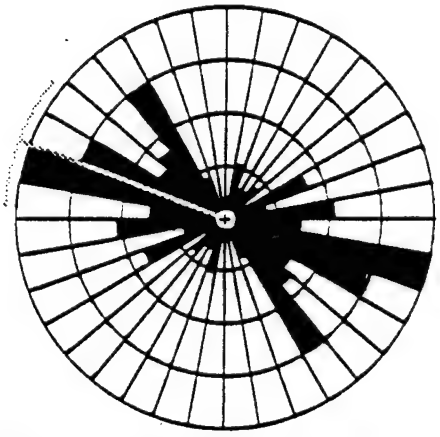

W=2.54 cm S=37.4% LAYER #2 (SHPB)	Statistics
N = 114	Vector Mean = 290.4
Class Interval = 10 degrees	Conf. Angle = 17.39
Maximum Percentage = 16.7	R Magnitude = 0.406
Mean Percentage = 5.88 Standard Deviation = 4.38	Rayleigh = 0.0000

Figure A.58. Results from statistical analysis using Rosy for W=2.54 cm (1.00 inch) and S=37.4% in layer #2 (SHPB).

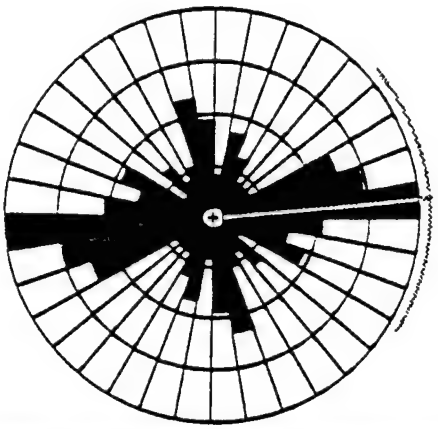

W=2.54 cm S=58.2% LAYER #2 (SHPB)	Statistics
N = 139	Vector Mean = 84.8
Class Interval = 10 degrees	Conf. Angle = 37.38
Maximum Percentage = 13.7	R Magnitude = 0.177
Mean Percentage = 5.56 Standard Deviation = 3.03	Rayleigh = 0.0126

Figure A.59. Results from statistical analysis using Rosy for W=2.54 cm (1.00 inch) and S=58.2% in layer #2 (SHPB).

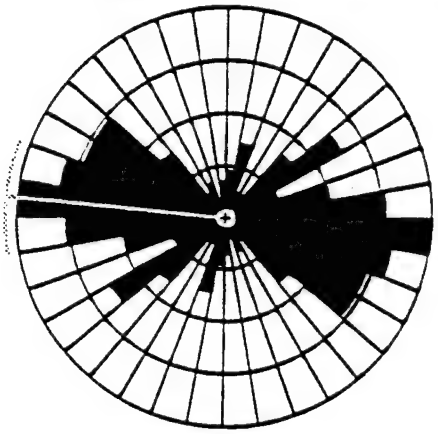

W=2.54 cm S=74.9% LAYER #2 (SHPB)	Statistics
N = 170	Vector Mean = 275.3
Class Interval = 10 degrees	Conf. Angle = 15.06
Maximum Percentage = 12.9	R Magnitude = 0.388
Mean Percentage = 5.56 Standard Deviation = 3.64	Rayleigh = 0.0000

Figure A.60. Results from statistical analysis using Rosy for W=2.54 cm (1.00 inch) and S=74.9% in layer #2 (SHPB).

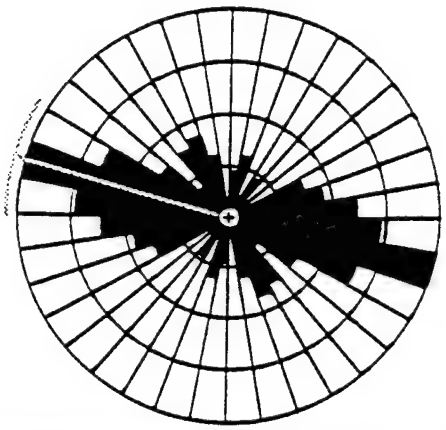

W=2.54 cm S=0% LAYER #3 (SHPB)	Statistics
N = 174	Vector Mean = 285.1
Class Interval = 10 degrees	Conf. Angle = 16.22
Maximum Percentage = 14.9	R Magnitude = 0.357
Mean Percentage = 5.56 Standard Deviation = 3.68	Rayleigh = 0.0000

Figure A.61. Results from statistical analysis using Rosy for W=2.54 cm (1.00 inch) and S=0% in layer #3 (SHPB).

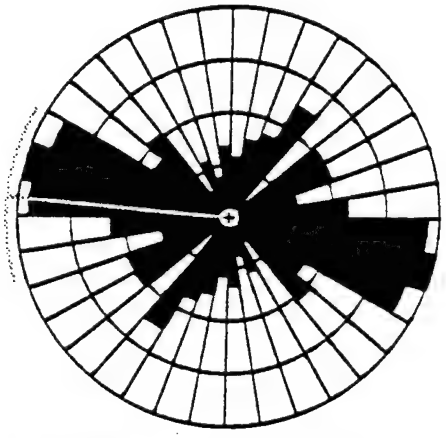

W=2.54 cm S=18.7% LAYER #3 (SHPB)	Statistics
N = 179	Vector Mean = 274.9
Class Interval = 10 degrees	Conf. Angle = 23.37
Maximum Percentage = 11.7	R Magnitude = 0.250
Mean Percentage = 5.56 Standard Deviation = 3.05	Rayleigh = 0.0000

Figure A.62. Results from statistical analysis using Rosy for W=2.54 cm (1.00 inch) and S=18.7% in layer #3 (SHPB).

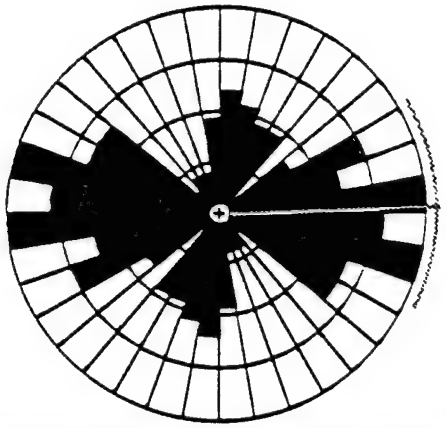

W=2.54 cm S=37.4% LAYER #3 (SHPB)	Statistics
N = 137	Vector Mean = 88.4
Class Interval = 10 degrees	Conf. Angle = 29.12
Maximum Percentage = 10.9	R Magnitude = 0.230
Mean Percentage = 5.88 Standard Deviation = 2.86	Rayleigh = 0.0007

Figure A.63. Results from statistical analysis using Rosy for W=2.54 cm (1.00 inch) and S=37.4% in layer #3 (SHPB).

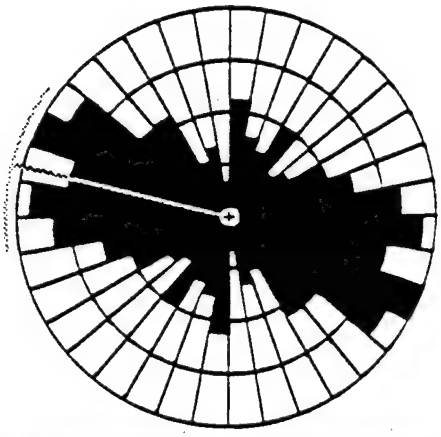

W=2.54 cm S=56.2% LAYER #3 (SHPB)	Statistics
N = 177	Vector Mean = 284.1
Class Interval = 10 degrees	Conf. Angle = 22.69
Maximum Percentage = 10.2	R Magnitude = 0.257
Mean Percentage = 5.56 Standard Deviation = 2.52	Rayleigh = 0.0000

Figure A.64. Results from statistical analysis using Rosy for W=2.54 cm (1.00 inch) and S=56.2% in layer #3 (SHPB).

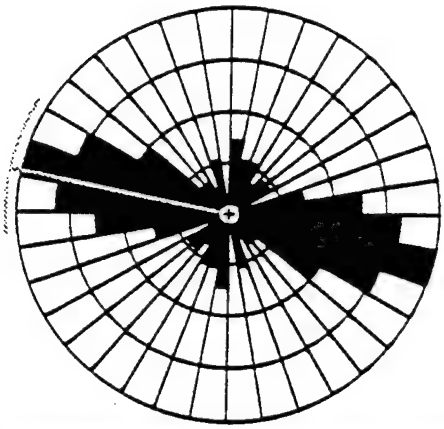

W=2.54 cm S=74.9% LAYER #3 (SHPB)	Statistics
N = 145	Vector Mean = 281.8
Class Interval = 10 degrees	Conf. Angle = 18.33
Maximum Percentage = 15.2	R Magnitude = 0.346
Mean Percentage = 5.56 Standard Deviation = 4.03	Rayleigh = 0.0000

Figure A.65. Results from statistical analysis using Rosy for W=2.54 cm (1.00 inch) and S=74.9% in layer #3 (SHPB).

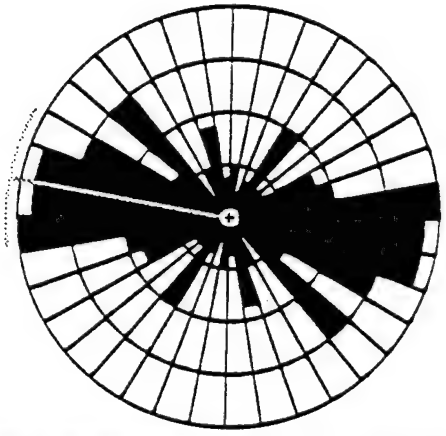

W=2.54 cm S=0% LAYER #4 (SHPB)	Statistics
N = 128	Vector Mean = 280.3
Class Interval = 10 degrees	Conf. Angle = 18.74
Maximum Percentage = 12.5	R Magnitude = 0.363
Mean Percentage = 5.56 Standard Deviation = 3.77	Rayleigh = 0.0000

Figure A.66. Results from statistical analysis using Rosy for W=2.54 cm (1.00 inch) and S=0% in layer #4 (SHPB).

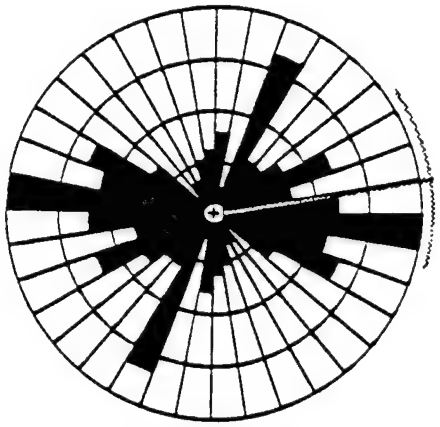

W=2.54 cm S=18.7% LAYER #4 (SHPB)	Statistics
N = 172	Vector Mean = 80.1
Class Interval = 10 degrees	Conf. Angle = 24.81
Maximum Percentage = 13.4	R Magnitude = 0.241
Mean Percentage = 5.56 Standard Deviation = 3.30	Rayleigh = 0.0000

Figure A.67. Results from statistical analysis using Rosy for W=2.54 cm (1.00 inch) and S=18.7% in layer #4 (SHPB).

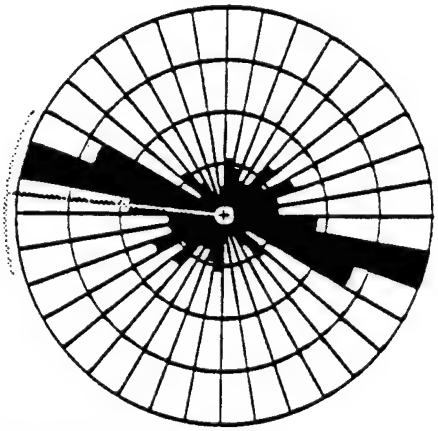

W=2.54 cm S=37.4% LAYER #4 (SHPB)	Statistics
N = 117	Vector Mean = 275.4
Class Interval = 10 degrees	Conf. Angle = 22.42
Maximum Percentage = 18.8	R Magnitude = 0.317
Mean Percentage = 5.56 Standard Deviation = 4.22	Rayleigh = 0.0000

Figure A.68. Results from statistical analysis using Rosy for W=2.54 cm (1.00 inch) and S=37.4% in layer #4 (SHPB).

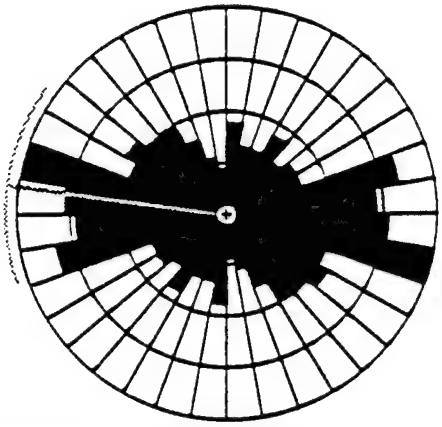

W=2.54 cm S=68.2% LAYER #4 (SHPB)	Statistics
N = 161	Vector Mean = 277.7
Class Interval = 10 degrees	Conf. Angle = 28.92
Maximum Percentage = 11.2	R Magnitude = 0.229
Mean Percentage = 5.56 Standard Deviation = 2.30	Rayleigh = 0.0002

Figure A.69. Results from statistical analysis using Rosy for W=2.54 cm (1.00 inch) and S=68.2% in layer #4 (SHPB).

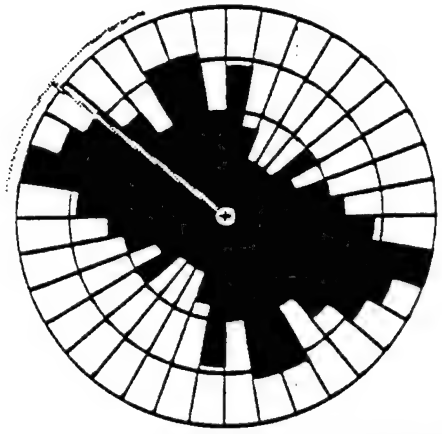

W=2.54 cm S=74.9% LAYER #4 (SHPB)	Statistics
N = 147	Vector Mean = 307.6
Class Interval = 10 degrees	Conf. Angle = 31.18
Maximum Percentage = 9.5	R Magnitude = 0.205
Mean Percentage = 5.56 Standard Deviation = 2.01	Rayleigh = 0.0020

Figure A.70. Results from statistical analysis using Rosy for W=2.54 cm (1.00 inch) and S=74.9% in layer #4 (SHPB).

REFERENCES

Allen, N.F., Richart, F.E., and Woods, R.D. "Fluid Wave Propagation in Saturated and Nearly Saturated Sands. " Journal of Geotechnical Engineering, ASCE, Vol. 106, No. GT3, (1980): pp. 235-254.

ASTM "Annual Book of Standards - Volume 04.08 Soil and Rock; Dimension Stone; Geosynthetics." American Society for Testing Materials, Philadelphia, PA, (1990): 1092 p.

Brewer, R. Fabric and Mineral Analysis of Soils, John Wiley and Sons, New York, NY, 1964: pp. 129-158.

Campbell, D.A. "Sand Fabric as an Indicator of Stress-Strain Response and Enhanced Techniques for its Measurement." PhD Thesis, Department of Civil, Environmental, and Architectural Engineering, University of Colorado, Boulder, CO., (1985): pp. 55-82.

Casagrande, A. "The Structure of Clay and its Importance in Foundation Engineering." In Contributions to Soil Mechanics; 1925-1940, (1932): pp. 72-126.

Chayes, F. "Discussion: Effect of Change of Origin on Mean and Standard Deviation of Two-Dimensional Fabrics." American Journal of Science, Vol. 252, (1954): pp. 567-570.

Curray, J.R. "The Analysis of 2-D Orientation Data." The Journal of Geology, Vol. 64, No. 2, (1956): pp. 117-131.

Das, B.M. Principles of Geotechnical Engineering, PWS Kent, Boston, MA, (1985): pp. 488-500.

DeGregorio, V.B. "Loading Systems, Sample Preparation, and Liquefaction." Journal of Geotechnical Engineering, Vol. 116, No. 4, ASCE, (1990): pp. 805-821.

Epoxy Technology, Inc., 14 fortune Drive, Billerica, Massachusetts 01821, Phone (508)-667-3805, "Epotek 301 Spectrally Transparent Epoxy Data Sheet." Low Viscosity Epoxy Used for the Development of Thin Sections, (1990).

Felice, C.W., Gaffney, E.S., Brown, J.A., and Olsen, J.M. "Dynamic High Stress Experiments on Soil." Geotechnical Testing Journal, ASTM, Philadelphia, PA, Vol. 10, No. 4, (1987): pp. 192-202.

Fredlund, D.G. "Appropriate Concepts and Technology for Unsaturated Soils." Canadian Geotechnical Journal, Vol. 16, (1979): pp. 121-139.

Fredlund, D.G. "Soil Mechanics Principles That Embrace Unsaturated Soils." Proceedings of the 11th International Conference on Soil Mechanics and Foundation Engineering, A. A. Balkema, Vol. 2, San Francisco, (1986): pp. 465-472.

Freitag, D.R., Green, A.J., and Melzer, K.J. Performance Evaluation of Wheels for Lunar Vehicles. U.S. Army Engineer Waterways Experiment Station, Vicksburg, MS, Technical Report No. M-70-2, (March, 1970): 207 p.

Gill, J.J., Miglionico, M., Andrews, M. Measurement of the Microstructural Response of Lightly Cemented Granular Soils Under Uniaxial Strain Conditions. Phillips Laboratory, Kirtland AFB, Albuquerque, NM, (1985): pp. 1-8.

Holtz, R.D. and Kovacs, W.D. An Introduction to Geotechnical Engineering, Prentice-Hall, Englewood Cliffs, NJ, 1981: pp. 109-124.

Hughes, D.S. and Kelly, J.L. "Variation of Elastic Wave Velocity With Saturation in Sandstone." Geophysics, Vol. 17, (1952): pp. 739-752.

Hunt, R.E. Geotechnical Engineering Techniques and Practices, McGraw-Hill, New York, NY, (1986): pp. 203-210.

Ishihara, K. "Propagation of Compressional Waves in Saturated Soil." JProceedings of the International Symposium on Wave Propagation and Dynamic Properties of Earth Materials, Albuquerque, NM, (1967): pp. 451-467.

Juang, C. and Holtz, R.D. "Fabric, Pore Size Distribution, and Permeability of Sandy Soils." Journal of Geotechnical Engineering, Vol. 112, No. GT9, ASCE, (1986): pp. 805-821.

Jizba, Z.V. "Mean and Standard Deviation of Certain Geological Data: A Discussion." American Journal of Science, Vol. 251, (1953): pp. 899-906.

Kolsky, H. Stress Waves in Solids, Dover Press, New York, NY, (1963): 213 p.

Krumbiem W.C. and Sloss L.L. Stratigraphy and Sedimentation, W.H. Freeman and Company, (1963): 660 p.

Ladd, R.S. "Specimen Preparation and Cyclic Stability of Sands." Journal of the Geotechnical Engineering Division, Vol. 103, No. GT6, ASCE, (1977): pp. 535-547.

Lafeber, D. "Aspects of Stress-Induced Differential Movements of Fabric in Elements in Mineral Soils." Proceedings of the 1st Australian Road Research Board, Canberra, Australia, (1962): pp. 1059-1067.

Lafeber, D. "On the Spatial Distribution of Fabric Elements in Rock and Soil Fabrics." Proceedings of the 4th Australian New Zealand Conference Soil Mechanics and Foundation Engineering, Adelaide, Australia, (1963): pp. 185-199.

Lafeber, D. "Soil Fabric in Soil Mechanics." Soil Micromorphology, Elsevier, Amsterdam, (1964): pp. 351-360.

Lafeber, D. "Soil Structural Concepts." Engineering Geology, Elsevier, Netherlands, (1966): pp. 261-290.

Lafeber, D. "Micromorphometric Techniques in Engineering Soil Fabric Analysis." Proceedings of the 3rd International Working Meeting on Soil Micromorphology, Wroclaw, Poland, (1972): pp. 669-687.

Lambe, T.W. "The Structure of Inorganic Soil." Proceedings of Soil Mechanics and Foundation Engineering, ASCE, Separate No. 315, (October, 1953): 49 p.

Lambe, T.W. and Whitman, R.V. Soil Mechanics, John Wiley and Sons, New York, NY, (1969): 553 p.

Mahmood, A, and Mitchell, J.K. "Fabric-Property Relationships in Fine-Grained Materials." Clays and Clay Minerals, Vol. 22, (1974): pp. 397-408.

Mitchell, J.K. Fundamentals of Soil Behavior, John Wiley and Sons, New York, NY, (1976): pp. 137-166.

Mitchell, J.K. The Influences of Sand Fabric on Liquefaction Behavior, Report Number S-76-5, U.S. Army Engineering Waterway Experiment Station, Soils and Pavement Laboratory, Vicksburg, MS, (1976): pp. 1-38.

Mulilis, J.P., Seed, H.B., Chan, C.K., Mitchell, J.K. and Arulanandan, K. "Effects of Sample Preparation Technique on Sand Liquefaction." Journal of the Geotechnical Engineering Division, ASCE, Vol. 103, No. GT2, (1977): pp. 91-108.

Oda, M. "Initial Fabrics and Their Relations to Mechanical Properties of Granular Material." Japanese Society of Soil Mechanics and Foundation Engineers, Tokyo, Japan, Vol. 12, No. 1, (1972a): pp. 17-36.

Oda, M. "The Mechanism of Fabric Changes During Compressional Deformation of Sand." Japanese Society of Soil Mechanics and Foundation Engineers, Tokyo, Japan, Vol. 12, No. 2, (1972b): pp. 1-18.

Olsen, R.E. "Effective Stress Theory of Soil Compaction." Journal of the Soil Mechanics and Foundation Engineering Division, ASCE, Vol. 89, No. SM2, (1963): pp 27-44.

Pettijohn, F.J. Sedimentary Rocks, Harper and Row, New York, NY, (1957): pp. 72-74.

Pincus, H.J. "The Analysis of Aggregates of Orientation Data in the Earth Sciences." Journal of Geology, Vol. 61, No. 6, (1953): pp. 482-509.

Pierce, S.J. "High Intensity Stress Wave Propagation Through Unsaturated Sands." Masters Thesis, Department of Civil Engineering, Colorado State University, Fort Collins, CO, (1989): 127 p.

Prakash, S. Soil Dynamics, McGraw Hill, New York, NY, (1981): pp. 46-124.

Rein, R.G. Microscopic Examinations of Surfaces Exposed By Cutting Ice-Rich Frozen Sands with a Wire Saw. U.S. Army Research Office, Report No. 29-79-C-0198, University of Washington, Research Triangle Park, NC 27709, (1983): 12 p.

Rinehart, J.S. Stress Transients in Solids. Hyperdynamics, Inc., Santa Fe, NM, (1975): 230 p.

Rock Ware Inc., 4251 Kipling Street, Suite 595, Wheatridge, Colorado 80033, Phone (303)-423-5645, "Digitize and Rosy." Computer Software developed by D. McEachran, for Particle Orientation Analysis, (1991).

Ross, C.A., Nash, P.T. and Friesenhahan, C.J. Pressure Waves in Solids Using a Split-Hopkinson Pressure Bar. ESL-TR-86-29, Air Force Engineering and Services Center, Tyndall AFB, FL, (1986): 83 p.

Ross, C.A. "Split-Hopkinson Pressure Bar Tests." Final Report No. ESL-TR-88-2, Air Force Engineering and Services Center, Tyndall AFB, FL, (1989): 80 p.

Rowe, P.W. "The Stress-Dilatancy Relation for Static Equilibrium of an Assembly of Particles in Contact." Proceedings of the Royal Society, Vol 269, (1962): pp. 500-527.

Rowe, P.W. " Stress-Dilatancy, Earth Pressures, and Slopes." Journal of the Soil Mechanics and Foundation Division, Vol. 89, No. SM3, (1963): pp. 37-61.

Summagraphics Corporation, 60 Silvermore Road, Seymour, Connecticut 06483, Phone (203)-881-5400, "SummaSketch II Series ADB Graphics Tablet", (1991).

Verhoogen, J. et. al. The Earth, Holt Rinehart and Winston, New York, (1970): pp. 8-27.

Veyera, G.E. Static and Dynamic Behavior of Compacted Unsaturated Sands. Final Report to US AFOSR/UES Under Contract Number F49620-87-0004, Engineering and Services Center, AFESC/RDCM, Tyndall AFB, FL, September, (1989): 20 p.

Veyera, G.E. and Fitzpatrick, B.J. A Specimen Preparation Technique for Microstructural Analysis of Unsaturated Soils." Final Report to US AFOSR Under Contract Number F49620-88-C-0053, Bolling AFB, Washington D.C., September, (1990a): 20 p.

Veyera, G.E. and Fitzpatrick, B.J. Stress Transmission and Microstructure in Compacted Moist Sand. Final Report to US AFOSR Under Contract Number F49620-88-C-0053/SB5881-0378, Bolling AFB, Washington D.C., December, (1990b): 56 p.

Wu, T.H. Soil Mechanics, Allyn and Bacon, Boston, MA, (1966): pp. 6-8.